Biomethane upgrading process : thermodynamic study of solid-liquid-vapor equilibrium form methane rich mixture

Mauro Riva

THÈSE DE DOCTORAT

de l'Université de recherche Paris Sciences et Lettres
PSL Research University

Préparée à MINES ParisTech

Biomethane upgrading process: thermodynamic study of solid-liquid-vapor equilibrium for methane rich mixtures

Procédés de purification du biométhane: étude thermodynamique des équilibres solide-liquide-vapeur de mélanges riches en méthane

École doctorale n°432

SCIENCES DES MÉTIERS DE L'INGÉNIEUR

Spécialité ÉNERGÉTIQUE ET PROCÉDÉS

Thèse confidentielle
(date de fin de 09/12/2021)

Soutenue par **Mauro RIVA**

Dirigée par **Paolo Stringari**

COMPOSITION DU JURY :

M. Eric May
University of Western Australia, Rapporteur

M. Paolo Chiesa
Politecnico di Milano, Rapporteur

M. Jerome Pauly
Université de Pau, Rapporteur

M. Vincent Gerbaud
Université de Toulouse, Membre du jury

M. Denis Clodic
Cryo Pur, Membre du jury

M. Arnaud Delebarre
Mines ParisTech, Président du jury

M. Paolo Stringari
Mines ParisTech, Membre du jury

MINES ParisTech | PSL RESEARCH UNIVERSITY PARIS

"Il faut pas courrir trop vite."
Denis G.

Acknowledgments

I wish to express my sincere gratitude to my advisor Paolo Stringari for his guidance during the last three years. His great motivation, curiosity and approach have been fundamental not only for this Ph.D study and research, but also for my future career.

I am thankful to Professor Christophe Coquelet, director of the Center Thermodynamique des Procédés, for giving me the possibility to work in his center and for its contribution in supervising my thesis.

I wish to thank Professor Denis Clodic and Dr. Joseph Toubassy from the company Cryo Pur for supporting this research and providing challenging questions to the thesis. They gave me the chance to work in a very innovative and dynamic company with motivated and competent people.

I would like to thank professor Eric May from the University of Western Australia, professor Paolo Chiesa from Politecnico di Milano and Mr. Jerome Pauly from Université de Pau et des Pays de l'Adour for accepting revising my work and for the useful comments provided. The rest of the thesis committee was composed by Vincent Gerbaud from Université de Toulouse and Arnaud Delebarre from Mines Paristech, who I would like to thank for the interesting questions and remarks during the Ph.D thesis discussion.

A special thanks goes to my office mate Marco Campestrini. I admire the dedication, accuracy and motivation you put in what you do: I wish you a fulfilling career as a researcher. Together with Paolo, you are an inspiration and a model in my work.

I warmly thank the Ph.D and post-doctoral fellows from the CTP and Cryo Pur for sharing this time and experience with me: Jamal, Fan, Tian, Charlie, Alfonso, Martha, Marco, Hamadi, Elie and Joseph. Special thanks to the CTP team in Amsterdam: Marco, Alfonso and Yohan, thank you for sharing with me 42 195 meters and a Ph.D thesis. It is a pleasure to thank all the colleagues from the CTP, and in particular Alain and Pascal for helping me in the lab, Jocelyne and Marie Claude for chatting with me, Hervé and David for being there.

Among the persons who contributed to this thesis I can't forget to mention my friends from Bulciago, who welcome me each time I go back home, and the friends I met in Fontainebleau: Manu, Bassam, Engue, Ben, Lydia, Gianni, Theo, Fanny, Andres, Anais, Simona, Gilles, Amira, Elise, merci les malakas, j'ai beaucoup appris et je me suis beaucoup amusé avec vous pendant ces trois dernières années.

Of course this thesis would not have been possible without the support of my beloved family: Milena, Giovanni, Valentina, nonna Gemma, nonno Franco (anche se hai visto solo l'inizio di questa tesi) and Elise, my future wife.

Contents

Part I

Introduction

Chapter 1

Introduction to the thesis

In this chapter a general introduction is proposed, explaining the scientific and technological problem and objectives of the study.

Résumé

Le biométhane est en train de devenir un acteur majeur dans le contexte des biocarburants et dans le cadre des politiques de décarbonation de l'énergie. Pour sa production, le biogaz brut obtenu à partir des déchets (agricoles ou de décharge), doit être traité pour éliminer le dioxyde de carbone et l'azote. Sa composition molaire est de 35% CO_2 and 65% CH_4 dans le cas du biomethane de digesteur et peut contenir jusqu'à 20% d'air dans le cas de biogaz de décharge. Grâce à la demande croissante de biogaz liquéfié (bioGNL), les techniques de purification cryogéniques sont de plus en plus compétitives par rapport aux technologies classiques. L'optimisation énergétique et les défis techniques tels que la solidification du CO_2, exigent des modèles fiables pour la simulation du procédé. L'objectif de cette thèse est l'étude d'une technologie cryogénique appliquée à la purification et la liquéfaction du biogaz.

Méthodes et résultats attendus:

- Production de mesures expérimentales d'équilibre solide-liquide-vapeur pour définir le diagramme de phases de mélanges ternaires (N_2-CH_4-CO_2) et quaternaires (N_2-O_2-CH_4-CO_2) ;
- Développement d'un modèle thermodynamique capable de prendre en compte les équilibres entre des phase solide, liquide et vapeur pour des mélanges binaires, ternaires et quaternaires du méthane et ses impuretés (CO_2, N_2, and O_2) ;
- Étude et optimisation d'un système innovant de séparation du CO_2 et des gaz de l'air appliqué au traitement et liquéfaction du biogaz.

Le partenaire académique est le Centre Thermodynamique des Procédés (CTP) de l'Ecole des Mines de Paris, installé à Fontainebleau. Les activités du CTP concernent principalement la décarbonation des procédés et les energies nouvelles et renouvelables, mais elles peuvent être étendues à d'autres domaines puisque la thermodynamique des fluides est un "thème-pilier" de l'ingénierie des procédés. Le coeur des travaux réalisés au CTP est la thermodynamique des équilibres de phases, qui associe le travail de modélisation, le travail expérimental mais aussi la conception d'outils innovants pour la mesure des propriétés thermo-physiques.

EReIE-Cryo Pur, Jeune Entreprise Innovante (JEI) fondée en déecembre 2010, est le partenaire industriel de ce projet. Le procédé Cryo Pur mis au point par la société EReIE-Cryo Pur est l'application d'une technologie brevetée (Clodic et Younes, 2001) pour la séparation

cryogénique du dioxyde de carbone présent dans le gaz de combustion par solidification à basse température (de -125 à -90 °C).

Ce manuscrit est divisé en neuf chapitres organisés en quatre parties. Dans la première partie, les défis du biométhane et de la production de biométhane liquéfié sont présentés. Dans la deuxième partie, une étude thermodynamique du mélange de biométhane est proposée en proposant un modèle thermodynamique et des mesures expérimentales. Dans la troisième partie, plus des détaillés sur les procèdes de séparation du CO_2, des gaz de l'air et de liquéfaction sont proposés en présentant la simulation du procédé Cryo Pur. Les simulations et les résultats obtenus dans cette troisième partie sont obtenus grâce aux modèles thermodynamiques et aux données expérimentales présentés dans la Partie II. Enfin, les conclusions et les perspectives de ce travail sont présentées dans la Partie IV.

1.1 Preface

The interest on biomethane as an alternative source of energy has grown over the past decade, driven by decarbonisation objectives in recent energy policy. In the European Union reducing the dependence from fossil fuels is strategic for reducing the EU energy dependence from natural gas and oil import. The EBA (European Biogas Association) forecasts that by 2030 and with the right policies in place, the biomethane industry could deliver 2-4% of the EU's electricity needs and take a 15-30% share of the methane market (EBA, 2014).

Biogas is produced by the anaerobic digestion of organic substrate from agricultural wastes, manure and industrial wastewater. Raw biogas consists mainly of methane (CH_4) and carbon dioxide (CO_2), along with water and traces of pollutants such as hydrogen sulphide (H_2S), ammonia and particulates. The content of methane is affected by the substrate and the production process. It is possible to distinguish two type of biogas:

- *biogas from digester*, produced from the fermentation of organic matter under controlled conditions in digestion chambers, called digesters. The molar composition is about 35% CO_2 and 65% CH_4.
- *landfill gas*, produced by spontaneous degradation of organic substances present in waste stocked in landfills. Compared to the biogas from digester, it contains air up to molar concentration of 20%, together with traces of other contaminants like siloxanes. Air gases are seeped into the biogas during the collection process, usually obtained by applying a low depression to the landfill. The molar ratio CH_4/CO_2 is about 1.5.

The CH_4 concentration determines the energy content in the gas since both CO_2 and N_2 are inert gases for the combustion: the highest the methane concentration in the biogas, the highest the heating power.

Raw biogas needs to be purified by removing water and pollutants (H_2S, siloxanes etc.), in order to prevent corrosion and mechanical wear of the equipment in which it is used. For some applications demanding a high energy content gas, namely vehicle fuels and injection in the natural gas grid, the biogas has to be upgraded into biomethane. It means that the concentration of methane in the biogas must be increased by removing carbon dioxide and nitrogen. The set of processes aiming to remove contaminants, such as siloxanes and H_2S, is called biogas purification. The term upgrading is used to refer to removal of carbon dioxide and nitrogen in order to raise the energy content of the biogas.

Different upgrading technologies allow carbon dioxide removal from biogas and some others nitrogen separation. When the desired final product is Liquified Biogas (LBG), cryogenic upgrading technologies becomes a very competitive alternative to the most established classical technologies, such as water scrubbers and pressure swing adsorber. Recent developments allow the integration of cryogenic upgrading technologies and biomethane liquefaction process. This technology is studied in the present work.

1.2 Objective

In the field of the non-fossil energy sources, this PhD project aims to improve the availability of the alternative and renewable resource that is the biomethane. Because upgrading process is fundamental for further applications of the biogas, suitable separation techniques have to be studied. Furthermore the liquefaction process allows new opportunities for biomethane final uses.

The objective of the thesis is the study of an optimized cryogenic technology applied to a biogas upgrading and liquefaction process. The base of the study is the knowledge of the thermodynamic behavior of biomethane mixture after purification from impurities, thus constituted of methane as a major component and N_2 (up to 20%), O_2 (up to 5%) and CO_2 (up to 40%). For this purpose, a thermodynamic model is developed and experimental measures carried out. The temperature range of interest for the process is from -90 and -161 ° C at pressure from atmospheric to 30 bar, thus phase diagrams including fluid and solid phases have to be studied. In order to define the phase diagrams and to verify and calibrate the thermodynamic model, original solid-liquid-vapor equilibrium data are produced, providing the composition of the vapor and liquid phase. Finally, results obtained from the model are used for understanding and optimizing the upgrading and liquefaction process.

Methods and expected results:

- New experimental measurements of solid-liquid-vapor equilibrium for defining the phase diagram of the ternary mixture of N_2-CH_4-CO_2 and quaternary system of N_2-O_2-CH_4-CO_2;
- Thermodynamic model able to compute the solid-liquid-vapor equilibrium for binary, ternary and quaternary mixtures of methane with CO_2, N_2, and O_2;
- Study and optimization of an innovative CO_2 and air gases separation system applied to biogas upgrading and liquefaction.

1.3 Academic partner: Centre of Thermodynamics of Processes (CTP) at Mines ParisTech

The Centre of Thermodynamics of Processes (CTP) is a joint research centre of MINES ParisTech and ARMINES and one of the 18 research centres of MINES ParisTech.

The activities of the CTP are mainly about *Decarbonation of the processes* and *New and Renewable Energies*, but they can be extended to other fields since the fluid thermodynamics is a "pillar theme" of process engineering.

The heart of the work done at CTP is the thermodynamics of phases equilibria that combine the modeling work, the experimental work but also the design of innovative tools for the thermophysical properties measurement. The CTP develops and/or modifies existing experimental tools in order to carry out its work. It develops new experimental protocols including the calibration and the estimation of the measurement uncertainties. The CTP attaches great importance to data treatment and to the comparison with data from the literature.

1.4 Industrial partner: EReIE/Cryo Pur

EReIE is a Jeune Entreprise Innovante (Young Innovative Company) created in December 2010, whose work follows the field of the New Energy Technologies. EReIE industrializes technologies coming from a laboratory level of development. Cryo Pur® process developed by the company EReIE is the application of a patented technology (Clodic and Younes, 2001) for the cryogenic separation of the carbon dioxide present in the flue gas through frosting at low temperature (from -125 to -90 ° C). In May 2015 EReIE created a branch company, Cryo Pur, focused on the development of the Cryo Pur process for biomethane upgrading and liquefaction. In the manuscript both names Ereie and Cryo Pur are used, referring substantially to the same industrial project.

1.5 Overview

This manuscript is divided in nine chapters organized in four main parts. In Part I, the challenges of the biomethane and liquefied biomethane production are presented: in Chapter 1, the context of this thesis is introduced and in Chapter 2 the state of the art of biogas upgrading technologies is presented, with particular attention to the cryogenic technologies. From this introduction it emerges that it is of fundamental importance for the study and optimization of the cryogenic system to understand and define the phase diagram of the biogas and landfill gas, including the solid phase.

In Part II, thus a thermodynamic study of to the biomethane mixture is proposed. A bibliographic research on existing phase equilibrium data for the systems of interest is presented in Chapter 3. The thermodynamic model able to compute phase equilibria and thermodynamic properties is described in Chapter 4, together with the comparison with data available in literature. Original experimental measures produced in this work are presented in Chapter 5.

In Part III, more details of the upgrading and liquefaction issues are proposed by presenting the simulation of the Cryo Pur process. The simulations and results obtained in this third Part are obtained thanks to the thermodynamic models and experimental data presented in Part II. The model for the heat and mass transfer in the heat exchanger for separating the CO_2 is presented in Chapter 6 and the behavior of the biomethane during the liquefaction step, with focus on the possibility of solid formation, is studied in Chapter 7. Chapter 8 completes the simulation of the upgrading process presenting the air separation unit. Finally conclusions and future perspectives of this work are presented in Part IV.

Chapter 2

State of the art

In this chapter a description of the context of biogas production and treatment is presented, with particular attention to existing cryogenic upgrading technologies and the Cryo Pur process.

Résumé

Le traitement de biogaz dépend de l'utilisation finale du biométhane: injection dans le réseau de gaz naturel, gaz pour véhicules ou liquéfaction. Dans le cas de l'injection dans le réseau de gaz naturel et gaz pour véhicules, la norme européenne prEN 16723 défini les spécifications du biométhane. Pour le CO_2, la teneur maximale déclarée est de 2.5%, pour l'oxygène de 0.1%. La norme européenne étant encore en phase d'approbation, pour l'instant les spécifications sont définies par différentes normes nationales: en France, la teneur en gaz inertes (CO_2 et N_2) ne doit pas dépasser le 3.5%, la teneur en oxygène ne doit pas dépasser le 0.1 ou 0.5%. Des limitations moins strictes pour la teneur en oxygène dans le biométhane sont admises dans certaines pays. Pour le biométhane liquéfié une limitation particulière sur la teneur de N_2 est appliquée à cause du phénomène appelé *rollover*. L'azote favorise en fait l'auto-stratification du bioGNL pendant le transport, ce qui peut causer l'évaporation soudaine d'une grande quantité de vapeur du réservoir. La limite pour éviter ce phénomène est généralement considérée de 1% de N_2.

Différentes technologies existent pour séparer le méthane du CO_2: les plus répondues aujourd'hui sont le lavage à l'eau et l'adsorption (PSA). Ces technologies permettent de produire du biométhane en phase gazeuse. La technologie cryogénique ne figure pas parmi les technologies les plus employées, mais elle devient compétitive lorsque l'on parle de production de biométhane liquéfié. Le procédé Cryo Pur en fait sépare les impuretés et le dioxyde de carbone en refroidissant le biogaz jusqu'à -125 °C à pression atmosphérique. Dans ces conditions, le CO_2 solidifie sur les ailettes des échangeurs et il est séparé du méthane.

Le system Cryo Pur présente des avantages remarquables pour la purification et production de biométhane liquéfié (bioGNL), mais présente aussi des enjeux technologiques concernant l'optimisation énergétique et le respect des spécifications du biométhane produit. C'est pour cela que la modélisation du procédé et des conditions de formation du CO_2 solide sont fondamentales, à plus forte raison dans le cas où les gaz de l'air sont présents dans le biogaz, car une étape ultérieure est nécessaire pour les séparer.

2.1 Biomethane specifications

The aim of biogas upgrading is to produce biomethane that meets the specifications in terms of minimum or maximum content of the components and impurities. Specifications may depend on final biomethane use or application (grid injection, liquefaction, vehicle fuel) and on the geographical region where they are applied. Specifications also define some indexes, such as the Heating Value, the Wobbe Index and the Methane Number, measuring the interchangeability of fuel gases.

2.1.1 Grid injection and vehicle fueling

The CO_2 and N_2 concentration in biomethane is subject to limitations since it decreases the heating power of the biomethane. The minimum value of the Wobbe Index and Heating Value can be translated into the maximum content of inert gases. In addition CO_2 content can be limited because of solidification issues. O_2 limitation are due to the risk of fouling in underground storage and enhanced corrosion rate in the presence of liquid water and elevate concentration of oxygen in metallic mains.

Concerning the biomethane grid injection and use as vehicle fuel, specifications are usually defined by national/regional distributors or transporters according to the national regulation. An example is the Southern California Gas Company (SoCalGas) defining the specifications for Biomethane injection in the grid (SoCalGas, 2011): maximum inert gases content is 4%, maximum CO_2 content is 3% and maximum O_2 content is 0.2%. In Europe, the European Organisation for Standardisation (CEN) is in charge of defining specifications common to all the member states for biomethane injection into natural gas grids and for use as transport fuel (EuropeanCommission, 2010). The development of these specifications is underway at the moment the thesis is written and only the drafts of the two documents prEN 16723-1 (CEN, 2015a) for grid injection and prEN 16723-2 (CEN, 2015b) for automotive fuels are available. The drafts contain specifications for the content of silicon, compressor oil, dust, chlorine, fluorine, polycyclic aromatic hydrocarbons, ammonia, amine, hydrogen cyanide, hydrogen sulphide and carbonyl sulphide. With respect to other properties, such as Wobbe Index, carbon dioxide, nitrogen and oxygen content, specifications refer to the H-gas specification for natural gas (CEN, 2015c). The CEN is in charge of writing also this standard. In this document CO_2 maximum content is declared as 2.5% and O_2 content limit is 1000 ppm (expressed as a moving average on 24 h). This specifications have to be applied at network entry points and interconnection points. However, where the gas can be demonstrated not to flow to installations sensitive to higher levels of oxygen and carbon dioxide, e.g. underground storage systems (which is usually the case for the injection in the distribution grid) higher limits of up to 4% for CO_2 and 1% for O_2 may be applied. For the Wobbe Index, defining the total amount of inert gases, at the moment of this thesis is written, there is still not a commonly accepted minimum and/or maximum values, as concluded by the CEN in the 2015 final draft (CEN, 2015c).

Until the European Standard will be validated, regulations of each member state sets the specifications for biomethane injection and vehicle fuels. In the French regulation the CO_2 limit is set to 2.5% and O_2 limit is 100 ppm (up to 5000 ppm depending for specific cases) (GRTgaz, 2015). Vehicle fuel has to attend the same standards as the national natural gas grid. Maximum content of inert gases (for a group H gas [1]) is 3.5%. In other European counties, this limits ranges between 2.5 to 6% for CO_2, and 0.5 to 1% for O_2 (Marcogaz, 2006). The application of a less strict oxygen limit for biomethane injection compared to natural gas specification is under

[1] Group H refers to high calorific value gas according to the European standard EN437 on natural gas quality, with a Wobbe Index ranging from 45.7 to 54.7 MJ/m^3. The majority of natural gas networks in Europe require the injection of group H gas.

discussion in different countries because of the high cost for O_2 separation and the absence of critical structures (e.g. molecular sieves at LNG storage sites, aquifer storage systems) in the distribution grid (HSE, 2013).

2.1.2 Biomethane liquefaction

Biomethane liquefaction offers interesting advantages for biomethane transport and storage at low (ambient) pressure. Its transport cost is less expensive compared to compressed biomethane (CBG) at 200 bar (Johansson, 2008). Furthermore, LBG allows to serve spots not reached by a pipeline or natural gas grid. Another developing technology is the LNG/LBG heavy truck fueling allowing greater autonomy compared to CBG fueled trucks.

In case of biomethane liquefaction, produced LBG needs to respect specification of biomethane in its final use. If LBG is regasified and injected in the gas grid or used as vehicle fuel, same specifications reported in sec. 2.1.1 have to be respected. For oxygen content, natural gas grid limits are normally considered sufficient.

In Liquified Natural Gas production process, some specific limits are set: the maximum concentration of CO_2 is considered to be 50 ppm in order to avoid solidification problems during liquefaction. At classical liquefaction pressure (40-50 bar) it has to be noticed that a much higher concentration of carbon dioxide could be tolerated because solid CO_2 is sufficiently soluble in hydrocarbons. The 50 ppm limit is empirically used since experience in the operation of cryogenic processing plants has shown that local freeze-out can occur at concentrations well below the solubility limit because of local cold spots on equipment surfaces, transient shifts in temperatures and pressures etc. (Timmerhaus and Flynn, 1989). Another point is that CO_2 solubility at ambient pressure is lower than 50 ppm. Solid formation can thus occurs during expansion and storage of LNG/LBG. This problem is discussed in Chapter 7.

The N_2 content in LBG and LNG is limited because it can cause auto-stratification, which is the precursor of roll-over problems during transport and storage for extended periods. If no nitrogen (or little) is present in the LNG/LBG stored or transported in the tank, a free convective circulation is set up (see fig. 2.1a). Since LNG/LBG tanks are not provided by external refrigeration but just highly insulated, a small leak of heat from the ambient warms the liquid in contact with the tank walls. The liquid becomes thus slightly less dense, moving upward close to the walls, and at the top of the tank it flashes: more volatile and lighter hydrocarbons (methane) preferentially evaporates. Relief valves garantee the control of the pressure in the tank by evacuating a certain amount of vapor (boil off). The flashed liquid is denser and moves downwards, producing the circulation in the tank. But as nitrogen is heavier than methane, and more volatile, auto-stratification instead of free convective circulation occurs in a tank with sufficient N_2 content (see fig. 2.1b). Nitrogen preferentially evaporates and leaves the tank boiling off and thus, if the nitrogen content is sufficient, the flashed liquid on the top becomes less dense (and not more dense, like in case of methane-rich boil off), producing a lighter top layer. The presence of two distinct layers in the tank is the cause of the roll over (another cause of stratification can be the addition of LNG of different density in the tank). At this point the bottom layer establishes its own convective circulation pattern but, because of the presence of the upper layer, it does not evaporate but superheats. The lower layer becomes progressively warmer and less dense, till the densities of the two layers approaches and the interface becomes unstable, producing the rapid mixing of the two layers (the so-called rollover phenomenon). As a consequence, since the lower layer was superheated, a large amount of vapor suddenly boils off from the tank. According to Baker and Creed (1996), when rollover happens, large amount of vaporized LNG is lost, but no explosions or structural damages occurs, thanks to the large overdimensioning of the valve systems. Arjomandnia et al. (2014) provide a recent review and

insights into the mechanisms of LNG rollover. For avoiding that auto-stratification and rollovers happens, it is considered that maximum N_2 content in LNG/LBG is 1% (Rufford et al., 2012).

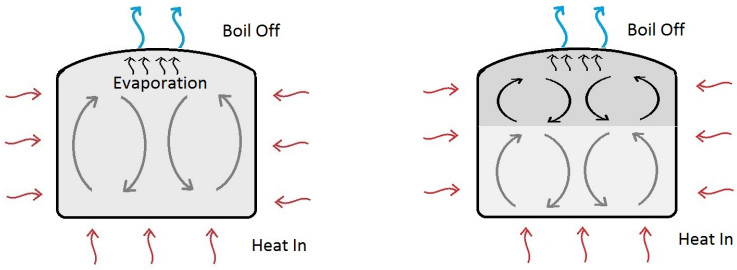

a. Normal tank behavior b. Stratified tank behavior

Figure 2.1: Scheme of the behavior of LNG stored in a tank.

Concluding, in the LNG industry, limits are mainly empirically defined by experience. Being the LBG industry very recent, this limits are still not tested and should be better defined.

2.2 Upgrading and liquefaction technologies

An overview of the worldwide upgrading market is here proposed, paying attention to the different technologies available. According to the information published by IEA Bioenergy Task 37 (Task37, 2014), updated to May 2014, 347 upgrading plants are operating worldwide. The most used technologies in biogas upgrading are (see fig. 2.2): water scrubbers (115 plants), pressure swing adsorption units, alone or coupled with water scrubbers or membranes (72 plants), chemical scrubbers (69 plants), membrane units (22 plants) and organic physical scrubbers (17 plants). An innovative technology is the CO_2 cryogenic separation, which is still not well established in the market (only one plant is operating according to the IEA, in Haarlem, The Netherlands, see sec. 2.3), mainly because of the high expected cooling cost (Song et al., 2012). Nevertheless it is in continuous development thanks to interesting advantages. In fact no absorbents are required and CO_2 can be captured at atmospheric pressure instead of high operating pressure needed for the other technologies. Another important advantage is the very low methane slip compared with other technologies (Bauer et al., 2013). Methane slip (or methane loss) is the volume ratio between the methane contained into the produced biomethane and the volume of the methane in the raw biogas as it enters the upgrading plant. It is so an indicator of the methane removed together with the carbon dioxide. It represents an evident loss in terms of produced biomethane, but also an environmental problem because methane has a great greenhouse effect, 28-34 times more than CO_2 on a 100 year frame and 84-86 times on a 20 year frame (Myhre et al., 2013) if released into the atmosphere. Finally, as Liquefied Biogas is gaining interest for biomethane transport and trucks fueling, cryogenic upgrading techniques coupled to a liquefaction process, requiring cryogenic temperature, could even present energetic advantages.

2.3 Cryogenic upgrading technologies

The term cryogenic stems from Greek and means the science and art of producing cold: this was how Kamerlingh Onnes first used the word in 1894 (Onnes, 1894) referring to the liquefaction of permanent gases. The term is used today as a synonym for the low-temperature state and used for all industrial processes dealing with temperatures significantly below $0°C$.

The research on cryogenic CO_2 capture technologies has made significant progresses in the last years, resulting in the development of different processes. Some processes have already been

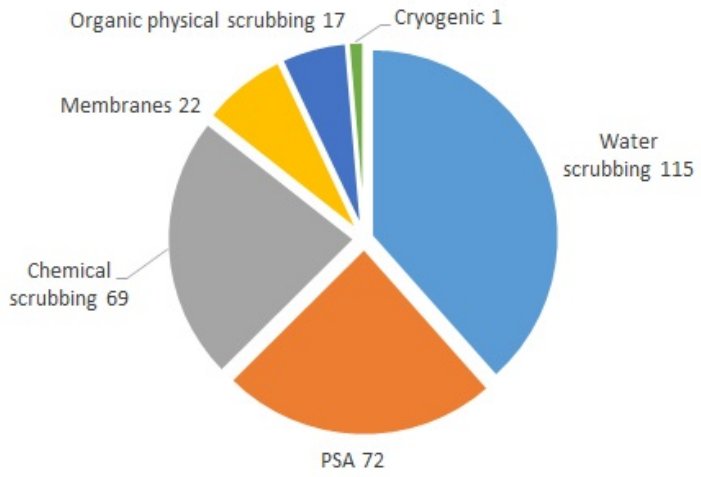

Figure 2.2: Operating biogas upgrading plants by technologies employed (Task37, 2014)

studied in the field of natural gas upgrading (see tab. 2.1). In case of natural gas upgrading application, low temperature processes have been developed for the exploitation of low quality gas reserves, with high CO_2 content. These processes can difficultly be applied for the biogas upgrading because they are designed for larger flow rate. The size of a biogas plant is much smaller than a natural gas process. For this reason, appropriate technologies should be studied for the application to the biogas upgrading.

A review of commercial technologies for biogas upgrading was published by the Swedish Gas Centre in 2013 (Bauer et al., 2013). It is reported that the first cryogenic upgrading plant suppliers was Prometheus Energy, which developed a cryogenic process for the up-grading of landfill gas in the early 1990s. A first pilot plant was built in Canada in 2000; and later in 2006, a larger plant with a capacity of 280 Nm^3/h was erected at the Bowerman Landfill in the USA. According to Bauer et al. (2013), *"there have been no updates or other news whatsoever on the plans of Prometheus Energy to further develop the technology"*. The same conclusion is reported in Allegue et al. (2012). Both documents also report the GPP technology by Gastreatment Services (GtS) from The Netherlands. Two pilot plants were built by GtS in the Netherlands, consisting of a unit for CBG production and another unit with higher capacity for liquefaction. Ryckebosch et al. (2011) reported in 2011 the existence of a pilot plant in the Netherlands for biogas cryogenic purification, upgrading and injection in the gas grid, and it is supposed to be the GtS pilot plant reported in Bauer et al. (2013). GPP process is implemented in 4 steps: gas drying, compression, gas cleaning and carbon dioxide removal. The upgrading process works at 10-26 bar and at temperature down to -85°C, so the CO_2 is captured as solid. By decreasing the temperature enough to produce liquid methane, it is also possible to separate nitrogen for landfill gas upgrading. Apart from the pilot plants, GtS has built commercial cryogenic upgrading plants in 2010 in Varberg, Sundsvall (Sweden) treating 100 Nm^3 raw biogas/h producing LBG. In 2011 a second GtS plant of 200 Nm^3 raw biogas/h plant was installed in Loudden, Stockholm (Sweden). Both plants have suffered several problems, according to Allegue et al. (2012). GtS does not give any statements on the state of the existing plants. According to Bauer et al. (2013) the two plants are not using cryogenic upgrading anymore. In the meantime, GtS have announced the delivery of a new plant for LBG production to the Schoteroog landfill in Haarlem in the northern part of the Netherlands. The plant treats gas from the nearby Waste Water Treatment Plant with a total raw gas flow of 280 Nm^3/h. The upgrading part of the plant is in operation since mid-2012 and is reported to work as expected. The liquefaction step has been commissioned in autumn 2012, but without any information on its operability at the hour of writing. According

to the IEA Bioenergy Task 37 (Task37, 2014), Haarlem plant is the only cryogenic upgrading (CO_2 removal) plant operating in the world. It has to be said that in Task37 (2014) information are often missing for upgrading plants operating in non-members countries, especially USA. A small startup company in Gothenburg called BioFriGas is aiming at developing a small scale, low budget cryogenic biogas upgrading and liquefaction process. They built the first pilot plant at the Sobacken waste treatment plant in Boras in Sweden with a capacity of 25 Nm^3/h. No further information is provided by the company about their technology because of confidentiality issue, according to Bauer et al. (2013). Different authors reports the process CO_2 Wash developed by Acrion Technologies (Cleveland, Ohio) among the cryogenic upgrading processes (Krich et al., 2005), (Ryckebosch et al., 2011). Since it doesn't remove CO_2 but impurities (halogenated hydrocarbons or siloxanes) that have a much higher solubility in carbon dioxide than methane, it is actually a purification process (not upgrading).

Others technologies aiming to capture CO_2 at low temperature but at ambient pressure are in development phase and laboratory scale: Song et al. (2012) and Chang et al. (2010) studied two cryogenic separating systems able to capture the CO_2 by solidification in heat exchangers. The adopted refrigerating systems are, respectively, a Stirling chiller and a Brayton refrigerator. The work by Jonsson and Westman (2011) is also worth mentioning. Their study on cryogenic biogas upgrading using plate heat exchangers, supported by an experimental work to validate the results concluded that biogas CH_4 purity exceeding 99% was measured and proven to be achievable. (Tuinier et al., 2010) exploited a novel cryogenic capture process using dynamically operated packed beds. The study is for applying the technology to CO_2 capture from flue gas. The presented advantages compared to technologies using heat exchangers are the tolerance to water content, the absence of an increasing heat transfer resistance due to the increasing frost layer on the walls and fins and and higher tolerance to temperature gradients during the regeneration cycles. They developed a lab-scale pilot plant with flue gas, which is still operational at Delft University.

In last few years, liquefaction of biomethane is gaining interest. One of the first biomethane liquefaction plants have been built in Livermore, California, operational since 2009, liquefying 4000 Nm^3/h of landfill gas (US EPA, 2010). The plant is one of the largest landfill gas-to-LBG plants in the world and employs scrubbers for biomethane upgrading and a liquefaction technology provided by Cryostar/Linde. In Albury, Surrey, UK a liquefaction plant was built in 2008 and produces biomethane from landfill gas since 2008, with a liquefaction technology provided by Linde (GasRec, 2014). The Lidkoping (Sweden) plant built in 2012 treats 800 Nm^3/h of biogas with a membrane upgrading system and a liquefaction technology provided by Air Liquide (N_2 closed loop) (AirLiquide, 2012). In 2014 in Nes, Romerike, Norway, an agricultural region close to Oslo, a biomethane plant is equipped with the liquefaction technology provided by Wartsila Oil and Gas (Wartsila, 2014). Other pilot plants are tested, like the iLNG by Osomo NL, developing a small scale liquefaction technology for biomethane, with a membrane pre-treatement stage (Osomo, 2015).

In this context, Cryo Pur technology proposes an innovative technology allowing integrated upgrading and liquefaction of biomethane. The development of the technology started in 2001, when Clodic and Younes developed a cryogenic separation process, in which the CO_2 could be captured as a solid on the fins of heat exchangers which were cooled thanks to an Integrated Cascade system (Clodic et al., 2003). This solution was tested at laboratory scale and with an industrial scale demonstrator, and in 2010 it has been brought to industrial scale by the company EReIE/Cryo Pur.

Table 2.1: List of low temperature upgrading technologies for natural gas and biomethane

Name	Vendor/ Licensor	Technology	Applied to	Operating T and p	State of the technology	Refs
Ryan-Holmes	Process System International, Inc.	Distillation with entrainer additive	Natural Gas			(Holmes and Ryan, 1982)
Controlled Freeze Zone (CFZ)	Exxon Mobile	Distillation	Natural Gas	-1 to -84°C, 34 bar	Ready, no commercial plant installed	(Haut and Thomas, 1989)
Cryocell	Process Group, Cool Energy Ltd, Shell	Expansion + Separation	Natural Gas	-106 to 55°C, 20-115 bar	Pilot Plant	(Amin et al., 2005)
SprexCO2	Total, IFPEN and Prosernat	Distillation + Amine	Natural Gas	-50 to -55°C, 70 bar	Pilot Plant	(Lallemand et al., 2005)
Twister process	Twister BV	Condensation in supersonic velocity torboexpander	Natural Gas	75-100 bar	Applied for water and NGL/LPG separation	(Schinkelshoek and Epsom, 2008)
Tecnimont	Tecnimont	Double step distillation	Natural Gas	50-40 bar	Pilot Plant	(Pellegrini, 2014)
Prometheus Energy	Prometheus Energy		Biogas/ Landfill gas		Pilot plant / no updates	
GPP	Gastreatment Services (GtS)		Biogas/ Landfill gas	-85°C,10 - 26 bar	One commercial plant	
CRYOSEP	Biofrigas, Sweden		Biogas gas		Pilot plant	
Cryo Pur	Cryo Pur / Ereie	CO_2 freez out in HX	Biogas/ Landfill gas	-115°C, 1 bar	Pilot Plant	(Clodic and Younes, 2006)
Chalmers	Chalmers University, SWE	CO_2 freez out in HX	Biogas	1 bar	Laboratory scale	(Jonsson and Westman, 2011)
Hong Ik	Hong Ik University, ROK	CO_2 freez out in HX	Biogas	1 bar	Laboratory scale	(Chang et al., 2010)
Tsukuba	University of Tsukuba, JPN	CO_2 freez out in HX	Flue gas	1 bar	Laboratory scale	(Song et al., 2012)
Delft	Delft University, NED	Dynamically operated packed beds	Flue gas	1 bar	Laboratory scale	(Tuinier et al., 2010)

2.4 Cryo Pur process

The Cryo Pur technology is a cryogenic technique for integrated CO_2 separation and biomethane liquefaction. The process integrates biogas purification from water and pollutants, through washing and cooling subsystems. The process is also conceived to be able to integrate a biogas liquefaction process. Thus, the main product of the process can be Compressed Biogas (CBG), or in case of liquefaction, Liquefied Biogas (LBG), both with high concentration of methane (greater than 97.5%). The captured CO_2 is stored as liquid and represents a co-product of the process. CBG can replace Compressed Natural Gas (CNG) for injection in natural gas grid or as fuel vehicle. Liquefied Biomethane (LBG) is, like for the Liquefied Natural Gas (LNG), interesting for trucks fuelling and for optimizing biomethane transportation and distribution. In the cryogenic capture technology, the operative temperature in the heat exchanger ranges, depending on the required upgrading level, between -130 ° C and the normal CO_2 sublimation temperature, around - 78 ° C at atmospheric pressure. In case of liquefaction of the biomethane,

the operating pressure is up to 15 bar.

The biogas produced by a digester or a landfill plant that enters the Cryo Pur process contains impurities, siloxanes and H_2S, and is saturated of water. Moreover it is rich in carbon dioxide, with a typical concentration of 35% in volume for dry biogas. The inlet flow must be purified from pollutants and water, and then upgraded reducing the carbon dioxide concentration by removal as solid. The process is designed with different subsystems dedicated to each purification step. The modular configuration guarantees flexibility and optimized design for different configuration and feeding conditions. Biogas introduced in the process is firstly treated for removing H_2S, water and impurities through biogas washing and cooling. The biogas flow is cooled from ambient temperature down to -90°C. At that point the biogas can be considered composed only of CO_2 and CH_4, with a concentration of carbon dioxide from 30 to 40%, depending on the feed source. The next step is the separation of the CO_2 from the biogas mixture in the finned heat exchanger, the so called antisublimation upgrading into biomethane, with temperature decreasing down to -120 °C.

At this point the produced biomethane meets the standards to be injected in the natural gas grid or used as a vehicle fuel, being the CH_4 molar ratio in the mixture greater than 97.5%. The biomethane flow can then be compressed at 8 bar for the injection in the gas grid or to 200-250 bar to be transported as Compressed Biogas (CBG). A possible further step is the liquefaction of the biomethane, in case Liquefied Biogas (LBG) is wanted as a final product. In this case the liquefaction subsystem operates a compression and a further cooling of the biomethane coming from CO_2 separation step. This liquefaction subsystem works at high pressure (6-15 bar) and low temperature, and if not well designed, the risk of uncontrolled formation of solid CO_2 during the liquefaction is high. The Cryo Pur system includes two heat exchangers in parallel for each step, in order to allow their regeneration. In fact, while the biogas flows through the first heat exchanger, a *hot* refrigerant flow passes through the second, recovering the cool power and defrosting the finned tubes. The regeneration of the heat exchanger is necessary to eliminate, by forming liquid CO_2, the solid layer that is present on the fins.

2.4.1 Heat exchanger

During the biogas upgrading operation the carbon dioxide is captured as a solid on the fins of the heat exchanger and forms a layer of CO_2 frost. The layer grows during the time that the biogas flows through the heat exchanger and the carbon dioxide is captured. At one point the thickness of the layer on the fins, is such that the solid CO_2 represents an excessive obstacle to the passage of the biogas stream (see fig. 2.3). The heat exchanger thus needs to be regenerated in order to defrost the finned tubes and recover the carbon dioxide in form of liquid.

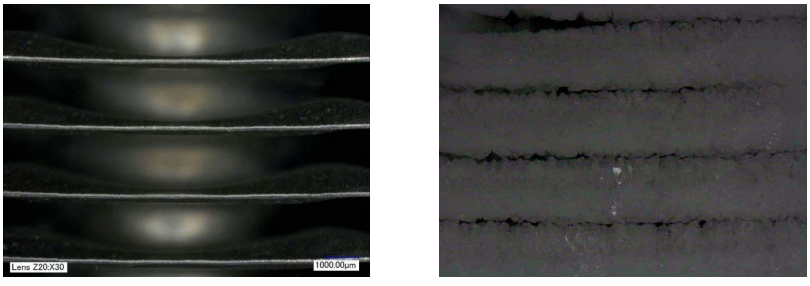

Figure 2.3: Solid CO_2 layer on the fins of the heat exchanger at the beginning and at the end of an operating cycle (Toubassy, 2012).

There are different types of heat exchanger. A first classification could be done according to the flow arrangement: parallel flow, counter flow, cross flow. Usually fins are used to increase the heat exchange surface. Different geometries are available for the fins: plate, wavy, round. In the case of Cryo Pur process, an unmixed cross flow heat exchanger with plate fins has been chosen as a base case for the pilot plant. The heat exchanger represents a key component of the whole process. It is the place where biogas is upgraded into biomethane by decreasing carbon dioxide concentration. The design of this component has a strong influence on the quality and cost of the product, providing the answer to two key questions: does the produced biomethane meet the expected standard? Does the cost of the produced biomethane allow the Cryo Pur technology being competitive with other upgrading technology? If the performances of the heat exchanger cannot be reliably simulated, the project designer should precautionary and conservatively under-estimate the captured CO_2, which means over-estimate the dimension of the heat exchanger surface, in order to be sure to obtain a biomethane which meets the desired standards (for injection in the gas grid, for the combustion in engines or for the production of LBG). At the same time, if solidification conditions, in terms of pressure and temperatures are not reliably predictable, the project needs to be set with preventively harder operating conditions (for example lower temperatures at same pressure) than actually necessary, resulting in higher energy consumption. Optimization, which is necessary to design a process with minimum capital and operating costs, lays on the capability of mastering physical phenomena happening in the heat exchanger. It is thus evident the importance of being able to simulate the capture of solid CO_2 in the heat exchanger and the modeling of the phase behavior for the biogas mixture. As example, the heat exchanger design has to take into account the frost distribution along the walls and fins surface: many studies have shown that the solid layer formed on a cold surface has a thickness profile with a peak in the first part of the surface, decreasing along the flow direction. This means that when the frost layer plugs the passage area for the biogas flow, determining the operating time before regeneration, there will be a dead surface of heat exchanger that could potentially capture more CO_2. If one manages to obtain a homogeneous surface of frost, as a consequence he maximizes the captured CO_2 in the heat exchanger, thanks to a longer operating cycles.

2.5 Conclusion: need for model and measures

From the introduction it emerges the importance of simulating the solidification and capture of the CO_2 in the heat exchanger. Tools for modeling the heat and mass transfer in the heat exchanger are needed, as well as tools for understanding and optimize the liquefaction conditions. In the air separation unit the risk of solid formation has to be avoided, and thus solid formation conditions have to be predicted and compared to operating conditions. Those tools are based on the computation of thermodynamic properties and phase equilibrium involving a solid phase for the biogas and landfill gas mixture. A reliable thermodynamic model is thus needed, which can be integrated in the heat exchanger model and used for the simulation of all the upgrading steps. For calibrating and testing the thermodynamic model, experimental data are used. A bibliographic research on data available in literature is carried out, and original measurements are performed.

Part II

Thermodynamic model and data

Chapter 3

Literature data

In this chapter, a bibliographic research on phase equilibrium data available in literature for the systems of interest is presented, with particular attention to the systems containing CO_2 and the equilibria involving a solid phase.

Résumé

Avant de modéliser les propriétés et le comportement des phases du biogaz (ou du gaz de décharge), les données d'équilibre de phases existantes pour les systèmes d'intérêt sont présentées, avec une attention particulière sur les systèmes impliquant la phase de CO_2 solide.

Pour une analyse critique des donnés existants en littérature, on étudie les différentes techniques expérimentales: suivant la classification de Muhlbauer (1997), elles peuvent être divisés selon la méthode employée pour établir l'équilibre (statique ou dynamique) ou selon la méthode employée pour analyser la composition des phases (synthétique ou analytique).

Le mélange CH_4-CO_2 a été largement étudié et un grand nombre de données sont disponibles. Pour des températures supérieures au point triple du méthane, tous les types d'équilibre ont été étudiés et un large intervalle de température est couvert. Un certain nombre de données impliquant une phase solide pour les systèmes N_2-CO_2 et O_2-CO_2 est disponible. En particulier, la solubilité du CO_2 en phase liquide (SLE) peut être comparée entre les trois mélanges: selon les données disponibles en littérature, la solubilité du CO_2 dans le méthane liquide est beaucoup plus importante que dans l'azote et l'oxygène liquide. Dans le cas du traitement du biogaz et de la liquéfaction, il est important de comprendre l'influence de l'azote et de l'oxygène sur la solubilité du dioxyde de carbone dans le méthane liquide.

A partir des données existantes, il est difficile d'estimer l'effet de l'addition d'azote et d'oxygène à un mélange CH_4-CO_2. En effet, les mesures d'équilibre de phases impliquant une phase solide pour le mélange multicomposant de CH_4-CO_2 avec N_2 et O_2 sont manquantes ou incomplètes. Shen et al. (2012) et Gao et al. (2012) proposent des données de solubilité à basse température pour le mélange N_2-CH_4-CO_2, fournissant seulement la composition de CO_2 en phase liquide. De plus, d'après la recherche bibliographique, aucune donnée pour le mélange de N_2-O_2-CH_4-CO_2 n'est disponible. Pour améliorer la compréhension de systèmes multicomposants dans des conditions où une phase solide peut apparaître, un modèle thermodynamique doit être validé par des valeurs expérimentales. Des mesures originales à basse température pour le mélange ternaire et quaternaire de méthane, de dioxyde de carbone, d'azote et d'oxygène sont ainsi produites dans ce travail.

3.1 Introduction

The necessity of predicting solid formation conditions and computing thermodynamic properties of the biomethane explains the need for a thermodynamic model of biomethane with particular attention to the phase equilibrium involving a solid phase. Thermodynamic models are supported, validated and calibrated by experimental data. Before modeling the biogas and landfill gas properties and phase behavior, existing phase equilibrium data for the systems of interest are presented with special focus on the systems involving the solid CO_2 phase. The phase diagram of each binary system is studied according to the classification of Van Konynenburg and Scott (1980). They proposed a general classification of phase equilibria for the fluid phases of binary mixtures generated using the van der Waals equation of state (EoS) and representative of the common phase diagrams encountered for real binary mixtures. Van Konynenburg and Scott (1980) classified the phase diagrams in five main types according to the p-T projections of the critical curves: both Type I and Type II presents a continuous vapor-liquid critical line linking the critical points of the two pure components, but Type II mixtures exhibit also a liquid-liquid critical line. For Type III to Type V mixtures, the critical curve is separated into two or more parts. Phase diagrams involving a solid phase have been studied by Luks (1986) and Yamamoto et al. (1989), showing six types of phase diagrams (from A to F) according to the solid-fluid-fluid locus behavior for binary mixtures of non polar or moderately polar non electrolytes.

3.2 Experimental techniques

Experimental techniques used for phase equilibrium measurements found in literature are studied and presented. The understanding of the principle and design of experimental methods for studying phase equilibria is of great importance in order to estimate the data accuracy and to critically analyze results.

According to Muhlbauer (1997) a first classification of experimental techniques for phase equilibrium measurements can be done according to the method employed to establish the equilibrium:

- **Static method**: the mixture is introduced into an equilibrium cell, where a stirrer allows the thermodynamic equilibrium and an homogeneous system to be reached;
- **Dynamic method**: the equilibrium is reached thanks to the circulation of one or more phases. In case of SVE measurements the circulating phase is the vapor phase.

The static method is largely the most used for phase equilibrium studies with a solid phase, thanks to the simplicity of the experimental setup. A second classification can be done according to the method to determine the composition of the phases:

- **Synthetic method** (or non-analytic method, or non-sampling method): a mixture of known composition is loaded into the cell, and the condition at which a second phase appears are observed.
- **Analytic method**: there is no need to know the global composition of the mixture, but the composition of each phase at the equilibrium is obtained by sampling and analyzing the samples.

Both methods are used for experimental measurements of phase equilibrium with solid phase. The main advantage of the synthetic method is the absence of a sampling device (it is also called non-sampling technique), which simplify the experimental apparatus. The main problem is the charge of the mixture, which can be done by weighting the components or by volume-pressure measurements. Weighting is the method that gives better results, but it does not allow

preparation of diluted solutions (lower than 500 ppm) with good accuracy. Furthermore it is necessary that the reserve weight is very small in comparison to the mixture one (De Stefani et al., 2004). Loading procedure by volume measurement is simple and accurate, but a very precise knowledge of pure components pvT properties is needed. For the analytic method, the advantage is the simplicity of the charging procedure, since the mixture does not need to be precisely prepared, but composition is analyzed by sampling liquid phase (or vapor, depending on the chosen condition). Liquid and vapor phase samplers represent a key component of the experimental apparatus, since the samples must be representative of the system and small enough for not changing significantly the equilibrium cell conditions. By far the most common methods for analyzing the samples in recent years has been by gas chromatography (Muhlbauer, 1997). A brief description of the operation is here provided.

Gas chromatography

Gas chromatography (GC) refers to a group of analytical separation techniques used to analyze volatile substances after separating each compound (Grob and Barry, 2004). The study and implementation of GC began in early 1900s , with a notable contribution by Mikhail Semenovich Twsett (which last name means color, from where the name *chromatography*). The essential objective of the technique is the separation of two or more compounds taking advantage from the specific distribution of each compound between a stationary phase (placed in a separation column) and a mobile phase. In a gas chromatography the samples of mixture to be analyzed can be liquid or vapor, since they are first vaporized and then carried to the separation column when the stationary phase is placed. The mobile phase (also called carrier gas) is a chemically inert gas, usually helium, hydrogen, nitrogen or argon, and serves to carry the molecules of the vaporized samples to and through the separation column. A schematic representation of a GC device is shown in fig. 3.1. The stationary phase can be both a solid adsorbent, termed gas-

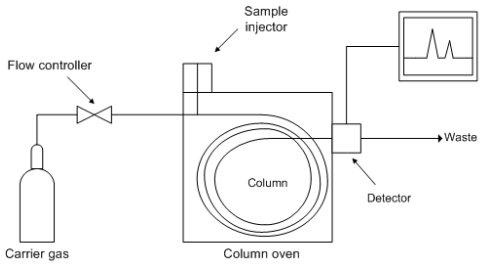

Figure 3.1: Scheme of a device for gas chromatography analysis.

solid chromatography (GSC) or a liquid on an inert support, termed gas-liquid chromatography. In both cases stationary phase consists of small homogeneous granules forming small channels between them.

The vapor sample enters the column carried by the mobile phase and each compound travels at rate determined by its interaction with the stationary phase. Thus, if the difference of retention and the length of the column are enough, each compound exits the column separately. Time needed for a compound to travel through all the column is called retention time (t_R). It depends on the affinity between the compound and the solid phase, summarized by the distribution constant (or partition coefficient) K, defined as the ratio between the concentration of component in the stationary phase divided by the concentration in the mobile phase. The column in a GC is contained in an oven, the temperature of which is precisely controlled electronically. The rate at which a sample passes through the column is directly proportional to the temperature of the column. The higher the column temperature, the faster the sample moves through the

column. However, the faster a sample moves through the column, the less it interacts with the stationary phase, and the less the analytes are separated. In general, the column temperature is selected to compromise between the length of the analysis and the level of separation. A method which holds the column at the same temperature for the entire analysis is called "isothermal". Most methods, however, increase the column temperature during the analysis: the initial temperature, the rate of temperature increase (the temperature "ramp"), and final temperature are called the "temperature program." A temperature program allows analytes that elute early in the analysis to separate adequately, while shortening the time it takes for late-eluting analytes to pass through the column.

Among the most used detectors, TCD, Thermal Conductivity Detector relies on the thermal conductivity of matter passing around a tungsten-rhenium filament with a current traveling through it. In this set up helium or nitrogen serve as the carrier gas because of their relatively high thermal conductivity which keep the filament cool and maintain uniform resistivity and electrical efficiency of the filament. However, when analyte molecules elute from the column, mixed with carrier gas, the thermal conductivity decreases and this causes a detector response. The response is due to the decreased thermal conductivity causing an increase in filament temperature and resistivity resulting in fluctuations in voltage. Detector sensitivity is proportional to filament current while it is inversely proportional to the immediate environmental temperature of that detector as well as flow rate of the carrier gas. FID, Flame Ionization Detector is another common detector where electrodes are placed adjacent to a flame fueled by hydrogen-air near the exit of the column. When carbon containing compounds exit the column, they are pyrolyzed by the flame forming ions that are detected by the electrodes. This detector works only for organic-hydrocarbon containing compounds due to the ability of the carbons to form cations and electrons upon pyrolysis which generates a current between the electrodes. The increase in current is measured and appears as a peak in a chromatogram. FIDs have low detection limits (a few picograms per second) and a wide linear operating range. FID compatible carrier gasses include nitrogen, helium, and argon.

The signals of detectors are elaborated, displayed and quantified by a software (see fig. 3.2). Each component is detected as a Gaussian peak in a signals vs. time diagram and the area of each peak is proportional to the amount of the component in the mixture. The relation between the number of moles of each analyzed component and the surface of the peak is determined during the calibration of the GC.

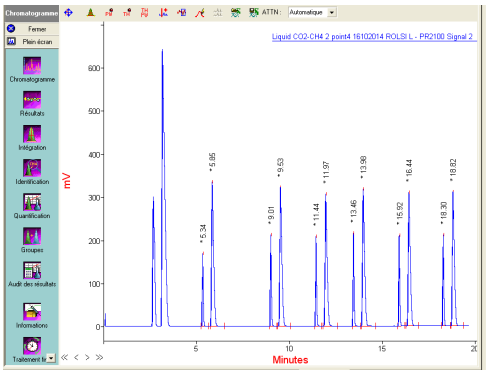

Figure 3.2: Results of a gas chromatographic analysis of a CH_4-CO_2 mixture. In the figure, 7 couples of peaks are visible; for each couple, the first peak is methane and the second is carbon dioxide.

3.3 The CH_4-CO_2 system

The binary system of methane and carbon dioxide has been widely studied and several phase equilibrium data exist in literature, including data involving a solid phase (fig. 3.3). According to the classification of Van Konynenburg and Scott (1980), the system is a Type-I. Considering the phase diagram including the solid phase, it can be classified as a type A according to the classification proposed by Luks (1986) and Yamamoto et al. (1989). The system is in fact characterized by a continuous vapor-liquid critical locus linking the critical point of the two pure components and a continuous SLVE locus from the triple point of the CO_2 to the quadruple point of the mixture (fig. 3.4). An important characteristic of this system is that the maximum of the SLVE locus has higher pressure (around 5 MPa) than the critical point of pure methane (4.6 MPa). As a consequence it is not possible separate the carbon dioxide from a mixture of CH_4-CO_2 for obtaining high purity methane through a classical distillation without incurring in solid CO_2 freeze-out.

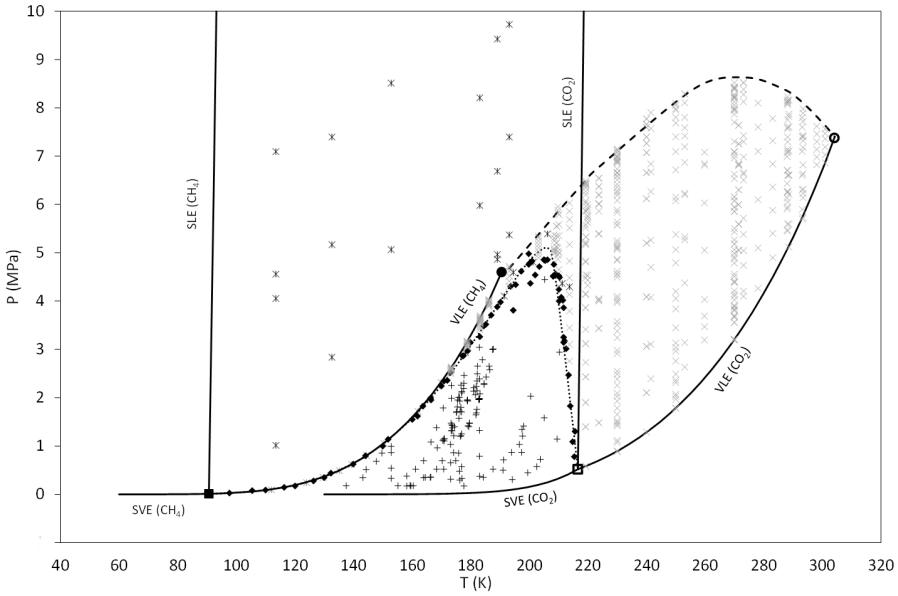

Figure 3.3: Available data for the CH_4-CO_2 system in the pT diagram: (■) CH_4 triple point; (•) CH_4 critical point; (□) CO_2 triple point; (∘) CO_2 critical point; (×) VLE data; (∗) SLE data; (⧫) SLVE data; (+) SVE data; (-) pure compound phase equilibria.

A large number of VLE data is available for this system covering a wide range of temperature, from 153 K to 300 K. A non exhaustive summary of existing VLE data is reported in table 3.1.

Phase equilibrium data involving a solid phase

Experimental values concerning the solid-liquid equilibrium (SLE), the solid-vapor equilibrium (SVE), and the solid-liquid-vapor equilibrium (SLVE) have been proposed by several authors since the 1950s (see tab. 3.2). Taking into account these works and the corresponding data, one can state at once that the solid phase is usually considered as composed of pure CO_2. Furthermore, because no experimental values for the CH_4-CO_2 mixture are available under 97 K, it follows that the mixture phase equilibrium behavior is still not well identified for temperatures lower than the pure CH_4 triple point temperature. For these temperatures also methane solidifies, thus giving a second solid phase in equilibrium with the pure solid CO_2. According to that, it can be stated that the mixture presents immiscibility in the solid phase.

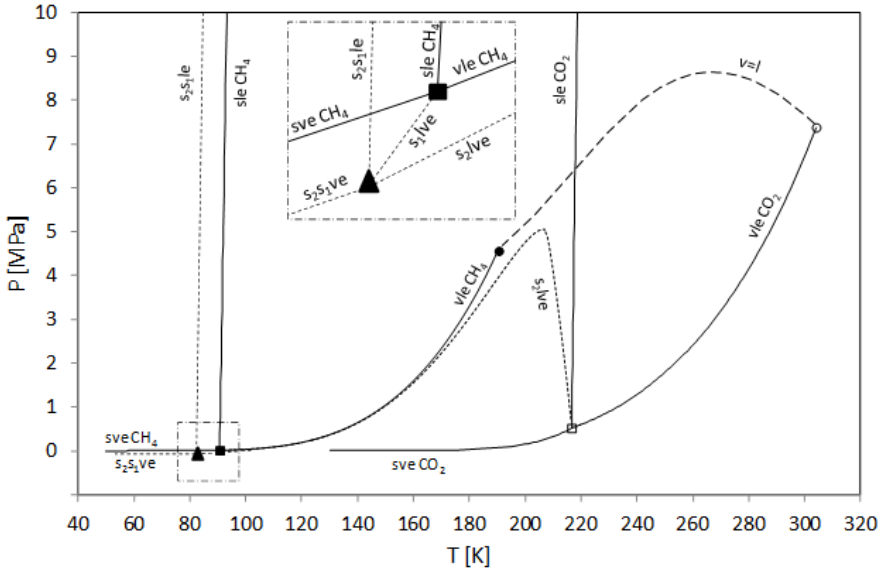

Figure 3.4: Pressure-temperature equilibrium behavior for the CH_4-CO_2 system: (■) CH_4 triple point; (•) CH_4 critical point; (□) CO_2 triple point; (○) CO_2 critical point; (▲) mixture quadruple point; (− −) vapor-liquid critical locus; (· · ·) three-phase locus; (-) pure compound phase equilibria (Riva et al., 2014)

As a consequence, the mixture should present a quadruple point, where a liquid, a vapor, and two solid phases coexist at equilibrium for appropriate values of pressure and temperature.

Even though the quadruple point, where liquid and vapor phases are in equilibrium with a carbon dioxide rich solid phase and a methane rich solid phase, has not been experimentally measured yet, a precious support in confirming this feature and in understanding the global phase equilibrium behavior of the mixture has been provided by Donnelly and Katz (1954). These authors obtained experimental results concerning the mixture critical locus, the vapor-liquid equilibrium (VLE), the SLVE and the SLE. Same authors extrapolated the fluid phase compositions along the SLVE locus toward an eutectic point, which corresponds to having a quadruple point temperature lower than the pure CH_4 triple point temperature.

Considering that this work does not deal with temperatures lower than the CH_4 triple point temperature and that all the experimental values involve only the pure CO_2 solid phase, a distinction between methane rich solid phases and pure carbon dioxide solid phase is useless in this context. As a consequence, the letter S is henceforth used for indicating the sole pure carbon dioxide solid phase occurring for temperature greater than the CH_4 triple point, for example for indicating the solid-liquid equilibrium (SLE), solid-vapor equilibrium (SVE) etc.

Table 3.2 presents a review of SLVE, SLE and SVE data proposed by different authors, specifying the corresponding type of equilibrium, the number of experimental values (N), and their temperature, pressure, and CO_2 mole fraction ranges. In fig. 3.5 it is possible to observe that the solubility of CO_2 in liquid methane has been studied from the triple point of the CO_2 down to 110 K, corresponding to a range of solubility down to 170 ppm.

Donnelly and Katz (1954) provided a complete study on the methane-carbon dioxide system providing also SLE and SLVE data in the range from 194.5 K to 215.4 K. Phase equilibrium data involving a solid phase were measured by loading a transparent constant volume cell with a synthetic mixture of known composition and recording temperature and pressure condition of solid formation determined by visual observation. Sterner (1961) extended the work of Donnelly

Table 3.1: Experimental VLE data for the CH_4-CO_2 mixture. N is the number of experimental points

Authors	Kind of data	N	Vapor composition (mol/mol) CO_2	Liquid composition (mol/mol) CO_2	Temperature (K)	Pressure (MPa)
Donnelly and Katz (1954)	VLE	85	0.19 - 0.95	0.03 - 0.92	200 - 271	1.5 - 7.9
Kaminishi et al. (1968)	VLE	18	0.003 - 0.012	0.069 - 0.52	233 - 283	3.7 - 8.2
Neumann and Walch (1968)	VLE	67	0.80 - 1	0.25 - 1	173 - 220	2.6 - 6.0
Arai et al. (1971)	VLE	34		0.04 - 0.56	253 - 288	2.6 - 8.5
Davalos et al. (1976)	VLE	36	0 - 0.77	0 - 0.59	230 - 270	0.9 - 8.5
Mraw et al. (1978)	VLE	46	0 - 1	0 - 1	153 - 219	0.6 - 6.5
Somait and Kidnay (1978)	VLE	12	0 - 0.4	0 - 0.30	270	3.2 - 8.4
Al-Sahhaf et al. (1983)	VLE	57	0 - 0.79	0 - 0.55	219 - 270	0.6 - 8.4
Vetere (1983)	VLE	14	0.40 - 0.79	0.03 - 0.58	230	1.1 - 5.2
Xu et al. (1992a)	VLE	23	0 - 0.20	0 - 0.18	289 - 293	5.1 - 8.2
Bian et al. (1993)	VLE	6	0 - 0.03	0 - 0.03	301	6.9 - 7.6
Webster and Kidnay (2001)	VLE	52	0 - 0.75	0 - 0.58	230 - 270	0.9 - 8.3

and Katz (1954) to temperatures down to 166.5 K for the SLVE through a dynamic method with gas chromatographic analysis of the liquid or vapor phase. Data on the SLVE curve have been provided for a wide range of conditions by Davis et al. (1962) using a constant volume cell in which three phase equilibrium was established and determined thanks to visual observation. The composition of the liquid phase was found by charging a mixture with known composition, while the vapor phase was sampled. Kurata and Im (1971) reported an experimental study of the vapor and liquid compositions at multiphase equilibrium of light paraffins in presence of solid CO_2. The authors report data along the SLVE locus of the binary CH_4-CO_2 mixture in the range of temperature from 165.2 to 210.2 K and pressure between 1.9 and 4.85 MPa based on Davis et al. (1962) SLVE data. Measurements on the solid-liquid equilibrium have been reported by Brewer and Kurata (1958) based on Donnelly and Katz (1954) data series. Different authors (see Tab.3.1) provided experimental data for the SLE of the methane and carbon dioxide mixtures at temperature down to 110 K. Cheung and Zander (1968) measured the SLE conditions of CH_4-CO_2 and CH_4-H_2S systems by means of a constant volume cell charged with a specific gas composition and analysis of the liquid phase composition by gas chromatography. The experimental procedure description states that the liquid level in the cell was allowed to build up until it reached the liquid sampler capillary. It means that some vapor remained in the cell, so the equilibrium conditions measured are SLVE, and not SLE. Recently Shen et al. (2012) and Gao et al. (2012) measured the SLE in the range of temperature between 112 and 170 K using a similar experimental apparatus corresponding to a static analytic method. Pikaar (1959) investigated the CH_4-CO_2 system for temperature down to 130 K, reporting a great amount of SVE, SLE and SLVE data obtained with two different experimental techniques: a non sampling technique consisting in a constant volume cell apparatus with investigation of the T-p behavior of the mixture, and a saturation cell apparatus with infra-red absorption analysis of vapor phase samples. Another set of data in the solid-vapor region for the CH_4-CO_2 mixture has been measured by Agrawal and Laverman (1974) in the range of condition of interest for the LNG industry by means of a non sampling visual technique in which the points of inception of solid formation on a cold spot created in the equilibrium cell are determined. Recently Le and Trebble (2007) studied the methane-carbon dioxide mixture at the solid-vapor equilibrium in a range of temperature from 168 to 187 K with a non sampling method similar to the experimental technique adopted by Agrawal and Laverman (1974), with observation of

solid formation on a cooled U-tube placed directly in the equilibrium cell, serving as a cold spot. Recently, experimental data are reported by Zhang et al. (2011) for the frost points of the CH_4-CO_2 systems for a wide range of CO_2 compositions (i.e. CO_2 mole fraction from 0.108 to 0.542). Also in this case the experimental technique adopted is a static-synthetic method but instead of a visual observation, a complete analysis of the p-T behavior during a cycle of cooling and heating of a mixture of known composition has been adopted.

Table 3.2: Experimental data involving a solid phase for the CH_4-CO_2 binary mixture.

Author	Kind of data	N	Molar fraction x_{CO_2} liquid phase y_{CO_2} vapor phase	Temperature (K)	Pressure (MPa)
Donnelly and Katz (1954)	SLE	4	0.205-0.865	194-214	4.29-4.59
	SLVE	21	-	194-215	0.78-4.86
Sterner (1961)	SLVE	9	x_{CO_2} 0.019-0.052	166-200	1.95-4.97
Davis et al. (1962)	SLVE	42	x_{CO_2} 0.0016-0.205	97-212	0.03-4.87
Kurata and Im (1971)	SLVE	10	x_{CO_2} 0.006-0.175 y_{CO_2} 0.02-0.74	165-210	1.90-4.85
Brewer and Kurata (1958)	SLE	8	0.18-1	190-215	-
Boyle (1987)	SLE	5	0.00027-0.00148	111-128	-
Cheung and Zander (1968)	SLE	9	0.0003-0.126	111-195	-
Streich (1970)	SLE	12	0.00031-1	110-218	-
Preston et al. (1971)	SLE	2	0.0007-0.0023	126-137	-
Voss (1975)	SLE	22	0.0002-0.128	112-193	-
Shen et al. (2012)	SLE	9	0.000213-0.02896	112-170	0.09-2.31
Gao et al. (2012)	SLE	9	0.000172-0.02896	113-170	-
Pikaar (1959)	SVE	103	0.000265-0.59	133-210	0.16-4.83
	SLE	21	0.01-0.2	143-204	0.75-5.20
Agrawal and Laverman (1974)	SVE	41	0.0012-0.11067	137-198	0.17-2.78
Le and Trebble (2007)	SVE	55	0.01-0.0293	168-187	0.96-3.00
Zhang et al. (2011)	SVE	17	0.108-0.54	196-210	0.29-4.45
Xiong et al. (2015)	SVE	64	0.001-0.34	153-193	0.2-3.00

About SLE data pressure

From the bibliographic research on experimental data on phase equilibrium involving the solid phase, it is possible to conclude that SLE pressure data are rarely reported. This is because for SLE influence of pressure is often considered negligible. At this purpose Donnelly and Katz (1954) reported that SLE lines have been drawn starting from the triple point: *"The equilibria were known to be such that the boundary was essentially a vertical line, and hence, one point in the region of the three-phase locus determines the line."* Similarly Pikaar (1959) states: *"After the triple point liquid composition has been determined [...] the solubility lines, which defined solid-liquid equilibrium, could be drawn".*

In the work of Donnelly and Katz (1954) and Shen et al. (2012) the pressure of the SLE measures is reported. In this case it is possible to observe that the pressure at which data are measured is very close to calculated SLVE pressure and they fit the p-T curve of three phase locus . Data by Shen et al. (2012) and Gao et al. (2012) are obtained using the same experimental apparatus consisting in a static analytic method, with a very similar procedure: both of them state that the equilibrium cell is filled of liquid for 2/3 or 80% only. SLVE data

reporting temperature and liquid phase composition (but not pressure) are considered as SLE data, as observed by Hlavinka et al. (2006).

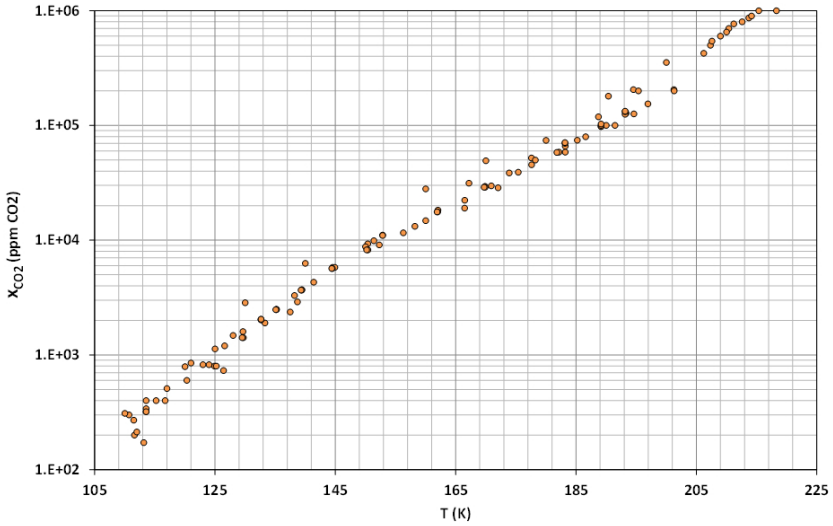

Figure 3.5: SLE data for the CH_4-CO_2 system in the xT diagram: (•) experimental values (see tab. 3.2)

3.4 The N_2-CO_2 system

For the binary system of nitrogen and carbon dioxide a large number of VLE data is available (tab. 3.3), all of them are at temperature greater than the CO_2 triple point. Two series of SLVE data are available, at temperature close to the CO_2 triple point. No SLVE data are available at temperature closer to the N_2 triple point. It is possible to classify the system as Type-III, according to the classification of Van Konynenburg and Scott (1980) and type F according to the classification proposed by Luks (1986) and Yamamoto et al. (1989) including the solid phase. The system presents in fact a branch of the vapor-liquid critical locus starting from the CO_2 critical point joining in an Upper Critical End Point (UCEP) the higher temperature branch of the solid-liquid-vapor locus starting from the CO_2 triple point (fig. 3.6). Solubility data are available from 67 to 115 K, being the nitrogen critical point of 126.2 K (see fig. 3.7).

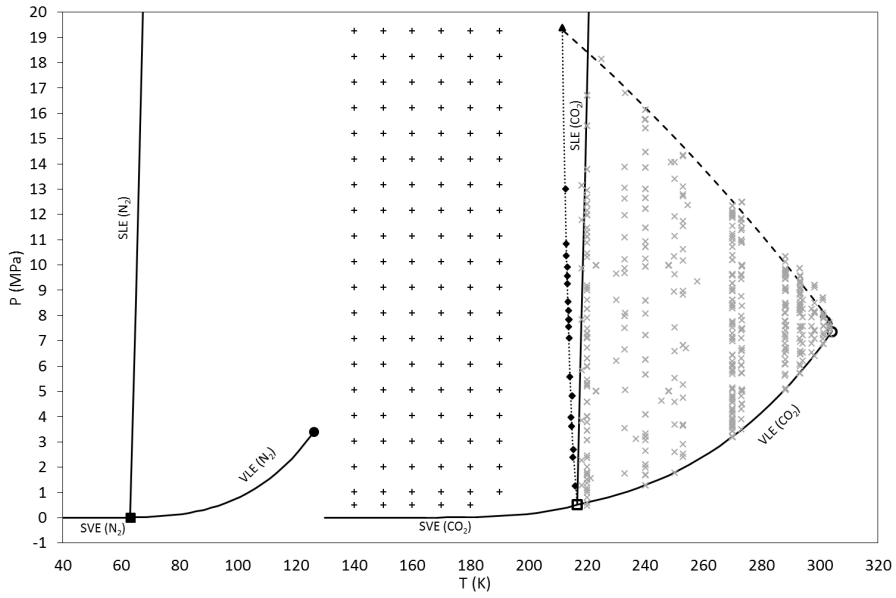

Figure 3.6: Pressure-temperature equilibrium behavior for the N_2-CO_2 system and available data for the binary N_2-CO_2 system: (■) N_2 triple point; (•) N_2 critical point; (□) CO_2 triple point; (∘) CO_2 critical point; (▲) upper critical end point (UCEP); (×) VLE data; (⧫) three-phase locus data; (+) SVE data; (-) pure compound phase equilibria.

Table 3.3: Experimental VLE data for the N_2-CO_2 mixture. N is the number of experimental points

Authors	Kind of data	N	Vapor composition (mol/mol) CO_2	Liquid composition (mol/mol) CO_2	Temperature (K)	Pressure (MPa)
Krichevskii et al. (1962)	VLE	27	0.79 - 1	0.81 - 1	288 - 301	5.1 - 10.3
Zenner and Dana (1963)	VLE	31	0.15 - 0.80	0.70 - 0.99	218 - 273	1.3 - 13.9
Arai et al. (1971)	VLE	43		0.43 - 1	253 - 288	2.4 - 14.4
Somait and Kidnay (1978)	VLE	40	0.58 - 1	0.65 - 1	270- 288	3.2 - 12.3
Al-Sahhaf et al. (1983)	VLE	58	0.17 - 1	0.52 - 1	220 - 240	0.6 - 16.7
Shi et al. (1984)	VLE	14	0.80 - 0.94	0.80 - 0.94	288	5.6 - 9.9
Yorizane et al. (1985)	VLE	34	0.79 - 0.98	0.60 - 0.94	273 - 298	4.5 - 11.4
Fall and Luks (1986)	VLE	17	0.86 - 0.98		294 - 301	6.2 - 8.6
Brown et al. (1989a)	VLE	17	0.38 - 1	0.70 - 1	250 - 270	1.8 - 14.1
Brown et al. (1989b)	VLE	68	0.17 - 1	0.81 - 1	220 - 270	0.5 - 13.0
Xu et al. (1992a)	VLE	20	0.80 - 1	0.85 - 1	288 - 293	5.1 - 9.7
Bian et al. (1993)	VLE	12	0.96 - 1	0.97 - 1	301 - 303	6.9 - 8.0
Yucelen and Kidnay (1999)	VLE	24	0.30 - 1	0.75 - 1	240 - 270	1.3 - 13.0

Table 3.4: Experimental data involving a solid phase for the N_2-CO_2 mixture.

Author	Kind of data	N	Molar fraction (ppm) CO_2	Temperature (K)	Pressure (MPa)
Fandino et al. (2015)	SLVE	4		213 - 215	4.8 - 13.0
Schweitzer (1962)	SLVE	16		213 - 216	1.2 - 10.8
Fedorova (1940)	SLE	4	2.2 - 7.3	67 - 98	-
Yakimenko et al. (1975)	SLE	9	1.6 - 166	75-115	-
Rest et al. (1990)	SLE	5	0.7 - 98	91 - 115	-
Sonntag and Van Wilen (1961)	SVE	64	190-78 800	140-190	0.5-10.1
Smith et al. (1964)	SVE	72	1300-54 800	140-190	5.1-20.3

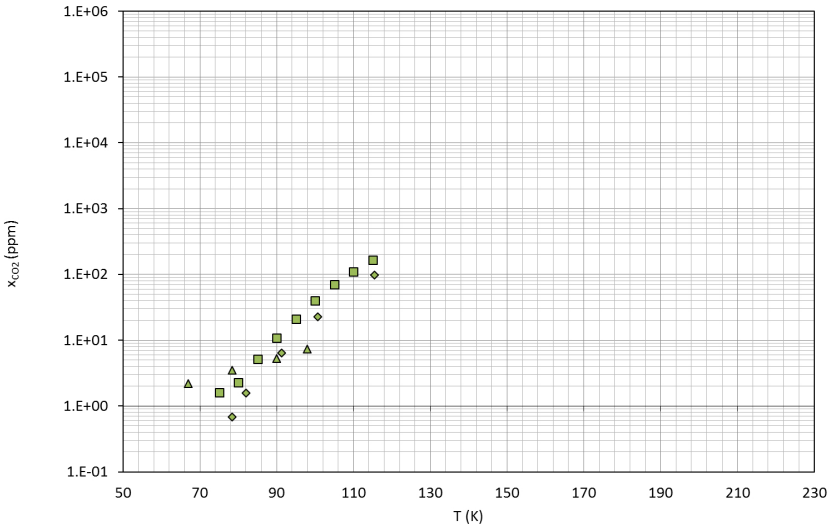

Figure 3.7: SLE data for the N_2-CO_2 system in the xT diagram: (▲)data from Fedorova (1940), (♦) data from Rest et al. (1990), (■) data from Yakimenko et al. (1975)

3.5 The O_2-CO_2 system

Similarly to the system N_2-CO_2, the O_2-CO_2 system presents a vapor-liquid critical locus starting from the CO_2 critical point joining the higher temperature branch of the SLVE locus starting from the CO_2 triple point in an Upper Critical End Point (UCEP) (fig. 3.8). Similarly to the other system including CO_2, immiscibility of solid phases can be assumed.

VLE data are available for this system covering the range from the CO_2 critical temperature to the CO_2 triple point temperature, see tab. 3.5. Concerning Solid-Fluid Equilibrium data, the solubility of CO_2 in oxygen has been studied by De Stefani et al. (2002) and De Stefani et al. (2004), proposing original measurements and reporting some data from literature. A partial list of SLE data sources is proposed in tab. 3.6. To the authors knowledge, no SVE and SLVE data are available for this system. The solubility of carbon dioxide in liquid oxygen is similar to the solubility of carbon dioxide in liquid nitrogen and lower than in liquid methane. SLE data are represented in a xT diagram in fig. 3.9. SLE available data are in the range of temperature of 67 - 110 K, considering that the O_2 critical point is 154.6 K.

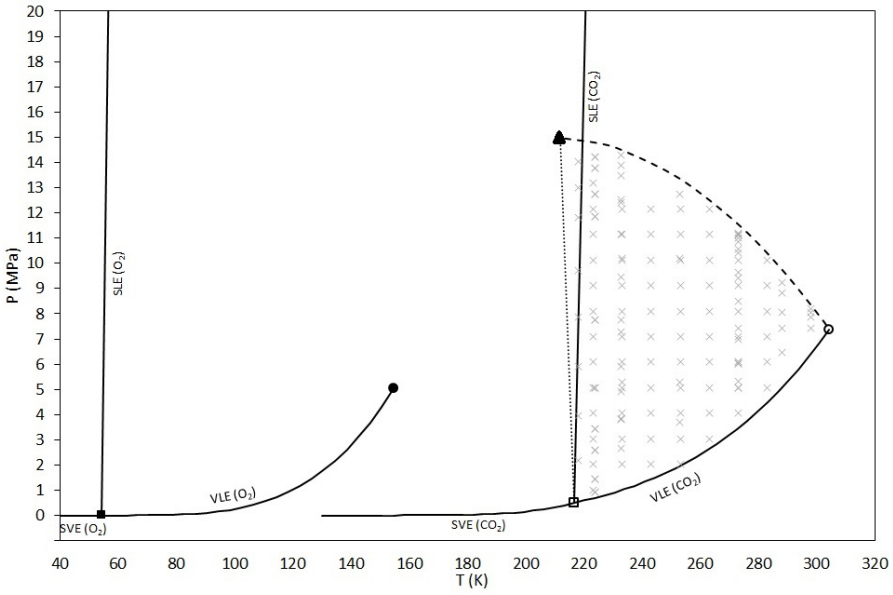

Figure 3.8: Pressure-temperature equilibrium behavior for the O_2-CO_2 system and available data for the binary O_2-CO_2 system: (■) O_2 triple point; (•) O_2 critical point; (□) CO_2 triple point; (○) CO_2 critical point; (▲) upper critical end point (UCEP); (×) VLE data; (-) pure compound phase equilibria.

Table 3.5: Experimental VLE data for the O_2-CO_2 mixture.

Authors	Kind of data	N	Vapor composition (mol/mol) CO_2	Liquid composition (mol/mol) CO_2	Temperature (K)	Pressure (MPa)
Zenner and Dana (1963)	VLE	33	0.147 - 0.746	0.469 - 0.967	218 - 273	2.2 - 14.3
Kaminishi and Toriumi (1966)	VLE	22	0.243 - 0.919	0.629 - 0.97	233 - 298	3.7 - 12.7
Fredenslund and Sather (1970)	VLE	91	0.18 - 0.939	0.554 - 0.996	223 - 283	0.9 - 14.2

Table 3.6: Experimental data involving a solid phase for the O_2-CO_2 mixture.

Author	Kind of data	N	Molar fraction (ppm) CO_2	Temperature (K)	Pressure (MPa)
Fedorova (1940)	SLE	5	1.8 - 5.6	67 - 98	-
Amamchyan et al. (1973)	SLE	7	0.2 - 12.6	76 -96	-
Rest et al. (1990)	SLE	3	4-36	91 - 107	-
De Stefani et al. (2002)	SLE	13	4-100	89 - 110	-

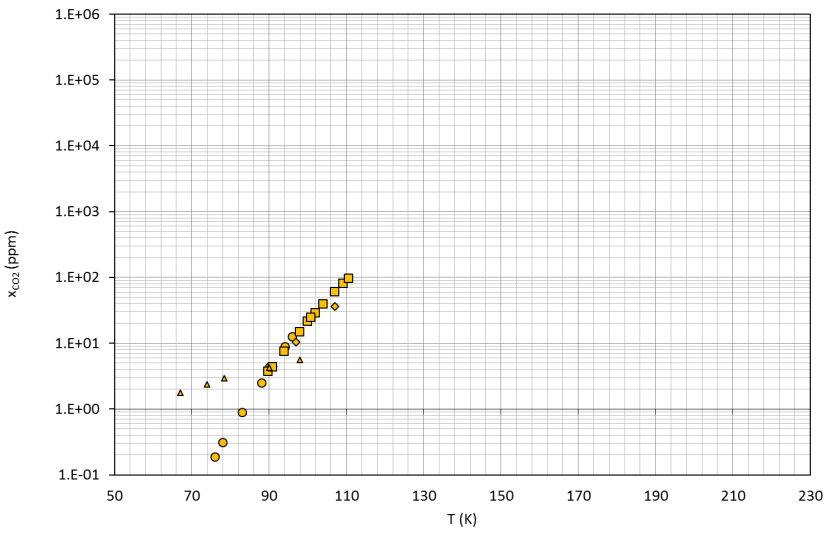

Figure 3.9: SLE data for the O_2-CO_2 system in the xT diagram: (▲) data from Fedorova (1940), (♦) data from Rest et al. (1990), (■) data from De Stefani et al. (2002), (●) data from Amamchyan et al. (1973)

3.6 The N_2-CH_4 system

The N_2-CH_4 system presents a phase diagram of Type-I, according to the classification of Van Konynenburg and Scott (1980) as it is possible to see in fig. 3.10. A large number of VLE data is available in literature, covering the whole VLE domain of the mixture down to 100 K, as reported in tab. 3.7. Both components have triple point at temperature significantly lower than the range of interest of this work ($T_{t,N_2} = 63.1K$, $T_{t,CH_4} = 90.7K$). Solid-Fluid Equilibrium (SFE) data are thus not studied for this system.

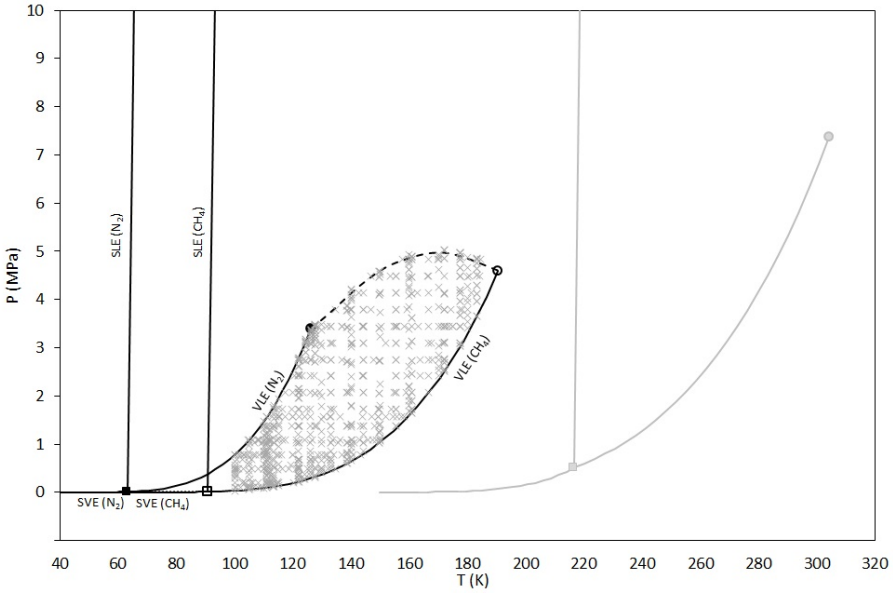

Figure 3.10: Pressure-temperature equilibrium behavior for the N_2-CH_4 system and available data for the binary N_2-CH_4 system: (■) N_2 triple point; (•) N_2 critical point; (□) CH_4 triple point; (○) CH_4 critical point; (×) VLE data; (-) pure compound phase equilibria; (-) CO_2 pure compound phase equilibria.

Table 3.7: Experimental VLE data for the N_2-CH_4 mixture.

Authors	Kind of data	N	Vapor composition (mol/mol) CH_4	Liquid composition (mol/mol) CH_4	Temperature (K)	Pressure (MPa)
Bloomer and Parent (1953)	VLE	141	0 - 1	0 - 1	101 - 184	0.10 - 4.80
Cines et al. (1953)	VLE	85	0 - 0.96	0.01 - 0.99	111 - 172	0.17 - 4.50
Fastovskii and Petrovskii (1957)	VLE	99	0 - 1	0 - 1	100 - 158	0.20 - 1.60
Brandt and Stroud (1958)	VLE	9	0.16 - 0.87	0.29 - 0.95	137 - 175	3.50
Skripka et al. (1970)	VLE	14	0 - 1	0 - 1	113	0.11 - 1.77
Stryjek et al. (1972)	VLE	123	0 - 1	0 - 1	114 - 183	0.12 - 5.00
Miller et al. (1973)	VLE	11	0 - 0	0.22 - 0.97	112	0.18 - 1.30
Parrish and Hiza (1995)	VLE	41	0 - 1	0 - 1	100 - 115	0.03 - 1.90
Stryjek et al. (1974)	VLE	109	0 - 1	0 - 1	122 - 183	0.22 - 5.00
Kidnay et al. (1975)	VLE	81	0.06 - 0.98	0.1 - 1	112 - 180	0.19 - 4.94
Wilson (1975)	VLE	16	0 - 1	0 - 1	111	0.09 - 1.57
Kremer (1982)	VLE	32	0.18 - 0.98	0.2 - 1	140 - 160	0.65 - 4.93
Liu et al. (1988)	VLE	10	0 - 0.57	0-0.95	123	0.42 - 2.58
Fontaine (1989)	VLE	171	0-1	0-1	114 - 183	0.28 - 4.89
Janisch et al. (2007)	VLE	35	0.30 - 0.91	0.41 - 0.99	130 - 180	0.58 - 5.10
Han et al. (2012)	VLE	84	0 - 1	0 - 1	100 - 123	0.04 - 2.91
Torocheshnikov and Levius (1941)	VLE	35	0 - 1	0 - 1	100 - 132	0.03 - 2.32

3.7 The N_2-O_2 system

The N_2-O_2 system presents a phase diagram of Type-I, according to the classification of Van Konynenburg and Scott (1980), as it is possible to see in fig. 3.11. Since the critical point of the heavier component, oxygen, is 154.6 K, measuring the vapor-liquid equilibrium for this system means performing measurements at cryogenic temperature: VLE data are available in literature for temperature from 100 to 136 K (see tab. 3.8)Both components have triple point at temperature significantly lower than the range of interest of this work ($T_{t,N_2} = 63.1K$, $T_{t,O_2} = 54.4K$). SFE data are thus not studied for this system.

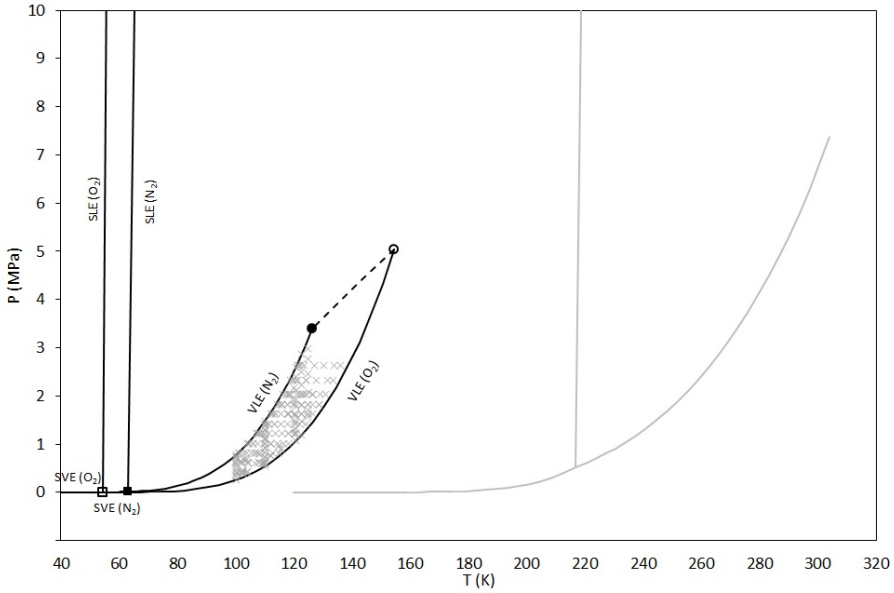

Figure 3.11: Pressure-temperature equilibrium behavior for the N_2-O_2 system and available data for the binary N_2-O_2 system: (■) N_2 triple point; (•) N_2 critical point; (□) O_2 triple point; (○) O critical point;(×) VLE data; (-) pure compound phase equilibria; (-) CO_2 pure compound phase equilibria.

Table 3.8: Experimental VLE data for the N_2-O_2 mixture.

Authors	Kind of data	N	Vapor composition (mol/mol) N_2	Liquid composition (mol/mol) N_2	Temperature (K)	Pressure (MPa)
Dodge and Dunbar (1927)	VLE	23	0.15 - 0.95	0.06 - 0.90	100 - 125	0.35 - 2.97
Din (1960)	VLE	35	0.19 - 0.84	0.10 - 0.69	100 - 116	0.39 - 1.02
Wilson et al. (1964)	VLE	113	0.11 - 0.99	0.05 - 0.99	101 - 136	0.40 - 2.63
Baba-Ahmed et al. (1999)	VLE	45	0 - 1	0 - 1	100 - 122	0.26 - 2.87

3.8 The O_2-CH_4 system

The O_2-CH_4 system is a mixture of an oxydant and a fuel. Operating with this binary mixture requires thus special devices made for working in explosive atmosphere. Experimental data are available in literature are few (a partial list of sources is presented in tab. 3.9). The pT diagram of this system should be similar to the N_2-CH_4 pT diagram beacause of the similar triple point and critical point temperatures and pressures of the pure components. The phase diagram is thus of Type-I, according to the classification of Van Konynenburg and Scott (1980) as shown in fig. 3.12. Both components have triple point at temperature significantly lower than the range of interest of this work. SFE data are thus not studied for this system.

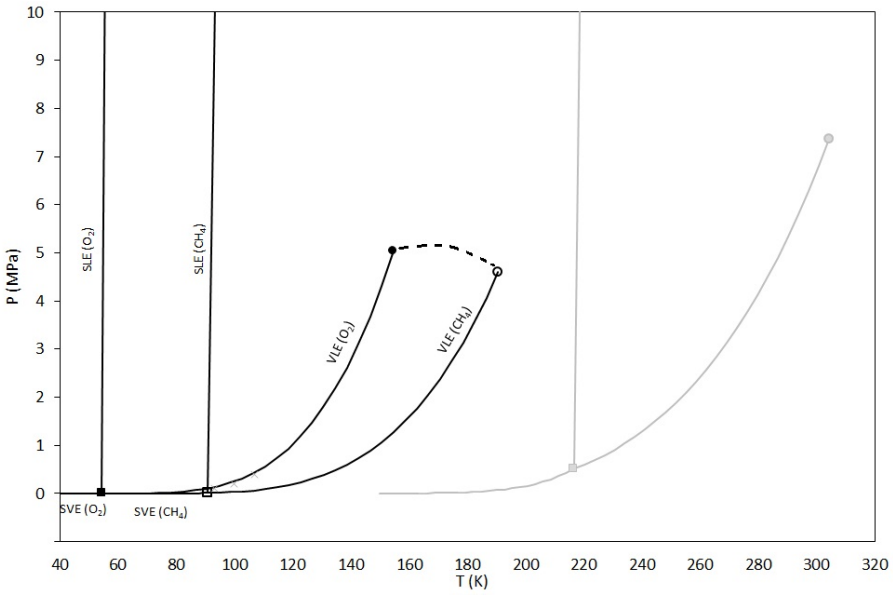

Figure 3.12: Pressure-temperature equilibrium behavior for the O_2-CH_4 system : (■) O_2 triple point; (●) O_2 critical point; (□) CH_4 triple point; (○) CH_4 critical point; (×) VLE data; (-) pure compound phase equilibria; (-) CO_2 pure compound phase equilibria.

Table 3.9: Experimental VLE data for the O_2-CH_4 mixture.

Authors	Kind of data	N	Vapor composition (mol/mol) O_2	Liquid composition (mol/mol) O_2	Temperature (K)	Pressure (MPa)
Hodges and Burch (1967)	VLE	3	-	0.99	93 - 107	0.10 - 0.40

3.9 The N_2-CH_4-CO_2 system

The N_2-CH_4-CO_2 system has been studied and some measurements are available in literature. VLE data for the ternary system have been produced for temperature higher than the triple point of the CO_2 (see tab. 3.10). Phase equilibrium data involving a solid phase are also available in literature and reported in table 3.11: the SVE and freezing point (solid formation from the vapor phase) for mixtures of nitrogen-methane-carbon dioxide has been measured in the 70' by Agrawal and Laverman (1974) and Haufe et al. (1972), and more recently by Le and Trebble (2007) and Xiong et al. (2015). Data obtained by Haufe et al. (1972) are for nitrogen-rich mixtures, while other data are useful for natural gas/biogas applications (see tab. 3.11). Shen et al. (2012) and Gao et al. (2012), reporting the CO_2 concentration in liquid phase in the ternary mixture at SLVE conditions. All the available data are reported in the pT diagram in figure 3.13.

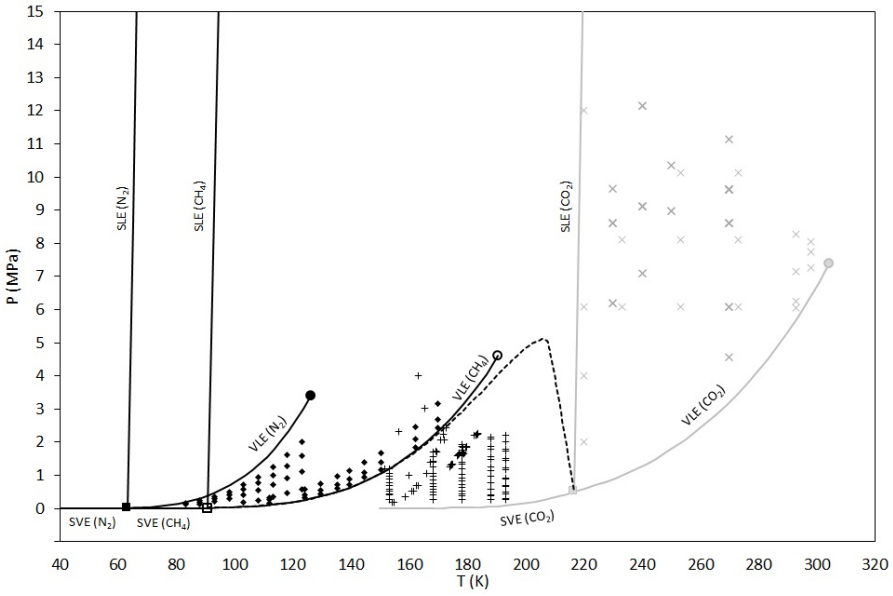

Figure 3.13: Pressure-temperature equilibrium behavior for the N_2-CH_4-CO_2 system : (■) N_2 triple point; (●) N_2 critical point; (□) CH_4 triple point; (○) CH_4 critical point;(×) VLE data; (⧫) SLVE data; (+) SVE data; (-) pure compound phase equilibria; (-) CO_2 pure compound phase equilibria.

Table 3.10: Experimental VLE data for the N_2-CH_4-CO_2 ternary system. N is the number of experimental points

Authors	Kind of data	N	Temperature (K)	Pressure (MPa)
Sarashina et al. (1971)	VLE	48	233-273	6.1 - 10.1
Somait and Kidnay (1978)	VLE	56	270	4.6 - 9.6
Al-Sahhaf et al. (1983)	VLE	37	220-240	6.0 - 12.2
Trappehl and Knapp (1989)	VLE	56	220	2.0-12.0
Al-Sahhaf (1990)	VLE	26	230 - 250	6.2-10.3
Xu et al. (1992a)	VLE	55	293	6.0-8.3
Xu et al. (1992b)	VLE	30	298	7.2-8.0

Table 3.11: Experimental data involving a solid phase for the N_2-CH_4-CO_2 system.

Author	Kind of data	N	Molar composition x liquid phase y vapor phase	Temperature $[K]$	Pressure $[MPa]$
Agrawal and Laverman (1974)	SVE	19	y_{CO_2}=0.02 y_{N_2}=0.01-0.03	154-173	0.17-2.44
Haufe et al. (1972)	SVE	5	y_{CO_2}=0.002-0.004 y_{N_2}=0.63	151-165	1.00-3.99
Le and Trebble (2007)	SVE	24	y_{CO_2}=0.02 y_{N_2}=0.01-0.02	174-183	1.24-2.26
Xiong et al. (2015)	SVE	77	y_{CO_2}=0.001-0.32 y_{N_2}=0.03-0.05	153-193	0.20-2.00
Shen et al. (2012)	SLVE	27	x_{CO_2}=0.0002-0.027	112-170	0.15-3.15
Gao et al. (2012)	SLVE	31	x_{CO_2}=3-300 ppm	83-123	0.12-2.02

3.10 Conclusion and discussion

Phase equilibrium data for the binary systems of the components of interest for the study have been collected. This allows the comparison and validation of the results of a thermodynamic model on the data of interest.

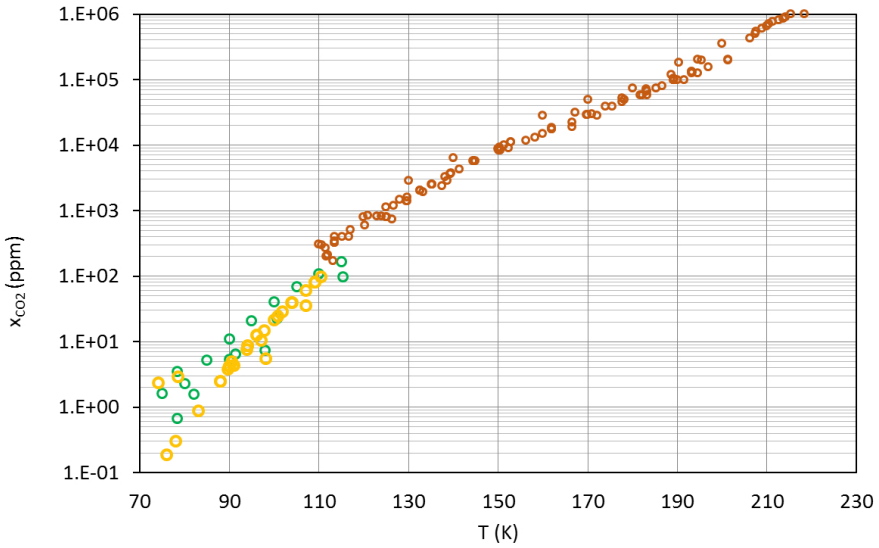

Figure 3.14: Comparison between the CO_2 solubility in liquid methane (○), nitrogen (○) and oxygen (○) according to SLE data available in literature (see tab. 3.2,3.4, 3.6)

Focusing on systems containing CO_2, the CH_4-CO_2 mixture has been largely studied, and a large number of data are available. All types of equilibria for temperature greater than the triple point of methane have been studied, and a wide range of temperature is covered. Some data involving a solid phase for the N_2-CO_2 and O_2-CO_2 systems are available. In particular, CO_2 solubility in liquid phase (SLE) can be compared among the three mixtures: according to data available in literature, CO_2 solubility in liquid methane is much larger than in liquid nitrogen and oxygen (fig. 3.14). In case of landfill gas upgrading and liquefaction, it is important to understand the influence of nitrogen and oxygen on the solubility of the carbon dioxide in liquid methane. From existing data, the effect of the nitrogen and oxygen addition to a CH_4-CO_2

mixture is difficult to be estimated. Phase equilibrium measurements involving a solid phase for multicomponent mixture of CH_4-CO_2 with N_2 and O_2 are, in fact, missing or incomplete. Shen et al. (2012) and Gao et al. (2012) propose solubility data in the low temperature range, providing only the CO_2 composition in the liquid phase for the ternary N_2-CH_4-CO_2. Furthermore, to the author's knowledge, no data for the quaternary mixture of N_2-O_2-CH_4-CO_2 are available. For improving the comprehension of complex multicomponent systems at conditions where a solid phase can appear, a thermodynamic model should be supported by experimental values. Original measurements in the low temperature region for ternary and quaternary mixture of methane, carbon dioxide, nitrogen and oxygen are thus produced in this work.

Chapter 4

Modeling thermodynamic properties and phase equilibrium

In this chapter thermodynamic models available in literature for computing phase equilibria are reviewed, then the author presents the approach chosen in this work.

Résumé

On rappelle dans ce chapitre le formalisme couramment utilisé en thermodynamique pour l'équilibre entre phases et examine les approches existantes pour la modélisation des phases fluide et solide. Affirmer qu'un système est en équilibre thermodynamique signifie qu'il n'y a pas de transfert net de matière ou d'énergie. Dans un processus de séparation, la force motrice du transfert de chaleur et de matière est donnée par l'écart à l'équilibre thermodynamique. L'étude de l'équilibre entre une phase solide et une phase fluide est donc une étape fondamentale dans la compréhension et la modélisation du processus de séparation d'intérêt.

Un système hétérogène est en équilibre thermodynamique lorsque toutes les phases ont la même température (équilibre thermique), pression (équilibre mécanique) et tous les composants de chaque phase ont le même potentifel chimique (équilibre chimique). L'équilibre chimique peut être exprimé grâce à l'isofugacité de tous les composants de chaque phase. Dans le cas d'équilibre entre une (ou plusieurs) phase fluide et une phase solide, on a besoin d'un modèle pour calculer la fugacité des phases fluides et d'un modèle pour calculer la fugacité de la phase solide. Parmi les modèles thermodynamiques pour les phases fluides et solides, dans ce travail on choisit deux approches:
1) une équation d'état cubique (Peng Robinson EoS) couplée avec un approche classique pour la phase solide (équation de Zabaloy) ;
2) une équation d'état multiparamétrique (Gerg 2008 EoS) couplée avec une équation d'état pour le CO_2 solide (Jager and Span EoS)

Les données présentées au chapitre 3 sont comparées aux résultats obtenus avec les modèles choisis et implémentés. La comparaison est faite sur la composition molaire de la phase vapeur et liquide à température et pression expérimentales. Pour les données d'équilibre solide-liquide (SLE), lorsque la pression expérimentale n'est pas fournie, on utilise la pression d'équilibre solide-liquide-vapeur (SLVE).

La régression des paramètres d'interaction binaire de l'équation d'état Peng Robinson sur les données SLVE ou SLE augmente sensiblement la précision de la prédiction de la solubilité du CO_2 en phase liquide et en phase vapeur. L'amélioration est particulier évidente pour la solubilité du CO_2 dans la phase liquide. Le premier model implémenté (PR EoS +équation de Zabaloy) a des résultats légèrement meilleurs que le model GERG + Jager and Span EoS pour prédire la solubilité du CO_2 dans le méthane liquide. Néanmoins, les résultats obtenus avec le

deuxième modèle reste satisfaisants et la solubilité du CO_2 dans le méthane en phase vapeur (SVE) est encore mieux prédite par le modèle GERG + Jager and Span Eos que par le modèle PR EoS + Zabaloy.

4.1 Introduction

In order to simulate the fluid behavior during the biogas treatments, thermodynamic properties of the biogas and solid phase formation conditions have to be known. A thermodynamic model able to simulate the vapor, liquid and solid phase of the biogas mixture is developed to compute needed properties.

In this chapter the theoretical basis undergoing the problem of multiphase equilibrium are recalled, with particular attention to the phase equilibrium involving solid and fluid phases. Models and approaches used by different authors in literature are reviewed, then the author presents the models and approaches chosen in this work: a Peng-Robinson cubic Equation of State coupled with a Classical Approach for the solid phase and a multiparametric Equation of State (GERG-2008) coupled with a fundamental Equation of State for the solid CO_2 (Jager and Span, 2012).

4.2 Thermodynamic framework

The aim of this section is to recall the formalism commonly used in thermodynamics for the phase equilibrium and review existing models and approaches for modeling fluid and solid phases. Far from providing an exhaustive description of the theory undergoing the physics of the separation processes, some words worth to be spent for arguing the reasons for studying the thermodynamic equilibrium of the system and for introducing the theory of the phase equilibrium problem involving a solid phase.

Stating that a system is in thermodynamic equilibrium means that no net material or energy transfer occurs. Thermodynamic equilibrium thus represents the asymptotic behavior with respect to the time of the studied system if stable conditions are maintained. In a separation process, the driving force of the mass and heat transfer is given by the departure from the thermodynamic equilibrium, which represent the limits that can be reached. Studying the phase equilibrium between a solid and a fluid phase is thus a fundamental step in the comprehension and modeling of the separation process of interest.

4.2.1 Equilibrium conditions

A system in which two or more phases coexists is called heterogeneous. A phase is a portion of the system that is separated from other phases by interfaces and is homogeneous in physical and chemical properties (or change continuously from one point to another). A heterogeneous system is in thermodynamic equilibrium when all phases have the same temperature T (thermal equilibrium, eq. (4.1)), pressure p (mechanical equilibrium, eq. (4.2)) and all components in each phase have the same chemical potential μ (chemical equilibrium, eq. (4.3)). This can be summarized by the following set of equations for every α or β phase, and i component:

$$T^\alpha = T^\beta \tag{4.1}$$

$$p^\alpha = p^\beta \tag{4.2}$$

$$\mu_i^\alpha = \mu_i^\beta \ ; \ i = 1, ..., nc \tag{4.3}$$

Fugacity f for the component i in the phase α is defined as follows

$$f_i^\alpha(T, p, \mathbf{x}) = f^0(T, p^0) \exp\left(\frac{\mu_i^\alpha(T, p, \mathbf{x}) - \mu_i^0(T, p^0)}{RT}\right) \tag{4.4}$$

where $\mathbf{x}$ is the molar composition of the phase and the superscript 0 refers to a reference state, or standard state of the phase. Setting the same reference state for all phases, for example

ideal gas at T^0 and p^0, one can combine equations (4.3) and (4.4) resulting into the equality of fugacity

$$f_i^{\alpha}(T, p, \mathbf{x}^{\alpha}) = f_i^{\beta}(T, p, \mathbf{x}^{\beta}) \tag{4.5}$$

It can be demonstrate that equation (4.3) is a consequence of the principle stating that at specified T and p, the total Gibbs free energy G of the system is a minimum at the equilibrium.

$$dG = 0 \tag{4.6}$$

4.2.2 Phase equilibrium calculation

Phase equilibrium calculation refers to the solutions of equations governing the equilibrium in order to obtain conditions (temperature T, pressure p, molar volume v, molar fractions x_i...) at which two or more phases coexist. With reference to equations (4.5) and (4.6), methods for determining phase equilibrium can be divided into:

- Isofugacity approach.
- Gibbs free-energy minimization techniques

In particular for the equilibrium between a solid phase (superscript S) and a fluid phase (superscript F), Gibbs free energy to be minimized can be calculated from

$$g(T, p, \mathbf{z}) = Sg^S(T, p, \mathbf{w}) + Fg^F(T, p, \mathbf{x}) \tag{4.7}$$

where g is the molar Gibbs free energy, $\mathbf{z}$ is the global molar composition of the mixture, $\mathbf{w}$ and $\mathbf{x}$ are the composition of the solid and fluid phase respectively. S and F are the molar fraction of solid and fluid phase, defined as the ratio between the mole of solid and liquid phase, n^S and n^F respectively, and the total number of moles:

$$S = \frac{x^S}{x^S + x^F} \tag{4.8}$$

$$F = \frac{x^F}{x^S + x^F} \tag{4.9}$$

Equality of fugacity (eq. (4.5)) applied for solving a SFE has to be respected for each component i present in the solid phase :

$$f_i^S(T, p, \mathbf{w}) = f_i^F(T, p, \mathbf{x}) \tag{4.10}$$

In both cases, for calculating solid-fluid phase equilibrium one needs to compute the fugacity or Gibbs free energy of solid and fluid phase. Fugacity f and Gibbs free energy g are thermodynamic properties and have to be obtained from a thermodynamic model.

Historically, thermodynamics models have been developed at the beginning for the vapor (gas) phase, then for vapor and liquid. Solid phase is usually treated apart from fluid phase, and only few thermodynamic models are able to compute properties for vapor, liquid and solid. In section 4.3 a non-exhaustive bibliography on solid phase models is presented, after which a brief selection of fluid models is proposed, in section 4.4. After that, the models used in this work are presented more extensively in section 4.5.

4.3 Solid phase models

The issue of phase equilibrium involving one or more solid phases is of interest for many industrial application (metallurgy, fractional crystallization, Liquified Natural Gas industry...). Thus, several researches have been carried out producing different models for the solid phase. In this work the focus is kept on molecular solid formed from carbon dioxide at low temperature, from a mixture including methane, nitrogen and oxygen.

For modeling the fugacity of the solid phase, different approaches are possible and can be summarized in:

- the solid phase fugacity is obtained from the subcooled fluid phase fugacity, using a classical *Fluid EoS* and a correction for considering the transition from the fluid and the solid phase;
- the solid phase fugacity is obtained from a *Solid phase EoS*, which can be an Equation of State developed to describe both solid and fluid or the solid phase only.

4.3.1 Fugacity of the solid phase obtained from the subcooled fluid

The Classical Approach (CA) is a typical application of the solid fugacity obtained from the fugacity of the subcooled fluid phase.

Classical Approach Equation

CA relates solid and liquid fugacity of a pure compound through the thermodynamic relation:

$$f^S_{pure,i}(T,p) = f^L_{pure,i}(T,p)\exp\left[\frac{\Delta h^{SL}(T_T,p_T)}{RT_T}\left(1-\frac{T_T}{T}\right)\right.$$
$$\left.+\frac{\Delta c_P^{SL}(T_T,p_T)}{R}\left(\frac{T_T}{T}-1-\ln\left(\frac{T_T}{T}\right)\right)-\frac{\Delta v^{SL}(T_T,p_T)(P-P_T)}{RT}\right] \tag{4.11}$$

Equation (4.11) linking solid to liquid fugacity of a pure component is a rigorous thermodynamic relation except for two assumption:

- the difference between the c_P of the solid and liquid phase at melting conditions is constant and equal to the same difference at triple point conditions $\Delta c_P^{SL}(T,p) = \Delta c_P^{SL}(T_T,p_T)$
- the difference between the molar volume v of the solid and liquid phase at melting conditions is constant and equal to the same difference at triple point conditions $\Delta v^{SL}(T,p) = \Delta v^{SL}(T_T,p_T)$.

Starting from equation (4.11) some assumption can be done for simplifying the expression of solid fugacity.

Classical Approach: first approximation

The first one is to neglect the effect of pressure on the ratio between solid and liquid fugacities, thus eq. (4.11) becomes

$$f^S_{pure,i}(T,p) = f^L_{pure,i}(T,p)\exp\left[\frac{\Delta h^{SL}(T_T,p_T)}{RT_T}\left(1-\frac{T_T}{T}\right)\right.$$
$$\left.+\frac{\Delta c_P^{SL}(T_T,p_T)}{R}\left(\frac{T_T}{T}-1-\ln\left(\frac{T_T}{T}\right)\right)\right] \tag{4.12}$$

Classical Approach: second approximation

The second often used assumption is to approximate $ln\left(\frac{T_T}{T}\right)$ to $\left(\frac{T_T}{T}-1\right)$ by expanding in series. In this way the Δc_p therm in eq. (4.11) is nil and the equation becomes

$$f^S_{pure,i}(T,p) = f^L_{pure,i}(T,p)\exp\left[\frac{\Delta h^{SL}(T_T,p_T)}{RT_T}\left(1-\frac{T_T}{T}\right)\right] \tag{4.13}$$

Classical Approach: Zabaloy equation

Rodriguez-Reartes et al. (2011) propose an expression of the solid fugacity obtained from eq. (4.11). In this work we refers to this approach as the *Zabaloy equation*.

$$f^S_{pure,i}(T,p) = f^L_{pure,i}(T,p)\exp\left(U\right) \tag{4.14}$$

with

$$\begin{aligned} U = \frac{\Delta v^{SL}(T_T,p_T)}{RT_T}\Bigg[&C1\left(1-\frac{T_T}{T}\right)+C2\left(\frac{T_T}{T}-1+ln\left(\frac{T}{T_T}\right)\right)\\ &+C3\left(\frac{T}{2T_T}-1+\frac{T_T}{2T}\right)+\frac{T_T(P-P_T)}{T}\Bigg] \end{aligned} \tag{4.15}$$

Details on the derivation of eq. (4.15) are presented in section 4.5.1.

Poynting factor

Another approach often used for computing Vapor-Solid Equilibrium is the Poynting correction factor. Fugacity of the solid phase is calculated in this case from the fugacity of the vapor phase of the pure solid former component at sublimation pressure and temperature of the system multiplying an exponential term called Poynting correction, as expressed in the following equation:

$$f^S_{pure,i}(T,p) = f^V_{pure,i}(T,p^{SVE}_{pure,i})\exp\left(\frac{\int_{p^{SVE}_{pure,i}}^{p} v^S\ \mathrm{d}p}{RT}\right) \tag{4.16}$$

The complete CA equation (4.11), the simplified CA equations (4.13) and (4.12), Rodriguez-Reartes et al. (2011) equation (4.14) and the Poynting factor equation (4.16) are all written for a solid composed of a pure substance. Solid mixtures are thus not considered. Pure solid fugacity can be equated with the fugacity of the same component in the fluid mixture for computing solid-fluid equilibrium.

4.3.2 Fugacity of the solid phase from a *Solid phase EoS*

For calculating solid phase fugacity, classical EoS such as cubic EoS or Viriale EoS are not adequate because they can only compute thermodynamic properties for liquid and vapor phases. Different authors thus elaborated EoSs able to account for liquid, vapor and solid phase with a single equation, other authors coupled two EoSs, one for the liquid and vapor phases and one for fluid and solid phases: these approaches result in an EoS that are called *SLV EoS* in this work. On the other hand, some authors proposed specific EoS for the solid carbon dioxide based on experimental data (*Solid CO_2 EoS*) .

SLV Equations of state

A Modified cubic EoS (MCEoS) has been proposed by Wenzel and Schmidt (1980) by adding a term of order 6 to a Van der Waals type EoS in order to taking into account the solid phase transition. The equation shows at certain temperature and pressure a solid-liquid critical point, which has never been demonstrated experimentally. Furthermore, as expressed by Salim and Trebble (1994) the capability of the equation to predict solid phase thermodynamic properties had not been tested. Guevara-Rodriguez and Romero-Martinez (2013) proposed an improved MCEoS adding a term of order 10 for considering the attractive contribution of the solid phase, applied to pure compounds with small molecules, like CO_2. Salim and Trebble (1994) proposed a system of two cubic EoS, the first, called Original Eos, for representing liquid-vapor transition and the second, called Translated EoS, for representing solid-vapor transition by adopting a volume translation at the triple point for representing the solid volume . Giraldo et al. (2009) applied the system of EoSs by Salim and Trebble for representing CO_2 solidification in binary mixtures with methane and ethane. Yokozeki (2004) proposed a quartic EoS allowing to analytically compute solid, liquid and vapor roots with the same equation, by modifying the repulsive term of a cubic EoS. This equation is characterized by a discontinuity between the fluid curve and the solid branch. The solid branch is in fact limited between a solid covolume c and the liquid covolume b, assuring that no solid-liquid critical point can be found because of the discontinuity. The equation has been applied to pure compounds and mixtures. Stringari et al. (2014) and Campestrini (2014) widely tested the equation and regressed pure and binary interaction parameters for large number of compounds and mixtures.

Solid CO_2 Equations of State

Instead of using an unique equation of state for vapor, liquid and solid phases, another approach can be the use of an EoS explicitly developed for solid CO_2: some examples are provided by the equations developed by Jager and Span (2012) and Trusler (2011, 2012). These EoSs are able to compute thermodynamic properties of the solid phase of carbon dioxide as pure compound. In particular Jager and Span (2012) developed a multiparametric Eos for solid phase of CO_2, regressing the parameters on available experimental data for the solid CO_2. Solid CO_2 is characterized by a relatively high number of experimental values for many thermodynamic properties and phase equilibrium conditions. More details on this model are given in section 4.5.2.

4.4 Fluid phase models

When a general EoS capable of representing liquid, vapor and solid phase is used, one can compute properties for fluid and solid phase using the same model/equation. Otherwise, fugacity, Gibbs free energy and other properties for the fluid phase have to be derived from a fluid Equation of State (EoS). A great number of EoS has been developed and tested for liquid and vapor phase, starting from the van der Waals work (Van der Waals, 1873), who described the continuity of liquid and gaseous states and wrote the van der Waals EoS (eq. (4.17)). Based on the same approach, a family of EoSs called Cubic Eos (CEoS) had been developed improving the results of the Van der Waals Eos. All the *two parameters* cubic Eos can be written in a general form reported in eq. (4.18). Coefficient for some of the most used CEoS are listed in table 4.1.

$$P(T,v) = \frac{RT}{v-b} - \frac{a_c}{v^2} \tag{4.17}$$

$$P(T,v) = \frac{RT}{v-b} - \frac{a_c \cdot \alpha(T)}{(v-b\cdot r1)(v-b\cdot r2)} \tag{4.18}$$

Table 4.1: Cubic Eos parameter for eq. (4.18)

Equation of State	r1	r2
VdW	0	0
RK	-1	0
SRK	-1	0
PR	$-1-\sqrt{2}$	$-1+\sqrt{2}$

Cubic Eos are largely used for performing phase equilibrium calculation thanks to their simple mathematical form allowing analytic solution.

Natural Gas Equations of State

For studying biogas behavior it can be convenient to refer to EoS developed for the natural gas industry. Since '70s in fact oil and gas industry has invested research on natural gas, developing different equations best applicable to mixtures composed mainly of methane and light hydrocarbons, with carbon dioxide and nitrogen as well. An example of cubic equations developed focusing on natural gas systems was the Peng-Robinson cubic Eos (PR EoS). Peng and Robinson managed to obtain improved performances compared with other cubic EoS, especially with respect to liquid density values and in the region close to the critical point, making this equation more suited for the natural gas industry (Peng and Robinson, 1976).

In classical natural gas region, from -20 to 80 $°C$ and pressure up to 300 bar, AGA8-DC92 (Starling and Savidge, 1994) equation was developed and considered the internationally accepted standard for calculation of compression factor. This EoS is limited to the vapor phase, thus is not of interest for this work.

Benchmark Eos for natural gas mixtures has been developed by the GERG consortium resulting in the GERG-2004 (Kunz et al., 2007) and updated in the GERG-2008 (Kunz and Wagner, 2012) equations. This GERG is a multiparametric EoS, also defined as an empirical equation because it is based on correlation whose functional form is not defined *a priori* through physical explanation, but obtained by regression on a large amount of experimental data. More details on this model are given in section 4.5.2.

4.5 Approach used in this work

For the purpose of this work, the choice of the model for solid-fluid equilibrium and calculation of thermodynamic properties is based on some criteria that can be here summarized:

- the model must provide good description of the VLE, SVE, SLE and SLVE.
- solid phase in the mixture of interest (CO_2+CH_4+N_2+O_2) can be assumed as pure CO_2.
- the model should not need slow numerical solution for the SFE in order to maintain the interest of a practical application which is the simulation of the CO_2 capture during the biogas purification process.
- the possibility of calculation of solid carbon dioxide properties is desirable.

Furthermore, the range of condition of interest is :

- temperature greater than the methane triple point: $-170\ ^{\circ}C < T < 25\ ^{\circ}C$;
- pressure from atmospheric to a maximum of 100 bar: $1\ bar < p < 100\ bar$;
- complete range of molar composition of CO_2, with attention to small concentration of CO_2: $0\% < x_{CO_2} < 100\%$.

As Yokozeki (2004) underlined, a single unified EoS for solid,liquid and vapor is *philosophically more pleasing*, but treating solid with a separated equation and vapor and liquid with a well developed fluid EoS is sufficient for practical application.

Two approaches have been chosen in this work:

- firstly a Classical Approach coupling a Peng Robinson EoS beacause of the simplicity of calculations and a tested good representation of the solid-fluid equilibria. Results of the application of this model to the CH_4-CO_2 system have been published in Riva et al. (2014).
- secondly, in order to increase the accuracy in the calculation of the VLE and for enabling accurate calculation of solid phase properties, a second model is implemented, coupling the GERG-2008 equation with the Jager and Span (2012) EoS for solid CO_2.

4.5.1 PR Eos plus Zabaloy equation model

A thermodynamic model able to compute solid-vapor equilibrium (SVE), solid-liquid equilibrium (SLE), and solid-liquid-vapor equilibrium (SLVE) is presented. A cubic Equation of State (Peng Robinson) is used for modeling the fluid phase coupled with an expression for calculating solid phase fugacity starting from the liquid fugacity of the pure subcooled liquid.

Zabaloy equation for the solid phase

The expression chosen for the solid fugacity is the one proposed by Rodriguez-Reartes et al. (2011). It is obtained as eq. (4.11) but assuming Δc_P^{SL} as a linear function of the temperature instead of constant. The solid fugacity can thus be calculated with eq. (4.14) and eq. (4.15).

For deriving these equations (or similarly eq. (4.11)) one can compare eq. (4.4) applied for the pure component in liquid and solid phase, resulting in eq. (4.19)

$$\frac{f^S_{pure,i}(T,p)}{f^L_{pure,i}(T,p)} = \exp\left(\frac{\mu^S_{pure,i}(T,p) - \mu^L_{pure,i}(T,p)}{RT}\right) = \exp\left(\frac{\Delta g^{S\to L}_{pure,i}(T,p)}{RT}\right) \tag{4.19}$$

being $\mu^L_{pure,i}(T,p) - \mu^S_{pure,i}(T,p)$ equal to the molar free Gibbs energy change from liquid to solid phase $\Delta g^{S\to L}_{pure,i}$ at temperature T and pressure p. A particular case is when T and p are equal to the melting temperature T_m and pressure p_m of the pure component: in this case $\Delta g^{S\to L}_{pure,i}$ is nil and fugacity of pure solid is equal to fugacity of pure liquid at T and p. In the general case in which T and p are different from T_m and p_m, it is convenient to relate solid and liquid molar free Gibbs energy through a thermodynamic path passing from the triple point of the pure component (fig. 4.1). Furthermore $\Delta g^{S\to L}_{pure,i}$ can be expressed through eq. (4.20) using enthalpy and entropy change, $\Delta h^{S\to L}_{pure,i}$ and $\Delta s^{S\to L}_{pure,i}$ respectively (for sake of readability index $_{pure,i}$ is omitted) .

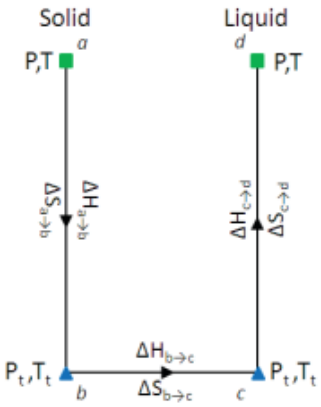

Figure 4.1: Thermodynamic path from solid to liquid phase at T,P

$$\Delta g^{S\to L} = \Delta h^{S\to L} - T\Delta s^{S\to L} \tag{4.20}$$

and following the thermodynamic path

$$\Delta g^{S\to L} = \Delta g^{a\to d} = \Delta g^{a\to b} + \Delta g^{b\to c} + \Delta g^{c\to d} \tag{4.21}$$

$$\Delta h^{S\to L} = \Delta h^{a\to d} = \Delta h^{a\to b} + \Delta h^{b\to c} + \Delta h^{c\to d} \tag{4.22}$$

$$\Delta s^{S\to L} = \Delta s^{a\to d} = \Delta s^{a\to b} + \Delta s^{b\to c} + \Delta s^{c\to d} \tag{4.23}$$

Property change from point b to c are properties of melting at triple point.

$$\Delta h^{b\to c} = \Delta h^{SLE}_{T_T,p_T} \tag{4.24}$$

$$\Delta s^{b\to c} = \Delta s^{SLE}_{T_T,p_T} = \frac{\Delta h^{SLE}_{T_T,p_T}}{T_T} \tag{4.25}$$

Enthalpy change from a to b and from c to d, thus from T,p to triple point temperature T_T and pressure p_T and reciprocal, can be calculated using following equations:

$$dh(T,p) = c_P dT - v(1 - T\beta)dp \tag{4.26}$$

$$ds(T,p) = \frac{c_P}{T}dT - v\beta dp \tag{4.27}$$

where β is the volumetric thermal expansion coefficient defined as:

$$\beta = \frac{1}{v}\left(\frac{\partial v}{\partial T}\right)_p \tag{4.28}$$

$$\Delta h^{a\to d} = \int_{T}^{T_T} c_p^S dT + \int_{p}^{p_T} v^S \left(1 - T\beta^S\right) dp + \Delta h^{SLE}_{T_T,p_T} + \int_{T_T}^{T} c_p^L dT + \int_{p_T}^{p} v^L \left(1 - T\beta^L\right) dp \tag{4.29}$$

$$= \int_{T_T}^{T} \left(c_p^L - c_p^S\right) dT + \int_{p_T}^{p} \left(v^L - v^S\right) dp - \int_{p_T}^{p} T\left(v^L\beta^L - v^S\beta^S\right) dp + \Delta h^{SLE}_{T_T,p_T} \tag{4.30}$$

$$= \int_{T_T}^{T} \left(\Delta c_p^{SL}\right) dT + \int_{p_T}^{p} \left(\Delta v^{SL}\right) dp - \int_{p_T}^{p} T\left(v^L\beta^L - v^S\beta^S\right) dp + \Delta h^{SLE}_{T_T,p_T} \tag{4.31}$$

$$\Delta s^{a\to d} = \int_{T}^{T_T} \frac{c_p^S}{T} dT - \int_{p}^{p_T} v^S\beta^S dp + \Delta s^{SLE}_{T_T,p_T} + \int_{T_T}^{T} \frac{c_p^L}{T} dT + \int_{p_T}^{p} v^L\beta^L dp \tag{4.32}$$

$$= \int_{T_T}^{T} \frac{c_p^L - c_p^S}{T} dT - \int_{p_T}^{p} \left(v^L\beta^L - v^S\beta^S\right) dp + \frac{\Delta h^{SLE}_{T_T,p_T}}{T_T} \tag{4.33}$$

$$= \int_{T_T}^{T} \frac{\Delta c_p^{SL}}{T} dT - \int_{p_T}^{p} \left(v^L\beta^L - v^S\beta^S\right) dp + \frac{\Delta h^{SLE}_{T_T,p_T}}{T_T} \tag{4.34}$$

Combining eq. (4.20) with eq. (4.31) and eq. (4.34), the Gibbs energy variation from solid to liquid at T,p can be written as follows:

$$\Delta g^{SL}(T,p) = \Delta h^{SLE}_{T_T,p_T}\left(1 - \frac{T}{T_T}\right) + \int_{T_T}^{T} \Delta c_p^{SL} dT - T\int_{T_T}^{T} \frac{\Delta c_p^{SL}}{T} dT - \int_{p_T}^{p} \Delta v^{SL} dp \tag{4.35}$$

Then, assuming Δv^{SL} constant and equal to $\Delta v^{SL}(T_T, p_T)$ and Δc_p^{SL} constant and equal to $\Delta c_p^{SL}(T_T, p_T)$, one obtains eq. (4.11). Otherwise, assuming Δv^{SL} constant and equal to $\Delta v^{SL}(T_T, p_T)$ but Δc_p^{SL} as a linear function of the temperature $\Delta C_P^{SL}(T) = A + BT$, one obtains the Zabaloy expression (eq. (4.14)), in which constants $C1$, $C2$, $C3$ are thus :

$$C1 = \frac{\Delta h^{SL}(T_T, p_T)}{\Delta v^{SL}(T_T, p_T)} \tag{4.36}$$

$$C2 = \frac{AT_T}{\Delta v^{SL}(T_T, p_T)} \tag{4.37}$$

$$C3 = \frac{BT_T^2}{\Delta v^{SL}(T_T, p_T)} \tag{4.38}$$

The Peng Robinson EoS for the fluid phase

The Peng-Robinson (Peng and Robinson, 1976) cubic Equation of State is chosen for representing the fluid phase. The classic form of a PR EoS is explicit in pressure, having the following form for a mixture

$$p(T, v, \mathbf{x}) = \frac{RT}{v - b(\mathbf{x})} - \frac{a(T, \mathbf{x})}{v(v + b(\mathbf{x})) + b(\mathbf{x})(v - b(\mathbf{x}))} \tag{4.39}$$

where $b(\mathbf{x})$ is the covolume and $a(T, \mathbf{x})$ is the attractive term parameter of the cubic equation, both depending on the molar composition of the mixture ($\mathbf{x}$) according to some equation modeling the interactions between the components, called mixing rules. For each component i, a_i and b_i are

$$a_i(T) = a_{c,i} \cdot \alpha(T) \tag{4.40}$$

$$a_{c,i} = 0.45724 \frac{R^2\ T_{c,i}^2}{p_{c,i}} \tag{4.41}$$

$$\alpha(T) = \left(1 + m_i \left(1 - \sqrt{T/T_{c,i}}\right)\right)^2 \tag{4.42}$$

$$m_i(T) = 0.37464 + 1.54226\omega_i - 0.26992\omega_i^2 \tag{4.43}$$

$$b_i = 0.07780 \frac{R\ T_c}{p_c} \tag{4.44}$$

$\alpha(T)$ is the same *alpha function* proposed by Soave (1972),where m_i depends on the acentric factor w_i.

Because of their simplicity and the good results provided for weakly polar and non-associated compounds, Classical van der Waals mixing rules have been chosen for combining pure compound parameters (geometric mean for $a(T)$ term with binary interaction parameter k_{ij} non-null between two different components i and j, and arithmetic mean for the covolume, with binary interaction parameter l_{ij} null):

$$a(T, \mathbf{x}) = \sum_{i=1}^{n} \sum_{j=1}^{n} x_i x_j \left(1 - k_{ij}\right) \sqrt{a_i(T) a_j(T)} \tag{4.45}$$

$$b(\mathbf{x}) = \sum_{i=1}^{n} x_i b_i \tag{4.46}$$

Three parameters are thus necessary and sufficient for defining the PR EoS for each pure compound: critical temperature T_c, critical pressure p_c and acentric factor ω. For the compounds of interest, parameters are reported in table 4.2. They have been taken from the NIST Standard Reference Database 23 (Lemmon et al., 2013). One binary interaction parameter k_{ij} for each binary mixture is also needed.

Table 4.2: Parameters for the Peng-Robinson EoS

Component	T_c (K)	p_c(MPa)	ω
CO_2	304.1282	7.3773	0.22394
CH_4	190.564	4.5992	0.01142
O_2	154.581	5.0430	0.0222
N_2	126.192	3.3958	0.0372

Binary interaction parameter k_{ij} is usually obtained from regression on VLE data, estimated through a correlation (for example, Nishiumi et al. (1988), Gao et al. (1992)) or predicted by a group contribution method, as in the work of Abdoul et al. (1991). For the PR EoS the binary

Table 4.3: Binary interaction parameters (k_{ij}) from Sandler (2006).

	N_2	O_2	CH_4	CO_2
N_2	-	-0.0119	0.03	-0.02
O_2	-0.0119	-	NA	NA
CH_4	0.03	NA	-	0.0919
CO_2	-0.02	NA	0.0919	-

interaction parameters k_{ij} for a large number of systems have been regressed on VLE data and proposed by Sandler (2006). For the systems of interest, values are reported in table 4.3.

For the binary mixtures of CO_2-O_2 and CH_4-O_2, the value of k_{ij} is considered nil, since these values are commonly not reported in literature and data are scarce.

Fugacity of the fluid phase from PR EOS

Fluid fugacity f_i^F can be derived, as other thermodynamic properties, from the Equation of State for the fluid phases. Starting from the definition of fugacity (eq. (4.4)) one can obtain following expression for the Peng Robinson EoS:

$$f_i^F(T,p,\mathbf{x}) = x_i p \ \exp\left[\frac{b_i}{b}(Z-1) - ln(Z-B) \right. \\ \left. -\frac{A}{2\sqrt{2}B}\left(\frac{2\sqrt{a_i}\sum_{j=1}^{nc} x_j\sqrt{a_j}\,(1-k_{ij})}{a} - \frac{b_i}{b}\right) ln\left(\frac{Z+\left(1+\sqrt{2}\right)B}{Z+\left(1-\sqrt{2}\right)B}\right)\right] \tag{4.47}$$

where Z is the compressibility factor defined as $Z = \frac{pv}{RT}$ and calculated from the cubic form of the PR EoS (taking the opportune liquid or vapor root):

$$Z^3 - (1-B)Z^2 + \left(A - 3B^2 - 2B\right)Z - \left(AB - B^2 - B^3\right) = 0 \tag{4.48}$$

being

$$A = \frac{ap}{R^2T^2} \tag{4.49}$$

$$B = \frac{bp}{RT} \tag{4.50}$$

Binary interaction parameter (k_{ij}) regression

In order to increase the capability of the model to represent phase equilibria involving a solid phase, in this work it has been chosen to regress k_{ij} parameters on SLVE data, when available, for the binary mixtures including carbon dioxide. According to the bibliographic research on phase equilibrium data presented in Chapter 3, SLVE data for the systems CH_4-CO_2 are available covering a wide range of the three phase locus. For the binary system of N_2-CO_2, some SLVE data are reported in the region close to the CO_2 triple point. For the CO_2-O_2 mixture, no SLVE data are available to the author's knowledge. The majority of the available SLVE data report triple point temperature and pressure, whereas no information on the phase compositions is available. The regression is performed by minimizing the objective function expressed in eq. (4.51), for N experimental points.

$$f_{obj} = \frac{1}{N}\sum_{i=1}^{N}\left(\frac{M_i^{calc} - M_i^{exp}}{M_i^{exp}}\right)^2 \tag{4.51}$$

As explained later in sec. 4.6.2, it is preferable to compute SLVE pressure from temperature because in some cases two SLVE temperatures exists at same pressure (i.e. for the CH_4-CO_2 triple phase locus). M is thus the triple point pressure for the N_2-CO_2 and the CH_4-CO_2 systems.

As stated before, no SLVE data are available for the CO_2-O_2 mixture. However, solubility data for CO_2 in liquid oxygen are available in the low temperature range (see Sec. 3.5). Comparing SLE data with model results for this system, a large deviation can be observed when k_{ij} parameter is equal to zero. The predicted solubility can be 150 times greater than measured solubility, and even greater than the solubility in liquid methane. Calibration of the model on SLE data for the O_2-CO_2 system is thus performed. A first comparison between data and model results shows that experimental values from Fedorova (1940) are not in agreement neither with data from other authors nor with the model behavior. As a consequence, it has been chosen not to consider this data for the regression of the k_{ij} (see fig. 4.4b). SLE data do not provide experimental pressure, and thus equation (4.51) is used with M being the CO_2 composition in liquid phase.

In figures 4.2a, 4.3a and 4.4a the behavior of the objective function as a function of k_{ij} for each binary mixture is shown. The regressed k_{ij} parameters are listed in table 4.4. For the others binary mixtures, the k_{ij} values available in literature have been used.

Table 4.4: Binary interaction parameters k_{ij} for the PR EoS used in this work, regressed on SLVE data. * from Sandler (2006)

	N_2	O_2	CH_4	CO_2
N_2	-	-0.0119*	0.03*	0.018
O_2	-0.0119*	-	0	0.16
CH_4	0.03*	0	-	0.119
CO_2	0.018	0.16	0.119	-

Comparison between results obtained using a PR with binary interaction parameters available in literature and regressed on SLVE data is presented in Sec. 4.7.

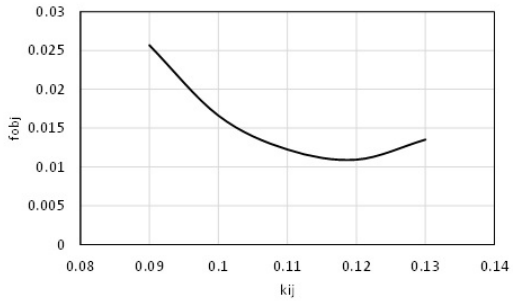

(a) f_{obj} from eq. (4.51)

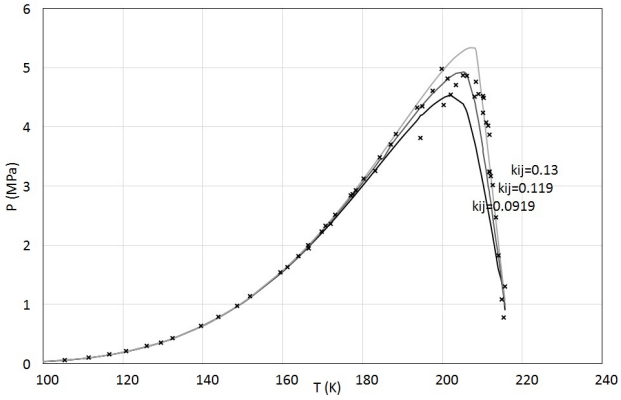

(b) Triple point locus obtained with different k_{ij} values (−) and experimental values (×)

Figure 4.2: Regression of the k_{ij} parameter of eq. (4.45) for the $CH_4 - CO_2$ mixture.

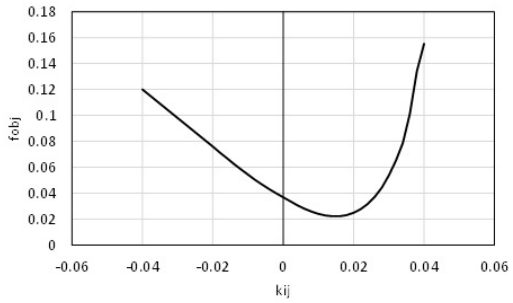

(a) f_{obj} from eq. (4.51)

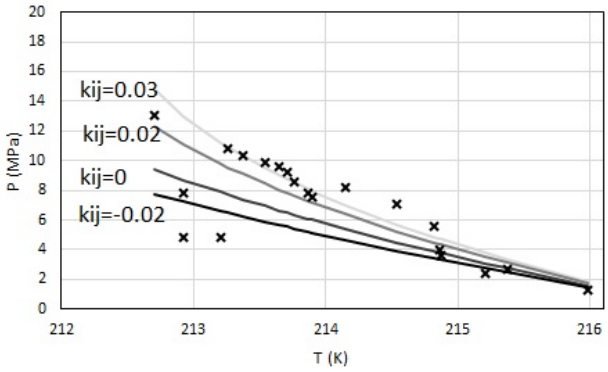

(b) Triple point locus obtained with different k_{ij} values − and experimental values ×

Figure 4.3: Regression of the k_{ij} parameter of eq. (4.45) for the $N_2 - CO_2$ mixture

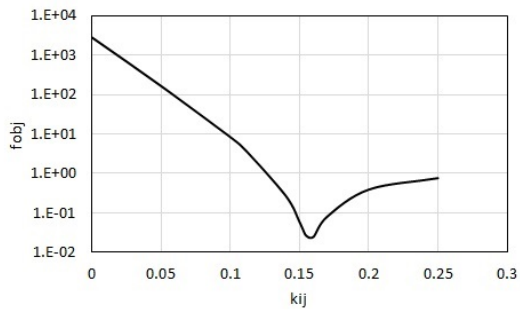

(a) f_{obj} from eq. (4.51)

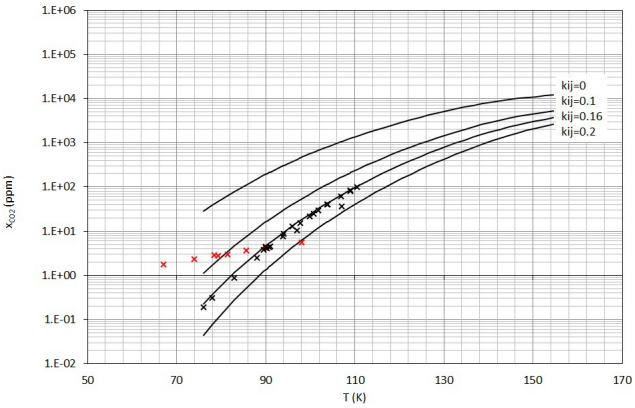

(b) SLE data used (×) and not used (×) for the regression; (−) results from model with different k_{ij} values;

Figure 4.4: Regression of the k_{ij} parameter of eq. (4.45) for the $O_2 - CO_2$ mixture

4.5.2 GERG plus Jager and Span model

In this section, a thermodynamic model able to compute vapor-liquid, fluid-solid phase equilibria and the thermodynamics properties of the solid phase is presented. The model used for the fluid phase is the GERG equation of state, and the model for the solid phase is the Equation of State for solid CO_2 proposed by Jager and Span (2012).

The Jager and Span EoS for the solid phase

In the Classical Approach for computing solid fugacity, the CO_2 volume in the solid phase at given temperature T and pressure p is calculated by computing the volume of the subcooled liquid CO_2 at same T and p and adding a factor Δv^{SL}, usually considered constant. The volume of the hypothetical subcooled liquid at T and p is just a mathematical derivation obtained from an EoS for the fluid phase, but it does not correspond to any physical (and thus measurable) property. CA is cannot rigorously compute thermodynamic properties of the solid phase, even if it provides good representation of Solid-Fluid Equilibrium (SFE) data. When the aim of the model is to compute thermodynamic properties of a fluid mixture in equilibrium with a solid CO_2, a proper model for the solid CO_2 has to be used. It is the case of the model proposed by Jager and Span (2012), which is an Equation of State for the solid CO_2 expressed in Gibbs free energy (eq. (4.52)).

$$\begin{aligned}\frac{g}{RT^0} &= g_0 + g_1\Delta\vartheta + g_2\Delta\vartheta^2 \\ &+ g_3\left\{\ln\left(\frac{\vartheta^2+g_4^2}{1+g_4^2}\right) - \frac{2\vartheta}{g_4}\left[\arctan\left(\frac{\vartheta}{g_4}\right) - \arctan\left(\frac{1}{g_4}\right)\right]\right\} \\ &+ g_5\left\{\ln\left(\frac{\vartheta^2+g_6^2}{1+g_6^2}\right) - \frac{2\vartheta}{g_6}\left[\arctan\left(\frac{\vartheta}{g_6}\right) - \arctan\left(\frac{1}{g_6}\right)\right]\right\} \\ &+ g_7\Delta\pi\left[e^{f_\alpha(\vartheta)} + g_8K(\vartheta)\right] + g_9K(\vartheta)\left[(\pi+g_{10})^{6/7} - (1+g_{10})^{6/7}\right]\end{aligned} \tag{4.52}$$

where ϑ and π are the reduced temperature and pressure:

$$\vartheta = \frac{T}{T^0};\ \Delta\vartheta = \vartheta - 1;\ \pi = \frac{p}{p^0};\ \Delta\pi = \pi - 1 \tag{4.53}$$

Reference state is set to

$$T^0 = 150\ K;\ p^0 = 0.101325\ MPa \tag{4.54}$$

The coefficients g_0 and g_1 has to be regressed by imposing the equality of molar Gibbs free energy of solid and fluid phases at the triple point:

$$g^S(T_t, p_t) = g^V(T_t, p_t) = g^L(T_t, p_t) \tag{4.55}$$

and

$$s^S(T_t, p_t) = s^L(T_t, p_t) - \frac{\Delta h^{SL}}{T_t} \tag{4.56}$$

Δh^{SL} is the enthalpy of melting at triple point, considered equal to 8875 $J\ mol^{-1}$ by Jager and Span (2012). According to Span and Wagner (1996), triple point temperature and pressure

of CO_2 are $T_t = 216.592\ K$ and $p_t = 0.517950\ MPa$. The values of the other parameters of eq. (4.52) are listed in Jager and Span (2012).

Functions $f_\alpha(\vartheta)$ and $K(\vartheta)$ are

$$f_\alpha(\vartheta) = g_0^\alpha \left(\vartheta^2 - 1\right) + g_1^\alpha \ln\left(\frac{\vartheta^2 - g_2^\alpha \vartheta + g_3^\alpha}{1 - g_2^\alpha + g_3^\alpha}\right) + g_4^\alpha \ln\left(\frac{\vartheta^2 + g_2^\alpha \vartheta + g_3^\alpha}{1 + g_2^\alpha + g_3^\alpha}\right) \tag{4.57}$$

$$+ g_5^\alpha \left[\arctan\left(\frac{\vartheta - g_6^\alpha}{g_7^\alpha}\right) - \arctan\left(\frac{1 - g_6^\alpha}{g_7^\alpha} -\right)\right] \tag{4.58}$$

$$+ g_8^\alpha \left[\arctan\left(\frac{\vartheta + g_6^\alpha}{g_7^\alpha}\right) - \arctan\left(\frac{1 + g_6^\alpha}{g_7^\alpha} -\right)\right] \tag{4.59}$$

$$K(\vartheta) = g_0^K \vartheta^2 + g_1^K \vartheta + g_2^K \tag{4.60}$$

For the development of the model, Jager and Span (2012) made some simplifying assumptions to overcome the problem of having only few experimental data for solid carbon dioxide in the pressure range from 0 MPa to the CO_2 triple point pressure:

1. The pressure dependence of the heat capacity $c_p(T, p)$ is negligible ;
2. The pressure dependence of the thermal expansion coefficient is negligible;
3. The pressure dependence of the compressibility is negligible.

Fugacity of the solid phase

Equation of State written in Gibbs free energy are called fundamental EoS because all thermodynamic properties can be obtained by derivation, without any integration, avoiding, thus all sort of integration constant. The fugacity of solid CO_2 is obtained by eq. (4.4), that for the pure CO_2 becomes

$$f^S_{CO_2}(T, p) = p^0 \exp\left(\frac{g^S_{CO_2}(T, p) - g^0_{CO_2}(T, p^0)}{RT}\right) \tag{4.61}$$

Reference state is taken as ideal gas at T^0 and p^0, and so $g^0_{CO_2}$ is the ideal gas Gibbs free energy obtained from reference quality equation of state explicit in the Helmholtz free energy for the CO_2 reported in Kunz et al. (2007). This equation provides great accuracy with respect to ideal gas heat capacity down to very low temperature: as shown in fig. 4.5, the maximum error ($\Delta c_p rel$) on pseudo-experimental data from Wooley (1954) and McBride and Gordon (1961) in the range of $50 - 500$ K is 0.068%, calculated as

$$\Delta c_p rel = \frac{c_p^{calc} - c_p^{exp}}{c_p^{exp}} \tag{4.62}$$

The GERG EoS for the fluid phase

The model chosen for the fluid phase model is the GERG-2008 EoS proposed by Kunz and Wagner (2012) for improving GERG-2004 EoS proposed by Kunz et al. (2007). This EoS had the objective to overcome the weaknesses and limitations of existing equations of state used in the natural gas industry and the development was led by the Chair of Thermodynamics of the Ruhr-Universität Bochum, supported by the DVGW (German Technical and Scientific

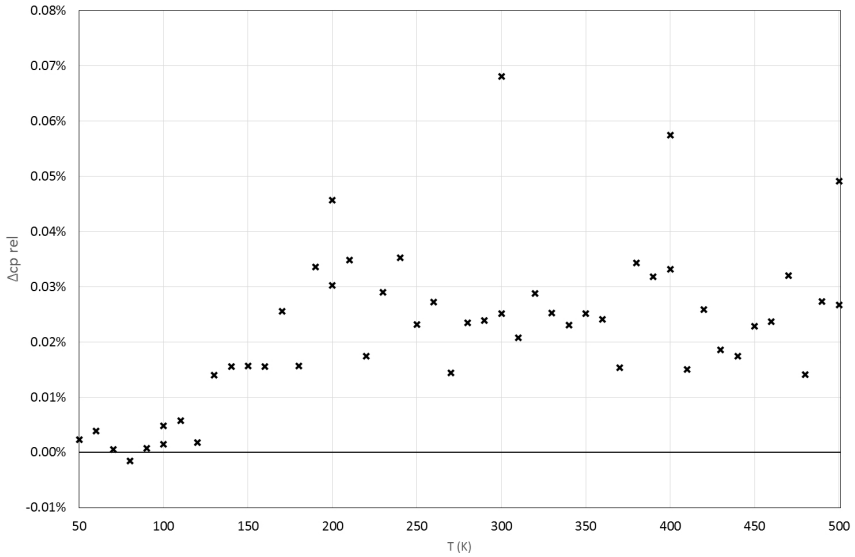

Figure 4.5: Comparison between ideal gas heat capacity of carbon dioxide calculated using reference equation from Kunz et al. (2007) and pseudo-experimental data from Wooley (1954) and McBride and Gordon (1961)

Association on Gas and Water) and European natural gas companies (E.ON Ruhrgas, Germany; Enagàs, Spain; Gasunie, The Netherlands; Gaz de France, France; Snam Rete Gas, Italy; and Statoil, Norway), which are members of GERG (Groupe Européen de Recherches Gaziéres).

The GERG EoS is based on a multi-fluid approximation expressed in the Helmholtz free energy, whose natural variables are temperature (T) and density (ρ) and can be written as the sum of an ideal part (a^{ig}) and a residual part (a^r):

$$a(T, \rho, \mathbf{x}) = a^r(T, \rho, \mathbf{x}) + a^{ig}(T, \rho, \mathbf{x}) \tag{4.63}$$

Two approaches are historically used for the development of an Equation of State for fluid mixtures: the one-fluid approximation or the multi-fluid approximation. When the one-fluid approximation is used, a mixture is considered as equivalent to a pseudo-pure fluid, thus the EoS for describing a mixture is the same as a pure fluid EoS with parameters obtained by combination of pure fluid parameters through mixing rules. Cubic Eos are examples of the application of the one-fluid approximation. Contrary to the one-fluid approximation, multi-fluid approximation computes the residual properties as a combination of pure components equations of state in the form of fundamental equations and adds a departure function developed for the binary mixtures of the components that takes into account the non-ideality of the mixture behavior. The GERG EoS is based on a multi-fluid approximation proposed by Tillner-Roth (1998) and Lemmon (1996). For a mixture of nc components of composition $\mathbf{x}$ the residual part $a^r(T, \rho, \mathbf{x})$ of the Helmholtz free energy can be expressed in the following form :

$$\frac{a^r(T, \rho, \mathbf{x})}{RT} = \alpha^r(\tau, \delta, \mathbf{x}) = \sum_{i=1}^{nc} x_i \alpha_i^r(\tau, \delta) + \Delta\alpha^r(\tau, \delta, \mathbf{x}) \tag{4.64}$$

being $\Delta\alpha^r(\tau, \delta, \mathbf{x})$ the departure function accounting for the mixture non ideality, while residual Helmholtz free energy for each component i ($\alpha_i^r(\tau, \delta)$) accounts for the pure-component non ideality. The first approximation to the mixture is via the use of a composition-dependent reducing function: the inverse of the reduced mixture temperature $\tau = T_r/T$ and the reduced mixture density $\delta = \rho/\rho_r$, which are non-linear functions and contains up to four binary interaction

parameters. These non-linear reducing functions play a role as important as the departure function. Reducing parameters T_r and ρ_r are pseudo-critical temperature and density, based on the quadratic mixing rules proposed by Klimeck (Kunz and Wagner, 2012).

The ideal part of the Helmoltz free energy of the mixture is obtained from Helmoltz free energy of each component i (α_i^{ig})in the ideal-gas state and a mixing contribution :

$$\frac{a^{ig}(T,\rho,\mathbf{x})}{RT} = \alpha^{ig}(T,\rho,\mathbf{x}) = \sum_{i=1}^{nc} x_i \left[\alpha_i^{ig}(T,\rho) + \ln x_i\right] \tag{4.65}$$

Equations for each pure components are proposed in Kunz et al. (2007), together with mixing rules for pseudo-critical parameters and parameters of the departure function $\Delta\alpha^r(\tau,\delta,\mathbf{x})$.

Main advantages of the EoS are the wide-range of validity for natural gases and other mixtures and good performances that enables the equation to be adopted as a standard international reference equation suitable for all natural gas applications where thermodynamic properties are required. Range of validity depends on the pure fluid EoS (see tab. 4.5) and on binary mixture data used for regressing the mixing parameters (see tab. 4.6). Kunz et al. (2007) reported that the range of validity for the binary CH_4-CO_2 system is down to 143 K, citing Yorizane et al. (1968). Nevertheless the cited article do not present VLE data for the binary CH_4-CO_2, but for the CH_4-CO system. Data at lower temperature on which GERG EoS are thus from Mraw et al. (1978) at 153 K. The range of validity of an empirical equation of state is typically limited by the temperature and pressure ranges which are covered by reliable experimental data used for the development and evaluation of the equation. Modern multi-parameter equations of state are designed to behave reasonably far beyond this range, even if some authors show that this is not always the case (Syed et al., 2014).

Table 4.5: Range of validity for pure components EoS according to Kunz et al. (2007) * Carbon dioxide Eos can be extrapolated down to 90 K

Component	Temperature range (K)	Maximum pressure (MPa)
CH_4	90-623	300
N_2	63-700	300
CO_2	216-900*	300
O_2	54-303	100

Table 4.6: Temperature, pressure and composition range for binary mixture data used in Kunz et al. (2007)

Binary mixture	Temperature range (K)	Pressure range (MPa)	Composition
$CH_4 - N_2$	78.4-673	0.02-750	0.00-1.00
$CH_4 - CO_2$	153-673	0.03-99.9	0.00-0.99
$N_2 - CO_2$	209-673	0.1-274	0.10-1.00
$CH_4 - O_2$	-	-	-
$N_2 - O_2$	63-333	0.0-15.7	0.01-1.00
$CO_2 - O_2$	-	-	-

The departure function developed for the binary mixtures is set to zero for the $CH_4 - O_2$ and $CO_2 - O_2$ mixtures, due to the scarcity of data available for these mixtures.

A comparison between GERG-2008 and PR EoS with respect to available $CH_4 - CO_2$ low temperature data have been performed and results are shown in sec. 4.7.

4.6 SFE and SFFE solution

In the previous section models for computing fluid and solid fugacity have been presented. The solution of the phase equilibria involving a solid phase involves nevertheless recursive procedures and a final stability test. The algorithms used in this work for solving phase equilibria are presented in this section. Phase equilibria between a solid and a fluid phase (SFE) are Solid-Vapor Equilibrium (SVE) and Solid-Liquid Equilibrium (SLE). Phase equilibria between a solid and two fluid phases are, in this work, limited to the Solid-Liquid-Vapor Equilibrium (SLVE).

The importance of a correct and robust solution of the phase equilibrium is fundamental for computing thermodynamic properties of a mixture since, as a first step, one needs to determine which is the most stable stable configuration of the studied system at given temperature T and pressure p, in terms of number of existing phases and their compositions.

As previously said in section 4.2.1, for computing phase equilibrium two methods are possible: Gibbs' free energy minimization or isofugacity approach. The advantage of using a Gibbs free energy minimization technique for multiphase calculation is that one can find directly the more stable configuration of the system at given conditions, without the need to add any *a priori* information on the type and number of phases involved. For the isofugacity approach, on the contrary, the number and type of phases at the equilibrium must be specified, but the advantages is that it can be implemented by simpler methods (flash calculation), compared to the numerical optimization method needed for finding the minimum of the Gibbs free energy.

In this work, since the number of components is limited to four (carbon dioxide, methane, nitrogen and oxygen) and possible phase equilibria known, the approach chosen in this work is the equality of fugacity. In the range of pressure and temperature of interest, possible phase equilibria for the studied systems are in fact Solid-Fluid Equilibrium (SFE), both Solid-Liquid (SLE) and Solid-Vapor (SVE), Solid-Liquid-Vapor Equilibrium (SLVE) and Vapor-Liquid Equilibrium (VLE). No Liquid-Liquid Equilibrium is known to exist for the systems of interest (see Sec. 3). For finding the more stable solution at given condition, typically temperature (T), pressure (p) and global composition ($\mathbf{z}$), all possible types of equilibrium calculations are performed and, finally, a stability criterion is applied. The more stable configuration is the one with the minimum Gibbs free energy of mixing (g^{mix}). The Gibbs free energy of mixing, as explained in a clear manner by Privat and Jaubert (2012), is defined for a mixture of N component at temperature T, pressure p and molar composition $\mathbf{x}$ as

$$g^{mix}(T,p,\mathbf{x}) = g(T,p,\mathbf{x}) - \sum_{i}^{N} x_i g_i^{pure,stable}(T,p) \tag{4.66}$$

where $g(T,p,\mathbf{x})$ is the molar Gibbs free energy of the mixture and $g_i^{pure,stable}(T,p)$ is the molar Gibbs free energy of the pure component i in its stable phase at T and p. For a mixture of global composition $\mathbf{z}$ that at temperature T and pressure p splits into a vapor, a liquid and a solid phases, of composition $\mathbf{y}$, $\mathbf{x}$, and $\mathbf{w}$ respectively and with molar fraction V, L and S respectively, the molar Gibbs free energy of mixing is

$$g^{mix}(T,p,\mathbf{z}) = Vg^{mix,V}(T,p,\mathbf{y}) + Lg^{mix,L}(T,p,\mathbf{x}) + Sg^{mix,S}(T,p,\mathbf{w}) \tag{4.67}$$

For each phase α of composition x^α, the molar Gibbs energy of mixture can be calculated as

$$g^{mix,\alpha}(T,p,\mathbf{x}^\alpha) = \sum_i^N x_i^\alpha \ln \frac{f_i^\alpha(T,p,\mathbf{x}^\alpha)}{f_i^{\alpha,pure,stable}(T,p)} \tag{4.68}$$

Finally, being the solid phase considered as pure CO_2, the Gibbs free energy of mixing results to be nil.

4.6.1 Solid-Fluid Equilibrium

For calculating SFE at given temperature T, pressure p and global composition $\mathbf{z}$ the isofugacity condition (eq. (4.5)) must be solved for the solid former component (i.e. carbon dioxide) in solid and fluid phase. Being the composition of the solid phase known (pure CO_2), the solution of the SFE at given T, p, $\mathbf{z}$, is reduced to the determination of the composition of the fluid phase $\mathbf{x}$ and the molar fraction of the solid S and fluid phase F.

Expressing eq. (4.5) by means of the fugacity coefficient ϕ results into:

$$\phi_{CO_2}^S(T,p) = x_{CO_2}\ \phi_{CO_2}^F(T,p,\mathbf{x}) \tag{4.69}$$

allowing to obtain the molar composition of CO_2 in fluid phase, while the material balance is used to determine molar composition of every $i \neq CO_2$ component in the fluid phase, as well as solid S and fluid F molar fraction.

Material balance

In a system at SFE, total number of moles n is the sum of the number of mole in the fluid phase n^F and in the solid phase n^S:

$$n^F + n^S = n \tag{4.70}$$

dividing by the total number of moles n one obtains:

$$F + S = 1 \tag{4.71}$$

Since the solid phase is composed of the only CO_2, the material balance for carbon dioxide is:

$$x_{CO_2}(1-S) + S = z_{CO_2} \tag{4.72}$$

The other $i \neq CO_2$ components are present only in the fluid phase and thus:

$$x_{i\neq CO_2} = \frac{z_{i\neq CO_2}}{F} \tag{4.73}$$

Solving algorithm

Since the fugacity coefficient of the fluid phase $\phi_{CO_2}^F(T,p,\mathbf{x})$ depends on the molar composition $\mathbf{x}$, an iterative procedure is needed for determining x_{CO_2} (and so $\mathbf{x}$). The algorithm is presented in fig. 4.6.

The initial estimate of $x_{CO_2}^{(0)}$ can be obtained from eq. (4.69) taking $\phi_{CO_2}^F(T,p,\mathbf{x})$ equal to one (ideal gas). Convergence is achieved when *test* is lower than the tolerance ϵ, assumed equal to 10^{-13} in this work.

$$test = \frac{|x_{CO_2}^{(k+1)} - x_{CO_2}^{(k)}|}{x_{CO_2}^{(k)}} \tag{4.74}$$

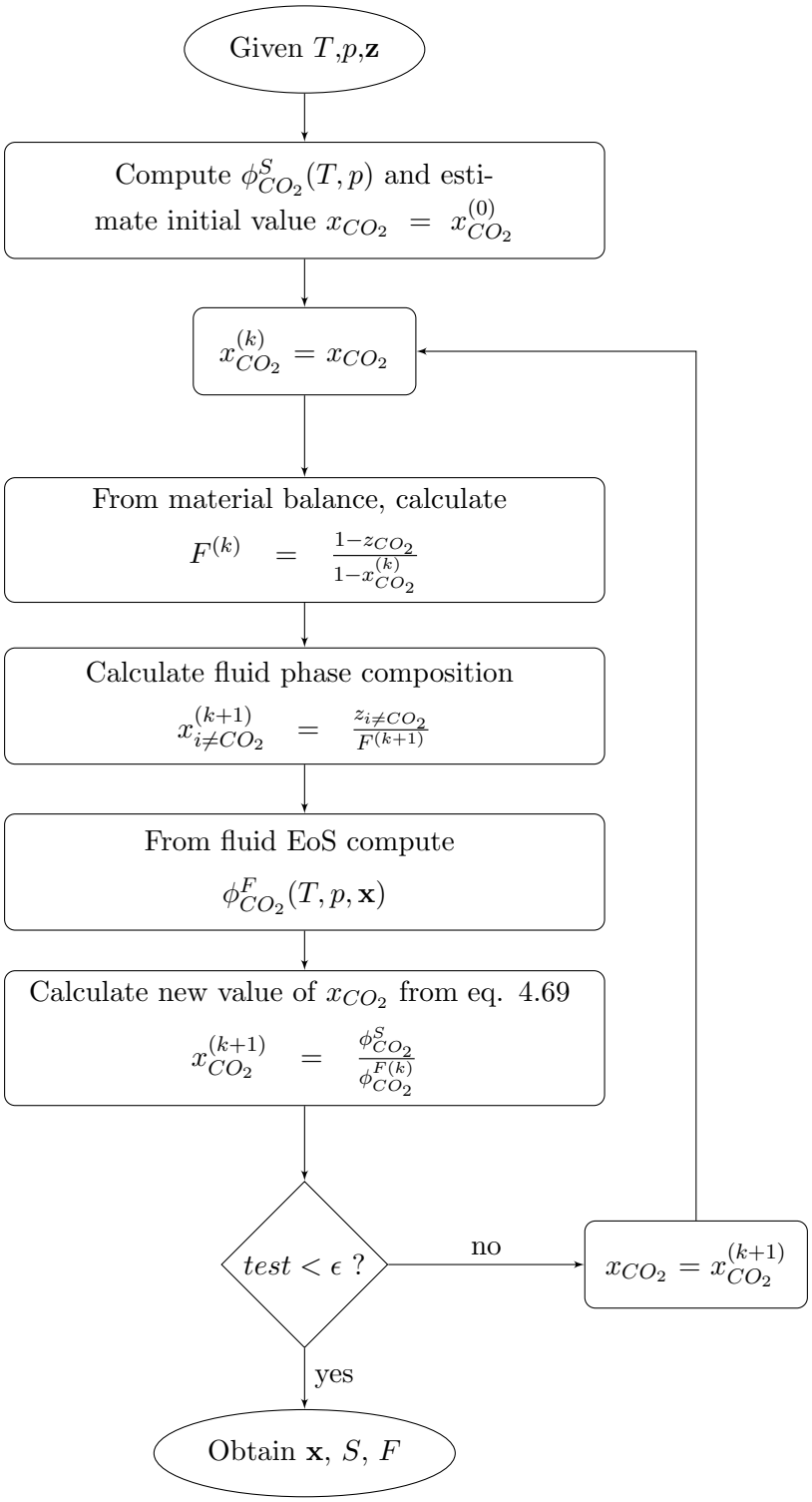

Figure 4.6: Flow diagram for SFE solving algorithm

4.6.2 Solid-Liquid-Vapor Equilibrium

According to Gibbs' phase rules in a system of nc components, when the number of phases (np) is 3, the number of degree of freedom is $nf = nc - np + 2 = nc - 3 + 2 = nc - 1$. For a pure component the system has no degree of freedom ($nf = 0$), which means that three phases exist only at a specific couple of temperature and pressure (T_t, p_t), namely the triple point of the component.

A binary system (nc=2) at SLVE is univariant ($nf = 1$) so one can calculate SLVE temperature T^{SLVE} at given pressure p or, conversely, SLVE pressure p^{SLVE} at given temperature T, but it is not possible to specify independently both temperature and pressure of the system. Calculation of pressure at given temperature is preferable because for many systems, like for instance the methane-carbon dioxide system, for a given temperature a unique SLVE pressure can exist, while for a given pressure, up to two SLVE temperature can exist. It may cause problems to the numerical solution when the two SLVE temperatures are similar, i.e. for pressure close to the maximum pressure of the SLVE locus (fig. 4.7). Composition of vapor and liquid phases at SLVE depends on chosen temperature.

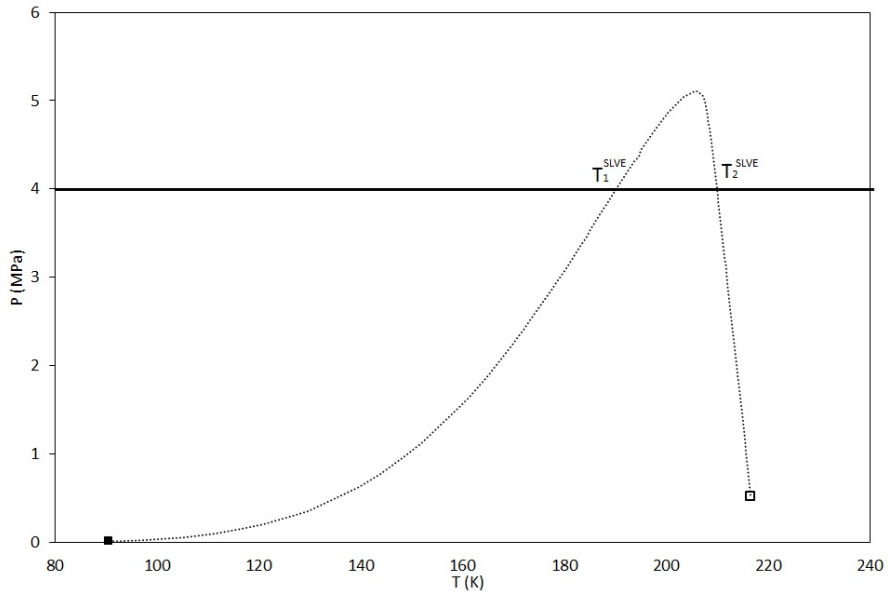

Figure 4.7: SLVE equilibrium line for the binary CH_4-CO_2 system. □ CO_2 triple point; ■ CH_4 triple point

For a number of components greater than 2, the number of degree of freedom is 2 or more. As a consequence it is possible to specify independently temperature and pressure for determining SLVE conditions. In order to calculate the liquid and vapor phase composition ($\mathbf{x}$ and $\mathbf{y}$) and molar fractions of liquid L, vapor V and solid S at SLVE conditions, it is necessary to specify global composition z of the system, together with T and p.

Material balance

In a system at SLVE, total number of moles n is the sum of the number of mole in the liquid phase n^L, in the vapor phase n^V and in the solid phase n^S :

$$n^L + n^V + n^S = n \tag{4.75}$$

and dividing by the total number of moles n one obtains liquid fraction L, vapor fraction V, and solid fraction S:

$$L + V + S = 1 \tag{4.76}$$

It can be convenient also to express n^F as the sum of the mole number in the liquid phase n^L and in the vapor phase n^V:

$$n^L + n^V = n^F \tag{4.77}$$

Fluid fraction F is obtained similarly:

$$L + V = F \tag{4.78}$$

and thus

$$F = 1 - S \tag{4.79}$$

The material balance on the CO_2 component is

$$x_{CO_2} L + y_{CO_2} V + S = z_{CO_2} \tag{4.80}$$

being $\mathbf{x}$ the composition of the liquid phase, $\mathbf{y}$ the composition of the vapor phase, $\mathbf{z}$ the global composition of the mixture. $\mathbf{z}'$ is defined as the composition of the fluid phase (vapor+liquid), and thus

$$z'_{CO_2}(1 - S) + S = z_{CO_2} \tag{4.81}$$

The other $i \neq CO_2$ components are present only in the fluid phase, so they can be calculated as:

$$x_{i \neq CO_2} L + y_{i \neq CO_2} V = z_{i \neq CO_2} \tag{4.82}$$

and, with reference to the subsystem F,

$$z'_{i \neq CO_2}(1 - S) + = z_{i \neq CO_2} \tag{4.83}$$

Solving algorithm for binary mixture

For the solution of the SLVE problem for a binary mixture the degree of freedom is one, so once the temperature of the system is fixed, it is possible to obtain SLVE pressure p^{SLVE}, liquid phase composition $\mathbf{x}$ and vapor phase composition $\mathbf{y}$. After solving the SLVE problem, it is necessary to specify global composition $\mathbf{z}$ and solve material balance (equations from (4.76) to (4.83)) for calculating vapor fraction V and liquid fraction L.

The algorithm combines VLE and SVE calculations at given temperature and pressure. The pressure is firstly set to an initial estimate, then iteratively modified until the objective function f is is less then tolerance ϵ. Objective function is defined as the difference between the composition of the vapor phase obtained from VLE and SVE calculation:

$$f = |y^{VLE}_{CO_2} - y^{SVE}_{CO_2}| \tag{4.84}$$

In figure 4.8 the algorithm is summarized in a flow diagram. The variation of the pressure p at the iteration $(k + 1)$ depends on the numerical method used. In case a Newton method is used the value is calculated as follow:

$$p^{(k+1)} = p^{(k)} - \Delta y \left(p^{(k)}\right) \left(\frac{d\Delta y}{dp}\right) \tag{4.85}$$

with $\left(\frac{d\Delta y}{dp}\right)$ obtained numerical, using forward difference scheme.

Excessive increments of pressure lead to T,p conditions at which the VLE calculation returns a single stable phase, causing the divergence of the algorithm. When this happens the pressure increment is reduced.

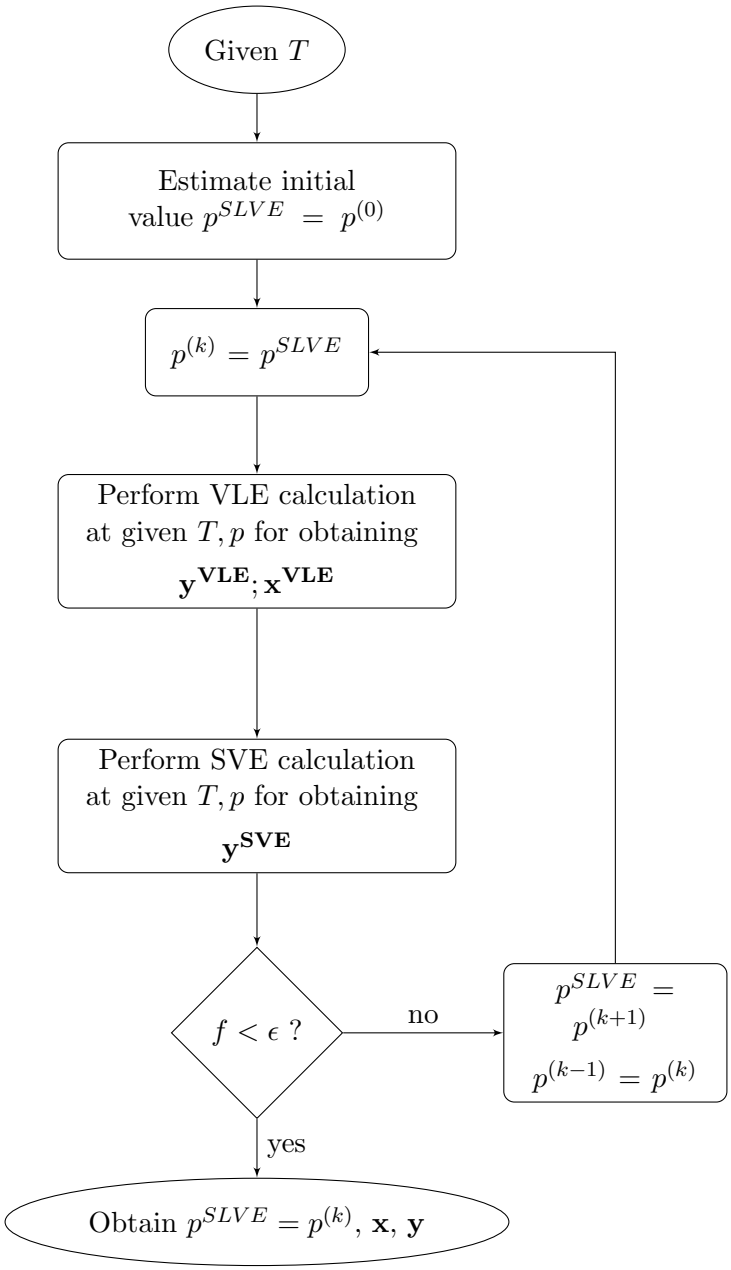

Figure 4.8: Flow diagram for SLVE solving algorithm for binary mixture

Solving algorithm for multicomponent mixture

As stated before, in a system of at least 3 components, at fixed temperature (or pressure) SLVE exists for a range of pressure (temperature). The solution of the SLVE given T, p and global composition $\mathbf{z}$ of the mixture, allows to obtain liquid and vapor molar composition, $\mathbf{x}$ and $\mathbf{y}$ respectively, and the molar fractions of liquid (L), vapor (V) and solid (S).

The fugacity at SLVE must be the same in all the three phases for the solid former component (CO_2).

$$f^S_{CO_2}(T,p) = f^L_{CO_2}(T,p,\mathbf{x}) = f^V_{CO_2}(T,p,\mathbf{y}) \tag{4.86}$$

This condition can be expressed through a system of two independent equations

$$\begin{cases} f^S_{CO_2}(T,p) = f^V_{CO_2}(T,p,\mathbf{y}) & (4.87) \\ f^L_{CO_2}(T,p,\mathbf{x}) = f^V_{CO_2}(T,p,\mathbf{y}) & (4.88) \end{cases}$$

All the $i \neq CO_2$ components have to respect the isofugacity condition between liquid and vapor phase:

$$f^L_{i\neq CO_2}(T,p,\mathbf{x}) = f^V_{i\neq CO_2}(T,p,\mathbf{y}) \tag{4.89}$$

The computation of the SLVE conditions is thus performed calculating the fugacity of the solid phase at system T and p and then performing a VLE calculation at same fixed T and p, and given fluid molar composition z' (TPz-flash calculation). Flash calculation guarantees that eq. (4.88) and eq. (4.89) are respected. At fixed T and p, fugacity of the fluid phases depends on the given fluid molar composition z', which is linked to solid molar fraction S by eq. (4.81) and eq. (4.83).

It is thus possible to express the fugacity of the fluid phases as function of the solid fraction S and compare it with solid fugacity of the CO_2. The difference between solid and liquid fugacity $\Delta f^{SL} = f^S_{CO_2} - f^L_{CO_2}$ has to be equal to 0 for solving SLVE, which is equivalent to affirm that eq. (4.86) is respected. The behavior of $\Delta f^{SL}(S)$ as a function of S is represented in fig. 4.9 for different temperature and pressures. In order to solve the root-finding problem a bisection method is performed, with initial interval limits set as $S_l = 0 + \epsilon$ and $S_r = x_{CO_2} - \epsilon$. If no zero is found, it means that at given conditions no SLVE exists for the system. Solving algorithm is summarized in fig. 4.9.

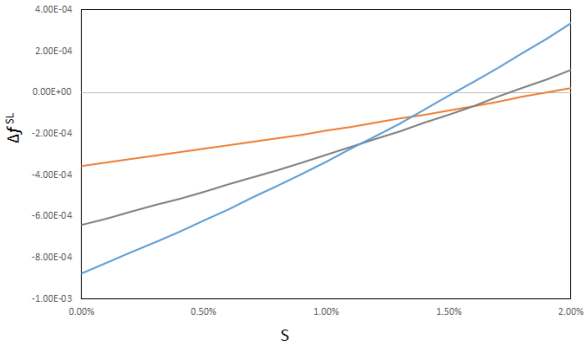

Figure 4.9: Difference between solid and liquid fugacity Δf^{SL} as function of solid molar fraction S for a mixture of 20% N_2,78% CH_4, 2% CO_2. $T = 144.5\ K$, $p = 1.4\ MPa$; $T = 135\ K$, $p = 1\ MPa$; $T = 124\ K$, $p = 0.6\ MPa$

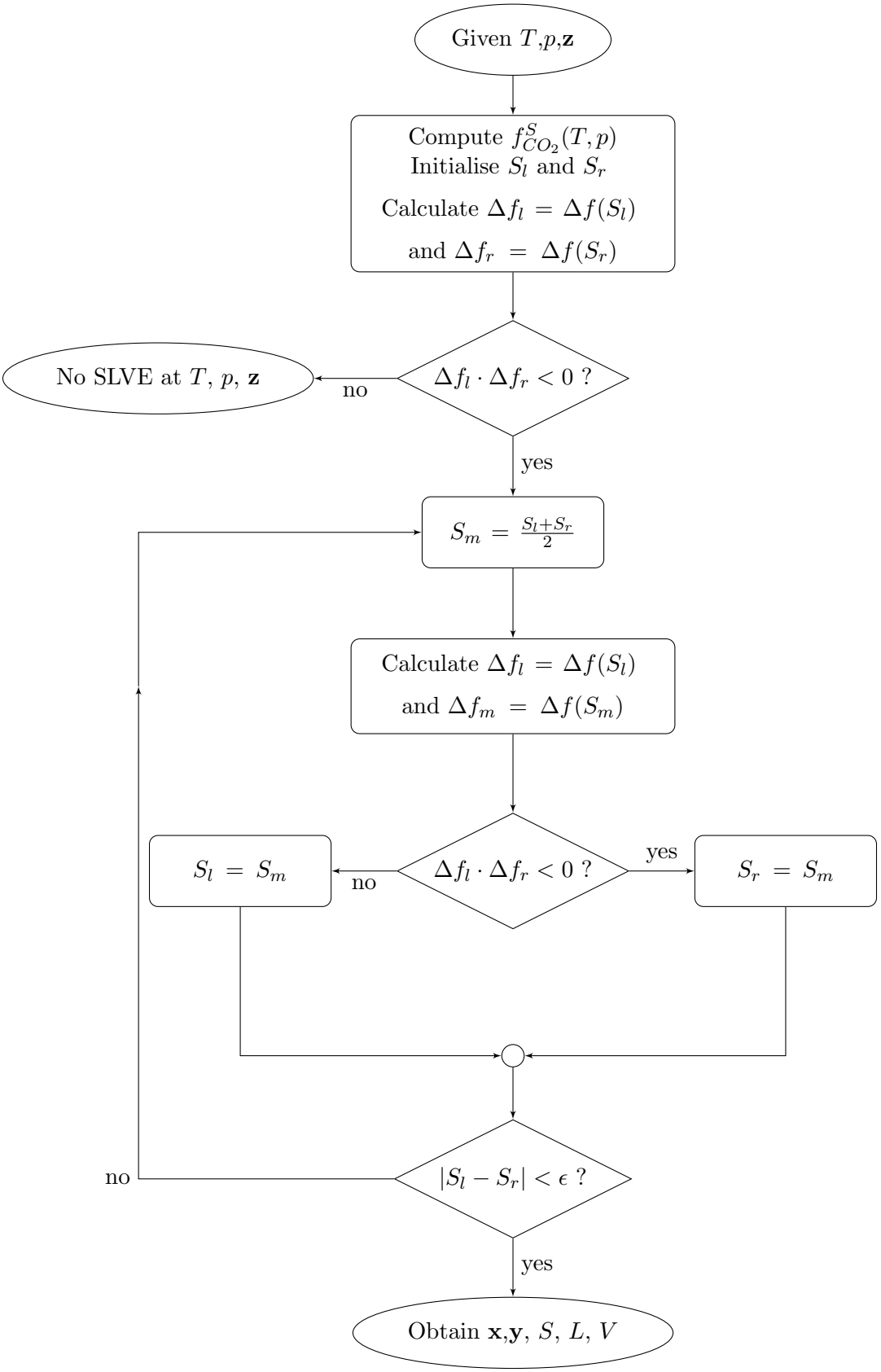

Figure 4.10: Flow diagram for SLVE solving algorithm for multicomponent mixture

4.6.3 Vapor-Liquid Equilibrium

A practical case of VLE solution is the case in which pressure p and temperature T of the system are specified and composition of each phase $\mathbf{y}$ and $\mathbf{x}$ has to be calculated. The commonly used Successive Substitution Method (SSM) is implemented for multicomponent flash problem. For binary mixture it can be convenient to implement a different algorithm, presented by Privat et al. (2013), allowing the solution of the VLE problem without the need of specifying the global composition of the mixture.

General pT-flash algorithm

The general pT-flash calculation allows to obtain composition of each fluid phase , $\mathbf{y}$ and $\mathbf{x}$, as well as vapor and liquid molar fractions, V and L respectively, specifying temperature T, pressure p and global composition $\mathbf{z}$ of the system. Necessary condition for Vapor-Liquid Equilibrium is the equality of fugacities of each component in each phase.

$$x_i f_i^L(T,p,\mathbf{x}) = y_i f_i^V(T,p,\mathbf{y}) \tag{4.90}$$

Material balance also need to be satisfied:

$$x_i L + y_i V = z_i \tag{4.91}$$

$$L + V = 1 \tag{4.92}$$

$$\sum_i^{nc} x_i = 1 \tag{4.93}$$

$$\sum_i^{nc} y_i = 1 \tag{4.94}$$

Defining the equilibrium ratio K_i as

$$K_i = y_i/x_i \tag{4.95}$$

and combining previous equations, one obtains

$$x_i = \frac{z_i}{1+V(K_i-1)} \tag{4.96}$$

and

$$y_i = \frac{K_i z_i}{1+V(K_i-1)} \tag{4.97}$$

Finally combining material balance equations to eq. (4.96) and eq. (4.97), the Rachford-Rice expression is obtained (Rachford and Rice, 1952):

$$f_{obj} = \sum_i^{nc} \frac{(K_i-1)z_i}{1+V(K_i-1)} = 0 \tag{4.98}$$

The VLE problem is solved when V satisfying eq. (4.98) is found and, at the same time, $\mathbf{x}$ and $\mathbf{y}$ that satisfy eq. (4.90) are found.

Iterative scheme can be expressed as follows (Firoozabadi, 1999)

$$K_i^{(k+1)} = K_i^{(k)} exp\left(-ln\frac{f_i^V(T,p,\mathbf{y^{(k)}})}{f_i^L(T,p,\mathbf{x^{(k)}})}\right) \tag{4.99}$$

Initial guess for K_i can be obtained from Wilson correlation (Wilson, 1969) using critical temperature T_{ci} and pressure p_{ci} and acentric factor ω_i:

$$lnK_i = 5.37(1+\omega_i)(1-T_{ci}) + ln(P/P_{ci}) \tag{4.100}$$

Solving algorithm is summarized in fig. 4.11.

Solution of the VLE for binary mixture: *petit-flash*

For binary mixture the Gibbs' phase rule states that the number of degrees of freedom is 2, thus 2 independent variables (temperature T and pressure p) are sufficient for completely defining the system. In this case the phase equilibrium problem is uncoupled from the material balance and thus there is no need to specify the global composition $\mathbf{z}$ of the mixture if ones do not need to calculate vapor and liquid fractions. The algorithm is presented in Privat et al. (2013) and it uses a successive substitution technique for solving the iterative scheme, written as:

$$x_1^{(k+1)} = \left[\frac{\phi_1^V \left(\phi_2^V - \phi_2^L \right)}{\phi_1^L \phi_2^V - \phi_2^L \phi_1^V} \right]^{(k)} \tag{4.101}$$

and

$$x_1^{(k+1)} = \left[\frac{\phi_1^L \left(\phi_2^V - \phi_2^L \right)}{\phi_1^L \phi_2^V - \phi_2^L \phi_1^V} \right]^{(k)} \tag{4.102}$$

The algorithm is presented in fig. 4.12, where tolerance ϵ is set to 10^{-10}. Differently from the general pT-flash, the *petit flash* algorithm is not able to indicate whether the system is more stable in a single phase or in a two phases configuration.

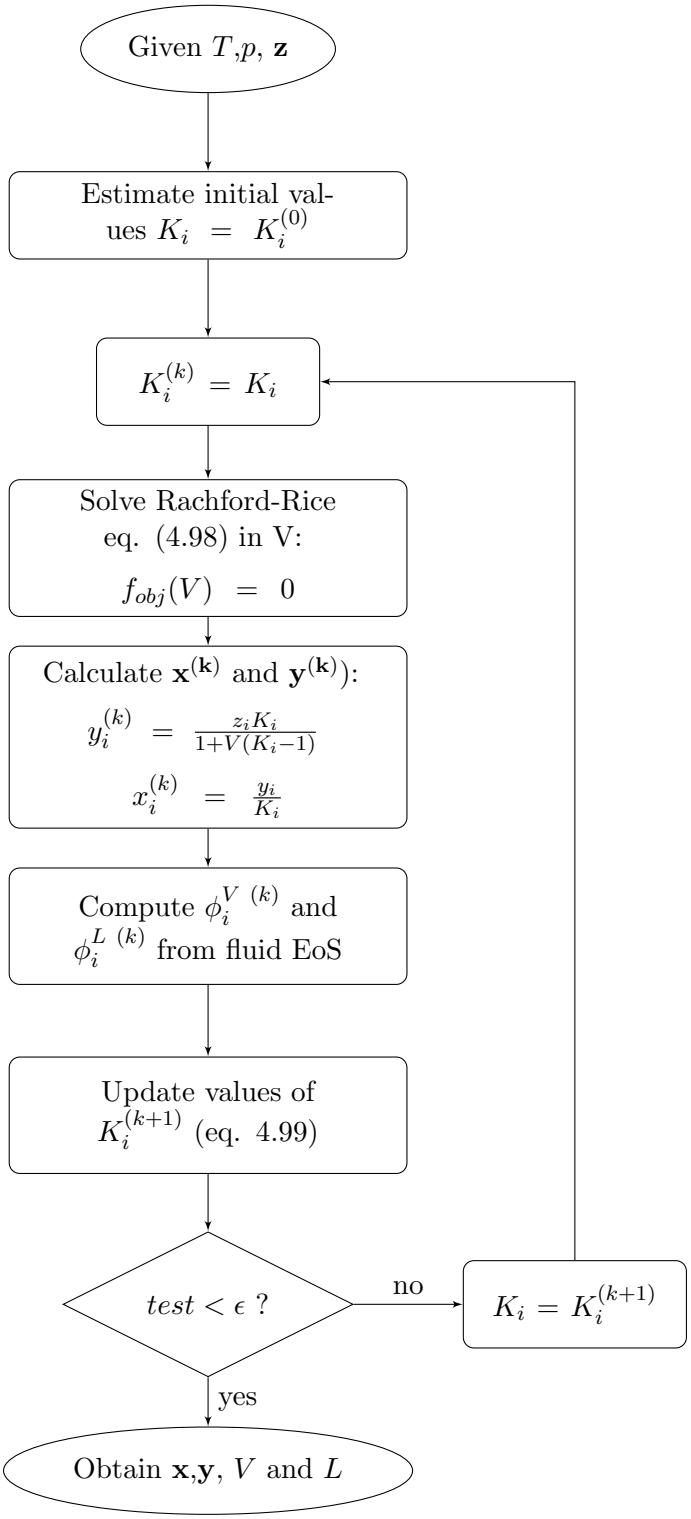

Figure 4.11: Flow diagram for pT-flash algorithm

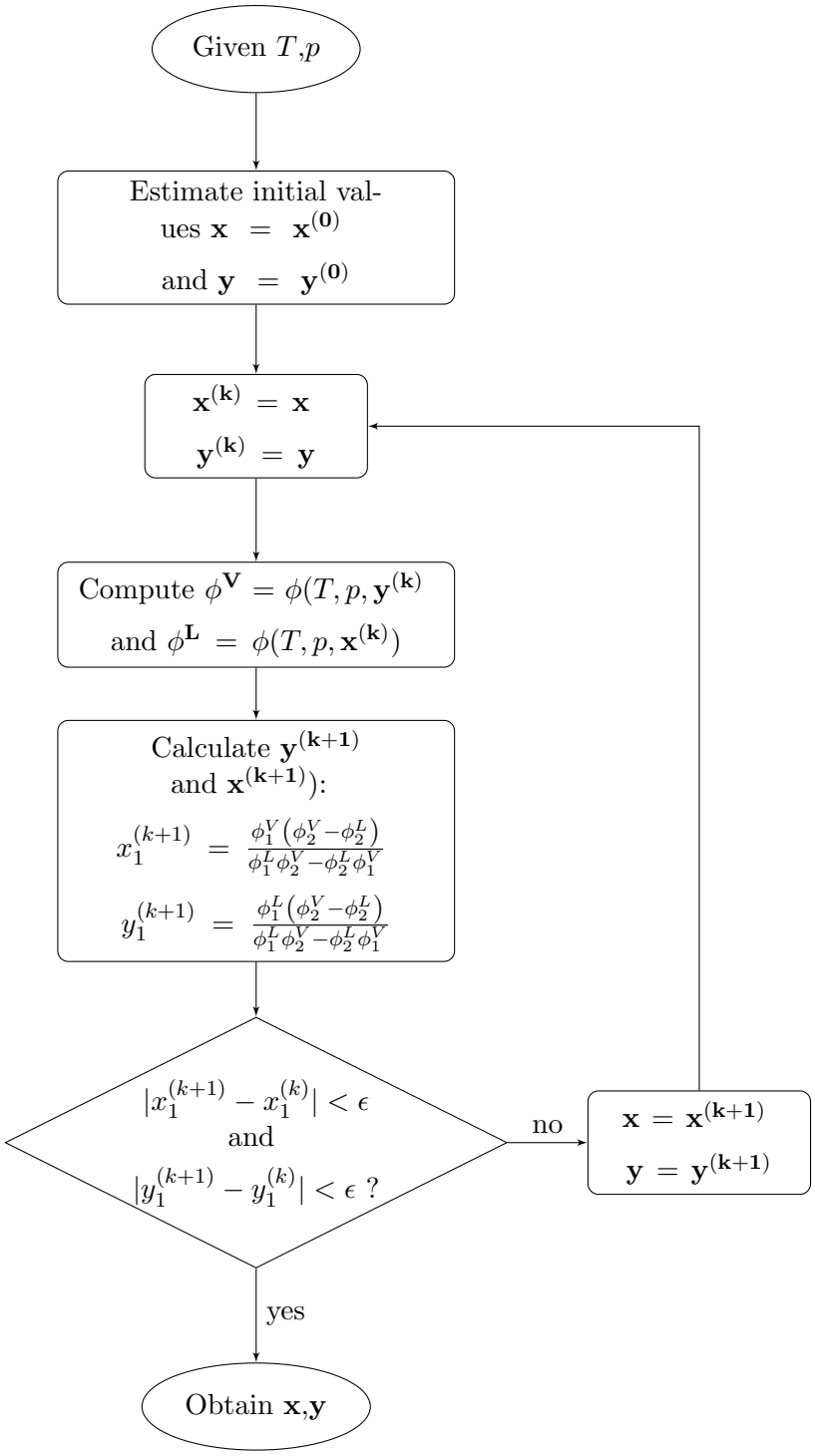

Figure 4.12: Flow diagram for *petit flash* algorithm

4.7 Results and comparison with data

A comparison between data and results obtained from the selected models, namely PR EoS+Zabaloy equation model and GERG+Jager and Span EoS, is proposed. The performances of the PR EoS have been tested using binary interaction parameters available in literature (see tab. 4.3) and binary interaction parameters regressed in this work on SLVE or SLE data (see tab. 4.4). Data presented in Chapter 3 are compared with results obtained with:

- PR EoS + Zabaloy model with k_{ij} available in literature (regressed on VLE data)
- PR EoS + Zabaloy model with k_{ij} regressed in this work (on SLVE and SLE data)
- Gerg 2008 EoS + Jager and Span model.

The comparison is made on vapor and liquid molar composition at experimental temperature and pressure. For SLE data, when experimental pressure is not furnished, calculated SLVE pressure is used, according to what observed on CO_2-CH_4 SLE data (see sec. 3.3).

The capability of each model in representing phase equilibrium literature data has been evaluated with reference to the following statistical indexes (for the generic property M):

$$AAD\% = \frac{100}{N}\sum_{i}^{N}\frac{\left|M_i^{calc} - M_i^{exp}\right|}{M_i^{exp}} \tag{4.103}$$

$$Bias\% = \frac{100}{N}\sum_{i}^{N}\frac{M_i^{calc} - M_i^{exp}}{M_i^{exp}} \tag{4.104}$$

$$MAD\% = max_{i=1,N}\left(100 \times \frac{\left|M_i^{calc} - M_i^{exp}\right|}{M_i^{exp}}\right) \tag{4.105}$$

Phase equilibrium data involving a solid phase have been compared and the results of the comparison are summarized in table 4.7 according to the type of equilibrium. A detailed list of results for all the binary system including carbon dioxide is proposed, according to the type of phase equilibrium data involving a solid phase: tab. 4.9 and tab. 4.10 for the SLE and SVE of the CH_4-CO_2 system, tab. 4.11 and tab. 4.12 for the SLE and SVE of the N_2-CO_2 system and tab. 4.13 for the SLE of the O_2-CO_2. Furthermore, the VLE of the binary CH_4-CO_2 system is studied in detail and results are presented in 4.8 and discussed in sec. 4.7.1.

Table 4.7: Results of the comparison between available data and results from models. (k_{ij} *lit*) refers to binary interaction parameters available in literature (tab. 4.3) and (k_{ij} *reg*) refers to binary interaction parameters regressed in this work (tab. 4.4)

Model	VLE (x_{CO_2})			SLE (x_{CO_2})			SVE (y_{CO_2})		
	BIAS	AAD	MAD	BIAS	AAD	MAD	BIAS	AAD	MAD
PR (k_{ij} *lit*)+Zabaloy	3.8%	6.9%	143.4%	505.7%	513.0%	2441.7%	20%	21%	32%
PR (k_{ij} *reg*)+Zabaloy	6.3%	9.9%	149.1%	3.0%	26.4%	50.6%	12%	13%	14%
GERG +Jager	2.2%	6.0%	100.7%	58.5%	66.9%	255.9%	21%	22%	42%

4.7.1 Discussion

Calibrating the PR EoS binary interaction parameters on SLVE or SLE sensibly increases the accuracy of the prediction of the CO_2 solubility in liquid or vapor phase. Performance improvement is evident, especially for the CO_2 solubility in the liquid phase. The PR EoS + Zabaloy equation model still overestimates the solubility of carbon dioxide in liquid methane

but BIAS is significantly reduced. PR EoS+Zabaloy equation model has slightly better results than GERG+Jager and Span EoS in predicting CO_2 solubility in liquid methane. This can be explained by the fact that 47% of the SLE data for the binary CH_4-CO_2 system are outside (being at lower temperature) the range of temperature of the data used for the regression of the GERG 2008 departure function (see tab. 4.6). Also for the N_2-CO_2 system, all SVE and SLE data are at temperature lower than the range in which the GERG 2008 EoS is calibrated. Nevertheless it must be said that the behavior of the GERG EoS remain reasonable, and solubility in the vapor phase for the CH_4-CO_2 system is even better predicted by the GERG+Jager and Span Eos model than the PR EoS+Zabaloy model. On the contrary the GERG EoS is limited to 90 K for systems involving carbon dioxide because of the limits of the pure CO_2 EoS (see tab. 4.5). For temperature lower than 90 K, calculation are thus not performed. For temperature higher than 90 K, CO_2 solubility in liquid phase obtained from the GERG+Jager and Span Eos model is greater than the results obtained from the PR EoS+Zabaloy equation.

The obvious consequence of regressing the binary interaction parameter not on VLE data but on SLVE data is a reduced accuracy of the model in predicting VLE conditions (see tab.4.8). An interesting conclusion, however, is that comparing the performances in representing the low temperature VLE of the binary $CH_4 - CO_2$ mixture, the PR EoS with with k_{ij} regressed on SLVE data has lower deviation: considering the range of temperature from 153 to 203 K (see fig. 4.13) the AAD for the PR with parameters from literature is 30.3%, while for the PR with parameters regressed in this work is 29.2%. The choice of using binary interaction parameter regressed on SLVE data is thus coherent with the aim of this work of representing the phase equilibrium of the biogas system at cryogenic temperature. On the other hand, as expected, the GERG EoS shows better results in calculating the vapor-liquid equilibrium on the entire range of temperature for the studied systems.

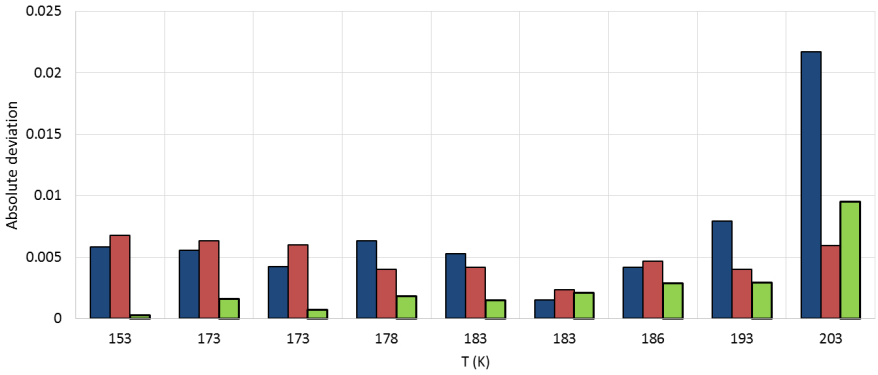

Figure 4.13: Absolute deviation between calculated and experimental CO_2 composition in liquid phase $|x_{calc} - x_{exp}|$ for low temperature VLE condition: ■ PR EoS with k_{ij} from literature, ■ PR EoS with k_{ij} from this work, ■ GERG2008 EoS

The bibliographic research on phase equilibrium data proposed in Chap. 3, together with the data analysis through thermodynamic models, allows identifying the regions where more measurements are needed for better defining the phase equilibrium behavior of a methane rich system including a solid phase. In particular, for studying the behavior of a biogas and landfill gas type mixture, it is interesting to investigate the influence of nitrogen and oxygen on the solid formation conditions of a mixture containing methane and carbon dioxide system. Ternary N_2-CH_4-CO_2 data are few and, to the authors' knowledge, phase equilibrium for the O_2-N_2-CH_4-CO_2 mixture has not been experimentally investigated at now. In next section, original data for the aforementioned systems are proposed.

				PR k_{ij} *lit*		PR k_{ij} *reg*		GERG2008	
Authors	T (K)	p (Mpa)		liq	vap	liq	vap	liq	vap
Donnelly and Katz (1954)	200-271	1.48-7.90	Ncalc	83	50	83	50	83	50
			BIAS	-3.6%	5.4%	7.2%	8.1%	-1.2%	8.6%
			AAD	4.5%	6.0%	7.4%	8.5%	3.6%	9.0%
			MAD	20.3%	36.5%	33.0%	48.6%	24.7%	47.0%
Kaminishi et al. (1968)	233-283	3.70-8.19	Ncalc	15	17	15	17	15	17
			BIAS	-0.3%	-1.3%	5.8%	-0.5%	1.7%	-0.5%
			AAD	0.9%	1.5%	5.8%	1.1%	1.8%	1.3%
			MAD	2.1%	5.2%	20.9%	5.1%	4.6%	5.4%
Neumann and Walch (1968)	173-220	2.58-6.00	Ncalc	55	49	54	48	56	56
			BIAS	31.3%	32.7%	30.1%	40.4%	-1.3%	-1.3%
			AAD	37.5%	33.8%	53.6%	40.4%	19.4%	33.7%
			MAD	143.4%	95.8%	149.1%	133.2%	73.6%	91.0%
Arai et al. (1971)	253-288	2.63-8.52	Ncalc	34		34		34	
			BIAS	15.1%		18.0%		16.6%	
			AAD	15.9%		18.1%		16.9%	
			MAD	67.0%		71.2%		69.2%	
Davalos et al. (1976)	230-270	0.89-8.52	Ncalc	33	33	33	33	36	36
			BIAS	0.6%	1.3%	8.1%	2.1%	2.3%	2.4%
			AAD	1.0%	3.1%	8.1%	3.7%	2.4%	3.6%
			MAD	4.4%	7.1%	27.5%	8.8%	7.9%	9.7%
Mraw et al. (1978)	173-219	0.58-6.49	Ncalc	43		44		45	
			BIAS	-1.3%		14.3%		-1.0%	
			AAD	9.8%		17.6%		5.1%	
			MAD	69.7%		114.4%		28.0%	
Somait and Kidnay (1978)	270	3.20-8.43	Ncalc	11	11	11	11	12	12
			BIAS	-0.5%	-1.0%	1.4%	-0.4%	0.6%	-0.5%
			AAD	0.7%	1.0%	1.4%	1.1%	0.6%	1.2%
			MAD	1.4%	5.4%	6.4%	5.3%	4.3%	5.8%
Al-Sahhaf et al. (1983)	219-270	0.58-8.41	Ncalc	61	55	61	55	58	58
			BIAS	0.4%	-1.9%	4.0%	-1.1%	2.3%	-0.7%
			AAD	1.3%	1.9%	7.6%	1.6%	2.4%	1.7%
			MAD	8.4%	9.1%	47.7%	9.9%	12.8%	9.1%
Vetere (1983)	230	1.12-5.25	Ncalc	14	14	14	14	14	14
			BIAS	33.9%	16.0%	40.1%	17.2%	37.4%	18.3%
			AAD	33.9%	18.7%	40.1%	19.3%	37.4%	20.1%
			MAD	74.9%	34.8%	87.1%	35.0%	80.8%	36.2%
Xu et al. (1992a)	288-293	5.12-8.16	Ncalc	21	21	21	21	23	23
			BIAS	0.0%	0.0%	0.7%	0.4%	0.7%	0.0%
			AAD	0.5%	0.6%	0.7%	0.7%	0.7%	0.5%
			MAD	1.7%	3.0%	3.6%	2.7%	3.9%	3.3%
Bian et al. (1993)	301	6.86-7.56	Ncalc	5	5	5	5	6	6
			BIAS	-0.5%	0.2%	-0.6%	-0.2%	-0.3%	-0.3%
			AAD	0.5%	0.3%	0.6%	0.2%	0.3%	0.3%
			MAD	1.0%	0.6%	1.2%	0.5%	0.6%	0.7%
Webster and Kidnay (2001)	230-270	0.89-8.38	Ncalc	49	49	49	49	52	52
			BIAS	0.2%	-2.0%	5.4%	-1.2%	1.8%	-0.8%
			AAD	1.0%	2.1%	5.4%	1.5%	1.8%	1.4%
			MAD	9.8%	12.2%	35.9%	11.1%	13.2%	10.3%
Total	173-301	058-8.52	BIAS	5.6%	6.3%	11.6%	7.6%	3.0%	1.8%
			AAD	9.5%	8.5%	15.5%	10.9%	7.2%	9.1%
			MAD	143.4%	95.8%	149.1%	133.2%	80.8%	91.0%

Table 4.8: Comparison between experimental and calculated liquid and vapor molar composition of CO_2 at experimental VLE temperature and pressure for the binary CH_4-CO_2 system. (k_{ij} *lit*) refers to binary interaction parameters available in literature (tab. 4.3) and (k_{ij} *reg*) refers to binary interaction parameters regressed in this work (tab. 4.4)

Authors	T(K)	p(Mpa)		PR (k_{ij} *lit*)	PR (k_{ij} *reg*)	GERG2008
Donnelly and Katz (1954)	194-213	4.29-4.59	Ncalc	3	3	2
			BIAS	11.9%	-13.6%	-8.5%
			AAD	24.9%	22.7%	22.9%
			MAD	44.0%	41.5%	31.4%
Brewer and Kurata (1958)	190-215	-	Ncalc	8	8	8
			BIAS	13.8%	2.0%	6.3%
			AAD	18.8%	14.5%	19.5%
			MAD	38.1%	45.8%	39.6%
Boyle (1987)	111-128	-	Ncalc	5	5	5
			BIAS	51.4%	7.4%	10.4%
			AAD	52.5%	7.7%	10.4%
			MAD	70.0%	15.5%	16.0%
Cheung and Zander (1968)	110-194	-	Ncalc		9	
			BIAS	63.4%	20.2%	24.0%
			AAD	67.1%	25.9%	33.8%
			MAD	144.7%	62.7%	90.5%
Streich (1970)	110-218	-	Ncalc	12	12	12
			BIAS	14.7%	-16.3%	-11.6%
			AAD	23.0%	23.3%	20.4%
			MAD	56.2%	53.8%	43.8%
Preston et al. (1971)	126-137	-	Ncalc	2	2	2
			BIAS	168.1%	83.9%	53.1%
			AAD	168.1%	83.9%	79.4%
			MAD	199.1%	100.2%	132.4%
Voss (1975)	112-193	-	Ncalc	22	22	22
			BIAS	67.8%	22.3%	25.8%
			AAD	67.8%	23.4%	24.6%
			MAD	131.3%	46.1%	50.7%
Shen et al. (2012)	112-170	0.09-2.31	Ncalc	9	9	9
			BIAS	85.1%	30.4%	30.8%
			AAD	85.1%	30.4%	30.8%
			MAD	127.8%	42.0%	48.7%
Gao et al. (2012)	113-170	-	Ncalc	9	9	9
			BIAS	92.1%	34.5%	49.2%
			AAD	92.1%	34.5%	49.2%
			MAD	222.9%	99.3%	159.6%
Pikaar (1959)	143-204	0.75-5.2	Ncalc	21	21	20
			BIAS	33.4%	6.9%	22.6%
			AAD	33.4%	9.4%	23.9%
			MAD	72.9%	28.1%	67.5%
Total	110-215	0.09-5.2	Ncalc	70	79	69
			BIAS	36.5%	9.6%	11.3%
			AAD	39.8%	19.0%	20.1%
			MAD	199.1%	100.2%	132.4%

Table 4.9: Comparison between experimental and calculated liquid composition of CO_2 at SLE conditions for the binary CH_4-CO_2 system. (k_{ij} *lit*) refers to binary interaction parameters available in literature (tab. 4.3) and (k_{ij} *reg*) refers to binary interaction parameters regressed in this work (tab. 4.4)

Authors	T(K)	p(Mpa)		PR (k_{ij} *lit*)	PR (k_{ij} *reg*)	GERG2008
Pikaar (1959)	132-210	0.16-4.83	Ncalc	103	103	103
			BIAS	11.2%	7.9%	5.3%
			AAD	11.2%	8.9%	5.4%
			MAD	16.3%	44.1%	24.0%
Agrawal and Laverman (1974)	137-198	0.17-2.78	Ncalc	41	41	41
			BIAS	3.6%	4.6%	3.4%
			AAD	11.5%	15.1%	15.3%
			MAD	28.0%	41.6%	41.6%
Le and Trebble (2007)	168-187	0.96-3.00	Ncalc	55	55	55
			BIAS	29.9%	27.3%	22.1%
			AAD	33.6%	31.5%	29.0%
			MAD	85.2%	80.6%	75.9%
Zhang et al. (2011)	196-210	0.29-4.45	Ncalc	17	17	17
			BIAS	4.5%	3.8%	0.2%
			AAD	6.2%	5.8%	5.0%
			MAD	15.1%	15.1%	9.8%
Xiong et al. (2015)	153-193	0.27-3.04	Ncalc	62	62	62
			BIAS	8.5%	7.7%	5.5%
			AAD	14.4%	14.0%	12.6%
			MAD	75.3%	73.0%	88.8%
Total	132-210	0.16-4.83	Ncalc	216	216	216
			BIAS	13.3%	11.0%	8.2%
			AAD	14.4%	12.7%	10.4%
			MAD	85.2%	80.6%	75.9%

Table 4.10: Comparison between experimental and calculated vapor composition of CO_2 at SVE conditions for the binary CH_4-CO_2 system. (k_{ij} *lit*) refers to binary interaction parameters available in literature (tab. 4.3) and (k_{ij} *reg*) refers to binary interaction parameters regressed in this work (tab. 4.4)

Authors	T(K)	p(Mpa)		PR (k_{ij} *lit*)	PR (k_{ij} *reg*)	GERG2008
Fedorova (1940)	67 - 98	-	Ncalc	4	4	2
			BIAS	132.8%	23.7%	135.0%
			AAD	204.0%	112.0%	135.0%
			MAD	495.9%	232.4%	179.0%
Yakimenko et al. (1975)	75-115	-	Ncalc	9	9	6
			BIAS	20.9%	-33.9%	-16.7%
			AAD	31.0%	33.9%	19.9%
			MAD	45.6%	79.0%	45.4%
Rest et al. (1990)	91 - 115	-	Ncalc	5	5	4
			BIAS	153.4%	31.3%	59.0%
			AAD	153.4%	31.3%	60.6%
			MAD	180.1%	51.5%	135.9%
Total	67-115	-	Ncalc	18	18	12
			BIAS	82.6%	-3.0%	33.8%
			AAD	103.5%	50.6%	52.6%
			MAD	495.9%	232.4%	179.0%

Table 4.11: Comparison between experimental and calculated liquid composition of CO_2 at SLE conditions for the binary N_2-CO_2 system. (k_{ij} *lit*) refers to binary interaction parameters available in literature (tab. 4.3) and ((k_{ij} *reg*) refers to binary interaction parameters regressed in this work (tab. 4.4)

Authors	T(K)	p(Mpa)		PR (k_{ij} *lit*)	PR (k_{ij} *reg*)	GERG2008
Sonntag and Van Wilen (1961)	140 - 190	0.5 - 10.1	Ncalc	64	64	64
			BIAS	25.1%	15.7%	23.8%
			AAD	25.1%	15.8%	23.8%
			MAD	40.0%	33.2%	61.8%
Smith et al. (1964)	140 - 190	5.1 - 20.3	Ncalc	64	64	64
			BIAS	38.3%	11.8%	61.0%
			AAD	38.3%	11.8%	61.0%
			MAD	62.9%	19.4%	122.5%
Total	140-190	0.5-20.3	Ncalc	128	128	128
			BIAS	31.7%	13.8%	42.4%
			AAD	31.7%	13.8%	42.4%
			MAD	62.9%	33.2%	122.5%

Table 4.12: Comparison between experimental and calculated vapor composition of CO_2 at SVE conditions for the binary N_2-CO_2 system. (k_{ij} *lit*) refers to binary interaction parameters available in literature (tab. 4.3) and (k_{ij} *reg*) refers to binary interaction parameters regressed in this work (tab. 4.4)

Authors	T(K)	p(Mpa)		PR (k_{ij} *lit*)	PR (k_{ij} *reg*)	GERG2008
Fedorova (1940)	67-98	-	Ncalc	5	5	2
			BIAS	1330.4%	-27.7%	568.5%
			AAD	1370.0%	92.0%	568.5%
			MAD	4474.8%	160.8%	808.1%
Rest et al. (1990)	91-107	-	Ncalc	3	3	3
			BIAS	3853.2%	-26.8%	326.4%
			AAD	3853.2%	39.1%	326.4%
			MAD	4810.7%	97.7%	369.9%
De Stefani et al. (2002)	90-110	-	Ncalc	13	13	13
			BIAS	2528.1%	-9.7%	191.5%
			AAD	2528.1%	9.7%	191.5%
			MAD	4727.2%	12.5%	358.5%
Total	67-110	-	Ncalc	21	21	18
			BIAS	2432.2%	-16.4%	255.9%
			AAD	2441.7%	33.5%	255.9%
			MAD	4810.7%	160.8%	808.1%

Table 4.13: Comparison between experimental and calculated liquid composition of CO_2 at SLE conditions for the binary O_2-CO_2 system. (k_{ij} *lit*) refers to binary interaction parameters available in literature (tab. 4.3) and (k_{ij} *reg*) refers to binary interaction parameters regressed in this work (tab. 4.4)

Chapter 5

Original phase equilibrium measurements

In this chapter the apparatus and procedure for producing original phase equilibrium measurements are presented and the results are commented and compared with model and other literature data.

Résumé

La recherche bibliographique sur les données d'équilibre entre phases proposée au Chap. 3, ainsi que l'analyse des données par des modèles thermodynamiques (Chap. 4), permet d'identifier les régions où davantage de mesures sont nécessaires pour mieux définir le comportement d'équilibre de phases d'un système riche en méthane incluant une phase solide. En particulier, pour étudier le comportement d'un mélange de type biogaz et de type gaz naturel, il est intéressant d'étudier l'influence de l'azote et de l'oxygène sur les conditions de formation d'un mélange contenant du méthane et du dioxyde de carbone. Les données pour le système N_2-CH_4-CO_2 sont rares et, d'après l'étude bibliographique, l'équilibre de phases pour le mélange O_2-N_2-CH_4-CO_2 n'a pas fait l'objet d'études expérimentales à ce jour. C'est pour cela que dans ce travail on produit des données originales d'équilibre solide-liquide-vapeur (SLVE) à basse température pour les systèmes susmentionnés. Le domaine de température et pression de ces mesures se rapproche des conditions opératoires du procédé Cryo Pur: température entre 125 et 146 K et pression inférieur à 20 bar.

L'apparat de mesure se compose d'une cellule d'équilibre (EC) placée dans un Dewar de 55 litres, partiellement rempli d'azote liquide (LN2). La cellule d'équilibre est aussi enveloppée par une résistance électrique régulée par un régulateur de température. La source froide (azote liquide) couplée à la résistance électrique permet la régulation de température dans la cellule. La température est mesurée en haut et en bas de la cellule au moyen de deux sondes de température PT100Ω (à 0 ° C). La température moyenne entre les deux sondes est calibrée sur les courbes saturées de méthane pur et d'oxygène pur. La pression dans la cellule est mesurée par un capteur de pression PTX611 Druck de 16 MPa. La cellule est équipée de deux échantillonneurs pneumatiques ROLSI, reliés au chromatographe à gaz (GC) par une ligne de transfert thermostatée. Le dispositif GC de type Perichrom PR 2100 est équipé d'un détecteur de conductivité thermique (TCD) et d'un détecteur d'ionisation de flamme (FID) pour analyser la composition des échantillons. Le mélange est chargé dans la cellule à température ambiante puis refroidi à trois températures différentes 146, 132 et 125 K en réglant le régulateur de température. Au total 4 séries différentes de mesures, à savoir quatre mélanges de composition globale différents sont effectués. En comparant les résultats expérimentaux obtenus dans ce travail et les données

de littérature sur la solubilité du CO_2 pour le mélange binaire de CH_4-CO_2, on peut observer

que l'ajout d'azote et d'oxygène dans le méthane diminue la solubilité du CO_2 en phase liquide. L'effet peut être expliqué en étudiant la solubilité du CO_2 dans l'oxygène liquide et l'azote, qui est beaucoup plus faible que dans le méthane liquide, suivant les données de la littérature. On peut donc conclure que la teneur en méthane en phase liquide a un effet majeur sur la solubilité du CO_2 en phase liquide. Lorsque de l'azote et de l'oxygène sont ajoutés au méthane, la teneur en méthane en phase liquide diminue et donc la solubilité du CO_2 diminue également. Cette conclusion n'est pas en accord avec les résultats expérimentaux de littérature.

5.1 Introduction

In order to allow good process simulation and understand the phase behavior at low temperatures, models need to be supported by, and compared with, experimental measurements. In literature, a number of measurements are available for the binary CH_4-CO_2 mixture involving the solid phase (see sec. 3.3). SLVE data usually do not provide the composition of fluid phases. Furthermore data involving a solid CO_2 phase in the multicomponent mixtures of CH_4-CO_2 with N_2 and O_2 are few. Solubility data for a mixture of CH_4-N_2-CO_2 in the low temperature range have been proposed by Shen et al. (2012) and Gao et al. (2012), but they only provide CO_2 content in the liquid phase.

Original low temperature SLVE measurements have been produced in this work. The measurement are performed in the range of conditions of interest for the process: temperature lower than 150 K and pressure lower than 20 bar. According to what previously expressed, both liquid and vapor CO_2 content are important to be known for determining solid formation conditions in the process. In this range of conditions expected CO_2 solubility is between 10000 and 1000 ppm in liquid phase and down to 20 ppm in the vapor phase. Particular attention has thus to be paid to the analytic method for CO_2 detection. The phase behavior of landfill gas at low temperature is studied by measuring the SLVE of the ternary mixture of N_2-CH_4-CO_2 and the quaternary mixture of N_2-O_2-CH_4-CO_2 with N_2/O_2 ratio similar to the ratio of these components in air.

Original measurements allow to test the model performances at low temperature for multicomponent mixtures. Furthermore model parameters for the O_2-CH_4 system are missing because of the lack of data. Original measurements with the quaternary mixture containing O_2 allow to compare the model prediction of vapor-liquid distribution ratio of oxygen in a mixture containing methane.

The measurement campaign is planned in order to have four series of three points for each series; each point is at different temperatures (148, 135 and 128 K). The first and second series of measurement are with two ternary mixtures of N_2-CH_4-CO_2 and the third and fourth are with two quaternary mixtures of N_2-O_2-CH_4-CO_2.

5.2 Experimental apparatus description

In this section, a description of the experimental apparatus employed for producing the original data is proposed. The facility is used for obtaining low temperature SLVE measurements for the ternary CH_4-CO_2-N_2 mixture and quaternary CH_4-CO_2-N_2-O_2 mixture. The gas mixture is loaded into an equilibrium cell (EC) and the solid presence is indirectly detected by composition analysis of the fluid phases. An image and a flow diagram of the apparatus are represented in fig. 5.1 and fig. 5.2. A focus on the cell assembly is presented in fig. 5.3.

The apparatus used in this work is a slightly modified version of the original apparatus used for low temperature VLE measurements (Baba-Ahmed et al., 1999) and solubility data (De Stefani et al., 2002; Stringari et al., 2012). Recently the apparatus has been used for determining solid formation conditions (Lange, 2015). A similar experimental apparatus is used by the Institute of Refrigeration and Cryogenics of the Shanghai Jiao Tong University for low temperature solubility measurements (Shen et al., 2012; Gao et al., 2012; Xiong et al., 2015) and by the Centre for Energy at School of Mechanical & Chemical Engineering At the University of Western Australia for low temperature VLE measurements (Kandil et al., 2010, 2011; Hughes et al., 2015).

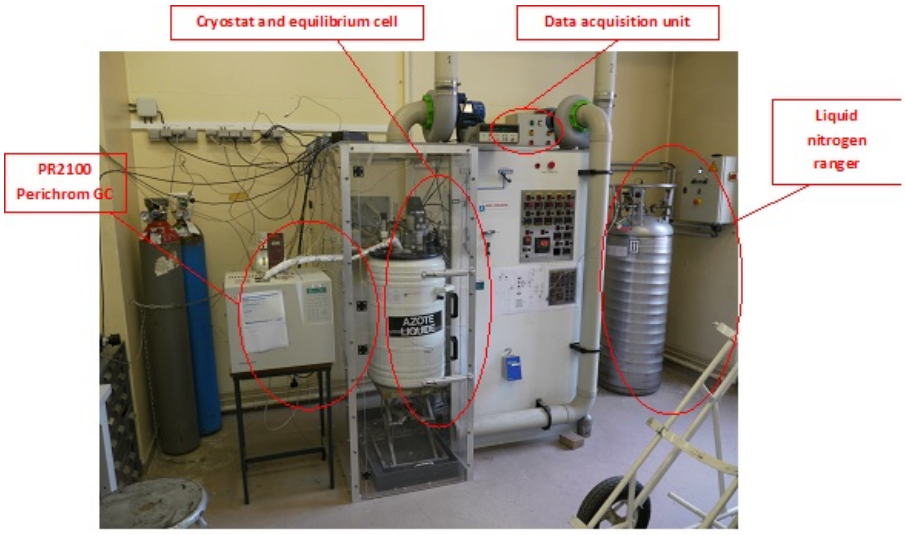

Figure 5.1: Overview of the experimental apparatus

5.2.1 Equilibrium cell and feed circuit

The 40 cubic centimeters equilibrium cell (EC) is made of Hastelloy C276 and it is surrounded by a brass shell (2) (fig. 5.3) closed with a brass cap (3). Inside the equilibrium cell there is an axis (9) holding a rotating magnetic bar covered with titanium (10) driven by a motor through the stirring assembly. The magnetic bar is raised by a support (11) in order to prevent blockages when the solid phase forms at the bottom of the cell. The stirrer is essential for assuring the equilibrium between existing phases. A key aspect when working at low temperature and moderate or high pressure is the nature of the seals used. In the apparatus described in this work, in-house made Teflon+stainless steel joints are used.

The loading of the gas mixture is done by the valve V1 (fig. 5.2) connecting the EC to the feed circuit. The pressure of the feed circuit is measured by a 200 bar PTX611 Druck pressure transducer (HP 200 bar). For emptying the cell and the circuit, the valve V5 and V6 are connected to a purge system equipped with a vacuum pump. The valve V3b is connected to a variable volume cell (PV) allowing loading liquid components in the cell. Suppliers and purity of all components used in this work are listed in tab. 5.1.

Table 5.1: Gas purities and suppliers of components used in this work

Component	Supplier	Declared purity (vol %)
N_2	Air Liquide	99.995
O_2	Air Liquide	99.999
CH_4	Air Liquide	99.995
CO_2	Air Liquide	99.995

5.2.2 Temperature regulation and data analysis devices

The equilibrium cell is placed into a 55 liters Dewar, partially filled with liquid nitrogen (LN2). In this way, the cell is surrounded by a nitrogen vapor atmosphere at temperature equal to the nitrogen normal boiling point (77.3 K). The equilibrium cell is surrounded by a brass shell closed with a brass cap. The brass shell is wrapped by an electric resistance regulated by a

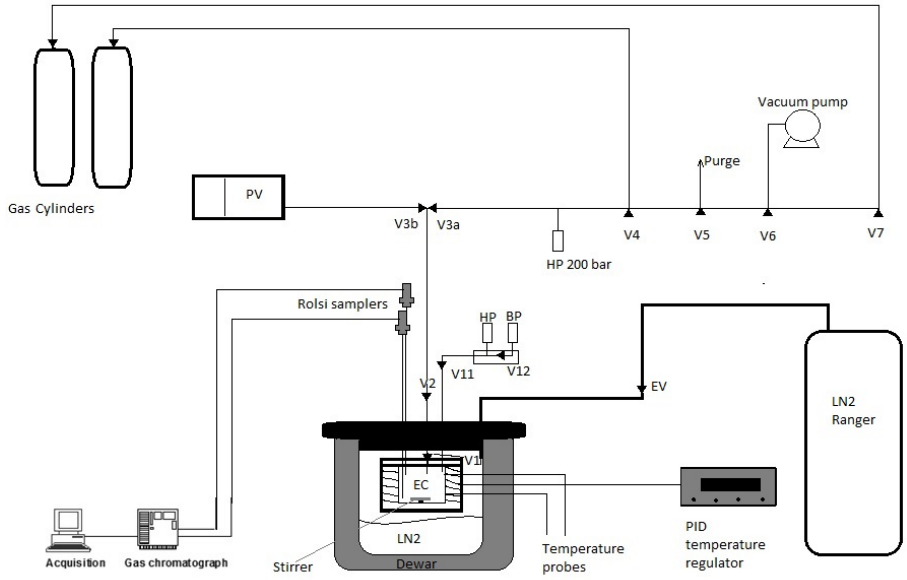

Figure 5.2: Scheme for the experimental unit used in this work

Fuji electric PXR PID temperature regulator. Another heater is in contact with the brass cap and connected to another independent PID regulator. The cold source (liquid nitrogen) coupled with the electric resistance allows temperature regulation in the cell. The liquid nitrogen should not touch the bottom of the cell to avoid its over-cooling. The liquid nitrogen is supplied from a 176 liters ranger intended for this purpose.

The temperature is measured at the top and at the bottom (see fig. 5.3), by means of two PT100Ω (at 0°C) temperature probes, in order to measure the temperature gradient established inside the cell that can be present due to the position of the cold source. The difference in temperature between lower and upper part of the cell has been initially estimated between 1 and 2 K, depending on the level of liquid nitrogen. It has to be noticed that with the calibration of the temperature probes performed in this work (see B) it is not possible to measurement the temperature gradient because each probe is not independently calibrated, but only the average temperature. According to a further calibration campaign, where the two probes are independently calibrated, the difference in the temperature measured in the upper and lower part of the cell is estimated to be less than 0.5 K.

The pressure in the EC is measured by a 160 bar PTX611 Druck pressure transducer and a 1.6 bar PTX611 Druck pressure transducer (which can be isolated by means of valve V12 when working pressure is higher than 1.6 bar). In addition, both the pressure transducers can be isolated from the cell by means of the valve V11.

The acquisition system (Agilent 34970A Data Acquisition / Switch Unit) collects temperature and pressure data from the temperature probes and pressure transducer, and sends it to a computer for the analysis.

5.2.3 Samples analysis

The cell is equipped with two pneumatic ROLSI^{TM} samplers with stainless steel capillaries. The nominal internal diameter of both the capillaries is 0.1 mm, and their length is 140 and 168

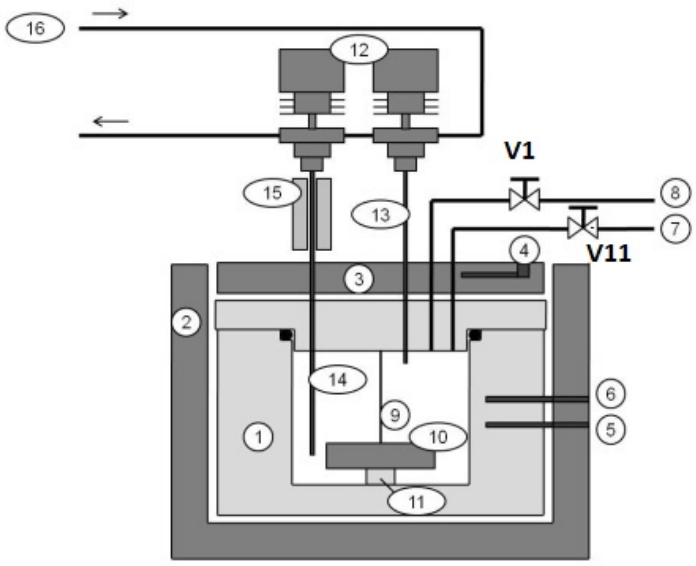

Figure 5.3: Details of the equilibrium cell assembly. 1, equilibrium cell; 2, brass shell; 3, brass cap; 4, position of the heating cartridge for temperature regulation of the brass cap; 5, 6 position of Pt100 probes for temperature measurement; 7, connection to the pressure transducers; 8, loading line; 9, axis; 10, titanium covered magnetic bar; 11, support; 12, ROLSI samplers; 13 and 14, capillaries for sampling vapor and liquid respectively; 15, heating cartridge; 16, transfer line. (Stringari et al., 2012)

mm respectively for vapor (ROLSIV) and liquid (ROLSIL) sampling. The temperature of the part of the liquid capillary between the cell and the ROLSI sampler is controlled by a heating cartridge connected to a PID regulator (see fig. 5.3) in order to avoid undesired solidification and condensation during the operations. The temperature of the core of the ROLSI samplers is also kept at 100°C by a heating system connected to a PID regulator. The ROLSI samplers are connected to the Gas Chromatograph (GC) through a thermostated transfer line. The samples are withdrawn thanks to the pressure difference between the cell and the transfer line. The minimum pressure that can be reach in the cell allowing sampling the mixture is thus around 5 bar.

The GC device is a Perichrom PR 2100 type equipped with a Thermal Conductivity Detector (TCD) and a Flame Ionisation Detector (FID) for analyzing the composition. In the gas chromatograph device, one or two Porapak Q column are placed (depending on the system to study), 80/100 mesh, 1/8" external diameter, 2 mm internal diameter and 4 m long made in Silcosteel. Operational temperatures of the oven is set for each series of measure, depending on the components to be analyzed. The carrier gas used is helium, and the flow is optimized depending on oven temperature and length of the column. GC operating conditions are resumed in tab. 5.2.

5.2.4 Methanizer

The CO_2 content in fluid phases at low temperature SLVE is expected to be in the range of 10000 to 20 ppm. For this reason the CO_2 peak cannot be observed, for the lowest quantities, on the Thermal Conductivity Detector (TCD). The detection of the CO_2 peak is performed by a Flame Ionisation Detector (FID). Since the FID cannot directly detect CO_2, a methanizer is installed for reducing CO_2 into methane, which can be detected by the FID. The methanizer is a U-tube containing 0.2 g of nickel catalyst, kept at 300°C for allowing the complete conversion

Table 5.2: GC operating conditions for the composition analysis of the SLVE measurements

Type of measurements	N_2-CH_4-CO_2 SLVE	N_2-O_2-CH_4-CO_2 SLVE
Column	4m Porapak Q	2 x 4m Porapak Q
Oven Temperature	70 °C	-25 °C for 6.5 min
		60 °C/min ramp
		70 °C for 14 min
N_2 Retention time (min)	0.9	5.3
O_2 Retention time (min)	-	6.3
CH_4 Retention time (min)	1.25	10.2
CO_2 Retention time (min)	2.5	16
Carrier gas	He	He
Carrier flow (ml/min)	21	21
Carrier gas pressure (kPa)	212	230 - 330
CarRef pressure (kPa)	74	65
TCD temperature	120 °C	120 °C
FID temperature	300 °C	300 °C
H_2 flow (injected to the FID) (ml/min)	3 (5 kPa)	3 (5 kPa)
H_2 flow (injected to the Methaniser) (ml/min)	30	30
Air flow (FID) (ml/min)	240 (50 kPa)	240 (50 kPa)

of CO_2 into CH_4 following the reaction

$$CO_2 \ + \ 4 \ H_2 \longrightarrow CH_4 \ + \ 2 \ H_2O \tag{5.1}$$

The hydrogen flow is assured by a Hydrogen Generator, providing a total flow of 34 ml/min of hydrogen to the FID, in part injected directly in the FID, in part injected to the methanizer. Maintenance of the methanizer is performed regularly by thermal conditioning at 430°C. At the end of the series of measurements the catalyst is replaced with a new one.A scheme of the GC circuit is presented in figure 5.4.

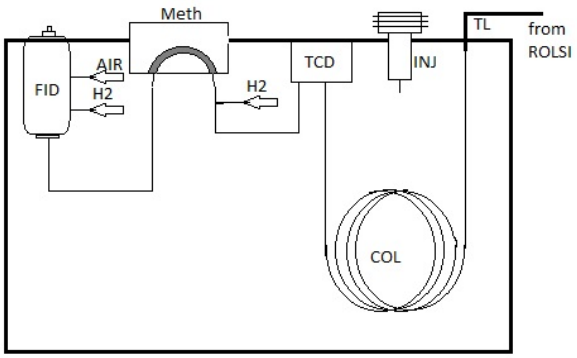

Figure 5.4: Schematic representation of the equipment installed in the GC: transfer line (TL), injector (INJ), packed column (COL), Thermal Conductivity Detector (TCD), hidrogen and air inlets (H2, AIR), methanizer (Meth), Flame Ionisation Detector (FID)

5.3 Experimental procedure

A static non-visual methodology is used for determining the SLVE data at low temperature for the ternary N_2-CH_4-CO_2 mixture and quaternary N_2-O_2-CH_4-CO_2 mixture. In order to

obtain temperature, pressure and liquid and vapor phase compositions at SLVE conditions, the adopted procedure is made of three main steps:

1. the loading of the cell;
2. the cooling program for reaching the desired temperature;
3. composition analysis of liquid and vapor phase.

Once the equilibrium cell is evacuated and put under vacuum, the mixture with desired composition is loaded into the cell. The loading pressure is calculated using the GERG Equation of State, while the loading temperature is ambient temperature. Each pure components is loaded into the cell separately from a gas cylinder. Once the mixture is completely loaded at ambient temperature and desired pressure, the cell is isolated from loading circuit by means of valve V1 (see fig. 5.2), the magnetic stirrer is activated for assuring perfect mixing in the cell and the global composition of the loaded mixture is checked by GC analysis. Before each sampling, ROLSI samplers are purged.

After the loading of the cell, the dewar is filled with liquid nitrogen at the half of its volume, to avoid the contact between the bottom of the cell and the liquid nitrogen. The temperature and the pressure inside the cell are continuously recorded and the system is cooled down by setting the temperature regulator. A first rapid cooling is performed down to a temperature set 5 K greater than the expected solid formation temperature. When the system stably reaches this temperature, a second slow cooling is executed down to 148 K. The cooling rate is set to 0.5 K/h, and once the temperature is reached, the system is kept at stable temperature for around 48h, checking the stability of pressure. During this period temperature and pressure of the mixture are constant, and thus the vapor and liquid phase are sampled for the composition analalysis. Once the composition is analyzed, the dewar is refilled with liquid nitrogen and temperature is slowly decreased down to 135 K with same cooling rate (0.5 K/h). The system is thus kept at stable temperature for around 48h, and composition analysis of vapor and liquid phase is performed. After that, the dewar is refilled again and temperature is decreased down to 128 K with same cooling rate (0.5 K/h) for another composition analysis. The temperature of the cell is then let increase up to ambient temperature for evacuating the cell and loading a new mixture.

5.4 Experimental results and discussion

The measured SLVE molar composition of liquid and vapor phases and estimated uncertainties at each temperature and pressure are tabulated in tab. 5.3. Uncertainty on temperature is 0.2 K and uncertainty on pressure is 0.003 MPa. Information on uncertainty estimation are available in Appendix C, while procedure for temperature, pressure and GC calibration are available in Appendix B. Ternary plot of phase diagrams for validating experimental results are proposed in fig. 5.5.

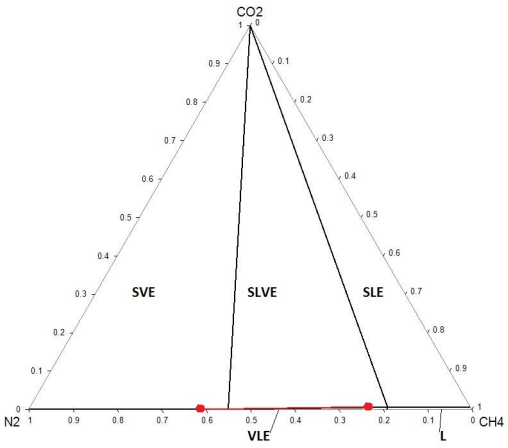

Point 1.1: T=145.9 K, p=2.044 MPa

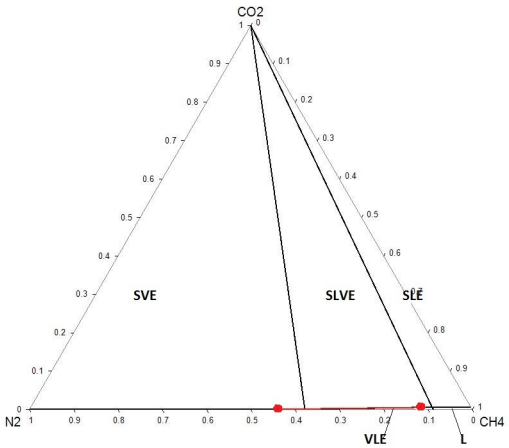

Point 2.1: T=145.8 K, p=1.123 MPa

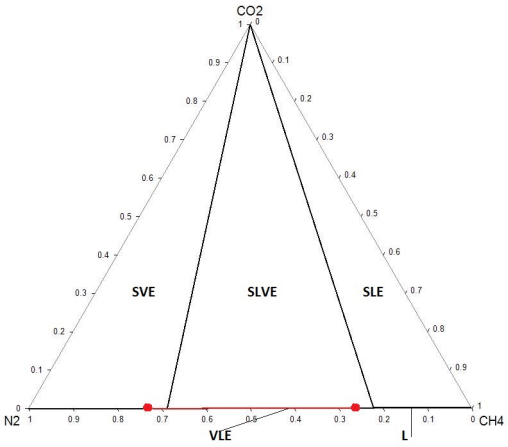

Point 1.2: T=132.1 K, p=1.355 MPa

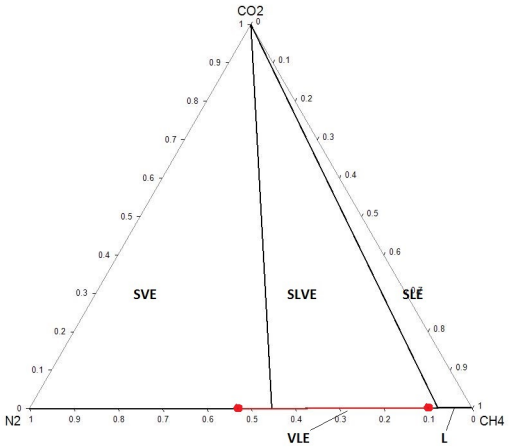

Point 2.2: T=132.1 K, p=0.772 MPa

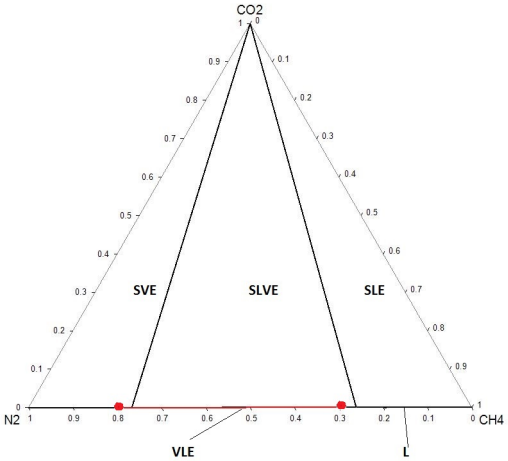

Point 1.3: T=124.9 K, p=0.772 MPa

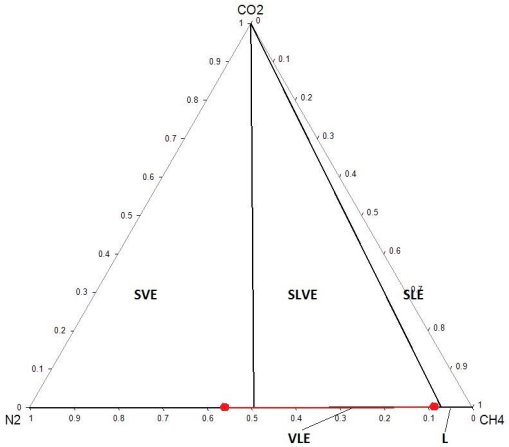

Point 2.3: T=124.5 K, p=0.517 MPa

Figure 5.5: Ternary phase diagram for the ternary mixture N_2-CH_4-CO_2 mixture: experimental point obtained in this work (-) and model results (-)

Table 5.3: SLVE liquid and vapor phase composition measured in this work for mixtures of N_2(1)-O_2(2)-CH_4(3)-CO_2(4). N indicates the measurement numeration according to the global composition of the loaded mixture

			Liquid composition						Vapor composition					
N	T	P	x_2	u(x_2)	x_3	u(x_3)	x_4	u(x_4)	y_2	u(y_2)	y_3	u(y_3)	y_4	u(y_4)
	(K)	(MPa)					(ppm)	(ppm)					(ppm)	(ppm)
1.1	145.9	2.044	-	-	0.764	0.002	6 945	40	-	-	0.388	0.014	473	27
1.2	132.1	1.355	-	-	0.734	0.001	1 640	52	-	-	0.265	0.016	46	33
1.3	124.9	0.772	-	-	0.706	0.006	753	36	-	-	0.205	0.009	16	10
2.1	145.8	1.123	-	-	0.885	0.012	5 750	35	-	-	0.559	0.017	576	23
2.2	132.1	0.772	-	-	0.902	0.006	1 191	56	-	-	0.471	0.035	52	14
2.3	124.5	0.517	-	-	0.919	0.004	534	52	-	-	0.444	0.015	15	15
3.1	146.1	2.105	0.070	0.003	0.745	0.004	6 977	112	0.117	0.005	0.400	0.005	1 604	54
3.2	132.4	1.349	0.082	0.005	0.714	0.012	1 733	85	0.127	0.005	0.278	0.006	217	68
3.3	125.0	0.964	0.083	0.003	0.711	0.004	365	66	0.131	0.003	0.238	0.002	41	23
4.1	146.5	1.389	0.027	0.004	0.892	0.007	6 507	245	0.072	0.004	0.609	0.006	1 465	61
4.2	132.5	0.839	0.033	0.015	0.883	0.023	1 560	110	0.087	0.004	0.476	0.006	181	44
4.3	125.1	0.576	0.033	0.040	0.882	0.326	356	83	0.090	0.003	0.420	0.003	36	38

As previously stated, the mixture is loaded in the cell at ambient temperature and then cooled down at three different temperatures 148, 135 and 128 K by setting the temperature regulator. Final calibrated average temperature in the cell resulted 3 K lower than the temperature set on the temperature regulator. In tab. 5.3 it is possible to see 4 different series of measurements, namely four different global composition mixtures. According to the number of series and their temperature, experimental points are named 1.1, 1.2, 1.3, ... 4.2, 4.3. The global composition of the mixtures loaded in the cell is reported in tab. 5.4. Global composition has been calculated from loading pressure of each component and checked by GC analysis. The formation of a solid phase at experimental temperature and pressure can be deducted from the material balance on the CO_2 component:

$$z_{CO_2} = y_{CO_2}V + x_{CO_2}L + w_{CO_2}S \tag{5.2}$$

where y_{CO_2}, x_{CO_2} and w_{CO_2} are the CO_2 molar compositions in the vapor, liquid and solid phases and V, L and S the molar fractions of vapor, liquid and solid respectively and z_{CO_2} the global CO_2 molar compositions. Assuming w_{CO_2} equal to unity (pure CO_2 solid), and taking measured y_{CO_2}, x_{CO_2}, S has to be greater than 0 in order to solve eq. (5.2) (being V and L in the range 0-1).

Table 5.4: Global composition of loaded mixture for each series of measurement N

N	z_{N_2}	z_{O_2}	z_{CH_4}	z_{CO_2}
1	0.40	-	0.57	0.02
2	0.19	-	0.79	0.02
3	0.31	0.09	0.58	0.02
4	0.15	0.04	0.79	0.02

CO_2 solubility

Comparing experimental results obtained in this work and literature data of CO_2 solubility for the binary mixture of CH_4-CO_2 (see fig.5.6) it is possible to observe that the addition of nitrogen and oxygen in methane decreases the solubility of CO_2 in the liquid phase, at least for temperatures lower than 145 K. The effect can be explained studying the CO_2 solubility in liquid oxygen and nitrogen, which is much lower than in liquid methane, according to literature data (see Chap.3). One can conclude that methane content in liquid phase has a major effect on CO_2 solubility in liquid phase. When some nitrogen and oxygen are added to methane, methane content in liquid phase decreases and thus the CO_2 solubility decreases too. This conclusion is in contrast with the experimental results obtained by Shen et al. (2012) and Gao et al. (2012). Data from aforementioned authors report higher CO_2 solubility compared to data obtained in this work. Even if the authors of Shen et al. (2012) and Gao et al. (2012) declare their data as SLE data, analysis of the experimental procedure and comparison with model results obtained at same T, p, **z**, show that they are actually SLVE data. CO_2 solubility in liquid phase obtained in this work is compared with model results and experimental values at similar conditions available in literature in fig. 5.6 and in fig. 5.7. The relative deviation ($\Delta x_{CO_2} rel$) between model results ($x_{CO_2,calc}$) and experimental values ($x_{CO_2,exp}$) calculated as

$$\Delta x_{CO_2} rel = \frac{(x_{CO_2,calc} - x_{CO_2,exp})}{x_{CO_2,exp}} \tag{5.3}$$

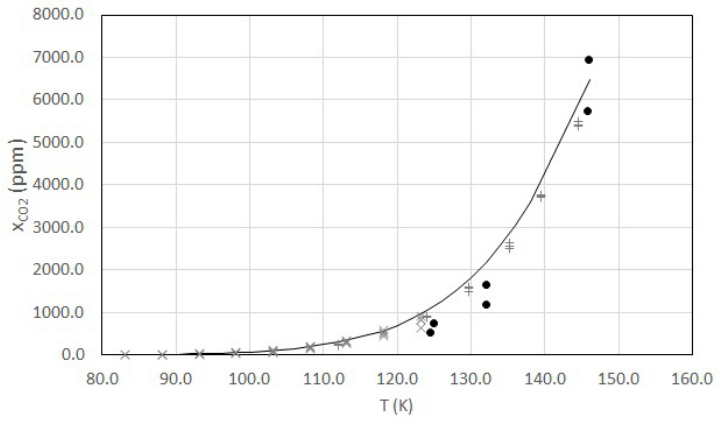

Figure 5.6: Comparison between CO_2 solubility in liquid phase for the ternary N_2-CH_4-CO_2 mixture obtained in this work (•), data from Shen et al. (2012) (+) and Gao et al. (2012) (×), and model results (−) obtained at constant pressure (10 bar) with the PR EoS+Zabaloy equation model

A comparison between measured solubility of CO_2 in liquid and vapor phase and results from PR+Zabaloy equation model is presented in figure 5.8. The measured CO_2 solubility in liquid is lower than solubility obtained performing a TP (SLVE) flash at experimental temperature, pressure and global composition (fig. 5.9). Both Gerg EoS+Jager and Span model and PR EoS+Zabaloy equation overestimate the solubility of the CO_2 in the liquid phase. The CO_2 solubility obtained with the Gerg EoS+Jager and Span model is 27% (in average) higher than the PR EoS+Zabaloy equation of over the temperature range covered by the experimental campaign (see tab. 5.5).

As previously stated, methane content in liquid phase has a major effect on CO_2 solubility. Since the methane content in liquid phase is very similar in ternary and quaternary mixture measurements, this can explain why CO_2 solubility is similar in both measurements with or without O_2. Furthermore, comparing experimental results obtained in this work and data for

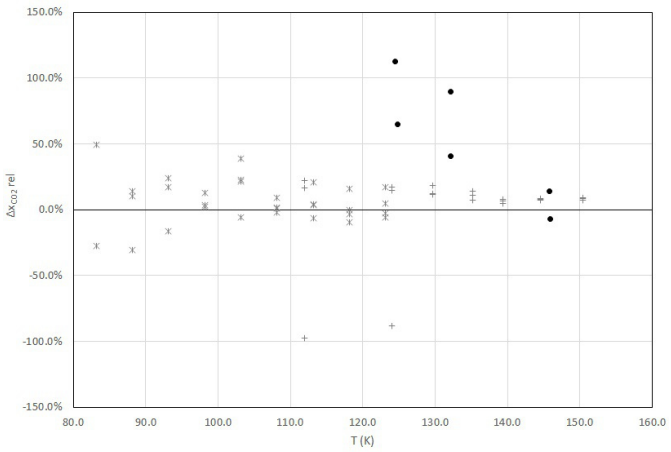

Figure 5.7: Relative deviation between CO_2 solubility in liquid phase obtained in this work (•) for the ternary N_2-CH_4-CO_2 mixture, data from Shen et al. (2012) (+) and Gao et al. (2012) (×). Model results are obtained with the PR Eos+Zabaloy equation model

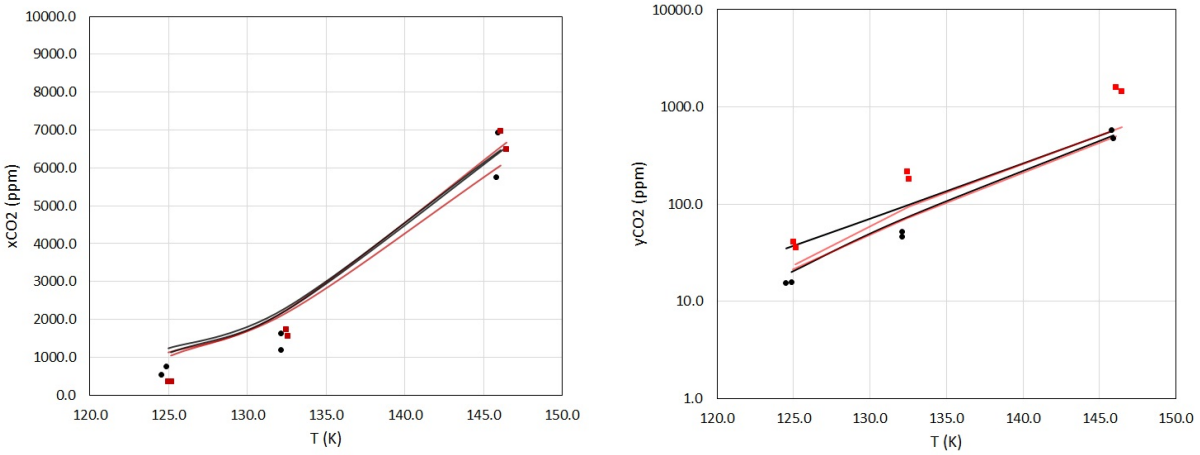

(a) CO_2 solubility in liquid phase

(b) CO_2 solubility in vapor phase

Figure 5.8: Comparison between CO_2 solubility in liquid and vapor phase: ternary N_2-CH_4-CO_2 data obtained in this work (•) and model results (-), the quaternary N_2-O_2-CH_4-CO_2 data obtained in this work (■), and model results (-). Model results are obtained with the PR Eos+Zabaloy equation model.

the binary mixture of CH_4-CO_2 (fig. 5.10) it is possible to conclude that the addition of nitrogen and oxygen decreases the solubility of CO_2 in the liquid phase. Also for the binary mixture, CO_2 solubility in liquid phase is overestimated by models. Contrary CO_2 solubility in vapor phase increases when O_2 is added, and the phenomenon is not predicted by the model (fig. 5.8b).

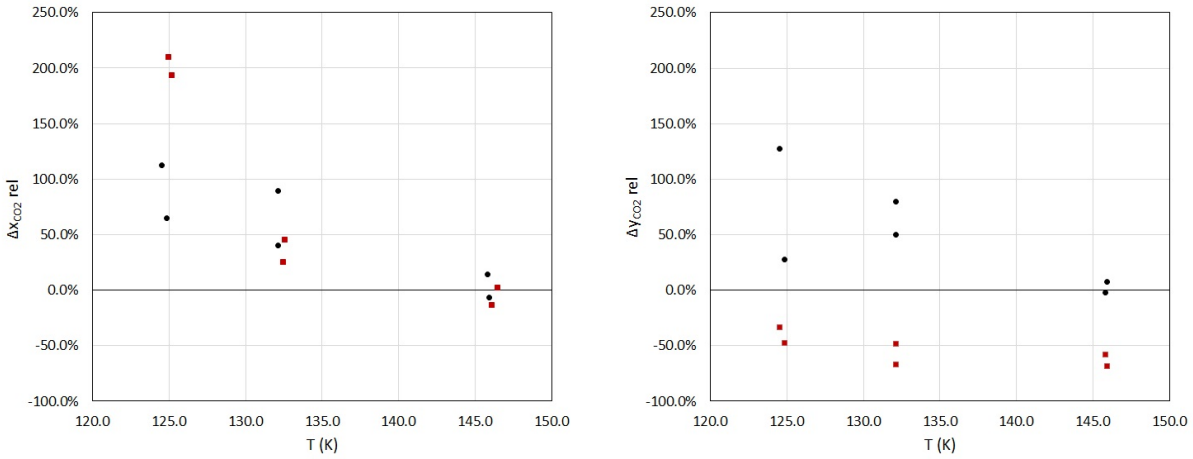

(a) Liquid phase **(b)** Vapor phase

Figure 5.9: Relative deviation between experimental data obtained in this work and calculated CO_2 solubility in liquid and vapor phase for the ternary N_2-CH_4-CO_2 mixture (●) and quaternary N_2-O_2-CH_4-CO_2 mixture (■). Model results are obtained with the PR Eos+Zabaloy equation model.

Table 5.5: Measured CO_2 solubility in liquid (x_{CO_2}) and vapor phase (y_{CO_2}) and results from th PR EoS+Zabaloy equation and Gerg EoS+Jager and Span model.

N	T (K)	x_{CO_2} exp ppm	x_{CO_2} PR ppm	x_{CO_2} GERG ppm	y_{CO_2} exp ppm	y_{CO_2} PR ppm	y_{CO_2} GERG ppm
1.1	145.9	6 945	6 474	7 846	473	510	633
1.2	132.1	1 640	2 305	2 853	47	70	92
1.3	124.9	753	1 240	1 573	16	20	28
2.1	145.8	5 750	6 551	7 674	576	563	689
2.2	132.1	1 191	2 257	2 669	52	93	120
2.3	124.5	534	1 135	1 349	15	35	40
3.1	146.1	6 977	6 065	7 831	1 604	502	631
3.2	132.4	1 733	2 167	2 901	217	72	96
3.3	125.0	365	1 130	1 551	41	21	30
4.1	146.5	6 507	6 672	7 986	1 465	615	750
4.2	132.5	1 560	2 266	2 787	181	94	121
4.3	125.1	356	1 047	1 451	36	30	41

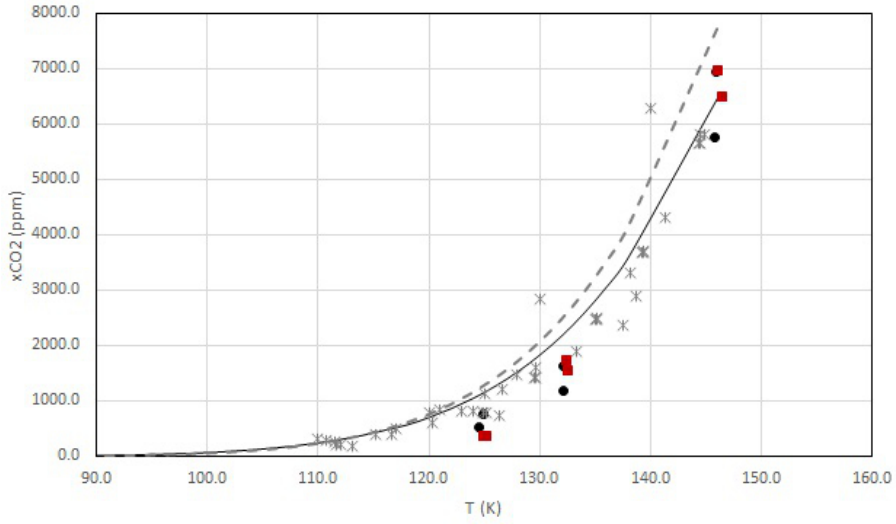

Figure 5.10: Comparison between CO_2 solubility in liquid phase for the ternary N_2-CH_4-CO_2 mixture obtained in this work (•), model results (−), for the quaternary N_2-O_2-CH_4-CO_2 mixture obtained in this work (■) and binary CH_4-CO_2 data from literature, see sec. 3.3 (⁕) and model results (−−). Results from model are obtained using the PR EoS+Zabaloy equation model.

Other components

Concerning the other components of the studied mixture, the vapor-liquid distribution ratio K_i is studied

$$K_i = \frac{y_i}{x_i} \tag{5.4}$$

The comparison between results from the two models and experimental values is reported in fig. 5.11. The relative deviation $\Delta Krel$ is calculated as:

$$\Delta Krel = \frac{(K_{i,calc} - K_{i,exp})}{K_{i,exp}} \tag{5.5}$$

where $K_{i,calc}$ is obtained from the PR EoS+Zabaloy equation model or the Gerg EoS+Jager and Span model. From fig. 5.11 it is possible to observe that, while from nitrogen and methane the two models are in agreement and the relative deviation is lower than 15% for all the experimental points, for oxygen the two models give opposite results (13 to 34 % for the Gerg Eos+Jager and Span model and -17 to -30% for the PR EoS+Zabaloy equation model). This is due to the fluid models, that are predictive for most of binary mixtures containing oxygen: the Gerg Eos has non-regressed parameter for the binary mixture O_2-CH_4 and O_2-CO_2 (because of the lack of available data) and the PR EoS has nil k_{ij} for the binary mixture O_2-CH_4 and k_{ij} regressed on SLE data for the O_2-CO_2. The different behavior is not due to the regressed k_{ij} parameter for the O_2-CO_2 parameter, as shown in fig. 5.11b, where results from the PR EoS with nil k_{ij} parameter for the O_2-CO_2 are also plotted.

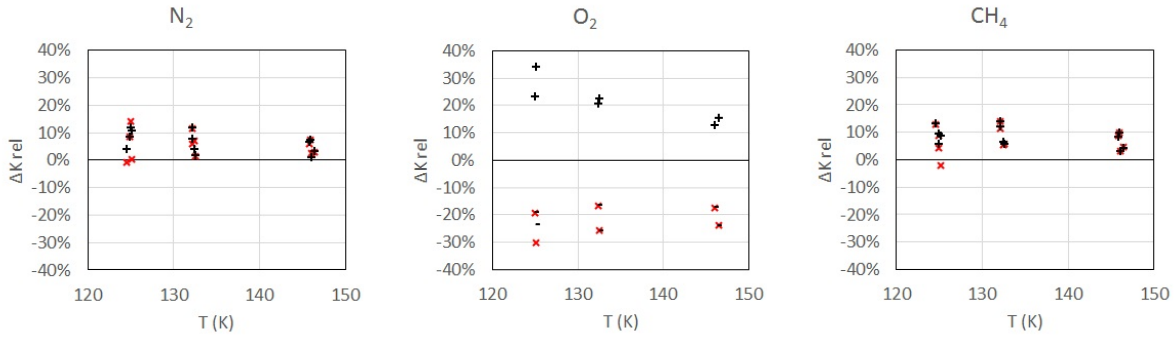

(a) **(b)** **(c)**

Figure 5.11: Relative deviation between nitrogen, oxygen and methane experimental and calculated vapor-liquid distribution ratio K_i using the Gerg+Jager and Span model(+), the PR EoS+Zabaloy equation with regressed parameter (×) and nil k_{O2CO2} parameter (-)

Uncertainties

Uncertainties on temperature and pressure can be considered sufficiently small (0.1 K and 3 kPa). On the contrary uncertainty on composition can be considered satisfactory for the CO_2 solubility in liquid phase but not in vapor phase. Studying the sources of the uncertainty (repeatability of the measurements u_{rep} and calibration of the GC u_{calib}) it is possible to observe that the ratio $\frac{u_{rep}}{u_{calib}}$ is close to one, which means that the two sources have the same importance in defining the uncertainty on composition. The high value of the uncertainty due to the repeataibility is caused by two factors:

1. both methane and carbon dioxide are detected by the FID, even if only the CO_2 peak is measured using the FID signal (being the FID set with high sensibility in order to detect small traces of CO_2, the CH_4 peak saturates the FID signal). Methane and carbon dioxide

retention time is quite close (10.2 and 16 min) and thus the CO_2 peak is overlapped to the tail of the CH_4 peak. This make the integration of the peak more difficult;

2. the opening time of the sampler cannot be increased as wished when the CO_2 peak is small, otherwise the CH_4 would saturate the FID signal for a period larger than the retention time of the CO_2, making impossible the iteration of the CO_2 peak. As a consequence, the CO_2 peak has to be kept small, and when the CO_2 content is lower than 50 ppm, the peak is no more than 50 times larger than the baseline noise.

Furthermore, the study of a multicomponent mixture increases the difficulty of the GC analysis. In our case the separation of N_2 and O_2 was possible with a temperature program at -25°C, which caused some problems of methane and carbon dioxide retention in the column increasing the baseline perturbation. For increasing the quality of the GC analysis and reducing the uncertainty on the composition, reducing the number of components and assuring perfect separation of the components in the GC should be considered. In case only the component present in traces is detected by the FID the problem does not exist because the other components are "filtered" by the detector. A different analytic method (high resolution gas chromatography or mass spectrometry) could be considered when analyzing two components with similar retention time and both detected by the FID.

The high value of the uncertainty associated to the GC calibration is in part caused by the same aforementioned problems. In particular the GC calibration by relative response factor (see Appendix B) is obtained by comparing the detector response of two components at the same time: CO_2 on the FID and CH_4 or N_2 on the TCD. The ratio between the number of moles (and the composition) of the two components is a perfect linear function of the ratio between the peak surfaces of the two components when the response of each detector is linear and passing for the point (0,0), namely nil intercept. If the ratio between the injected moles of a component and the intercept of the calibration equation is not negligible, the peak surface ratio depends on the amounts of moles analyzed (and not only the mole ratio between the two components). In the GC calibration performed in this work the two causes of uncertainty previously mentioned may cause a detector response with intercept non-nil.

Some comments on the experimental procedure and apparatus: the sampling devices allows to withdraw liquid and vapor samples at low temperature; the only problem that has been encountered is the plugging of the liquid capillary likely because of solid formation inside the capillary plunging in the cell. For avoiding this it is necessary to set the temperature control of the liquid capillary and the brass cap at temperature higher than 135 K. The mixing inside the cell is very important for reaching a stable equilibrium in the cell. It happened that the transmission from the motor to the magnetic bar had some problems: in this case the phenomenon observed was a continuously and slowly decreasing pressure even after the temperature was controlled at a stable set value.

The auto-refilling of the liquid nitrogen dewar should be considered for avoiding excessive temperature perturbation during the loading of important amount of LN2 and allowing longer measurement campaigns. A filled dewar allows to maintain the temperature in the EC for 35 hours at 173 K or 60 hours at 128 K.

Part III

Landfill gas upgrading process

Chapter 6

CO_2 capture by antisublimation

In this chapter the formation of solid CO_2 in the upgrading heat exchangers is simulated. The equations and the numerical method used for modeling and solving the transient problem of the CO_2 capture are described and results are shown and commented.

Résumé

L'élimination du CO_2 à basse température est discutée dans ce chapitre: le biogaz brut précédemment purifié de l'H_2S et d'autres impuretés est pré-refroidi avant d'entrer dans l'échangeur de chaleur de séparation du CO_2, où il est ensuite refroidi à -95°C. A cette température, le CO_2 solidifie et est séparé du flux de biogaz. Dans le but de comprendre la capture du CO_2 dans l'échangeur de chaleur, on simule la formation de la couche solide à partir d'un flux de biogaz (ou gaz de décharge). Le phénomène est un processus dynamique impliquant une couche solide croissante le long du temps. Un modèle d'échangeur de chaleur simplifié est développé et le modèle thermodynamique mis en oeuvre dans ce travail et présenté dans la partie précédente est utilisé pour calculer les propriétés du biogaz, ainsi que les conditions de formation du CO_2 solide.

Étant donnée la complexité du problème, des simplifications dans la géométrie de l'échangeur et de l'agencement des écoulements ont été effectuées et on choisit le modèle des capacités concentrées pour résoudre le problème de conduction thermique en régime dynamique. De cette manière, les équations du bilan d'énergie et de matière) sont écrites et discrétisées grâce à la méthode numérique des *volumes finis*. On considère que la solidification a lieu lorsque la température de la paroi de l'échangeur est inférieure à la température de givrage du biogaz. La couche de CO_2 solide qui croît sur les parois de l'échangeur de chaleur modifie le transfert de chaleur. Les propriétés du CO_2 solide doivent donc être connues, notamment la densité, la capacité calorifique et la conductivité thermique. Une recherche bibliographique sur les valeurs expérimentales de ces propriétés est proposée dans l'Annexe A.

La simulation permet de dessiner les profils de température dans l'échangeur de chaleur à différents pas de temps, ainsi que la croissance de l'épaisseur de la couche de CO_2 solide. Les résultats du problème dynamique par rapport à la solution stationnaire montrent que, lorsque la température de la paroi est supérieure à la température de givrage (température SVE), les profils de température tendent vers la solution stationnaire. Cependant, lorsque la température de la paroi est inférieure à la température de givrage, le CO_2 solide commence à se former et une couche solide commence à croître. A ce stade, les températures de la paroi et du biogaz ne suivent plus le profil de température de la solution stationnaire. Cela peut s'expliquer par la réaction exothermique de solidification, qui tend à libérer de l'énergie dans le biogaz et la paroi, modifiant ainsi leur température. La teneur en CO_2 du biogaz diminue en raison de la capture de dioxyde de carbone solide: il s'ensuit que la température de givrage (SVE) diminue également, selon le diagramme de phase du biogaz.

Malgré la solubilité du CO_2 dans la vapeur de méthane, azote et oxygène soit similaire, l'influence de l'azote et de l'oxygène présents dans le gaz de décharge est principalement la dilution du mélange CH_4-CO_2 avec de l'azote et de l'oxygène, ce qui entraîne une plus faible teneur en CO_2 dans l'écoulement de gaz entrant dans l'échangeur de chaleur et donc une température de givrage inférieure, donc moins solide est formé et le transfert de chaleur est amélioré. Une certaine variation des propriétés thermodynamiques du biogaz peut également être observée: la densité du biogaz est légèrement plus élevée en présence d'azote et la capacité calorifique légèrement inférieure. Le résultat dans la simulation de l'échangeur de chaleur est une amélioration du transfert de chaleur et donc un refroidissement plus efficace du gaz de décharge. La conséquence est une meilleure répartition de la couche solide le long de la paroi de l'échangeur de chaleur, ce qui correspond à des cycles plus longs de givrage et de dégivrage de chaque échangeur de chaleur par rapport au cas de base sans azote.

6.1 Presentation of the problem

The upgrading of biogas and landfill gas is the set of processes aiming to produce the so-called biomethane. Compared to raw biogas, biomethane has a higher energy content and meets the standards for the injection in the natural gas grid or vehicle fueling. Biogas upgrading generally consists in different steps: CO_2 separation, liquefaction, nitrogen removal. The CO_2 removal at low temperature is discussed in this chapter: the raw biogas is previously purified from H_2S and other impurities and pre-cooled before entering the upgrading heat exchanger where it is further cooled down to -95°C. At this temperature CO_2 solidifies and is separated from the biogas flow.

With the aim of understanding the CO_2 capture in the heat exchanger, the solid formation from a biogas or landfill gas flow is simulated. The phenomenon is a dynamic process involving a solid layer growing along the time. A simplified heat exchanger model is developed and the thermodynamic model implemented in this work and presented in previous Part is used for computing vapor and solid properties, as well as solid formation conditions.

Heat transfer with solidification is a complex task involving combined heat and mass transfer within the cooled biogas. In the heat exchanger, the biogas is cooled down by a refrigerant; a wall divides the two fluids, participating to the heat transfer by conduction. When the temperature in the biogas side is low enough to start solid formation (antisublimation), a solid phase consisting in pure CO_2 starts to freeze out on the wall and fins. The temperature at which the solidification process starts (TSVE) is computed through a thermodynamic model developed in this work (see Chap. 4). This temperature is the condition of the thermodynamic equilibrium between the forming solid phase and the biogas vapor phase, therefore the model does not take into account the phenomenon of supercooling. Supercooling occurs when the solute crystallize at temperature lower then the thermodynamic equilibrium temperature, because of an energy barrier to nucleation. It is mainly due to the energy needed to form the nucleus of solid CO_2, which starts the development of the solid phase. In the case of the upgrading heat exchanger of the studied process, the crystallization process starts from existing nuclei of solid CO_2 remaining on the wall of the heat exchangers after a regeneration cycle. The process can thus be considered a secondary nucleation, characterized by a small supercooling (or supersaturation), according to the Classical Nucleation Theory.

The formation and accumulation of the solid phase on the walls of the heat exchangers is, by definition, a transient/dynamic problem. Transient conduction happens within the frost layer and the wall. The boundary conditions are the convective heat flow between the biogas bulk temperature and the frost layer, and between the refrigerant bulk temperature and the wall surface. The geometry changes with the accumulation of solid CO_2, so a further difficulty is given by the moving boundaries. As soon as the carbon dioxide is captured, the total mass flow of the biogas decrease, and, at the same time, the composition changes. In fact the process aims to produce an outgoing biogas (biomethane) having an higher content of methane. Finally, the thermodynamic properties of the biogas change all along the heat exchanger because of temperature and composition variations.

6.2 State of the art

First a review of existing methods to simulate the heat exchange with phase change in a counter flow finned tube heat exchanger is provided. Concerning design and performance calculations, two analytic methods are commonly used: LMTD (Logarithmic Mean Temperature Difference) and ϵ-NTU (effectiveness - Number of Transfer Units) methods. They are purely analytical calculations methods. The two methods are equivalent, even if the first one is commonly use for

sizing and the second one for performances rating. Both assumes that the heat exchanger has no external losses, constant fluid properties and constant overall heat transfer coefficient over the entire heat transfer surface. The two last aforementioned assumptions are often not verified, in particular when phase change occurs. In this last case, thermo-physical properties and heat transfer coefficient show important variations and LMTD or ϵ-NTU cannot be applied for the whole heat exchanger. Opportune corrections to both methods have been proposed to extend their application to the case in which condensation occurs. It is the case of LMED (Logarithmic Mean Enthalpy Difference), in which enthalpy differences are used instead of temperature differences, or modified ϵ-NTU method following the Threlkeld approach (Perrotin, 2004; Kuehn et al., 1998). The same kind of correction could also be adapted to the antisublimation problem.

Analytic methods or modified analytic methods are useful tools for solving steady state problems. In case of solidification, with CO_2 solid layer growth, the problem is indeed dynamic. The aforementioned methods are thus exploitable only considering a succession of quasi-steady states. Another approach to the heat exchanger problem with solid formation is an empirical study of the solid layer growth, as proposed by Song et al. (2013). In this case an experimental heat exchanger surface is exposed to a N_2-CO_2 gas flow and different properties are measured, such as density, thickness profile, temperatures and heat exchanger performances. Nevertheless results are strictly linked to the characteristics of the experimental set-up and it can be hardly apply to different geometries and operating conditions. Focusing on the conductive problem within the solid layer, many studies have been proposed, especially for water frost formation (see App. A). Interesting models considering the solid layer as a porous medium, with temperature/time dependent density have been proposed by Le Gall et al. (1997) and Tao and Besant (1993). This approach provides a complete description of the temperature profile within the solid layer, for given boundary conditions defined by the convective heat flux between the biogas bulk and the frost surface and the conductive flux between the frost and the wall. Finally, a possible approach for modeling the heat exchange is the lumped capacitance model, which neglects the conductive heat transfer within the wall, but allows solving the dynamic heat transfer problem with phase change. Complete description of the temperature profiles of biogas, refrigerant and wall all along the heat exchanger can be found. As better explained in the next paragraph, the assumption of neglecting conductive heat resistance of wall and frost is valid only for small thickness of the solid layer, namely short simulation time.

The aim of this work is not the design of the heat exchanger, but to understand the phenomenon of the solid capture in the heat exchanger, taking into account the dynamic characteristic of the solidification problem. Small frost thickness can be considered and thus a lumped capacitance method is used, coupled with the solution of the transient conduction problem.

6.3 Simulation of the heat exchanger

It has been chosen to develop a model starting from a simplified geometry, allowing to compare the results with analytic solutions. In particular the configuration chosen is a plane heat exchanger with parallel or counter flow. Fig. 6.1 represents the geometry of the problem with parallel flow configuration. Lumped capacitance model is used to solve the transient problem: the temperature of the wall is considered spatially uniform in every control volume at any instant of time. The assumption implies that the temperature gradient within the wall is negligible. This condition is closely approximated if the resistance to conduction within the wall is small compared to resistance to convective heat exchange between the wall and the fluids.

In neglecting temperature gradient within the solid, the problem has to be considered not as a transient conduction problem within the wall with convective boundary conditions, but by

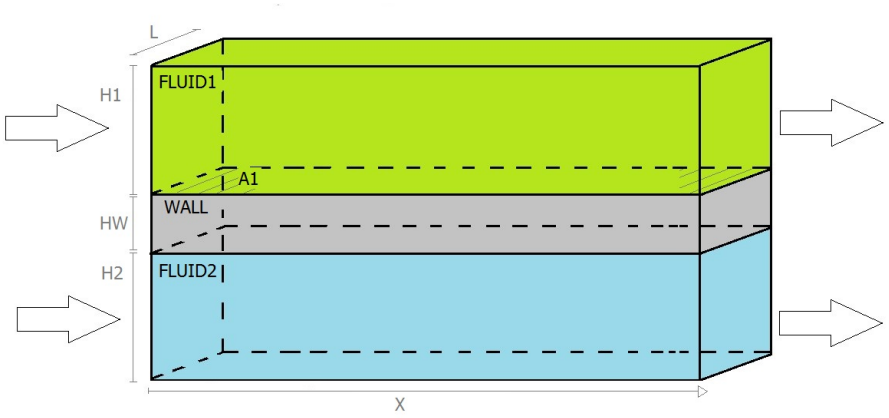

Figure 6.1: Scheme of an heat exchanger with parallel flow configuration.

formulating an overall energy balance in the control volume. As said, this method is valid if the resistance to conduction (R_{cond}) through the solid is small compared to the resistance to convection (R_{conv}) across the fluids. This criterion can also be expressed using the Biot number, a dimensionless parameter defined as:

$$Bi = \frac{hL}{\lambda} = \frac{R_{cond}}{R_{conv}} \tag{6.1}$$

where, h is the convective heat transfer coefficient of fluid 1 or 2, λ the thermal conductivity of the wall and L is the thickness of the wall.

Considering the biogas side of the heat exchanger, the Bi number is now briefly evaluated: a realistic value of the convective heat transfer coefficient is 20 W/m^{2}K (later in this report the value will be calculated from opportune correlations), thermal conductivity of the wall is 230 W/mK for aluminium, and the thickness of the wall is 1 mm; Biot number is of order of magnitude of 10^{-5}, much less than 1. The assumption can be thus considered valid and the use of the lumped capacitance model justified.

In case of frost formation, the limit of validity of the approximation is checked, calculating Biot number for the total conductive resistance of the solid layer made of CO_2 and the wall. Conductivity of solid CO_2 is considered equal to 0.3 W/mK, from extrapolated data by Sumarokov et al. (2006)) and Cook and Davey (1976) (see App. A). The two layers (frost and wall) are considered as a series circuit of thermal resistances, so the value is calculated as follows:

$$R_{tot} = R_{frost} + R_{wall} = \frac{t_{frost}}{\lambda_{frost}} + \frac{t_{wall}}{\lambda_{wall}} \tag{6.2}$$

where t is the thickness of the frost and wall and λ the thermal conductivity. Results are reported in fig. 6.2 showing the Biot number variation as a function of frost thickness. Biot number has to be largely less than 1 for the assumption of negligible conduction in the frost layer to be valid. For Bi number equal to 3×10^{-2} the values of the frost layer thickness is equal to 0.5 mm. Since Bi grows linear with frost thickness, the criterion can be considered verified with a maximum frost thickness of 0.15 mm. This is the validity limit of the lumped capacitance model for simulating the heat transfer in the heat exchanger in case of frost formation.

The limit of this method is that, in case of CO_2 frost formation, the temperature gradient inside the frost and the wall is not studied. The temperature of the solid CO_2 will be considered equal to the temperature of the wall, as explained later. Together with the aforementioned hypothesis, the most important assumptions considering the dynamic behavior of the heat exchanger are:

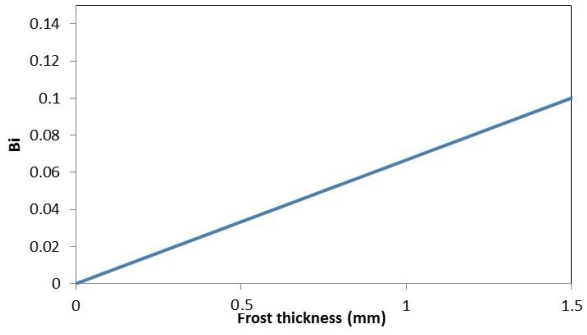

Figure 6.2: Biot number variation relative to the problem of CO_2 frost formation on the wall of an heat exchanger, depending on the frost thickness.

- axial conduction is negligible in both fluids and wall;
- overall heat losses are negligible;
- heat generation and viscous dissipation within the fluid are negligible;
- momentum balance relating pressure drop and velocity is not considered in the model.

From the last assumption it results that the pressure in the heat exchanger remains constant and set equal to 1 bar.

Energy balance

Considering the aforementioned approach and assumptions, the global energy balance within a control volume is given by convective exchange between fluid and the wall ($Q_{ex,i}$) and enthalpy change associated to the mass flow. The governing equations are now written for the fluids and wall: for the generic fluid i (biogas or refrigerant), the energy balance can be written as :

$$V_i \frac{\delta(\rho_i c_{p,i} T_i)}{\delta t} = V_i \frac{\delta\left(u_i \rho_i c_{p,i} T_i\right)}{\delta x} + Q_{ex,i} \tag{6.3}$$

The left term of eq. (6.3) is the stored energy (ρ is the density, c_p is the heat capacity, T is the temperature). The derivative term in space is the enthalpy flow (u is the bulk velocity of the fluid) and the last term $Q_{ex,i}$ represents the energy exchanged between fluid and wall. Similarly for the wall, the energy balance can be written. Since no fluid flow term is present, the stored energy is equal to the difference between inlet and outlet energy exchanged with the two fluids:

$$V_w \frac{\delta \rho_w c_{p,w} T_w}{\delta t} = Q_{ex,1} - Q_{ex,2} \tag{6.4}$$

Energy exchanged between each fluid and wall depends on the convective heat transfer coefficient h_i, temperature differences and, in case of frost formation, latent heat of solidification (Δh_{S-V}) of the CO_2 mass experiencing phase change (m_{solid}):

$$Q_{ex,1} = h_1 A_1 \left(T_1 - T_w\right) + m_{solid} \Delta h_{S-V} \tag{6.5}$$

$$Q_{ex,2} = h_2 A_2 \left(T_w - T_2\right) \tag{6.6}$$

Mass balance

The mass balance for component different from CO_2 states that the component flow is constant, since the solid captured is pure carbon dioxide, thus the accumulation term is nil:

$$\frac{\delta m_{i \neq CO_2}}{\delta t} = 0 \tag{6.7}$$

The mass balance for the carbon dioxide must consider the storage of antisublimated mass on the wall of the heat exchanger. The solidification is governed by the crystal growth, while the nucleation step is neglected since solid CO_2 crystals are already present in the heat exchanger, acting as nuclei for the new crystals. In this case the *Two steps crystal growth theory* (Valeton, 1924; Seader and Henley, 2011) explains the solid formation process as the succession of two phenomena: first a convective mass transfer step drives the CO_2 from the bulk to the solid layer surface, then a first order reaction at the interface allows the solidification and integration into crystal-lattice structure (kinetic step). In our case we can consider negligible the kinetic of integration in the solid structure compared to the mass transfer within the biogas flow, so that we can neglect the kinetic constant that should be experimentally found. This simplification allows the use of the mass transfer coefficient, obtainable using the Chilton-Colburn analogy (Chilton and Colburn, 1934). Solidification occurs if temperature of the wall is lower than the saturation temperature T_{SVE}.

$$\frac{\partial m_{CO_2}}{\partial t} = \begin{cases} 0 & \text{if } T \geq T_{SVE} \\ h_m S(\rho_1 X_{CO_2,1} - \rho_S X_{CO_2,S}) & \text{if } T < T_{SVE} \end{cases} \tag{6.8}$$

In eq. (6.8) h_m is the convective mass transfer coefficient (m/s), ρ_1 and ρ_S are the density of the biogas respectively at fluid bulk and at the surface temperature (kg/m^3), $X_{CO_2,1}$ and $X_{CO_2,S}$ the mass fraction of CO_2 (kg_{CO_2}/kg) at bulk and surface. In the same equation, S is the wall surface, T is wall temperature. Considering the accumulation term to be equal to the solidified mass of carbon dioxide, the outlet mass flow is equal to the difference between inlet mass flow and captured mass. Total flow of biogas $\dot{m}_1$ is given by the product of biogas density (ρ_1), velocity (u_1) and flow section ($H_1 \times L$, according to fig. 6.1):

$$\dot{m}_1 = \rho_1 u_1 (H_1 L) \tag{6.9}$$

and

$$\dot{m}_1 = \dot{m}_{CO_2} + \sum \dot{m}_{i \neq CO_2} \tag{6.10}$$

Numerical method

The method chosen to solve the system of differential equations provided by energy and mass balances is a finite volumes numerical method. This method is similar to the finite difference method or finite element method: values are calculated at discrete places on a meshed geometry. *Finite volume* refers to the small volume surrounding each node point on a mesh. In the finite volume method, volume integrals in a partial differential equation that contain a divergence term are converted to surface integrals, using the divergence theorem. The main steps of the method consist in:

- dividing the domain into small control volumes;
- evaluating energy and mass balance on each control volume, considering constant temperatures and properties inside every small volume

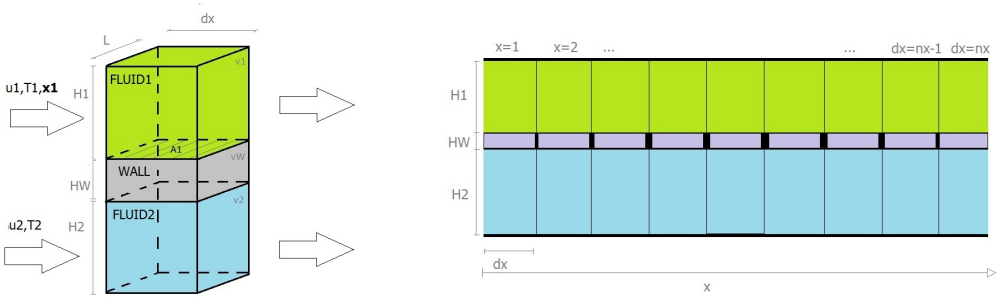

Frost layer growth period

Figure 6.3: Discretization of the geometry of the heat exchanger.

This numerical method is fully conservative because the fluxes entering and leaving a given volume are considered. Simulation of the dynamic behavior of the heat exchanger, for a given geometry of the heat exchanger is thus possible knowing the boundary conditions, namely the inlet conditions of the fluids.

The model is explained for two cases. First (Case 1: No solidification), energy balances are expressed and solved for the case in which antisublimation of carbon dioxide in fluid 1 does not take place. The properties of fluid 1 (biogas) are function of temperature, while the biogas composition is constant. In the second case (Case 2: Solidification) antisublimation of CO_2 is considered. Properties of fluid 1 are also function of biogas composition, since the concentration of CO_2 in the fluid decreases as consequence of the capture by solidification on the wall of the heat exchanger.

Case 1: No solidification

Energy balances are discretized to solve the systems of differential equation of above for the case of no CO_2 antisublimation. It is the case of wall temperature greater than saturation temperature of biogas with given composition. Time is discretized in intervals of constant step dt. The length of the heat exchanger is divided into a mesh of nx constant step dx.

Focus is kept on the properties of fluid 1 (biogas), which are considered function of temperature. Fluid 2 (refrigerant) and wall properties are assumed constant. For fluid 2, a refrigerant fluid in liquid phase (R-22 at 5 bar) is considered. Wall material is aluminium with thickness of 1 mm. Properties for biogas/landfill gas are calculated using a termodynamic model, as explained in Chap. 4. Biogas pressure is assumed constant all along the heat exchanger and equal to 1 bar. Composition does not change since there is no mass transfer, because no antisublimation of the CO_2 takes place. Since the density of biogas changes, also its velocity along the channel of the heat exchanger changes, in agreement with the mass balance. For each iteration velocity is calculated as

$$u_{1,x}^{t} = \frac{\dot{m}_1}{\rho_{1,x}^{t} A_1} \tag{6.11}$$

Energy balances (eqs. (6.3) and (6.4)) are discretized as follow:
Fluid 1:

$$V_1 \rho_{1,x}^{t-dt} c_{p,1,x}^{t-dt} \frac{T_{1,x}^{t} - T_{1,x}^{t-dt}}{dt} + V_1 u_{1,x-dx}^{t} \rho_{1,x-dx}^{t} c_{p,1,x-dx}^{t} \frac{T_{1,x}^{t} - T_{1,x-dx}^{t}}{dx} = -h_{1,x}^{t-dt} A_1 \left(T_{1,x}^{t-dt} - T_{w,x}^{t-dt} \right) \tag{6.12}$$

Fluid 2:

$$u_{1,x}^{t} = \frac{\dot{m}_1}{\rho_{1,x}^{t} A_1} \tag{6.13}$$

Wall:

$$u^t_{1,x} = \frac{\dot{m}_1}{\rho^t_{1,x} A_1} \tag{6.14}$$

From these equations it is possible to calculate temperature of Fluid 1, Fluid 2 and Wall at time t and position x.

Case 2: Solidification

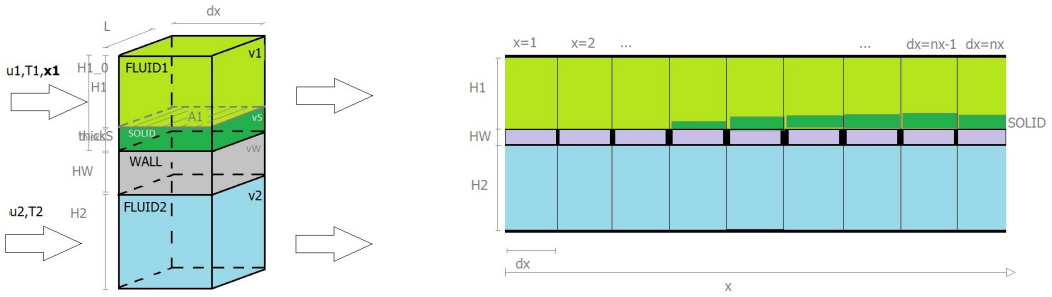

Frost layer growth period

Figure 6.4: Discretization of the geometry of the heat exchanger in case of frost formation.

Solidification of CO_2 takes place on the biogas side wall of the heat exchanger, where the biogas has the lowest temperature, and so the first place where solid formation condition is reached. So if the temperature of the wall (T_W) is lower than the Solid-Vapor Equilibrium temperature at biogas composition, part of the CO_2 on the biogas will be captured and stored as solid on the wall, creating a solid layer of thickness $thick_S$. Different frost density models have been developed and discussed in App. A. In this case, solid CO_2 density and heat capacity are considered as function of temperature as expressed by Maass and Barnes (1926) for the crystal CO_2 solid.

Thickness of solid layer is thus calculated from captured mass $M_{s,capt}$ and solid CO_2 density ρ_s:

$$thick_s = \frac{M_{s,capt}}{\rho_s} \tag{6.15}$$

$M_{s,capt}$ is obtained from the law governing the mass transfer (6.8).

The mass transfer coefficient h_m is calculated from the convective heat transfer coefficient h using the Chilton Colburn analogy (Chilton and Colburn, 1934) :

$$h_m = \frac{h}{\rho\ c_p Le^{1/3}} \tag{6.16}$$

where Le is the Lewis number, defined as the ratio between thermal and mass diffusivity, equivalent to the ratio between Schmidt and Prandtl numbers; ρ is density and c_p is the heat capacity. The convective heat transfer coefficient is calculated using an empirical correlation. Correlation developed for the CO_2 frosting problem are not availeble, to the author's knowledge. The correlation developed by Wang et al. (2000) is used in this work. The solid layer surface is considered to be at saturation condition (Solid-Vapor Equilibrium).

Solidification process contributes to the heat exchange through the latent heat of phase change: in particular solidification is an exothermic process, and thus it tends to rise solid/wall temperature. Energy balance for the wall becomes (6.4) discretized as:

$$V^{t-dt}_{w,x} \rho^{t-dt}_{w,x} c^{t-dt}_{p,w,x} \frac{T^t_{w,x} - T^{t-dt}_{w,x}}{dt} = h^{t-dt}_{1,x} A_1 \left(T^{t-dt}_{1,x} - T^{t-dt}_{w,x}\right) + M_{s,capt} \Delta h_{s-v} - h^{t-dt}_{2,x} A_2 \left(T^{t-dt}_{w,x} - T^{t-dt}_{2,x}\right) \tag{6.17}$$

where Δh_{s-v} is the latent heat of change of phase (from vapor to solid) considered constant with temperature and equal to 1019.37 kJ/kg (Lemmon et al., 2010).

If the accumulated amount of CO_2 is small, the thermal resistance of the solid layer can be neglected. In this case we can assume negligible the heat conduction process through the frost layer. We can so consider the temperature of the solid layer equal to the temperature of the wall. The influence of solid CO_2 formation on the heat transfer is considered modifying wall properties (density, heat capacity and volume). The density of the wall+solid CO_2 rho_{w+s} is calculated as the average of wall density rho_w and solid CO_2 density rho_s weighted on the volume of each layer (note that the surface is the same for wall and frost layer):

$$\rho_{w+s} = \frac{\rho_w V_w + \rho_s V_s}{V_w + V_s} = \frac{\rho_w H_w + \rho_s H_s}{H_w + H_s} \tag{6.18}$$

For the isobaric heat capacity of the wall+ solid CO_2 $c_{p,w+s}$ is calculated as the average of wall density $c_{p,w}$ and solid CO_2 density $c_{p,s}$ weighted on the mass of each layer :

$$c_{p,w+s} = \frac{c_{p,w} m_w + c_{p,s} m_s}{m_w + m_s} \tag{6.19}$$

The solid layer also changes the geometry of the flow section for the fluid 1. The value of the height of the channel ($H1$) is given by the height of the channel of the heat exchanger without solid CO_2 ($H1_0$) minus the thickness of the solid CO_2 layer $thick$:

$$H1_x^t = H1_0 - thick_x^t \tag{6.20}$$

So the velocity of fluid 1 is modified by three phenomena:

- change in mass flow (part of the CO_2 solidifies);
- change in density;
- change in flow section.

The three phenomena are taken into account to calculate the velocity at each iteration.

Initial and boundary condition

For our study we consider the case of fixed temperature for the inlet of biogas and refrigerant, and initial conditions for which initial temperature at initial time t_0 is fixed. It is a realistic case since in the heat exchanger inlet temperature can be controlled for both biogas and refrigerant.

6.4 Results

A model for simulating the global operation of a heat exchanger experiencing solid formation has been applied for a cryogenic biogas upgrading system, where the solid phase is pure CO_2 formed from a biogas flow, considered as a binary mixture of CO_2-CH_4. The complexity of the problem obliges to make some assumptions. Simplifications in geometry and flow arrangement have been done, and a lumped capacitance model assumption chosen. In this way, governing equations, including energy and mass balance have been written and discretized thanks to a finite volume numerical method. Solidification is considered to take place when temperature of the wall is lower than the solidification temperature of the biogas, at given composition and pressure, according to heat and mass transfer coefficients. The solid CO_2 layer growing on the walls of the heat exchanger modifies the heat transfer. Properties of solid CO_2 are thus to be known, in particular density, heat capacity and thermal conductivity. A bibliographic research

on experimental values of these properties is proposed in Appendix A and a model for computing thermodynamic properties of both solid CO_2 and biogas is presented in Chapter 4.

The simulation allows drawing temperature profiles in the heat exchanger at different time steps, as well as the growth of the thickness of solid CO_2 layer. Results obtained are compared with the analytic solution of the steady state problem considered without frost formation and no temperature dependent properties. The solution is given by following equations:

$$T_{1,steady} = A - B\frac{k_1}{k_2}\exp(-kx) \tag{6.21}$$

$$T_{2,steady} = A + B\frac{k_2}{k}\exp(-kx) \tag{6.22}$$

where A and B are obtained by imposing boundary conditions and k_i and k are:

$$k_i = \frac{AU}{\rho_i V_i u_i c_{p,i}} \tag{6.23}$$

$$k = k_1 + k_2 \tag{6.24}$$

Being ρ_i the density, V_i the volume, u_i the speed and $c_{p,i}$ the heat capacity of fluid i, and AU the global heat transfer coefficient of the heat exchanger:

$$\frac{1}{AU} = \frac{1}{h_1 A_1} + \frac{1}{h_2 A_2} \tag{6.25}$$

Results of the dynamic problem, compared with steady state solution are shown in fig. 6.5. In figure 6.6 it is possible to observe the evolution of the frost layer with time along the heat exchanger surface. As temperature of the wall is greater than the freezing temperature (SVE temperature) at biogas composition and pressure, temperature profiles tends to the steady state solution (fig. 6.5a). But when the temperature of the wall is lower than the freezing temperature (fig. 6.5b, 6.5c and 6.5d), solid CO_2 starts to form and a solid layer starts to grow. At this point temperatures of wall and biogas stop following the steady state solution, but they remains greater than the respective temperature profiles obtained in the case with no solid formation. This can be explained with the exothermic reaction of solidification, which tends to release energy to the biogas and wall. The CO_2 content in the biogas decreases thanks to the capture of solid carbon dioxide on the wall. It follows that the SVE temperature also decreases, according to the biogas phase diagram (fig. 6.7), obtained using the thermodynamic model presented in Chapter 4.

The influence of nitrogen and oxygen present in the landfill gas is analyzed by replacing biogas with a quaternary mixture of N_2-O_2-CH_4-CO_2. Results are based on the thermodynamic model (Chapter 4) and the experimental study (Chapter 5). The freezing temperature at ambient pressure of a landfill gas containing high amount of nitrogen (up to 20% in volume) is mainly a function of the CO_2 content in the feed gas. CO_2 solubility in vapor methane or vapor nitrogen and oxygen is in fact similar. The main impact, anyway, is the dilution of the mixture CH_4-CO_2 with nitrogen and oxygen, resulting in a lower CO_2 content in the gas flow entering the heat exchanger and thus a lower freezing temperature, less solid is formed (see fig. 6.8) and then the heat transfer is improved. Some variation in thermodynamic properties of fluid 1 can be also observed: the density of the fluid to be cooled is slightly higher in presence of nitrogen, and the heat capacity slightly lower. The result in the heat exchanger simulation is an improvement of the heat transfer and thus a more effective cooling of the landfill gas. The consequence is a better distribution of the solid layer along the wall of the heat exchanger, corresponding to longer cycles of frosting and defrosting of each heat exchanger compared to base case without nitrogen.

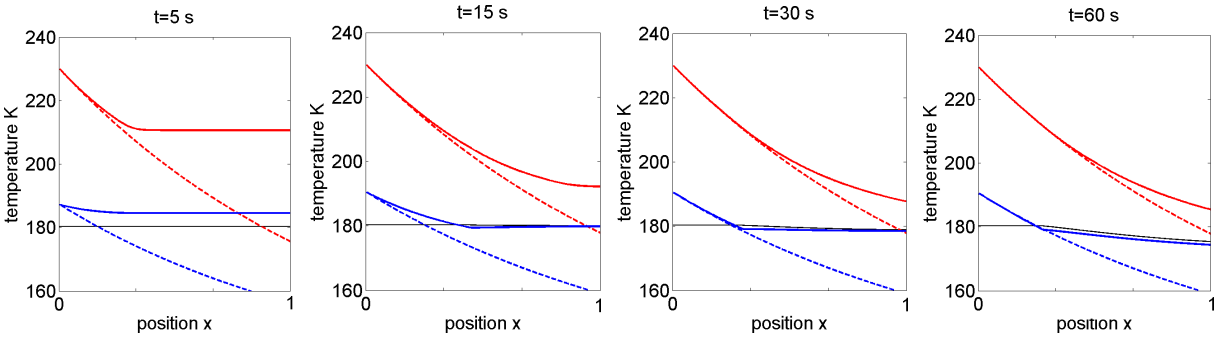

Figure 6.5: Temperature profiles at different time steps resulting from simulation of the solid CO_2 capture in the heat exchanger at ambient pressure. Biogas temperature -, wall temperature - and freezing temperature -. Dotted lines are temperature profiles resulting from analytic solution of steady state problem, without solid formation.

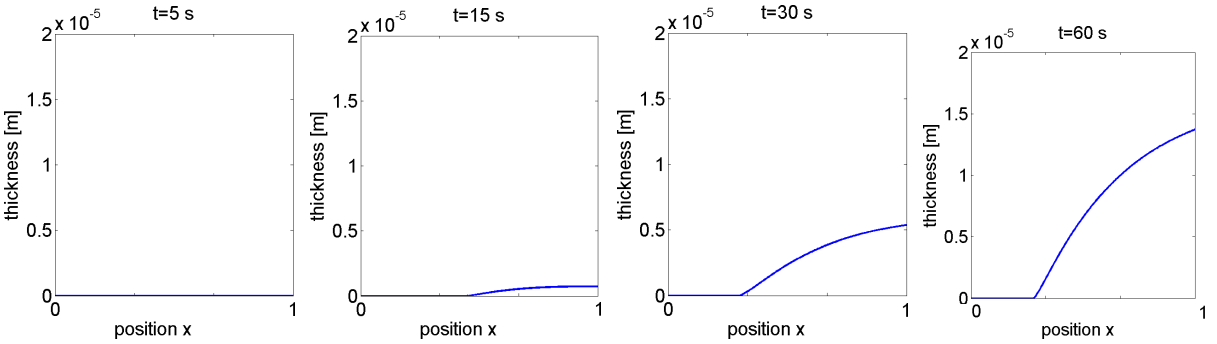

Figure 6.6: Solid layer thickness at different time steps resulting from simulation of the solid CO_2 capture in the heat exchanger at ambient pressure. Biogas temperature -, wall temperature - and freezing temperature -. Dotted lines are temperature profiles resulting from analytic solution of steady state problem, without solid formation.

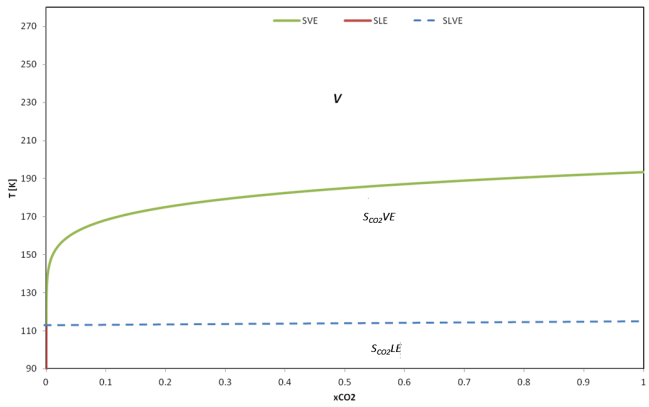

Figure 6.7: T-x phase diagram at the pressure of 1 bar for the binary CH_4-CO_2 system : (-) SVE boundary, (-) SLE boundary, (- -) SLVE temperature

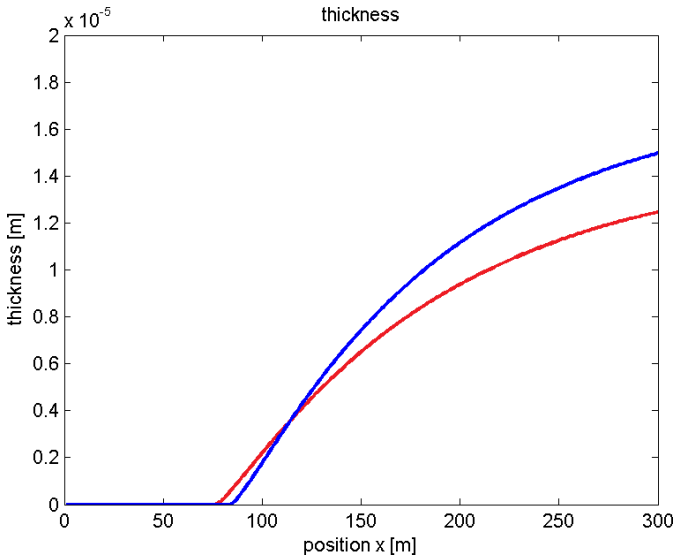

Figure 6.8: Comparison between solid layer thickness of a CH_4-CO_2 mixture (-) and a $N2$-CH_4-CO_2 mixture containing 20% (volume) of nitrogen (-)

Chapter 7

Biomethane liquefaction

In this chapter, the risk of uncontrolled solid formation during biogas liquefaction is studied and compared to the case of the liquefaction natural gas.

Résumé

Pour la liquéfaction du biométhane, le débit de gaz doit être comprimé à environ 15 bar et refroidi de nouveau à -120°C. Le procédé peut être comparé à la liquéfaction du gaz naturel, la principale différence étant la plus petite échelle et la pression de fonctionnement inférieure pour la liquéfaction du biométhane. De la même faon que le processus de production de GNL, un problème important est le risque de givrage de CO_2 pendant la liquéfaction, ce qui peut provoquer une obstruction des équipements. Comme présenté au chapitre 2.1, la concentration maximale de CO_2 dans le gaz naturel est estimée à 50 ppm afin d'éviter des problèmes de solidification lors de la liquéfaction. Dans le débit du biométhane entrant dans le systèeme de liquéfaction, la teneur en CO_2 est de 2,5% et donc la formation de solide est prévue dans l'échangeur de chaleur de production LBG. Pour cette raison, les échangeurs de chaleur sont similaires à ceux en charge de la capture de CO_2 présentés au Chap. 6. Plus précisément, le biométhane entrant dans l'échangeur de liquéfaction atteint la température de givrage autour de -98 °C, comme on peut le constater sur le diagramme de phase CO_2-CH_4 à 15 bar. Les diagrammes de phases et les calculs dans ce chapitre sont obtenus en utilisant un modèle thermodynamique présenté au Chap. 4. Une partie du CO_2 givre sur les ailettes de l'échangeur de chaleur et est ainsi capturé et séparé du flux de biométhane, qui devient plus riche en méthane. La formation et la séparation du CO_2 solide se termine lorsque le biométhane commence à se liquéfier: à la fin du processus de liquéfaction, la teneur en CO_2 du biométhane est proche de (idéalement égale à) la teneur en CO_2 de la phase vapeur au point triple (environ 0,3%).

Dans le cas où le GNL est produit à partir de gaz de décharge, une quantité importante d'azote peut rester dans le biométhane pendant la liquéfaction. L'effet de l'azote sur le procédé de liquéfaction est d'abord de baisser la température de liquéfaction. A 15 bar, un biométhane contenant 20% d'azote commence à se liquéfier à 152 K au lieu de 159 K. Dans la plage des conditions du procédé, la solubilité du CO_2 en phase vapeur ne change pas significativement avec la composition de la phase vapeur. En conséquence, plus de CO_2 est capturé dans l'échangeur de chaleur, puisque le biométhane suit la ligne d'équilibre SVE jusqu'à une température plus basse. Pour liquéfier complètement le courant de gaz, une température plus basse doit également être atteinte. En raison des spécifications sur le pouvoir calorifique et la teneur en azote et oxygène, les gaz de l'air doivent être éliminés: ce processus est couplé au processus de liquéfaction et est étudié au chapitre suivant.

7.1 Presentation of the problem

In the Cryo Pur process, after the CO_2 capture and separation in the heat exchanger, the biomethane has a molar composition of 97.5% of methane. At this point the biomethane can be further treated for the production of Liquefied BioGas (LBG).

For the liquefaction of biomethane, the gas flow needs to be compressed at higher pressure (around 15 bar) and cooled down again to -120° C. The process can be compared to the liquefaction of natural gas, with the principal difference being the smaller scale and the lower operating pressure for the biomethane liquefaction. Similarly to the LNG production process, an important issue is the risk of CO_2 freeze-out occurring during the liquefaction, that may cause equipment plugging. As said in Chapter 2.1, the maximum concentration of CO_2 in the natural gas is considered to be 50 ppm in order to avoid solidification problems during liquefaction. In the inlet biomethane flow the CO_2 content is 2.5% and thus solid formation is expected in the LBG production heat exchanger. For this reason, the heat exchangers are similar to the ones in charge of the CO_2 capture presented in Chap. 6. More precisely, the biomethane entering the liquefaction heat exchanger reaches the freezing temperature at around -98°C, as can be observed on the CO_2-CH_4 phase diagram at 15 bar (fig. 7.1). Phase diagrams and calculation in this chapter are obtained using a thermodynamic model presented in Chap. 4. Some CO_2 antisublimates on the fins of the heat exchanger and it is thus captured and separated from the biomethane flow, which changes its composition becoming richer in methane. The solid CO_2 formation and separation ends when the biomethane starts to liquefy: at the end of the liquefaction process the CO_2 content in the biomethane is close to (ideally equal to) the CO_2 content of the vapor phase at the triple point (around 0.3%). Following the cooling path on the CO_2-CH_4 phase diagram at 15 bar (fig. 7.1), the cooled biomethane reaches the SLVE temperature, around -114°C , where a liquid phase starts to form. Nevertheless, the biomethane do not enter the Liquid + Solid region , because its composition becomes richer in methane thanks to the solid CO_2 formation and separation. During the vapor to liquid transition, no more carbon dioxide can be capture since no solid is formed, so that the global composition of the Liquefied BioGas (LBG) is expected to be the same as the composition of the vapor phase at the SLVE temperature (less than 0.5%).

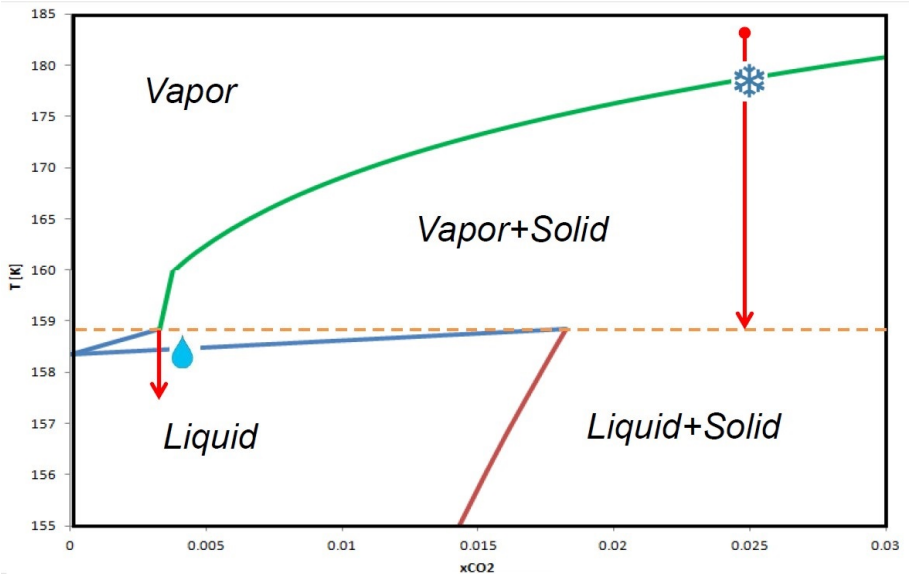

Figure 7.1: CO_2-CH_4 phase diagram at 15 bar. - SVE line, - VLE line, - SLE line, - - Triple Point temperature. Temperature scale on the y-axis is modified from 160 K for allowing the visualization of the freezing and the liquefaction points

7.2 About the maximum content of CO_2

Technical and scientific literature (Fisher and Ferschneider, 2010; Rufford et al., 2012) reports 50 ppm of CO_2 as LNG specification because of crystallization issues. This value is in fact considered the maximum content of CO_2 in the natural gas in order to avoid solid formation during liquefaction. As previously stated, at classical liquefaction pressure (40-50 bar) the solubility of CO_2 in methane and heavier hydrocarbons is much higher than 50 ppm, but this limit is empirically determined for avoiding freeze-out caused by local cold spots on equipment surfaces and transient shifts in temperatures and pressures (Timmerhaus and Flynn, 1989). In this section a study of the thermodynamic conditions that may cause solid formation during the liquefaction process is proposed and resulting limitations are compared to the existing ones.

Liquefaction processes of natural gas typically works at pressure around 40-50 bar, because the feed stream is already available at high pressure. In case of LBG production, the biomethane is available at lower pressure, 1-10 bar, and thus liquefaction is performed at lower pressures compared to natural gas (5-15 bar) for limiting compression costs. The effect of pressure on liquefaction is evident, in fact liquefaction temperature significantly increase with increasing pressure (from -160°C at ambient pressure to -90°C at 40 bar). Another difference between biomethane and natural gas is the presence of heavier hydrocarbons (ethane, propane, butane and pentane) which mainly increase the CO_2 solubility in liquid phase. For a simplified approach, the study of the binary CH_4-CO_2 without any heavier compound allows to understand the CO_2 freeze-out risk and obtained results are conservative compared to the results that would be obtained studyng a natural gas type mixture.

According to the T-x phase diagram of a CH_4-CO_2 binary mixture (fig. 7.1), a vapor stream to be liquefied encounters the SVE line before starting to condense when it is cooled down. As a consequence it forms solid CO_2 from the vapor phase, before being liquefied. This happens when the CO_2 content in the natural gas (or biomethane) is greater then the CO_2 content of the vapor phase at the SLVE temperature. On the contrary, if the natural gas composition is poorer in CO_2 than this value, the mixture will pass from the vapor to the liquid phase without solid formation. The CO_2 solubility in the vapor phase at the triple point can thus be considered as the maximum CO_2 content in order to avoid solid formation during liquefaction (fig. 7.1). It has to be noticed that the CO_2 solubility is much lower in the vapor phase than in liquid phase. At the SLVE at 15 bar, for example, CO_2 solubility in vapor phase is around 3200 ppm, while in liquid phase is 17000 ppm. This limit is, anyway, much larger than the 50 ppm limit usually reported. Contrary to the solubility in liquid phase, SVE boundary changes significantly with pressure: in tab. 7.1 maximum CO_2 content values in the binary mixture CH_4-CO_2 for pressures ranging from 1 to 40 bar are listed.

Once the inlet natural gas/biomethane is completely liquefied, the CO_2 solubility in the liquid phase is much higher than it was in vapor phase before the liquefaction, thus solid can only form if the temperature is significantly decreased. The degree of subcooling (ΔT_{sub}) of the LNG/LBG usually results from a trade-off between the cost of further cooling the fluid and the degree of vaporization accepted after the expansion at LNG storage pressure. Liquefied biomethane or natural gas is generally stored at lower pressure (often ambient pressure) in a highly insulated tank (fig. 7.2). Focusing on the solidification risk, for a binary mixture of methane with traces of carbon dioxide, the maximum subcooling before solid formation is reported in tab. 7.1. For obtaining this value, the SLE temperature of a mixture containing the maximum CO_2 content expressed in table 7.1 is computed (see fig. 7.3). It is slightly dependent from liquefaction pressure, since the variation of triple point temperature and the SLE temperature (at maximum CO_2 content) changes at almost the same rate with pressure.

In case the desired subcooling is greater than the maximum subcooling listed in table 7.1, the maximum CO_2 content in the natural gas or biomethane in order to avoid solid formation

Table 7.1: Maximum CO_2 content in the biomethane for avoiding solid formation during the liquefaction and the maximum subcooling from liquefaction temperature before encountering the Solid-Liquid boundary, at different pressures. Values are obtained using the PR+Zabaloy equation model presented in section 4.5

P (bar)	maxCO2 (ppm)	max ΔT_{sub} (°C)	P (bar)	maxCO2 (ppm)	max ΔT_{sub} (°C)	P (bar)	maxCO2 (ppm)	max ΔT_{sub} (°C)
1	7	23	11	1604	24	22	8401	22
2	30	24	12	1976	24	24	10469	21
3	80	24	13	2381	24	26	12882	21
4	156	24	14	2817	24	28	15662	20
5	256	25	15	3292	24	30	18980	20
6	382	25	16	3824	23	32	22579	19
7	541	25	17	4432	23	34	26800	18
8	738	25	18	5129	23	36	31737	18
9	981	24	19	5891	23	38	37498	17
10	1270	24	20	6617	22	40	44208	16

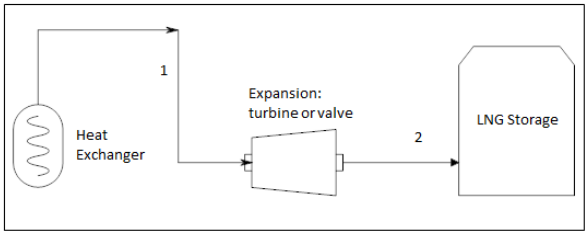

Figure 7.2: Scheme of a liquefaction process including the heat exchanger, the expansion valve or turbine and the storage tank.

depends on the final LNG/LBG temperature. In fig. 7.4 the maximum CO_2 content according to the final temperature of the liquefaction is reported. As an example, for LNG production at 40 bar and -150 °C the maximum CO_2 content is around 1000 ppm.

Another point of the liquefaction process where solid CO_2 formation may occur is during the expansion from liquefaction pressure to lower pressure. The expansion is in fact followed by a cooling and, in certain cases, vaporization of the LNG/LBG . The variation of the maximum CO_2 content with pressure has to be studied. As shown in figure 7.5, the triple point temperature of the binary mixture decreases with decreasing pressure (for temperature lower than -75 °C). The corresponding CO_2 content in the vapor phase decreases too. When the LNG/LBG is expanded to be stored at ambient pressure, the CO_2 content should not be greater than the solubility of CO_2 in liquid methane at -162 °C (methane boiling point), which is 275 ppm (fig. 7.4), in order to avoid the risk of solid formation in the storage tank. In case the storage pressure is higher, for example 6 bar, the boiling temperature of methane is -134°C and thus the limit is much higher (4300 ppm of CO_2).

Finally, potential solid formation problems can have place when the LNG/LBG is expanded and regasified at ambient pressure. In fact passing from the liquid to the vapor phase, the solubility of CO_2 sensibly decreases and thus CO_2 may frost in the expansion valve. To be sure that no solid will form during the expansion and gasification, the maximum CO_2 content in the biomethane or natural gas should be less than the CO_2 content of the vapor at the

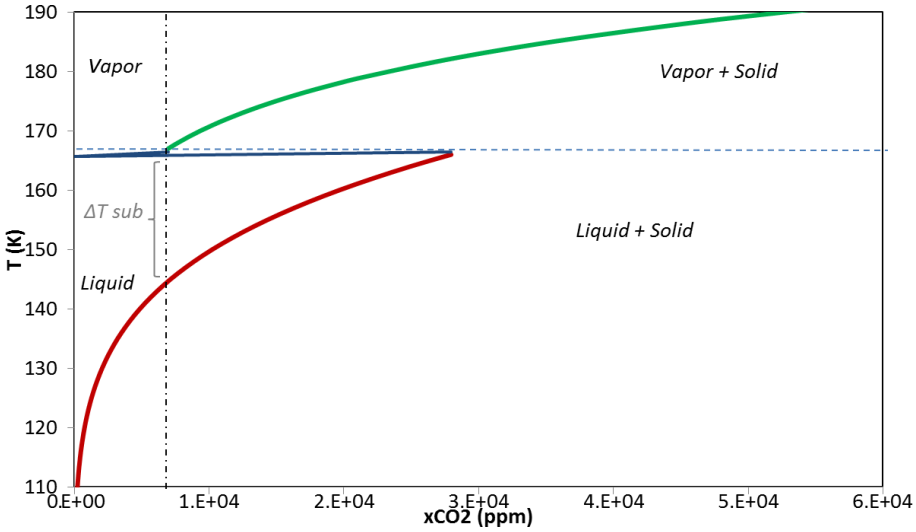

Figure 7.3: Tx phase diagram of the binary CH_4-CO_2 system at 20 bar. - SVE line, - SLE line,- VLE line and - - SLVE temperature.

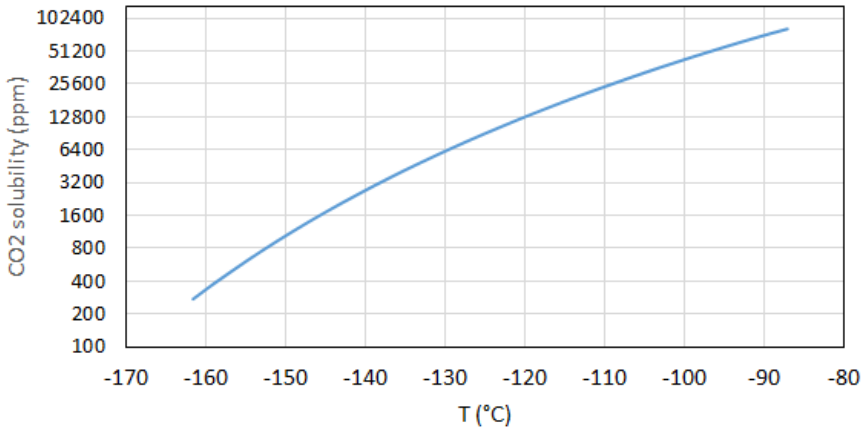

Figure 7.4: Variation of the CO_2 solubility with temperature

lower pressure triple point (7 ppm at 1 bar, as reported in tab. 7.1). Nevertheless, in actual operation, expanders and valves do not internally obey to equilibrium thermodynamics. Internal velocities of the fluid can be relevant and resident time not sufficient for allowing thermodynamics equilibrium to be established. This means that solid formation may not occurs even if CO_2 content is greater than indicated by thermodynamic limits (but not the contrary).

7.3 Influence of nitrogen

In case the LBG is produced from landfill gas, an important amount of nitrogen may remain in the biomethane during the liquefaction. The effect of the nitrogen on the liquefaction process is, firstly, to lower the liquefaction temperature. At 15 bar, a biomethane containing 20% of nitrogen starts liquefying at 152 K instead of 159 K.

In the range of conditions of the process, the solubility of CO_2 in the vapor phase does not change significantly with the composition of the vapor phase. As a consequence more CO_2 is capture in the heat exchanger, since the biomethane follows the SVE line down to lower

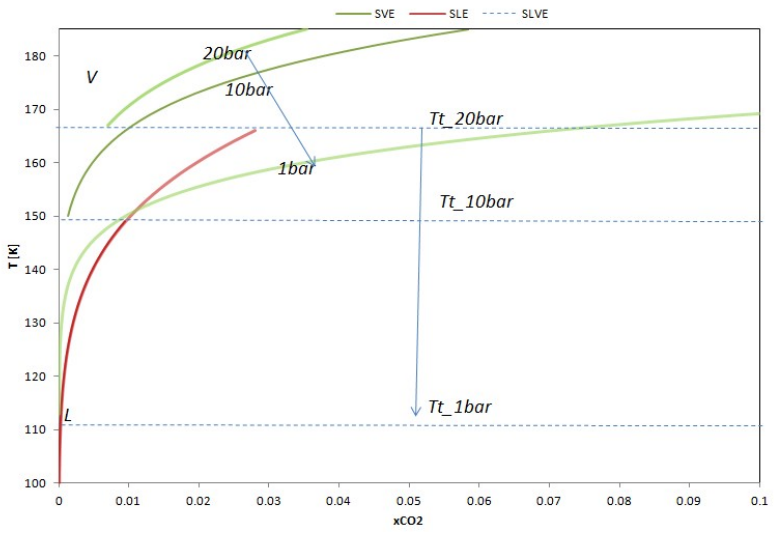

Figure 7.5: Variation of - SVE line, - SLE line and - - Triple Point temperature with pressure.

temperature (see fig. 7.6). To completely liquefying the gas stream, lower temperature has to be reached as well. Because of specification on Heating Value and nitrogen content, nitrogen has to be removed: this process is coupled with the liquefaction process and is studied in next chapter.

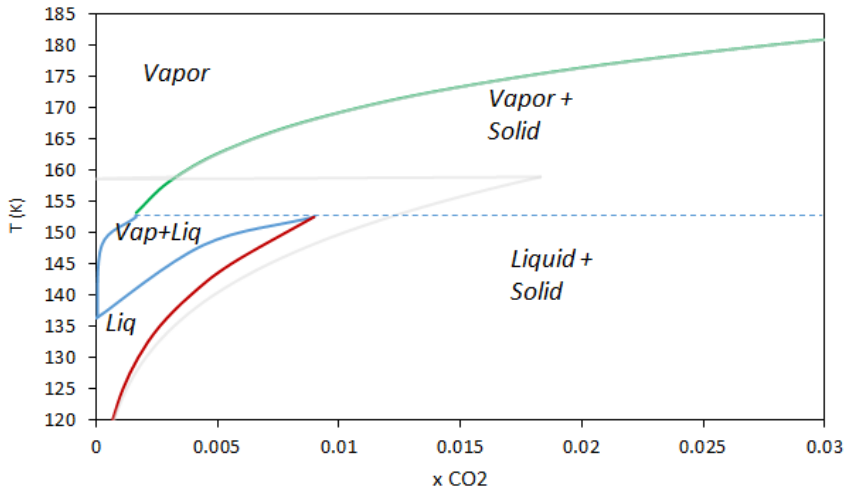

Figure 7.6: Phase diagram of the mixture N_2-CH_4-CO_2 at 15 bar with 20% nitrogen. - SVE line, - VLE line, - SLE line, - phase boundaries for the binary mixture of CH_4-CO_2.

7.4 Conclusion and discussion

As it can be seen in this chapter, the issue of solid formation risk during LNG and LBG production is a complicated and not well studied subject. The consequence is the existence of specifications for the CO_2 content in the natural gas liquefaction industry that seems to be extremely conservative and may be not necessary. The same specifications might be applied to biomethane liquefaction, as reported in Chap. 2.1. The interest of better understanding the

CO_2 freeze-out phenomenon is justified by the potential costs of further CO_2 removal in the LBG production. As explained before in fact, in the process studied in this work, the liquefied biomethane is produced with a CO_2 composition that is estimated to be 3200 ppm.

In order to study the phenomenon and have reliable predictions of CO_2 content limits, a thermodynamic model for phase equilibrium involving a solid phase is necessary tool for computing CO_2 solubility in liquid and vapor phase, phase diagrams, triple point conditions, liquefaction temperature as a function of pressure etc. Furthermore, the model has to be tested and calibrated against experimental data.

Chapter 8

Air removal

In this chapter a solution for the air removal from landfill gas is studied and designed.

Résumé

La teneur en azote et en oxygène dans le gaz de décharge est due à l'entrée d'air dans le système d'enfouissement et de collecte du gaz. Généralement, le gaz de décharge est extrait en employant un léger vide dans les tuyaux enfouis dans la décharge. Généralment, la teneur en air dans les gaz de décharge est de 20% de la fraction volumique. Dans un digesteur anaérobique, le biogaz est collecté directement dans le digesteur et donc l'air n'est généralement pas présent. Dans certains cas, de l'air peut être injecté (jusqu'à 8% en volume) dans le digesteur de biogaz afin de réduire la teneur en sulfure d'hydrogène par oxydation bactérienne, ce que l'on appelle la désulfuration biologique.

D'autre part, il est souhaitable de fournir du méthane de qualité correspondant aux spécifications vente, habituellement une teneur en gaz inertes inférieure à 3,5% (voir le chapitre 2.1). Un tel carburant de qualité supérieure est facilement commercialisable et largement utilisable pour l'injection dans le réseau du gaz naturel (gaz type H) ou comme combustible pour véhicule (GNV). Pendant la séparation cryogénique du CO_2, l'air n'est enlevé et donc à la fin d'une installation classique de valorisation de biogaz, le biométhane produit à partir de gaz de décharge est encore riche en azote et en oxygène. Dans le cas où la teneur en air est importante, une unité de séparation d'azote et d'oxygène est nécessaire.

Parmi les technologies existantes et les développements potentiels possibles, la distillation cryogénique semble être la plus adaptée pour une installation de valorisation cryogénique de biogaz. Dans le procédé CryoPur, le biométhane est produit à environ -115 ° C avec 2,5% de CO_2 et ensuite liquéfié à une pression plus élevée (15 bar). Les technologies d'adsorption présentent des problèmes d'inhibition cinétique à basse température, tandis que les technologies d'absorption ajoutent au procédé un traitement complexe du solvant. Enfin, les membranes sont exclues en raison des pertes élevées en méthane (*methane slip*). Parmi les différentes configurations de cryo-distillation, selon MacKenzie et al. (2002), le procédé à double colonne a une consommation d'énergie la plus faible pour une teneur élevée en N_2 (supérieure à 30%), mais dans le cas du gaz de décharge, la teneur en N_2 est inférieure (environ 20%). Pour limiter le coût d'investissement, une configuration avec une seule colonne a été considérée comme la solution la plus appropriée et a donc été simulée.

Une pré-simulation de la colonne a été réalisée afin d'estimer le nombre d'étages théoriques et le taux de reflux. On a utilisé la méthode Gilliland, Underwood, Winn, basée sur la corrélation de Gilliland (1940) pour calculer le rapport de reflux requis pour un nombre déterminé d'étages, la corrélation de Underwood (1948) pour le rapport de reflux minimal et la corrélation de

Winn (1958) pour le nombre minimum d'étages. À ce moment de la conception de la colonne, aucune information sur la taille et le type de colonne n'est disponible. Cette simulation est utile pour avoir une première estimation de la température et de la puissance du condenseur et du rebouilleur, ainsi que le nombre minimal d'étages théoriques et le rapport de reflux minimal.

Une seconde simulation rigoureuse a été réalisée à l'aide du logiciel de simulation Aspen Plus. Le modèle RADFRAC est utilisé pour simuler la colonne, étant capable de résoudre les bilans d'énergie et de masse à chaque étage de la colonne et donc de fournir des profils de composition et de température à l'intérieur de la colonne. On choisit une colonne à garnissage en raison de l'efficacité garantie malgré le petit diamètre de la colonne imposé par le faible débit du procédé étudié. Le but de la simulation est de dimensionner la colonne de distillation en respectant la spécification du bioGNL (97,5% de méthane, moins de 1% d'azote), d'assurer un faible methane-slip (moins de 1% du débit massique de méthane) et d'optimiser la consommation énergétique. La hauteur de la colonne a été limitée à des valeurs raisonnables (3,5 m de garnissage) afin de rendre la construction possible sur l'installation existante. En conséquence, le nombre d'étages théoriques est limité à 14, en fonction de l'efficacité du garnissage structuré. Le diamètre de la colonne est choisi selon les règles et corrélations communément utilisés en ingénierie, pour assurer une bonne distribution de liquide et de vapeur. Le diamètre choisi est de 120 mm.

La formation de CO_2 solide doit être évitée en raison du risque de bouchage dans le garnissage structuré de la colonne, ce qui provoque des problèmes de fonctionnement et une efficacité réduite de la colonne. Les conditions de givrage au CO_2 doivent être vérifiées à différents points de la colonne, suivant les profils de température et de composition établis dans la colonne. Pour chaque étage de la colonne, la teneur en CO_2 en phase vapeur et en phase liquide est donc comparée à la solubilité prédite à partir du modèle thermodynamique implémenté et présenté au Chapitre 4. Si la composition de CO_2 dans la colonne est supérieure à la solubilité du CO_2, du solide peut se former. La simulation effectué dans ce chapitre montre que le design choisi ne présente pas des risques de formation de solide.

8.1 Presentation of the problem

Air content is present in the landfill gas, typically 20% of volume fraction, so its removal is needed for respecting the biomethane specifications in terms of heating value and composition.

The nitrogen and oxygen content in the landfill gas is due to the air ingress to the landfill and gas-collection system. Generally, the landfill gas is extracted by employing a slight vacuum on pipes buried in the landfill. Typical air content in landfill gas is 20% of volume fraction. In an anaerobic digester, the biogas is collected directly from the vessel and thus air is not usually present. In certain cases some air can be injected (up to 8% by volume) in the biogas digester in order to reduce the hydrogen sulfide content through bacterial oxidation, the so-called biological desulfurization.

On the other hand, it is desiderable to provide methane of fuel-grade or sales-gas quality, typically with no more than 3.5% of molar concentration of inert gases (see Chap. 2.1) from biogas and landfill gas. Such high-grade fuel is readily marketable and widely useful for gas grid injection or as vehicle fuel. During the CO_2 cryogenic separation, no air is removed and thus at the end of a classical upgrading plant biomethane produced from landfill gas is still rich in nitrogen and oxygen. In case air content is important, a simple end-flash may not be sufficient for obtaining a fuel with less than 1% of nitrogen. A further process, the air removal unit, is necessary.

8.2 State of the art

Usually biogas upgrading plants are limited to the CO_2 removal after dehydration and purification from H_2S, siloxanes etc. Air removal is still not an established technology for biogas upgrading. Nevertheless it is a necessary treatment for allowing landfill gas to be injected in the natural gas grid, used as a vehicle fuel or liquefied for transport. In the natural gas field, nitrogen is removed when low quality gas sources are exploited. In this case a Nitrogen Rejection Unit (NRU) is needed. Different separation technologies exists for N_2 removal, exploiting differences in the molecular properties or thermodynamic and transport properties of nitrogen and methane. Four main technologies exist on the market, exploiting different separation mechanism:

- Distillation (separation trough creation of a second phase by heat transfer)
- Absorption (in a liquid solvent)
- Adsorption (on a porous solid)
- Membranes (separating molecules by permeation)

Distillation

Distillation is the most diffused technology for large scale plants. For separating methane and nitrogen by distillation, cryogenic temperatures are needed. Increase in pressure is an advantage for the separation, increasing the difference in volatility. For this reason cryogenic distillation is usually operate at high pressure (25-30 bar). The maximum operating pressure allowing to have a quasi-pure nitrogen stream at the top of the column is represented by the nitrogen critical pressure (33.96 bar). With the cryogenic distillation is possible to obtain methane with purity meeting the desired standards (less than 2.5% of nitrogen content) and with low methane slip (methane volume fraction in the vented nitrogen can be less than 0.1%), treating a wide range of N_2 feed contents (from 1% to 60%). Cryogenic distillation is a mature technology, but advancement in the technology can still be applied to make it suitable for small scale applications. Different configurations are possible; the most common process configurations are: single column process, double column process, two or three columns process.

Absorption

Absorption is not a common practice for nitrogen rejection. Nevertheless commercial processes exists operating by physical absorption (AET, 2003). The physical solvent is hydrocarbon oil that selectively absorbs methane. The CH_4 is recovered from the solvent through a series of flash vessels. The large amount of solvent needed and the cost of re-compression of methane after recovery from solvent make this technology too expensive for large scale plants.

Adsorption

Gas adsorption takes advantage from the different interaction of methane and nitrogen molecules with the surface of a solid adsorbent. It is one of the most suitable processes for small scale nitrogen rejection units in the liquefied natural gas production industry. Solid adsorbent can be zeolites, activated carbon or titanosilicates (Rufford et al., 2012). The adsorption is mainly governed by the thermodynamic equilibrium and the kinetic of adsorption. The equilibrium adsorption capacity increases with pressure and decrease with temperature. This principle is used for the regeneration (desorption) of the sorbent: in Temperature Swing Adsorption (TSA) processes, the desorption is achieved by increasing the temperature, while in Pressure Swing Adsorbtion (PSA) processes by lowering the pressure. Recently Saleman et al. (2015) described a dual-reflux pressure swing adsorption process capable of methane-nitrogen separation at ambient temperature and around 5 bar with activated carbon, which could be of relevance to biogas upgrading. On the other hand, low temperature inhibits the kinetic of adsorption, making difficult to exploit an adsorption process at cryogenic conditions.

Membranes

Membranes operate as semi-permeable barrier where a component passes through the membrane given a sufficient driving force (difference in partial pressure). Main advantages are the simplicity of the process configuration, low modification to the existing plant and low thermal energy requirements. However, the use of membrane for N_2 removal is sparse, mainly because of cost increasing with nitrogen content in the inlet flow and with degree of purity demand. The existing technology can treat natural gas with 20% of nitrogen and gives a purity of 96% of methane. Another negative point is the high methane content remaining in the nitrogen rich stream (methane slip).

Concluding, among the existing technologies and feasible potential developments, cryogenic distillation seems to be the more adapted for a cryogenic upgrading plant. In CryoPur process, the biomethane is produced at around -115°C with 2.5% of CO_2 and then liquefied at higher pressure (15 bar). Adsorption processes present problems of kinetic inhibition at low temperatures, while absorption adds complicated solvent treatments to the process. Finally membranes are excluded because of the characteristic high methane slip and low quality methane recovery. Among the different cryo-distillation configurations, according to MacKenzie et al. (2002), the double column process has the lowest energy consumption for high N_2 content (higher than 30%). In case of landfill gas, the N_2 content in the feed is lower (about 20%): the two or three columns process has slightly lower energy consumption than single column process at low N_2 content, but investment cost can be assumed to be two or three times higher than the single column. For this reasons, a single column distillation has been considered the more suitable solution and has been simulated.

8.3 Simulation and design of a cryogenic distillation column

A distillation column is the unit operation for separation through distillation. It is composed of a tower containing a number of distillation plates or a packing for increasing the surface of

contact between liquid and gas. The methane rich product is collected as a liquid at the bottom where the liquid is partially vaporized in the reboiler and then re-circulated in the column. The nitrogen rich stream is extracted from the top of the column where a condenser condensate a fraction of the distillate for re-circulating in the column. The fraction of the top stream that is condensate and re-circulate is called Reflux Ratio (RR). The reflux ratio is defined as the ratio between the Reflux and the vapor entering the condenser.

A key parameter for designing the process is the operating pressure. In fact both top and bottom temperatures increase with increasing pressure (see fig 8.1).

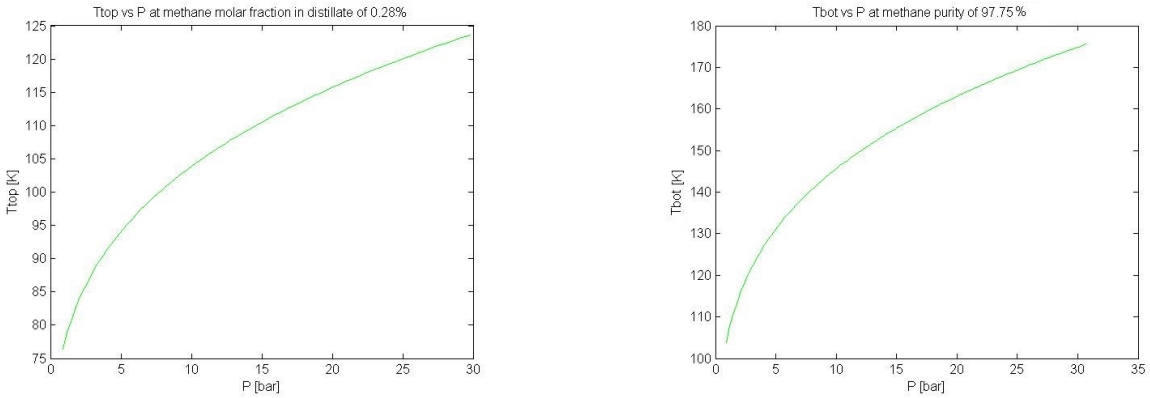

Figure 8.1: Condenser and reboiler temperatures vs pressure of the air separation column

At cryogenic distillation operating conditions (temperature ranges from -156 and -117°C), CO_2 may solidify and thus the air separation unit has to be placed downstream of the CO_2 removal heat exchangers. The biomethane liquefaction system should be placed upstream to the column in order to take advantage of the further CO_2 separation. Since the column is designed to be installed on an existing upgrading plant, cryogenic distillation operating pressure is chosen as the liquefaction pressure, 15 bar, avoiding the addition of a further compressor. The landfill gas is thus firstly cooled down and upgraded removing CO_2 at ambient pressure, then compressed and liquefied at 15 bar. The biomethane at this point contains 0.3 mol% of CO_2 (see Chap. 7) and finally enters the air removal distillation column where nitrogen is removed at the top of the column and LBG is collected at the bottom, with a methane content of 97.5 mol%.

Air separation unit is auto-thermal since it does not requires external refrigeration: the required low temperature duty of the condenser is provided by expanding and evaporating a fraction of the produced Liquefied Biogas (LBG). With reference to figure 8.2, a fraction of the LBG bottom product (C1) is expanded throught the expansion valve (D430) and sent to the condenser. A further heat exchanger (HE2) is used for cooling the liquefied biomethane (7-8) exiting the liquefaction heat exchanger (SS400) by heating the expanded LBG stream (C3-C4), which is finally re-injected in the process before the compressor (CP410). A chiller allows to cool the compressed biomethane down to 10°C (5), and the heat exchanger HE1 to further cool it down to -90°C (6) recovering the heat of the biomethane at 1 bar (2-3). The reboiler duty is recovered by the refrigerant stream (R1-R2) coming from the integrated cascade in charge of the refrigeration of the upgrading process. The distillate is a nitrogen and oxygen rich streaming, while the bottom product is the liquefied biogas (LBG).

A pre-simulation of the column has been performed in order to estimate the number of theoretical stages and the reflux ratio. The Gilliland, Underwood, Winn shortcut method has

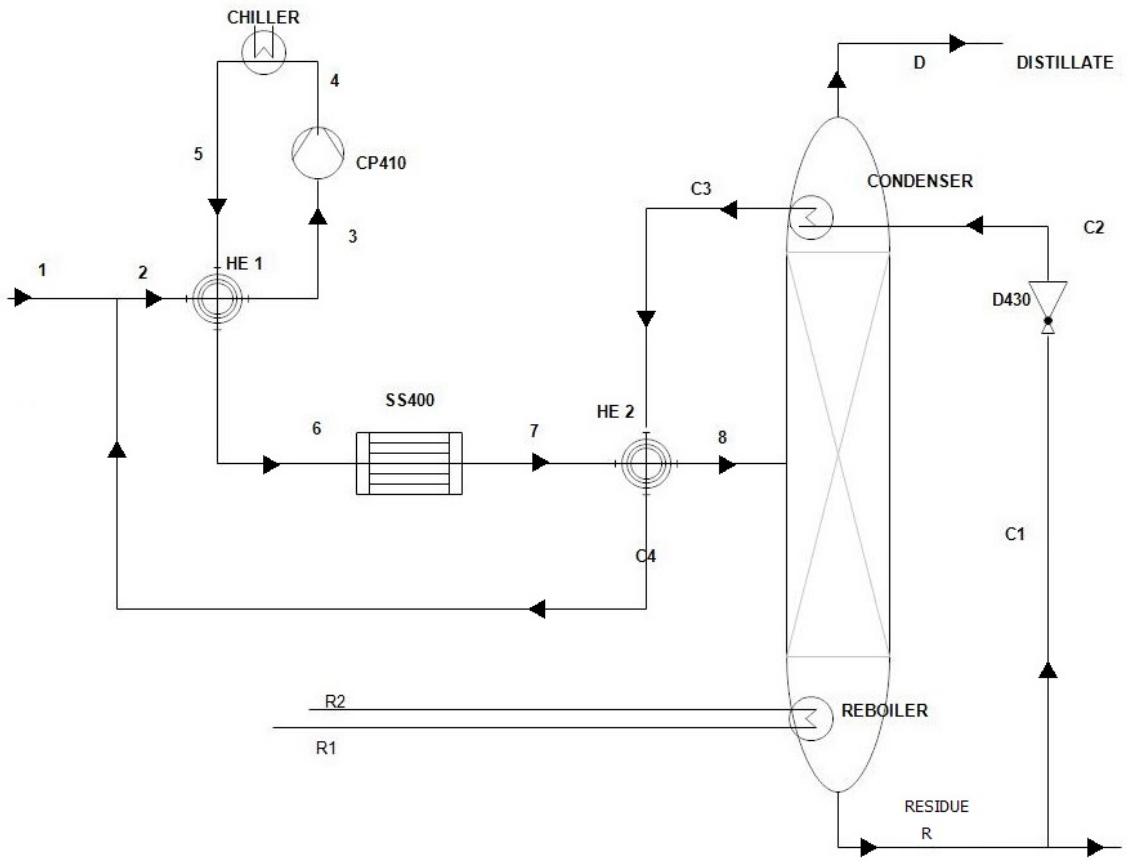

Figure 8.2: Scheme of the air removal system integrated with the liquefaction system

been used, based on the Gilliland (1940) correlation for computing the required reflux ratio for a specified number of stages, the Underwood (1948) correlation for the minimum reflux ratio and the Winn (1958) for the minimum number of stages. At this moment of the column design, no information about the size and type of column are available. The shortcut method is useful for having a first estimation of the condenser and reboiler temperature and duty, as well as the minimum number of theoretical stages and the minimum reflux ratio. Results are summarized in tab. 8.1.

Table 8.1: Results of the simulation using the Gilliland, Underwood, Winn shortcut method

Pressure (bar)	Minimum Number of stages	Minimum RR
15	6	4.11

A second and rigorous simulation have been performed using the Aspen Plus simulation software. The RADFRAC model is used for simulating the column, being able to solve energy and mass balances at each stage of the column and thus to provide composition and temperature profiles inside the column. The choice between a plate or packed column has been made by considering the advantages and disadvantages of each type of column. In particular, a packed column is chosen, mainly because of the small diameter of the column imposed by the small flowrate of the studied process (90 Nm^3/h). Structured packing is considered more suitable, thanks to its better efficiency that allows to reduce the height of the column compared to random packing.

The aim of the simulation is to size the distillation column respecting LBG product specification (97.5% of methane, less than 1% of nitrogen), assuring low methane slip (less than 1% of the methane mass flowrate) and optimize energy consumption for the liquefaction and separation process. A further constraint is given by the minimum temperature of the condenser, equal to the temperature of the expanded LBG at atmospheric pressure (-162°C). The height of the column was limited to reasonable values (3.5 m of packing section) in order to make the construction feasible on the existing plant. As a consequence, the number of theoretical plates is limited to 14, according to the efficiency of the structured packing. The diameter of the column is chosen according to the common engineering rules and correlations, for ensuring good liquid and vapor distribution without exceeding the flooding velocity. The chosen diameter is 120 mm. Furthermore, flammability of the gas mixture is checked along the process, verifying that the methane oxygen ratio is outside the flammability limits.

One of the parameters to be set is the outlet temperature of the liquefaction heat exchanger SS400, defining the vapor fraction of the stream entering the column. With reference to figure 8.2, the outlet of the liquefaction heat exchanger is indicated as point 7, thus the outlet temperature is called T7. Reducing this temperature has a double effect: firstly the heat exchanger duty increases and the performances of the refrigeration cycle decreases, resulting in a greater energy consumption. On the other hand the condenser duty decreases since the feed stream of the column is colder. Decreasing condenser duty means less LBG recirculated for providing the refrigeration to the condenser and thus lower energy consumption for the compression, together with a larger amount of LBG produced. Results are represented in fig. 8.3. The variation of the total energy consumption per Nm^3 of produced LBG with T7 is weak in a range of temperature close to the dew point of the LBG. T7 is thus set so that the quality of the stream at the outlet of the heat exchanger SS400 is less than 0.1.

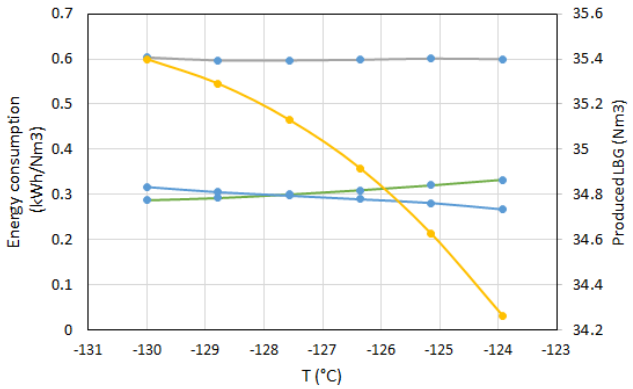

Figure 8.3: Energy consumption per Nm^3 of produced LBG as function of the outlet temperature of the liquefaction heat exchanger (T7). The air content of the landfill gas treated is 20%. - compressor duty, - liquefaction heat exchanger duty (COP=0.45), - total, - produced LBG

In order to obtain desired methane concentration in the bottom product and methane slip, two main parameters are optimized: the reflux ratio and the distillate to feed ratio. Results of the simulation are presented in tab. 8.2

8.4 Risk of solid formation in the column

Heavy components like carbon dioxide tends to concentrate at the bottom of the column. The risk that the concentration of CO_2 at one point of the column is high enough to form a solid phase has to be checked. Solid formation has to be prevented because of plugging risk in the structured

Table 8.2: Results of the simulation using the RADFRAC model from Aspen Plus

Pressure (bar)	Condenser temperature (°C)	Condenser duty (kW)	Reboiler temperature (°C)	Reboiler Duty (kW)
15	-156.1	1.2	-116.9	1.7
Inlet biomethane (Nm^3/h)	Air content at the inlet	Produced LBG (Nm^3/h)	CH_4 content	
46.7	20%	36.5	97.5%	

packing of the column, causing operation problems and reduced efficiency of the column. CO_2 frosting conditions should be verified at different point of the column, since temperature and composition profiles are established in the column. Solid formation prediction can be performed in order to prevent uncontrolled solid formation. For each stage of the column, CO_2 content in vapor and liquid phase has to be compared with predicted solubility at same temperature and pressure obtained from the model presented in Chapter 4. If the CO_2 composition in the stream is greater than the CO_2 solubility, solid can form. Otherwise there is no risk of solid formation in the column. Results of the simulation are proposed in fig. 8.4: it is possible to see that in the column with chosen configuration solid CO_2 formation risk is avoided. From composition profile it is possible to recognize the plate where feed stream is located, corresponding to an net change of slope. The zone below the feed stream plate is where CO_2 content is closer to the solubility limit. Nevertheless, there is a safety temperature margin of around 10 K before solid formation condition is reached.

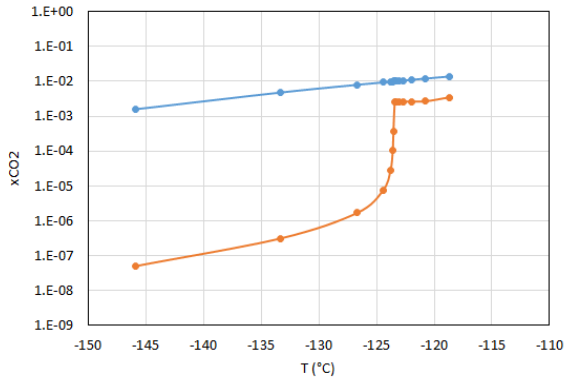

CO_2 concentration in the liquid phase vs temperature of each theoretical plate and estimated CO_2 solubility in the liquid phase.

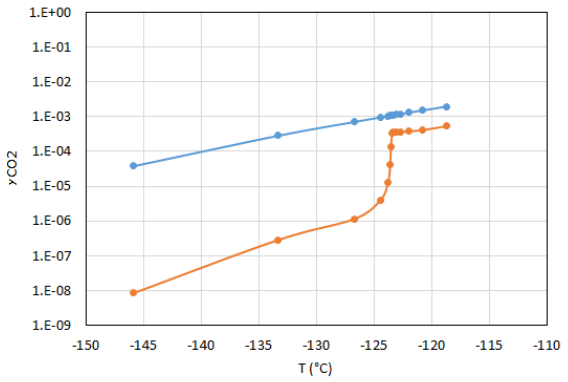

CO_2 concentration in the vapor phase vs temperature of each theoretical plate and estimated CO_2 solubility in the vapor phase.

Figure 8.4: - CO_2 concentration in the liquid and vapor phase, - CO_2 solubility

Once again, in order to perform this kind of verification, a thermodynamic model able to predict the Solid-Liquid and Solid-Vapor equilibrium is necessary. Furthermore, the influence of nitrogen and oxygen on the CO_2 solubility in liquid and vapor phase has to be investigated through a model but also by experimental verification.

Part IV

Conclusions and perspectives

Chapter 9

Conclusions and perspectives

Résumé

La simulation du processus cryogénique de valorisation et liquéfaction du biogaz montre la nécessité d'un modèle thermodynamique capable de prédire les conditions de solidification du CO_2. Deux modèles thermodynamiques ont été comparés: d'une part, une équation d'état de Peng Robinson a été couplée à l'expression de fugacité solide proposée par Rodriguez-Reartes et al. (2011) (équation de Zabaloy). Pour améliorer la capacité du modèle à représenter l'équilibre entre des phases fluides et solides, les paramètres d'interaction binaires de l'équation Peng Robinson ont été régressés sur les données SLVE des systèmes CH_4-CO_2 et N_2-CO_2 et SLE pour l'O_2-CO_2. La représentation de la solubilité du CO_2 dans le méthane, azote et oxygène liquide est significativement améliorées en utilisant les paramètres régressés dans ce travail. La déviation absolue moyenne (AAD) sur les données d'équilibre solide-liquide (SLE) est réduite de 513% à 26.4%. Un second modèle couplant l'équation d'état GERG-2008 et l'équation d'état de Jager et Span (2012) pour le CO_2 solide a été testé. La comparaison avec les données montre que ce modèle présente une meilleure représentation des données d'équilibre vapeur-liquide (VLE) et des performances dans la représentation des données SLE et SVE qui sont légèrement moins bien que l'équation PR EoS + Zabaloy avec les paramètres régressés dans ce travail. Les deux modèles tendent à surestimer la solubilité du CO_2 en phase liquide. L'intervalle de validité de l'EoS GERG-2008 couvre les conditions de fonctionnement du processus étudié et l'opinion de l'auteur est donc que cette équation d'état, couplé avec l'équation de Span and Wagner pour le CO_2 solide, convient pour être utilisé dans la simulation et la conception du procédé cryogénique et pour la prédiction de la formation du CO_2 solide.

Néanmoins, rien ne garantit que l'EoS GERG-2008 soit plus précis que l'EoS Peng Robinson dans les régions où les données disponibles au moment du développement de l'équation GERG étaient limitées, en particulier dans la région à basse température, comme le montrent May et al. (2015) et Rowland et al. (2016). Dans les régions où très peu de données sont disponibles mais une précision élevée est requise, la procédure appropriée sera de produire des données expérimentales d'équilibre de phases et de régredir les nouveaux paramètres pour l'EoS, comme proposé par Rowland et al. (2016).

Concernant le procédé, la liquéfaction du biométhane présente, de la même manière que la liquéfaction du gaz naturel, l'enjeu du risque de givrage du CO_2. Pour la production de gaz naturel liquéfié, la teneur en CO_2 est limitée à 50 ppm afin d'éviter la formation de solides. Dans ce travail, on montre que cette limite est conservatrice et donc, surtout pour l'application au bioGNL, une meilleure connaissance du phénomène et des conditions de formation de solide, ainsi qu'une prédiction de solubilité fiable peuvent permettre d'éviter des coûts de séparation et les risques de bouchage des équipements. L'approche utilisée dans ce travail montre des résultats encourageants concernant les mesures observées sur l'exploitation de la centrale pilote.

La concentration de CO_2 mesurée dans le LBG produit est d'environ 3000 ppm, comme prédit dans ce travail. La question de la formation de solides et des limites de CO_2 dans le GNL / bioGNL est d'une grande importance pour réduire les coûts de séparation. Les spécifications utilisées pour le moment ne sont pas vraiment justifiées par des résultats expérimentaux ou modélisés, mais elles ne sont que des valeurs conservatrices permettant d'éviter le problème de la formation de solide. La définition de spécifications plus rigoureuses pourrait conduire à des conditions de fonctionnement moins strictes et des solutions technologiques optimisées.

Dans ce travail, une colonne de cryo-distillation pour la séparation de l'air de biogaz de décharge a été étudiée et conçue. La simulation permet de vérifier le dimensionnement et l'absence de formation de CO_2 solide dans la colonne. Les résultats montrent que le bioGNL produit répond aux normes en termes de teneur en méthane et en azote et que le risque de formation de solides est évité dans la colonne. L'unité de séparation d'air sera installée et testée sur le pilote dans les prochains mois. De cette manière, les résultats de la simulation peuvent être comparés aux conditions de fonctionnement réel. Cela permettra d'optimiser la conception de la colonne et l'intégration dans le processus de liquéfaction.

Conclusions and perspectives

The biogas and landfill gas upgrading process is a necessary step for the increasing utilization of biomethane as vehicle fuel or in the natural gas grid. Recently, particular interest has been shown on the production of Liquefied BioGas (LBG) and different plants have been built. LBG presents advantages for its transport and storage compared to the compressed biogas, and innovative truck fueling solution are developed. Biomethane is in fact an *advanced liquid bio-fuel* (also called *second generation bio-fuel*) with environmental advantages compared to gasoline: low NOX and particle emission and greenhouse gas emission reduced up to 90%. Cryogenic upgrading is thus gaining interest compared to other available technologies because it is particularly suitable for being coupled with biomethane liquefaction thanks to its low operating temperature. Low temperatures and high CO_2 concentration means that the process has to deal with solid CO_2 formation. The Cryo Pur process takes advantages from solid formation for separating carbon dioxide from the biogas flow. The solidification needs to be controlled in order to optimize the design of the equipments and obtain a final product that meets the standards defined by its final use.

In order to provide reliable tools for solid formation comprehension in the treated landfill or biogas flow, and accurate prediction of CO_2 solubility in vapor and liquefied biomethane, a thermodynamic model has been developed. The model is able to handle coexisting solid CO_2 and fluid phases in a landfill gas mixture (CH_4-CO_2-N_2-O_2) and compute thermodynamic properties of the system. Two thermodynamic models have been compared: firstly a Peng Robinson Equation of State has been coupled with the solid fugacity expression proposed by Rodriguez-Reartes et al. (2011) (Zabaloy equation). For improving the capability of the model in representing phase equilibrium involving a solid phase, binary interaction parameters have been regressed on SLVE data of the CH_4-CO_2 and N_2-CO_2 systems. For the O_2-CO_2 systems no SLVE data are available but, comparing data of solubility CO_2 in liquid oxygen and results from model with non regressed parameters, high deviation is shown. Predicted solubility in liquid oxygen results even higher than the solubility in liquid methane and thus, binary interaction parameter for the O_2-CO_2 system is regressed on selected data available in literature. The performances of the model with parameters regressed in this work are significantly improved for representing Solid-Fluid phase equilibrium, as shown by the comparison with literature data. The AAD on CO_2 solubility (SLE) is reduced from 513% to 26.4% using parameters regressed in this work instead of parameters available in literature. For improving the prediction of the Vapor-Liquid Equilibrium and thermodynamic properties, a second model coupling the GERG-2008 Equation of State and the Jager and Span Equation of state for solid CO_2 has been tested. Comparison with data shows that this model has a better representation of VLE data and performances in representing SLE and SVE data that are slightly worse than the PR EoS+Zabaloy Equation with parameters regressed in this work. Furthermore, both models tends to overestimate the CO_2 solubility in liquid phase. The range of validity of the GERG-2008 EoS covers the operating conditions of the studied process and thus, the opinion of the author is that this model is suitable for being used in the simulation and design of the process, and for the prediction of solid formation as well.

Nevertheless, there is no guarantee that the GERG EoS is more accurate than the PR EoS, as shown by May et al. (2015) and Rowland et al. (2016), in particular in the regions where data available at the time of the GERG EoS development were limited, especially the low temperature region. In regions whee high accuracy is needed and very few data are available, the suitable procedure is the production of original data and the regression of new parameters for the EoS, as proposed by Rowland et al. (2016).

The thermodynamic model implemented and tested in this work is of interest for engineering purposes, for the design and optimization of the process. For this reason a further effort should

be done in order to provide a practical and user-friendly tool allowing the calculation of phase equilibrium conditions and thermodynamic properties, as well as the representation of phase diagram involving a solid phase. Coupling an existing GERG-2008 model implemented by Refprop with the Jager and Span model for the solid phase can be suitable at this purpose. For the simulation of the process thermodynamic and transport properties are needed. The capability of the model in representing the properties of interest in the low temperature domain has not been tested in this work. In a future work, the most important properties needed in the simulation have to be identified and then, a bibliographic research should be performed for finding available data to test and calibrate the model.

The influence of nitrogen and oxygen on the solid formation conditions has been studied through model prediction and measurements. CO_2 solubility in liquid nitrogen and oxygen is lower than in liquid methane and thus, high air content in the biogas stream increases the solid risk in the LBG. On the contrary, the influence of nitrogen and oxygen on the CO_2 solubility in vapor phase is weak. In order to validate and test the accuracy of the model results on landfill gas type mixture composed of N_2-O_2-CH_4-CO_2, data are needed. According to the bibliographic research, ternary N_2-CH_4-CO_2 data are few and incomplete. Furthermore, to the author's knowledge, phase equilibrium for the O_2-N_2-CH_4-CO_2 mixture has not been experimentally investigated at now. Original SLVE data for the ternary and quaternary mixture have been produced. Results seem not to be in agreement with available solubility data for the ternary system of N_2-CH_4-CO_2. Nevertheless, to the author's opinion, the deviation showed between model and data produced in this work can be considered of the same order as the deviation between the model and binary solubility data. Further studies and measurements could add some information to the discussion and clarify the influence of nitrogen and oxygen on the solubility of carbon dioxide in liquid phase. The experimental procedure for obtaining low temperature SLVE data could also be applied to the study of the problem of crystallization in LNG type mixture. Solidification of CO_2 and other compounds is in fact a common drawback in the natural gas treatment and liquefaction. Being able to accurately predict solid formation and compute thermodynamic properties of CH_4 rich mixtures at cryogenic conditions is of interest for applications of increasing importance in the energy domain.

The complexity of the solid formation and CO_2 separation process brings the interest on the simulation of the heat exchangers for upgrading and liquefaction, as well as the air separation unit. The simplified heat exchanger model developed in this work is able to simulate the dynamic process of solid deposit on the fins of the heat exchanger. It emerges the necessity of a thermodynamic model for the prediction of solid formation conditions. Some improvements in the model can be done in the next works: the assumption of neglecting thermal conduction in the solid layer brings a loss of information about frost layer. An improved model can be developed by coupling lumped capacitance model already implemented with a conductive heat transfer model. In this way a more complete description of the phenomenon can be achieved. Nevertheless, for sizing the heat exchanger a modified LMTD method including a solid phase formation should be more suitable. A challenging issue is to extend the simulation to the liquefaction heat exchanger. In this case two fluid phases are flowing in the heat exchanger, each one with a different velocity. Thermodynamic equilibrium may not be sufficient for completely describe the problem. An important approximation introduced in the heat exchanger simulation is that the model only consider the thermodynamic of the heat and mass transfer. When dealing with a solid phase, the kinetics of crystal formation can play an important role, which is not considered in this study. An interesting perspective to the study of the solid formation in the heat exchanger could be the introduction of a kinetic model able to take into account the non-equilibrium effects in the mass transfer and crystallization. This approach could be based on the observation of the behavior of the operating heat exchanger on the pilot plant and experimental studies.

The need of a thermodynamic model able to predict solid formation conditions is shown in the simulation of the liquefaction process. Liquefaction of biomethane presents, similarly to the natural gas liquefaction, the issue of solid CO_2 solidification risk. For Liquefied Natural Gas production, CO_2 content is limited to 50 ppm in order to avoid solid formation. In this work it is showed that the limit is conservative, and thus, especially for the LBG application, better knowledge of the solidification phenomenon and conditions, together with reliable solubility prediction can allow to avoid separation costs and plugging risks. The approach used in this work for studying the problems has encouraging results when compared to measurements observed on the pilot plant operation. The CO_2 concentration measured in the produced LBG is around 3000 ppm, as predicted in this work. The issue of solid formation and CO_2 limits in the LNG/LBG is of great importance for reducing separation costs. Specifications used at the moment are not really justified by experimental or predicted results, but they are just conservative values allowing avoiding the problem of solidification. The definition of more rigorous specification would results in less strict operating conditions or optimized technological solution. New product entering the market (LBG) and the decreasing prizes of oil and natural gas will probably push industries to better investigate the issue.

In this work, a cryodistallation column for the separation of air from landfill gas has been studied and designed. The simulation allows to verify if solid CO_2 formation occurs in the column. Results show that the produced LBG meets the standards in terms of methane and nitrogen content and that solid formation risk is avoided in the column. The air separation unit will be installed and tested on the pilot in next months, so that the results of the simulation could be compared to actual operation in real conditions. This will allow to optimize the design of the column and the integration in the liquefaction process.

Bibliography

Abdoul, W., Rauzy, E., and Pneloux, A. (1991). Group-contribution equation of state for correlating and predicting thermodynamic properties of weakly polar and non-associating mixtures: binary and multicomponent systems. *Fluid Phase Equilibria*, 68:47–102.

AET (2003). Advanced Extraction Technologies, Inc., Nitrogen Rejection.

Agrawal, G. M. and Laverman, R. J. (1974). Phase behavior of the methane-carbon dioxide system in the solid-vapor region. CO2-CH4 and N2-CH4-CO2 mixtures at compositions and pressures of industrial importance. *Advances in Cryogenic Engineering*, 19:327–338.

AirLiquide (2012). The liquefaction of biomethane, Lidkping, Sweden > Air Liquide Advanced Technologies.

Al-Sahhaf, T. A. (1990). Vapor-liquid equilibria for the ternary system N2 + CO2 + CH4 at 230 and 250 K. *Fluid Phase Equilibria*, 55(12):159–172.

Al-Sahhaf, T. A., Kidnay, A. J., and Sloan, E. D. (1983). Liquid + vapor equilibriums in the nitrogen + carbon dioxide + methane system. *Industrial & Engineering Chemistry Fundamentals*, 22(4):372–380.

Allegue, L. B., Hinge, J., and All, K. (2012). Overview of biogas technologies for production of liquid transport fuels. *Danish Technological Institute*.

Amamchyan, R. G., Bertsev, V. V., and Bulanin, M. O. (1973). Analysis of cryogenic solutions according to IR absorption spectra. *Zavod. Lab*, 39:432–434.

Amin, R., Jackson, A. T., and Kennaird, T. (2005). The Cryocell: An Advanced Gas Sweetening Technology. International Petroleum Technology Conference.

Arai, Y., Kaminishi, G.-I., and Saito, S. (1971). The experimental determination of the PVTX relations for the carbon dioxide-nitrogen and the carbon dioxide-methane systems. *Journal of Chemical Engineering of Japan*, 4(2):113–122.

Arjomandnia, P., Tade, M. O., Pareek, V., and May, E. F. (2014). Analysis of available data from liquefied natural gas rollover incidents to determine critical stability ratios. *AIChE Journal*, 60(1):362–374.

Baba-Ahmed, A., Guilbot, P., and Richon, D. (1999). New equipment using a static analytic method for the study of vapourliquid equilibria at temperatures down to 77 K. *Fluid Phase Equilibria*, 166(2):225–236. 00013.

Baker, N. and Creed, M. (1996). Stratification and rollover in liquefied natural gas storage tanks. *Process safety and environmental protection*, 74(1):25–30.

Bauer, F., Persson, T., Hulteberg, C., and Tamm, D. (2013). Biogas upgrading technology overview, comparison and perspectives for the future. *Biofuels, Bioproducts and Biorefining*, 7(5):499–511.

Bian, B., Wang, Y., Shi, J., Zhao, E., and Lu, B. C.-Y. (1993). Simultaneous determination of vapor-liquid equilibrium and molar volumes for coexisting phases up to the critical temperature with a static method. *Fluid phase equilibria*, 90(1):177–187.

Bloomer, O. T. and Parent, J. D. (1953). Liquid-vapor phase behavior of the methane-nitrogen system. *Chemical Engineering Progress Symposium Series*, 49:11–24.

Boyle, G. J. (1987). Shell Res. LTD Thornton Res. Centre P. O. Box. 1 Chester. *(as reported in Knapp, H.; Teller, M.; Langhorst, R. Solid-liquid equilibrium data collection, Vol. VIII, part 1, Chemistry Data Series, Dechema, 1987).*

Brandt, L. W. and Stroud, L. (1958). Phase Equilibria in Natural Gas Systems. Apparatus with Windowed Cell for 800 PSIG and Temperatures to320 F. *Industrial & Engineering Chemistry*, 50(5):849–852.

Brewer, J. and Kurata, F. (1958). Freezing points of binary mixtures of methane. *AIChE Journal*, 4(3):317–318. 00015.

Brown, T. S., Niesen, V. G., Sloan, E. D., and Kidnay, A. J. (1989a). Vapor-liquid equilibria for the binary systems of nitrogen, carbon dioxide, and n-butane system. *Fluid Phase Equilib.*, 53:7–14.

Brown, T. S., Sloan, E. D., and Kidnay, A. J. (1989b). Vapor-liquid equilibria in the nitrogen + carbon dioxide + ethane system. *Fluid Phase Equilibria*, 51:299–313.

Campestrini, M. (2014). *Thermodynamic study of solid-liquid-vapor equilibrium : application to cryogenics and air separation unit.* PhD thesis, Paris, ENMP.

CEN (2015a). prEN 16723-1 – Natural gas and biomethane for use in transport and biomethane for injection in the natural gas network – Part 1: Specifications for biomethane for injection in the natural gas network, Committee Draft.

CEN (2015b). prEN 16723-2 – Natural gas and biomethane for use in transport and biomethane for injection in the natural gas network – Part 2: Automotive fuel specifications, Committee Draft.

CEN (2015c). prEN 16726 – Gas infrastructure – Quality of gas – Group H, Committee Draft.

Chang, H. M., Chung, M. J., and Park, S. B. (2010). Integrated Cryogenic System for CO2 Separation and Lng Production from Landfill Gas. *Advances in Cryogenic Engineering*, 1218:278–285.

Cheung, H. and Zander, E. H. (1968). Solubility of Carbon Dioxide and Hydrogen Sulfide in Liquid Hydrocarbons at Cryogenic Temperatures. *Chemical Engineering Progress Symposium Series*, 64:34–43.

Chilton, T. H. and Colburn, A. P. (1934). Mass transfer (absorption) coefficients prediction from data on heat transfer and fluid friction. *Industrial & engineering chemistry*, 26(11):1183–1187.

Cines, M. R., Roach, J. T., Hogan, R. J., and Roland, C. H. (1953). Nitrogen-methane vapor-liquid equilibria. In *Chemical Engineering Progress Symposium Series*, volume 49, pages 1–10. Amer Inst Chemical Engineers 345 E 47th St, New York, Ny 10017.

Clodic, D. and Younes, M. (2001). Procede d'extraction du dioxide de carbone par anti-sublimation en vue de son stockage. *ARMINES French patent FR*, 1(01):232.

Clodic, D. and Younes, M. (2006). Method and system for extracting carbon dioxide by anti-sublimation for storage thereof.

Clodic, D., Younes, M., Gale, J., and Kaya, Y. (2003). A new Method for CO2 Capture: Frosting CO2 at Atmospheric Pressure. *Proceedings of the 6th International Conference on Greenhouse Gas Control Technologies*, I:155–160.

Cook, T. and Davey, G. (1976). The density and thermal conductivity of solid nitrogen and carbon dioxide. *Cryogenics*, 16:363–369.

Cui, J., Li, W. Z., Liu, Y., and Jiang, Z. Y. (2011). A new time- and space-dependent model for predicting frost formation. *Applied Thermal Engineering*, 31(4):447–457. 00015.

Davalos, J., Anderson, W. R., Phelps, R. E., and Kidnay, A. J. (1976). Liquid-vapor equilibria at 250.00.deg.K for systems containing methane, ethane, and carbon dioxide. *Journal of Chemical & Engineering Data*, 21(1):81–84.

Davis, J. A., Rodewald, N., and Kurata, F. (1962). Solid-liquid-vapor phase behavior of the methane-carbon dioxide system. *AIChE Journal*, 8(4):537–539. 00047.

De Stefani, V., Baba-Ahmed, A., and Richon, D. (2004). A review of experimental methods for solid solubility determination in cryogenic systems. *Cryogenics*, 44(9):631–641.

De Stefani, V., Baba-Ahmed, A., Valtz, A., Meneses, D., and Richon, D. (2002). Solubility measurements for carbon dioxide and nitrous oxide in liquid oxygen at temperatures down to 90 K. *Fluid Phase Equilibria*, 200(1):19–30.

Din, F. (1960). The liquid-vapour equilibrium of the system nitrogen+ oxygen at pressures up to 10 atm. *Transactions of the Faraday Society*, 56:668–681.

Dodge, B. F. and Dunbar, A. K. (1927). An investigation of the coexisting liquid and vapor phases of solutions of oxygen and nitrogen. *Journal of the American Chemical Society*, 49(3):591–610.

Donnelly, H. G. and Katz, D. L. (1954). Phase Equilibria in the Carbon Dioxide-Methane System. *Industrial & Engineering Chemistry*, 46(3):511–517.

EBA (2014). Strategy for the Biogas Industry.

EuropeanCommission (2010). *M/475 EN Mandate to CEN for standards for biomethane for use in transport and injection in natural gas pipelines.* Brussel.

Fahlen, P. (1996). *Frosting and defrosting air-coils.* PhD thesis, Chalmer University of Technology, Goteborg, Sweden.

Fall, J. L. and Luks, K. D. (1986). Effect of additive gases on the liquid-liquid-vapor immiscibility of the carbon dioxide+ n-nonadecane mixtures. *Journal of Chemical and Engineering Data*, 31(3):332–336.

Fandino, O., Trusler, J. P. M., and Vega-Maza, D. (2015). Phase behavior of (CO2 + H2) and (CO2 + N2) at temperatures between (218.15 and 303.15) K at pressures up to 15 MPa. *International Journal of Greenhouse Gas Control*, 36:78–92.

Fastovskii, V. G. and Petrovskii, Y. V. (1957). Liquid and vapor equilibriums in the nitrogen-methane system. *Zhurnal Fizicheskoi Khimii*, 31.

Fedorova, M. F. (1940). The solubility of C2h2 and CO2 in liquid nitrogen and oxygen. *Zhurnal Fizicheskoi Khimii*, 14:422–426.

Firoozabadi, A. (1999). *Thermodynamics of hydrocarbon reservoirs.* McGraw-Hill.

Fisher, B. and Ferschneider, G. (2010). Liquefaction du gaz naturel. *Techniques de l'Ingnieur*.

Fontaine, M. (1989). *The phase equilibrium of helium-methane and its representation with a new mixture equation of state*. Ph.D. Dissertation, Techn. Univ. Braunschweig, Braunschweig, Germany.

Fredenslund, A. and Sather, G. A. (1970). Gas-liquid equilibrium of the oxygen-carbon dioxide system. *Journal of Chemical and Engineering Data*, 15(1):17–22.

Gao, G., Daridon, J.-L., Saint-Guirons, H., Xans, P., and Montel, F. (1992). A simple correlation to evaluate binary interaction parameters of the Peng-Robinson equation of state: binary light hydrocarbon systems. *Fluid phase equilibria*, 74:85–93.

Gao, T., Shen, T., Lin, W., Gu, A., and Ju, Y. (2012). Experimental Determination of CO2 Solubility in Liquid CH4/N2 Mixtures at Cryogenic Temperatures. *Industrial & Engineering Chemistry Research*, 51(27):9403–9408. 00002.

GasRec (2014). LBM http://gasrec.co.uk/solution/lbm/.

Giauque, W. F. and Egan, C. J. (1937). Carbon Dioxide. The Heat Capacity and Vapor Pressure of the Solid. The Heat of Sublimation. Thermodynamic and Spectroscopic Values of the Entropy. *Journal of Chemical Physics*, 5:45–54.

Gilliland, E. R. (1940). Multicomponent rectification estimation of the number of theoretical plates as a function of the reflux ratio. *Industrial & Engineering Chemistry*, 32(9):1220–1223.

Giraldo, C. A., Clarke, M. A., and Trebble, M. A. (2009). Prediction of CO2 freeze-out conditions and CO2 hydrate formation conditions with a single equation of state. *Chemical Engineering Communications*, 197(4):571–583.

Grob, R. L. and Barry, E. F. (2004). *Modern Practice of Gas Chromatography*. John Wiley & Sons, Inc., 4th edition.

GRTgaz (2015). Prescriptions techniques applicables aux canalisations de transport de GRTgaz et aux installations de transport, de distribution et de stockage de gaz raccordees au reseau de GRTgaz.

Guevara-Rodriguez, F. d. J. and Romero-Martinez, A. (2013). An empirical extension for a generalized cubic equation of state, applied to a pure substance with small molecules. *Fluid Phase Equilibria*, 347:22–27.

Han, X. H., Zhang, Y. J., Gao, Z. J., Xu, Y. J., Wang, Q., and Chen, G. M. (2012). Vapor-Liquid Equilibrium for the Mixture Nitrogen (N2)+ Methane (CH4) in the Temperature Range of (110 to 125) K. *Journal of Chemical & Engineering Data*, 57(5):1621–1626.

Haufe, S., Mueller, H. D., and Tietze, G. (1972). Solubility of solid carbon dioxide in a methane -nitrogen mixture. *Chem thec*, 24:619–621.

Haut, R. and Thomas, E. (1989). Development and Application of the Controlled-Freeze-Zone Process. *SPE Production Engineering*, 4(03):265–271.

Hayashi, Y., Aoki, A., Adachi, S., and Hori, K. (1977). Study of Frost Properties Correlating With Frost Formation Types. *Journal of Heat Transfer*, 99(2):239–245. 00260.

Hlavinka, M. W., Hernandez, V. N., and McCartney, D. (2006). Proper interpretation of freezing and hydrate prediction results from process simulation. In *The 85th GPA Annual Convention Proceedings, Grapevine, USA*. 00005.

Hodges, R. J. and Burch, R. J. (1967). The equilibrium distribution of methane between the liquid and vapour phases of oxygen. *Cryogenics*, 7(14):112–113.

Holmes, A. S. and Ryan, J. M. (1982). Cryogenic distillative separation of acid gases from methane.

HSE (2013). 1 percent Oxygen Limit For Biomethane Injection Agreed By Hse.

Hughes, T. J., Kandil, M. E., Graham, B. F., Marsh, K. N., Huang, S. H., and May, E. F. (2015). Phase equilibrium measurements of (methane + benzene) and (methane + methylbenzene) at temperatures from (188 to 348) K and pressures to 13 MPa. *The Journal of Chemical Thermodynamics*, 85:141–147.

Jager, A. and Span, R. (2012). Equation of State for Solid Carbon Dioxide Based on the Gibbs Free Energy. *Journal of Chemical & Engineering Data*, 57(2):590–597.

Janisch, J., Raabe, G., and Khler, J. (2007). Vapor-liquid equilibria and saturated liquid densities in binary mixtures of nitrogen, methane, and ethane and their correlation using the VTPR and PSRK GCEOS. *Journal of Chemical & Engineering Data*, 52(5):1897–1903.

Johansson, N. (2008). Production of liquid biogas, LBG, with cryogenic and conventional upgrading technology-Description of systems and evaluations of energy balances.

Jonsson, S. and Westman, J. (2011). Cryogenic biogas upgrading using plate heat exchangers. Technical report, Chalmers University of Technology, Goteborg, Sweden.

Kaminishi, G.-I., Arai, Y., Saito, S., and Maeda, S. (1968). Vapor-Liquid Equilibria for Binary and Ternary Systems Containing Carbon Dioxide. *Journal of Chemical Engineering of Japan*, 1(2):109–116.

Kaminishi, G.-i. and Toriumi, T. (1966). Vapor- Liquid Phase Equilibrium in the CO2-H2, CO2-N2 and CO2-O2 Systems. *The Journal of the Society of Chemical Industry, Japan*, 69(2):175–178.

Kandil, M. E., May, E. F., Graham, B. F., Marsh, K. N., Trebble, M. A., Trengove, R. D., and Huang, S. H. (2010). VaporLiquid Equilibria Measurements of Methane + 2-Methylpropane (Isobutane) at Temperatures from (150 to 250) K and Pressures to 9 MPa. *Journal of Chemical & Engineering Data*, 55(8):2725–2731.

Kandil, M. E., Thoma, M. J., Syed, T., Guo, J., Graham, B. F., Marsh, K. N., Huang, S. H., and May, E. F. (2011). VaporLiquid Equilibria Measurements of the Methane + Pentane and Methane + Hexane Systems at Temperatures from (173 to 330) K and Pressures to 14 MPa. *Journal of Chemical & Engineering Data*, 56(12):4301–4309.

Kidnay, A. J., Miller, R. C., Parrish, W. R., and Hiza, M. J. (1975). Liquid-vapour phase equilibria in the N2 CH4 system from 130 to 180 K. *Cryogenics*, 15(9):531–540.

Kremer, H. (1982). *Experimentelle untersuchung und berechnung von hochdruck-flussigkeits-dampf und flussigkeits-flussigkeits-dampf-gleichgewichten fur tiefsiedende gemische.* Ph.D. Dissertation, University of Berlin, Berlin, Germany.

Krich, K., Augestein, D., Batmale, J. P., Benemann, J., Rutledge, B., and Salour, D. (2005). Biomethane from dairy waste: a sourcebook for the production and use of renewable natural gas in California. pages 47–69. California: Western United Dairymen.

Krichevskii, I. R., Khazanova, N. E., Lesnevskaya, L. S., and Sandalova, L. Y. (1962). Liquid-gas equilibrium in the nitrogen-carbon dioxide system under elevated pressures. *Khim. Promst.(Moscow)*, 38:169–171.

Kuehn, T., Ramsey, J. W., and Threlkeld, J. L. (1998). *Thermal Environmental Engineering*. Prentice hall edition.

Kunz, O., Klimeck, R., Wagner, W., and Jaeschke, M. (2007). The GERG-2004 Wide-Range Equation of State for Natural Gases and Other Mixtures. Technical Report GERG TM15.

Kunz, O. and Wagner, W. (2012). The GERG-2008 Wide-Range Equation of State for Natural Gases and Other Mixtures: An Expansion of GERG-2004. *Journal of Chemical & Engineering Data*, 57(11):3032–3091.

Kurata, F. and Im, K. U. (1971). Phase equilibrium of carbon dioxide and light paraffins in presence of solid carbon dioxide. *Journal of Chemical & Engineering Data*, 16(3):295–299.

Lallemand, F., Lecomte, F., and Streicher, C. (2005). Highly Sour Gas Processing: H2s Bulk Removal With the Sprex Process. International Petroleum Technology Conference.

Lange, S. (2015). *Purification of natural gas by means of a new low temperature distillation process*. PhD Thesis, Politecnico di Milano, Milano.

Le, T. T. and Trebble, M. A. (2007). Measurement of Carbon Dioxide Freezing in Mixtures of Methane, Ethane, and Nitrogen in the Solid-Vapor Equilibrium Region. *Journal of Chemical & Engineering Data*, 52(3):683–686.

Le Gall, R., Grillot, J. M., and Jallut, C. (1997). Modelling of frost growth and densification. *International Journal of Heat and Mass Transfer*, 40(13):3177–3187. 00081.

Lemmon, E. W. (1996). *A Generalized Model for the Prediction of the Thermodynamic Properties of Mixtures Including Vapor-Liquid Equilibrium*. Ph.D. Dissertation, University of Idaho, Moscow.

Lemmon, E. W., Huber, M. L., and McLinden, M. O. (2013). NIST: Reference Fluid Thermodynamic and Transport Properties-REFPROP, Version 9.1.

Lemmon, E. W., Huber, M. L., McLinden, M. O., and others (2010). NIST Standard Reference Database 23. *NIST Reference Fluid Thermodynamic and Transport PropertiesREFPROP, version*, 9:55.

Liu, K., Wang, W., Du, Y., and Jin, Z. L. (1988). VLE Measurement and Correlation of N2-Ar-CH4 System at 122.89 K. *Chem. Eng. (China)*, 16:58–63.

Luks, K. D. (1986). The occurrence and measurement of multiphase equilibria behavior. *Fluid Phase Equilibria*, 29:209–224.

Maass, O. and Barnes, W. H. (1926). Some Thermal Constants of Solid and Liquid Carbon Dioxide. *Proceedings of the Royal Society of London. Series A, Containing Papers of a Mathematical and Physical Character*, 111(757):224–244.

MacKenzie, D., Cheta, I., and Burns, D. (2002). Removing nitrogen. *Hydrocarbon engineering*, 7(11):57–63.

Marcogaz (2006). Injection of Gases from Non-Conventional Sources into Gas Networks.

May, E. F., Guo, J. Y., Oakley, J. H., Hughes, T. J., Graham, B. F., Marsh, K. N., and Huang, S. H. (2015). Reference Quality VaporLiquid Equilibrium Data for the Binary Systems Methane + Ethane, + Propane, + Butane, and + 2-Methylpropane, at Temperatures from (203 to 273) K and Pressures to 9 MPa. *Journal of Chemical & Engineering Data*, 60(12):3606–3620.

McBride, B. J. and Gordon, S. (1961). Thermodynamic functions of several triatomic molecules in the ideal gas state. *The Journal of Chemical Physics*, 35(6):2198–2206.

McCain, W. D. (1990). *The Properties of Petroleum Fluids*. PennWell Books.

Miller, R. C., Kidnay, A. J., and Hiza, M. J. (1973). Liquid-vapor equilibria at 112.00 K for systems containing nitrogen, argon, and methane. *AIChE Journal*, 19(1):145–151.

Mraw, S. C., Hwang, S.-C., and Kobayashi, R. (1978). Vapor-liquid equilibrium of the methane-carbon dioxide system at low temperatures. *Journal of Chemical and Engineering Data*, 23(2):135–139.

Muhlbauer, A. (1997). *Phase Equilibria: Measurement & Computation*. CRC press.

Myhre, G., Shindell, D., Bron, F.-M., Collins, W., Fuglestvedt, J., Huang, J., Koch, D., Lamarque, J.-F., Lee, D., Mendoza, B., and others (2013). Anthropogenic and natural radiative forcing. In *Climate Change 2013: The Physical Science Basis. Contribution of Working Group I to the Fifth Assessment Report of the Intergovernmental Panel on Climate Change*, volume 423.

Neumann, A. and Walch, W. (1968). Vapour/liquid equilibrium carbon dioxide/methane at low temperatures and in region of low carbon dioxide mole fractions. *Chemie Ingenieur Technik*, 40(5):241.

Nishiumi, H., Arai, T., and Takeuchi, K. (1988). Generalization of the binary interaction parameter of the Peng-Robinson equation of state by component family. *Fluid Phase Equilibria*, 42:43–62.

Ogunbameru, A. N., Brian, P. L. T., and Reid, R. C. (1973). On Carbon Dioxide Frost Formation. *Industrial & Engineering Chemistry Fundamentals*, 12(3):385–387. 00003.

Onnes, D. H. K. (1894). On the cryogenic laboratory at Leiden and on the production of very low temperatures. Technical report.

Osomo (2015). http://www.osomo.nl.

Parrish, W. R. and Hiza, M. J. (1995). Liquid-vapor equilibria in the nitrogen-methane system between 95 and 120 K. In *Advances in Cryogenic Engineering*, pages 300–308. Springer.

Pellegrini, L. A. (2014). Process for the removal of co2 from acid gas.

Peng, D.-Y. and Robinson, D. B. (1976). A New Two-Constant Equation of State. *Industrial & Engineering Chemistry Fundamentals*, 15(1):59–64. 06771.

Perrotin, T. (2004). *Airside investigation of high efficiency heat exchangers used in room air-conditioners*. PhD thesis, Ecole des Mines de Paris, Paris.

Pikaar, M. J. (1959). *Study of phase equilibria in hydrocarbon-CO2 systems*. PhD Thesis, Imperial College of Science and Technology, London. OCLC: 9847564.

Preston, G. T., Funk, E. W., and Prausnitz, J. M. (1971). Solubilities of hydrocarbons and carbon dioxide in liquid methane and in liquid argon. *The Journal of Physical Chemistry*, 75(15):2345–2352.

Privat, R. and Jaubert, J.-N. (2012). Discussion around the paradigm of ideal mixtures with emphasis on the definition of the property changes on mixing. *Chemical Engineering Science*, 82:319–333. 00003.

Privat, R., Jaubert, J.-N., and Privat, Y. (2013). A simple and unified algorithm to solve fluid phase equilibria using either the gammaphi or the phiphi approach for binary and ternary mixtures. *Computers & Chemical Engineering*, 50:139–151.

Rachford, H. and Rice, J. (1952). Procedure for Use of Electronic Digital Computers in Calculating Flash Vaporization Hydrocarbon Equilibrium. *Journal of Petroleum Technology*, 4(10):19–3.

Rest, A. J., Scurlock, R. G., and Wu, M. F. (1990). The solubilities of nitrous oxide, carbon dioxide, aliphatic ethers and alcohols, and water in cryogenic liquids. *The Chemical Engineering Journal*, 43(1):25–31.

Riva, M., Campestrini, M., Toubassy, J., Clodic, D., and Stringari, P. (2014). Solid-Liquid-Vapor Equilibrium Models for Cryogenic Biogas Upgrading. *Industrial & Engineering Chemistry Research*, 53(44):17506–17514. 00000.

Rodriguez-Reartes, S. B., Cismondi, M., and Zabaloy, M. S. (2011). Computation of solid-fluid-fluid equilibria for binary asymmetric mixtures in wide ranges of conditions. *The Journal of Supercritical Fluids*, 57(1):9–24. 00007.

Rowland, D., Hughes, T. J., and May, E. F. (2016). Extending the GERG-2008 equation of state: Improved departure function and interaction parameters for (methane + butane). *The Journal of Chemical Thermodynamics*, 97:206–213.

Rufford, T. E., Smart, S., Watson, G. C. Y., Graham, B. F., Boxall, J., Diniz da Costa, J. C., and May, E. F. (2012). The removal of CO2 and N2 from natural gas: A review of conventional and emerging process technologies. *Journal of Petroleum Science and Engineering*, 9495:123–154.

Ryckebosch, E., Drouillon, M., and Vervaeren, H. (2011). Techniques for transformation of biogas to biomethane. *Biomass and Bioenergy*, 35(5):1633–1645.

Saleman, T. L., Li, G. K., Rufford, T. E., Stanwix, P. L., Chan, K. I., Huang, S. H., and May, E. F. (2015). Capture of low grade methane from nitrogen gas using dual-reflux pressure swing adsorption. *Chemical Engineering Journal*, 281:739–748.

Salim, P. H. and Trebble, M. A. (1994). Modelling of solid phases in thermodynamic calculations via translation of a cubic equation of state at the triple point. *Fluid Phase Equilibria*, 93:75–99.

Sanders, C. T. (1974). *Frost formation: the influence of frost formation and defrosting on the performance of air coolers*. PhD thesis, TU Delft, Delft University of Technology. 00088.

Sandler, S. I. (2006). *Chemical, biochemical, and engineering thermodynamics*. John Wiley & Sons Hoboken, NJ, 4th edition.

Sarashina, E., Yasuhko, A., and Shozaburo, S. (1971). Vapor-liquid equilibria for nitrogen-methane.carbon dioxide system.

Schinkelshoek, P. and Epsom, H. D. (2008). Supersonic gas conditioning-commercialisation of twister technology. In *87th GPA annual convention, Grapevine, USA*.

Schweitzer, O. R. (1962). Solid-liquid-vapor Phase Equilibria in the Binary Systems: Ethylene-carbon Dioxide, Propane-carbon Dioxide, Nitrogen-carbon Dioxide, and Helium-carbon Dioxide.

Seader, J. D. and Henley, E. J. (2011). *Separation process principles*. Wiley, 2nd edition.

Shchelkunov, V. N., Rudenko, N. Z., Shostak, Y. V., and Dolganin, V. I. (1986). Surface desublimation of carbon dioxide from binary gas mixtures. *Journal of engineering physics*, 51(6):1432–1435.

Shen, T., Gao, T., Lin, W., and Gu, A. (2012). Determination of CO2 Solubility in Saturated Liquid CH4 + N2 and CH4 + C2h6 Mixtures above Atmospheric Pressure. *Journal of Chemical & Engineering Data*, 57(8):2296–2303. 00000.

Shi, M., Wei, M., Zhang, J., and Wang, L. (1984). Simple and speedy measurement of bubble point and dew point for VLE binary system under pressure. *Chemical Engineering (China)*, 6:51–54.

Skripka, V. G., Nikitina, I. E., Zhdanovich, L. A., Sirotin, A. G., and Benyaminovich, O. A. (1970). Liquid-vapor phase equilibrium at low temperatures in binary systems, components produced from natural gas. *Gazov Promst*, 15(12):35–36.

Smith, G. E., Sonntag, R. E., and Wylen, G. J. V. (1964). Solid-Vapor Equilibrium of the Carbon Dioxide-Nitrogen System at Pressures to 200 Atmospheres. *Advances in Cryogenic Engineering*, 9:197–206. DOI: 10.1007/978-1-4757-0525-6_24.

Soave, G. (1972). Equilibrium constants from a modified Redlich-Kwong equation of state. *Chemical Engineering Science*, 27(6):1197–1203.

SoCalGas (2011). Rule 30: Biomethane gas delivery specifications limits and action levels.

Somait, F. A. and Kidnay, A. J. (1978). Liquid-vapor equilibriums at 270.00 K for systems containing nitrogen, methane, and carbon dioxide. *Journal of Chemical & Engineering Data*, 23(4):301–305.

Song, C.-F., Kitamura, Y., Li, S.-H., and Jiang, W.-Z. (2013). Analysis of CO2 frost formation properties in cryogenic capture process. *International Journal of Greenhouse Gas Control*, 13:26–33. 00000.

Song, C.-F., Kitamura, Y., Li, S.-H., and Ogasawara, K. (2012). Design of a cryogenic CO2 capture system based on Stirling coolers. *International Journal of Greenhouse Gas Control*, 7:107–114.

Sonntag, R. E. and Van Wilen, G. J. (1961). The solid-vapor equilibrium of carbon dioxide-nitrogen. *Advances in Cryogenic Engineering*, 7:99–105.

Span, R. and Wagner, W. (1996). A New Equation of State for Carbon Dioxide Covering the Fluid Region from the TriplePoint Temperature to 1100 K at Pressures up to 800 MPa. *Journal of Physical and Chemical Reference Data*, 25(6):1509–1596.

Starling, K. E. and Savidge, J. L. (1994). *Compressibility factors of natural gas and other related hydrocarbon gases*. AGA, American Gas Association.

Sterner, C. J. (1961). Phase Equilibria in the CO2-Methane Systems. *Advances in Cryogenic Engineering*, (6):467–474.

Streich, M. (1970). N2 Removal from Natural Gas. *Hydrocarbon Process.*, 49:86–88.

Stringari, P., Campestrini, M., Coquelet, C., and Arpentinier, P. (2014). An equation of state for solid-liquid-vapor equilibrium applied to gas processing and natural gas liquefaction. *Fluid Phase Equilibria*, 362:258–267. 00000.

Stringari, P., Theveneau, P., Coquelet, C., and Lauermann, G. (2012). Solubility measurements of solid n-hexane in liquid methane at cryogenic temperature. *91st Annual Convention of the GPA, New Orleans*.

Stryjek, R., Chappelear, P. S., and Kobayashi, R. (1972). Low Temperature VLE of the N2-Methane, N2-Ethane, and N2-Methane-Ethane Systems, 1972. *Rice University: Houston*.

Stryjek, R., Chappelear, P. S., and Kobayashi, R. (1974). Low-temperature vapor-liquid equilibriums of nitrogen-methane system. *Journal of Chemical and Engineering Data*, 19(4):334–339.

Sumarokov, V. V., Stachowiak, P., Mucha, J., and Jeowski, A. (2006). Low-temperature thermal conductivity of cryocrystals formed by linear three-atom molecules. *Physical Review B*, 74(22):224302.

Syed, T. H., Hughes, T. J., Marsh, K. N., and May, E. F. (2014). Isobaric Heat Capacity Measurements of Liquid Methane + Propane, Methane + Butane, and a Mixed Refrigerant by Differential Scanning Calorimetry at High Pressures and Low Temperatures. *Journal of Chemical & Engineering Data*, 59(4):968–974.

Tao, Y.-X. and Besant, R. W. (1993). Prediction of Spatial and Temporal Distributions of Frost Growth on a Flat Plate Under Forced Convection. *Journal of Heat Transfer*, 115(1):278–281.

Task37, I. B. (2014). IEA Bioenergy Task37 Up-grading Plant Lists.

Tillner-Roth, R. (1998). *Fundamental Equations of State*. Aachen, shaker verlag edition.

Timmerhaus, K. D. and Flynn, T. M. (1989). *Cryogenic Process Engineering*. Springer US, Boston, MA.

Torocheshnikov, N. and Levius, M. (1941). Liquid Vapor Equilibrium in the System Nitrogen - Methane,. *Zh. Khim. Prom.*, 18(5):19–22.

Toubassy, J. (2012). *Study and modeling of the CO2 frosting on a gliding temperature evaporator*. PhD thesis, Paris, ENMP.

Trappehl, G. and Knapp, H. (1989). Vapour-liquid equilibria in the ternary mixture N2-CH4-CO2 and the quaternary mixture N2-CH4-C2h6-C3h8. *Cryogenics*, 29(1):42–50.

Trusler, J. P. M. (2011). Equation of State for Solid Phase I of Carbon Dioxide Valid for Temperatures up to 800 K and Pressures up to 12 GPa. *Journal of Physical and Chemical Reference Data*, 40(4):043105.

Trusler, J. P. M. (2012). Erratum: Equation of State for Solid Phase I of Carbon Dioxide Valid for Temperatures up to 800 K and Pressures up to 12 GPa [J. Phys. Chem. Ref. Data40, 043105 (2011)]. *Journal of Physical and Chemical Reference Data*, 41(3):039901.

Tuinier, M. J., van Sint Annaland, M., Kramer, G. J., and Kuipers, J. A. M. (2010). Cryogenic capture using dynamically operated packed beds. *Chemical Engineering Science*, 65(1):114–119.

Underwood, A. J. V. (1948). Fractional distillation of multicomponent mixtures. *Chem. Eng. Prog*, 44(8):603–614.

US EPA, O. (2010). Altamont Landfill Gas to Liquefied Natural Gas Project.

Valeton, J. J. P. (1924). I. Wachstum und Auflsung der Kristalle. III. *Zeitschrift fr Kristallographie-Crystalline Materials*, 60(1):1–38.

Van der Waals, J. D. (1873). *On the Continuity of the Gaseous and Liquid States*. PhD thesis, Leiden University, Leiden.

Van Konynenburg, P. H. and Scott, R. L. (1980). Critical Lines and Phase Equilibria in Binary Van Der Waals Mixtures. *Philosophical Transactions of the Royal Society of London. Series A, Mathematical and Physical Sciences*, 298(1442):495–540. 01057.

Vetere, A. (1983). Vapor-liquid equilibria calculations by means of an equation of state. *Chemical Engineering Science*, 38(8):1281–1291.

Voss, G. (1975). *PhD Thesis*. PhD thesis, Technical University of Berlin, Berlin, Germany.

Wang, C.-C., Lin, Y.-T., and Lee, C.-J. (2000). Heat and momentum transfer for compact louvered fin-and-tube heat exchangers in wet conditions. *International Journal of Heat and Mass Transfer*, 43(18):3443–3452.

Wartsila (2014). Biogas liquefaction plant supplied by Wartsila to produce biofuel for buses in Norway.

Webster, L. A. and Kidnay, A. J. (2001). Vapor-liquid equilibria for the methane-propane-carbon dioxide systems at 230 K and 270 K. *Journal of Chemical & Engineering Data*, 46(3):759–764.

Wenzel, H. and Schmidt, G. (1980). A modified van der Waals equation of state for the representation of phase equilibria between solids, liquids and gases. *Fluid Phase Equilibria*, 5(1):3–17.

Wilson, G. M. (1969). A Modified Redlich-Kwong Equation-of-State, Application to General Physical Data Calculations. *AIChE Natl. Meeting*.

Wilson, G. M. (1975). Vapor-liquid equilibria of nitrogen, methane, ethane, and propane binary mixtures at LNG temperatures from total pressure measurements.[For use in design of equipment for storage and handling of LNG]. *Adv. Cryog. Eng.;(United States)*, 20.

Wilson, G. M., Silverberg, P. M., and Zellner, M. G. (1964). Argon-oxygen-nitrogen three component system experimental vapor-liquid equilibrium data. Technical report, DTIC Document.

Winn, F. W. (1958). New relative volatility method for distillation calculations. *Petrol. Refin*, 37(5):216–218.

Wooley, H. W. (1954). Thermodynamic functions for carbon dioxide in the ideal gas state. *J. Res. Nat. Bur. Stand*, 52:289–292.

Xiong, X., Lin, W., Jia, R., Song, Y., and Gu, A. (2015). Measurement and Calculation of CO2 Frost Points in CH4 + CO2/CH4 + CO2 + N2/CH4 + CO2 + C2h6 Mixtures at Low Temperatures. *Journal of Chemical & Engineering Data*, 60(11):3077–3086.

Xu, N., Dong, J., Wang, Y., and Shi, J. (1992a). High pressure vapor liquid equilibria at 293 K for systems containing nitrogen, methane and carbon dioxide. *Fluid Phase Equilibria*, 81:175–186.

Xu, N., Dong, J., Wang, Y., and Shi, J. (1992b). Vapor Liquid Equilibria for N2-CH4-CO2 system near critical region. *Journal of chemical industry and engineering-china-*, 43:640–640.

Yakimenko, N. P., Gluch, G. M., Iomtev, M. B., and Abramova, R. I. (1975). Solubility of solid carbon-dioxide in liquid-nitrogen. *Zhurnal Fizicheskoi Khimii*, 49(1):209–210.

Yamamoto, S., Ohgaki, K., and Katayama, T. (1989). Phase behavior of binary mixtures of indole or quinoxaline with CO2, C2h4, C2h6, and CHF3 in the critical region. *The Journal of Supercritical Fluids*, 2(2):63–72.

Yokozeki, A. (2004). Solid-liquid-vapor phases of water and water-carbon dioxide mixtures using a simple analytical equation of state. *Fluid Phase Equilibria*, 222-223:55–66.

Yorizane, M., Sadarmoto, S., Yoshimura, S., Masuoka, H., Shiki, N., Kimura, T., and Toyama, A. (1968). Vapor-Liquid Equilibria at Low Temperature. *Chemical engineering*, 32(3):257–264,a1.

Yorizane, M., Yoshimura, S., Masuoka, H., Miyano, Y., and Kakimoto, Y. (1985). New procedure for vapor-liquid equilibria. Nitrogen+ carbon dioxide, methane+ Freon 22, and methane+ Freon 12. *Journal of Chemical and Engineering Data*, 30(2):174–176.

Yucelen, B. and Kidnay, A. J. (1999). Vapor-liquid equilibria in the nitrogen+ carbon dioxide+ propane system from 240 to 330 K at pressures to 15 MPa. *Journal of Chemical & Engineering Data*, 44(5):926–931.

Zenner, G. H. and Dana, L. I. (1963). Liquid-vapor equilibrium compositions of carbon dioxide-oxygen-nitrogen mixtures. In *Chemical engineering progress symposium series*, volume 59, pages 36–41.

Zhang, L., Burgass, R., Chapoy, A., Tohidi, B., and Solbraa, E. (2011). Measurement and Modeling of CO2 Frost Points in the CO2-Methane Systems. *Journal of Chemical & Engineering Data*, 56(6):2971–2975.

Appendix A

Solid CO_2 properties data

Before introducing solid CO_2 properties data it is worth to spend some words on the frost formation theory. Different models exists to simulate frost formation and growth, and they are presented in this paragraph. In fact, as better explained later, properties of solid layer formed on the walls of the heat exchanger strongly depends on the conditions at which it is formed.

CO_2 frost formation process

During the process of frost deposition on a cold surface, three main steps may be distinguished, as observed by Hayashi et al. (1977):

- the crystal growth period
- the frost layer growth period
- the frost layer full growth period

The first correspond to a very short period of the early stage of the process in which CO_2 antisublimate into small crystals frosted on the wall of the heat exchanger (fig. A.1a). Song et al. (2013) states this process is almost instantaneous. The new crystals grows on existing CO_2 crystals plays the role of nucleus for further crystallization. The second is characterized by a porous frost structure growing (fig. A.1b). The structure consists in solid CO_2 and traces of residual gas. The third period corresponds to a fully developed frost formation process (fig. A.1c). The increase rate of deposition slows and the density increase. It is also call the densification step.

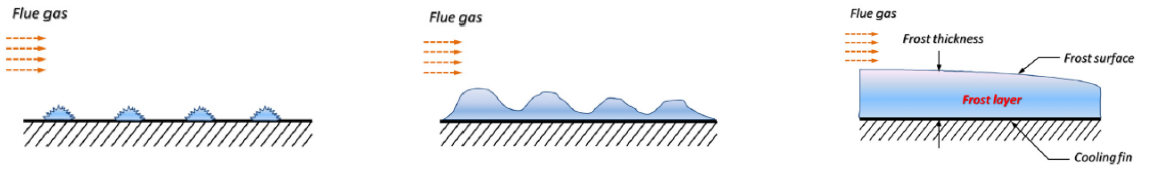

Crystal growth period | Frost layer growth period | Frost layer full growth period

Figure A.1: Sketch diagram of frost formation process from Cui et al. (2011)

Frost growth models and properties

Frost formation is a common phenomenon existing in various fields, such as refrigeration industry, civil engineering, aerospace industry. Many investigations have thus been developed, especially for water frosting. This is a very diffuse problem in refrigeration systems: when a heat pump

or, in general, the air side of a condenser works at ambient temperature below 0 $\circ C$, the air moisture solidifies on the walls of the chiller. This problem has stimulated many studies on frost growth simulation and frost properties calculation. A complete literature survey until 1996 has been made by Fahlen (1996). Among the number of studies, the most important references are:

- Hayashi et al. (1977) studied frost formation process by photographic observation, and classified frost formation types into several groups according to their structure. It concluded that frost type has strong influence on frost properties.

- Sanders (1974) has applied a theoretical model, considering physics of the frost growth and the particular aspects of finned coils, resulting in spatial variation model for properties. It validates the model with experimental data, concluding that results were in agreement with literature data and theoretical consideration. It concludes that frost density is great for higher temperatures of the wall, for higher air humidity and higher air velocity.

- Le Gall et al. (1997) and Tao and Besant (1993) proposed a frost growth model considering the frost layer as a porous medium with porosity $\epsilon = V_{crystal}/V_{frost}$. Properties of frost are function of porosity. All the properties can be thus expressed as function of porosity, but no direct relation porosity-frosting conditions has been described. They focused on the conduction and densification in the frost layer.

Conversely studies on CO_2 frosting processes are scarce. Ogunbameru et al. (1973) studied the frost CO_2 formation from a gas flow on a cold solid surface. Values of the total mass deposited were determined in situ by measuring the attenuation of low energy gamma radiation from a thin disk of cobalt-57 imbedded in the plate upon which frost was deposited. The thickness of the deposit was found by focusing a microscope on the frost surface and relating the focal length to a fixed calibration point. Values of solid density were expressed as function of gamma radiation. It concluded that both thickness and mass of frost deposited increased continuously with time but the rates of increase decreased and approached zero asymptotically: this behavior is attribute to the decreasing of the concentration difference between surface and gas flow, which is the driving force of the mass transfer. The average density of the frost layer was found to be high at short times but then it decreased as the frost continued to accumulate. According to Ogunbameru et al. (1973) data, the frost behavior of carbon dioxide is different from moisture and in contrast with the crystallization/ frost growth theory. This behavior is believed to be caused to the co-deposition of water frost during CO_2 frost experiments of the author, even if the concentration of water is much lower than CO_2 concentration in the gas flow.

Maass and Barnes (1926) have measured the solid CO_2 density at different temperatures for measuring the solid CO_2 coefficient of expansion. A known mass of carbon dioxide and propane was enclosed in a glass bulb and cooled at temperature lower than the CO_2 triple point. Carbon dioxide antisublimated and propane condensed. Knowing the total volume of the glass bulb, as well as the density of the liquid, they managed to calculate the density of the solid phase, considered as pure CO_2. Results can be represented by a polynomial correlation suggested by Toubassy (2012):

$$\rho = -0.0035T^2 + 0.031T + 1694.006 \tag{A.1}$$

Density in kg/m^3 and T in K, valid in the range $90.15 - 193.5\ K$. The process of deposition of solid CO_2 from liquid propane allows to consider values of density measured by Maass and Barnes (1926) as the density of carbon dioxide crystals, as observed by Cook and Davey (1976), too.

Cook and Davey (1976) experimentally found a relation between solid CO_2 properties (density and conductivity) and condensation rate in a cryopump, so at very low pressure (lower than $810^{-5}bar$). Results are shows in A.3 and A.4. Temperatures at which data are taken is

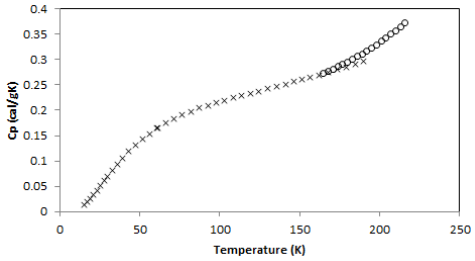

Figure A.2: Heat Capacity c_P versus temperature T for carbon dioxide: o Maass and Barnes (1926),x Giauque and Egan (1937)

100 K. In their work, the authors reported that measurements from other authors at temperatures deposition between 60 and 80 K gave values of density between 1300 kg/m^3 and 1400 kg/m^3 (Cook and Davey, 1976), even if they are not strictly comparable with data obtained in their work because of the difference in temperature deposition. It has to be said that values of condensation rate for our application are between 100 and 500 mg/m^2s

Shchelkunov et al. (1986) conducted studies on solid CO_2 formation on a plate from a binary gas mixture. He concludes that:

- The thickness of the layer of solid phase increases through- out the desublimation process
- The temperature of the plate and the pressure of the mixture have the greatest influence on the rate of growth of the thickness of the layer.
- The law of time variation of the thickness of the layer is nearly parabolic, which agrees with the results obtained in the freezing out of moisture .
- The density of the cryogenic precipitate increases with time.
- The solid phase becomes denser through internal diffusion and the effect of recrystallization of CO_2 molecules from "warm" sections of the layer to "cooler" sections under the action of the internal drop in the partial pressure of CO_2 due to the temperature gradient in the layer.
- A decrease in the temperature of the plate leads to an increase in the size and number of crystals formed, as well as lower density of their packing.

The values found by this work are hardly exploitable because of the low quality graphical representation available in the paper.

Giauque and Egan (1937) measured heat capacity of solid CO_2 with a low temperature calorimetric apparatus, for temperatures from 15 to 190 K. Also Maass and Barnes (1926) measured solid CO_2 heat capacity (fig A.2). A fitting equation for these data is reported in Toubassy (2012):

$$c_P = 1.25 \cdot 10^{-5} T^2 - 2.83 \cdot 10^{-3} T + 0.4 \tag{A.2}$$

Heat capacity in $cal/g \cdot K$ for temperature range between 165 and 216 K. The two sets of data differs for temperature higher than 170 K, see fig. A.2

Sumarokov et al. (2006) presented an experimental work on thermal conductivity for pure solid carbon dioxide up to 35K. Authors concludes that the thermal conductivity of solid CO_2 is much higher than any value measured at that time for simple molecular crystals like N_2, NO_2 and parahydrogen.

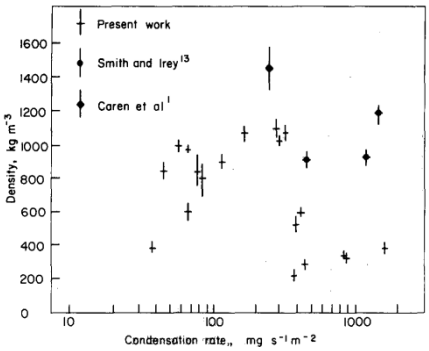

Figure A.3: Density versus condensation rate for carbon dioxide from Cook and Davey (1976)

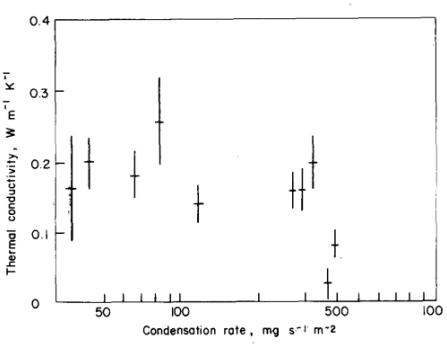

Figure A.4: Thermal conductivity versus condensation rate for carbon dioxide from Cook and Davey (1976)

Finally, interesting measurements have been carried out by Toubassy (2012). He studied the solidification of carbon dioxide on plane fins of an heat exchanger and provides data on solid layer thickness, mass and porosity.

Appendix B

Calibrations

B.1 Pressure calibration

The system pressure is measured by means of a 16 MPa PTX611 Druck pressure transducer. The sensor has been calibrated using a Druck PACE 5000 manometer as a secondary measurement standard. The calibration and the measurements have been performed maintaining the pressure transducer at 50 °C. The calibration allows to find a correlation between the pressure observed by the pressure transducer (p_{raw}) and the reference pressure measured by the secondary measurement standard (p_{true}).

Results obtained show that a second order correlation and linear correlation has very similar behavior, with very similar maximum deviation (see fig. B.1), and thus a linear correlation (eq. (B.1)) is used for the pressure calibration. The maximum deviation between calibrated pressure (p_{corr}) and reference pressure (p_{true}) is 26.16 mbar.

$$p_{corr} = 0.999942439 p_{raw} - 0.011686705 \tag{B.1}$$

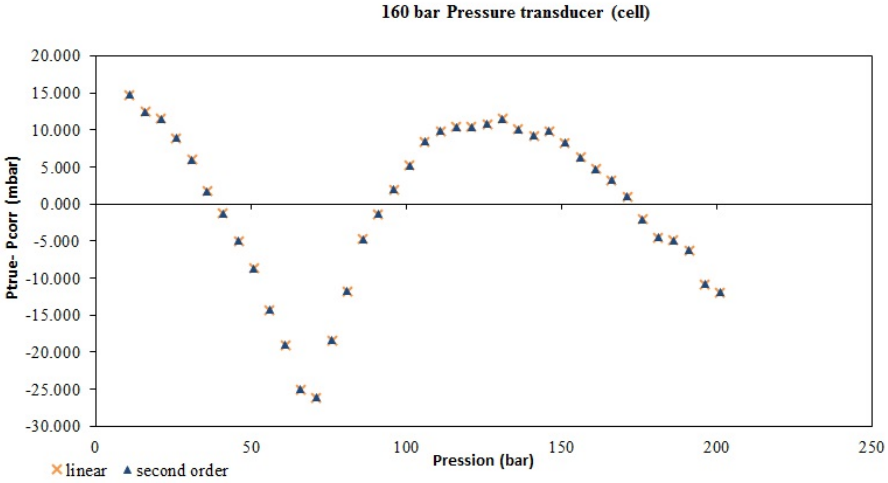

Figure B.1: Deviation between observed pressure and pressure obtained by applying the calibration correlation in the range 1-200 bar using a linear and a second order correlation for pressure calibration of 16 MPa PTX611 Druck pressure transducer.

B.2 Temperature calibration

The temperature measured in the equilibrium cell has been calibrated measuring the saturated pressure of methane, for a temperature range between 102 and 144 K, and oxygen from 140 to 166 K. The cell is equipped with two PT100 (at 0°C) temperature probes placed one at the top of the cell, measuring $T_{raw,top}$, and one at the bottom of the cell, measuring $T_{raw,bot}$. The temperature that has been calibrated (T_{raw}) is the average between $T_{raw,top}$ and $T_{raw,bottom}$.

The calibration is performed by calculating the average temperature in the cell (T_{raw}) from the observed temperature of the two temperature probes ($T_{raw,top}$ and $T_{raw,bot}$) and comparing it with the saturated temperature (T_{sat}) of pure oxygen and pure methane calculated from the measured saturated pressure (p_{sat}) using the following equation:

$$p_{sat} = exp\left(A + \frac{B}{T} + C\ln(T) + DT^E\right) \tag{B.2}$$

with p_{sat} expressed in Pa and temperature T in K. Coefficients A,B,C,D,E are reported in table B.1.

Table B.1: Coefficients of eq. (B.2) for calculating $p_{sat}(T)$

Component	A	B	C	D	E
Methane	39.205	-1324.4	-3.4366	3.10E-05	2
Oxygen	51.245	-1200.2	-6.4361	0.028405	1

The procedure for measuring the saturated pressure is to set the temperature of the cell through the temperature regulator and then to load pure methane (or pure oxygen) in vapor phase from a cylinder, until the pure compound starts to liquefy. This phenomenon is easily detectable because the pressure in the cell becomes constant during the liquefaction. Saturation pressure is thus measured and saturation temperature calculated from eq. (B.2). Oxygen is used for a temperature range between 102 and 144 K and methane from 140 to 166 K. A correlation between the average temperature observed in the cell (T_{raw}) and the saturation temperature, considered as the reference temperature (T_{true}) is then obtained.

Results obtained show that a second order correlation presents smaller maximum deviations compared to a linear correlation (see fig. B.2), and thus a second order correlation (eq. (B.3)) is used for the temperature calibration. The maximum deviation between calibrated temperature T_{corr} and reference temperature T_{true} is 0.09 K.

$$T_{corr} = -2.41191\ 10^{-5}T_{raw}^2 + 0.993074174T_{raw} - 0.288239505 \tag{B.3}$$

B.3 Gas Chromatograph detectors calibration

Two types of Gas Cinematography calibration have been used and compared in this work. The first one is by injection of a known volume of pure components by means of a syringe. The second one is by sampling a synthetic binary mixture of known composition. The first method allows to estimate the number of moles of each component from the integration of the GC detector response (peak surface). It cannot be used in case of very low composition of one component (down to 20 ppm) since the smallest amount of substance that can be injected by a syringe is much bigger than the amount of substance corresponding to 20 ppm in the analyzed sample. The second method does not allow to know the absolute amount of sampled component but only the molar composition of the sample. It has the advantage to allow the calibration of the GC down to very low concentration of one component.

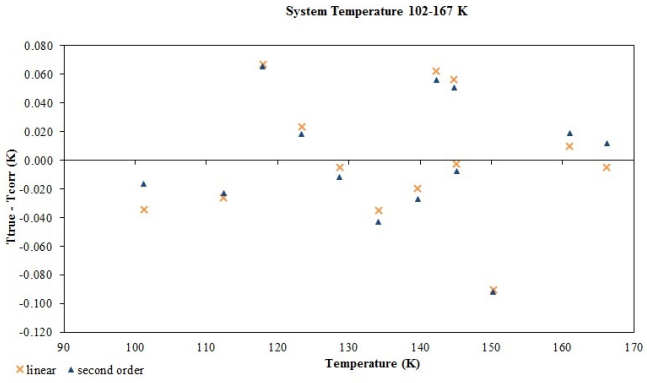

Figure B.2: Deviation between average temperature in the cell and temperature obtained by applying the calibration correlation in the range 102-167 K using a linear and a second order correlation for temperature calibration.

B.3.1 Calibration by injecting a known volume

The GC calibration method described in this section has been used for the N_2-O_2-CH_4-CO_2 quaternary system SLVE measurements: the GC has been calibrated by injecting samples of pure methane, pure oxygen and pure nitrogen by means of an Evol XR electronic automated syringe, with a nominal volume of 500 μl. For calibrating the FID for measuring the CO_2 content, a different calibration method has been used (see sec. B.3.2). For each of the three components, different volumes have been injected: 50 , 100, 200, 300, 400 and 500 μl. For the oxygen, a calibration with smaller volumes (down to 20 μl) has been performed. Surfaces of the peaks obtained from the GC analysis have been correlated to the number of moles. The theoretical number of moles injected has been calculated dividing the volume of injected gas by its molar volume obtained from the Van der Waals equation of state. Parameters for the attractive term (a_{vdW}) and the covolume (b_{vdW}) of the equation of state have been obtained from literature (McCain, 1990) and reported in tab. B.2. The ambient temperature has been measured by means of a PT100Ω (at 0°C) temperature probe placed close to the septum for samples collection attached to the manometer of the gas cylinders. The temperature probe has been connected to an electronic display and the system has been calibrated using a 25Ω Hart Scientific reference probe. The measurement of ambient pressure has been performed using a calibrated Druck DPI 141 precision pressure indicator. The gas chromatograph operating conditions are reported in tab. 5.2.

Parameters of eq. (B.4) correlating peak surfaces of each component (S_i) to the corresponding number of moles (n_i), are reported in tab. B.3. For the O_2 a second correlation for low concentration has been used. Results of the correlation of the GC are shown in figures from B.3 to B.6.

$$n_i = aS_i^2 + bS_i + c \tag{B.4}$$

In the quaternary mixture SLVE measurements, for determining the number of moles of CO_2 (n_{CO_2}) eq. (B.5) has been used, relating the CH_4 number of moles (n_{CH_4}) and the ratio of the peak surfaces of CO_2 and CH_4 (S_{CO_2} and S_{CH_4}), through a coefficient $F_{CO_2CH_4}$ obtained by calibration, as explained in sec. B.3.2.

$$n_{CO_2} = n_{CH_4} \frac{S_{CO_2}}{S_{CH_4}} F_{CO_2CH_4} \tag{B.5}$$

Table B.2: Parameters of the vdW EoS used for calculating the number of moles from the injected volumes, for each component.

Component	a_{vdW}	b_{vdW}
CH_4	2.253	0.04278
N_2	1.39	0.03913
O_2	1.36	0.03183

Table B.3: Parameters of eq. (B.4) and maximum deviation between injected and calculated moles for each component.

Component	a	b	c	$max(n_{inj} - n_{corr})$
CH_4	3.10022E-14	2.58162E-09	2.51786E-07	6.27806E-08
N_2	-7.42047E-15	2.61677E-09	1.11486E-07	9.69507E-08
O_2	0	2.77714E-09	1.70198E-07	8.09728E-08
$O_{2\ low}$	0	2.75234E-09	1.44073E-07	1.05117E-08

B.3.2 Calibration by sampling a synthetic mixture

The GC calibration method described in this section has been used for the N_2-CH_4-CO_2 ternary system SLVE measurements and the CO_2 content measured by the FID for the N_2-O_2-CH_4-CO_2 quaternary system SLVE measurements. GC conditions are reported in tab. 5.2.

Expected CO_2 concentration in vapor and liquid phase is too small (down to 30 ppm) to allow accurate enough TCD and FID calibration by injecting known quantities of CO_2 through a syringe.The method used for calibrating GC is thus by sampling binary mixtures of known composition and determining the relative response factor F_{ij} between two components. This method allows to obtain the relation between the ratio of the peaks surfaces (S_i/S_j) and the ratio of the number of moles (n_i/n_j) of two components. For components i and j, the response factor F_i and F_j are the proportionality factor between the number of moles and the surface of the peaks:

$$n_i = F_i \times S_i \tag{B.6}$$

$$n_j = F_j \times S_j \tag{B.7}$$

and thus

$$\frac{n_i}{n_j} = F_{ij} \times \frac{S_i}{S_j} = \frac{x_i}{x_j} \tag{B.8}$$

allowing to obtain the composition of each component using the following equation:

$$x_i = \frac{1}{1 + \sum_j F_{ij} \frac{S_j}{S_i}} \tag{B.9}$$

Preparation of mixtures of known composition

CO_2-CH_4 and CO_2-N_2 mixtures of known composition are thus prepared in the equilibrium cell, covering the expected range of composition of the measurements. Particular attention has been paid on the procedure for loading the mixture with composition obtained by measuring the loading pressure of each component: the number of moles of CO_2 (n_{CO_2}) has been calculated by dividing the volume of the cell (V_{cell}) by the CO_2 molar volume ($v_{CO_2}(T,p)$) calculated from the GERG EoS at measured pressure and temperature:

$$n_{CO_2} = \frac{V_{cell}}{v_{CO_2}(T,p)} \tag{B.10}$$

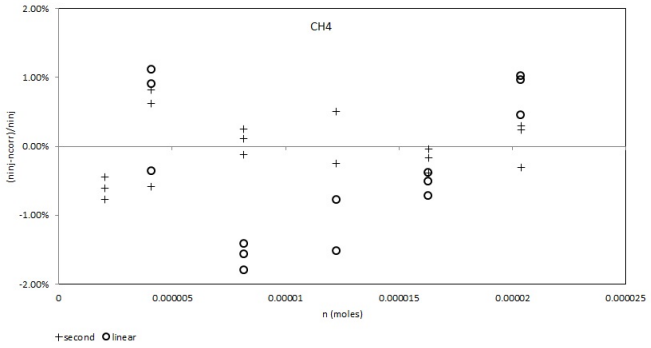

Figure B.3: Deviation between the number of moles injected in the GC and the number of moles obtained using a linear and a second order correlation for the Perichrom PR2100 GC TCD calibration for CH_4.

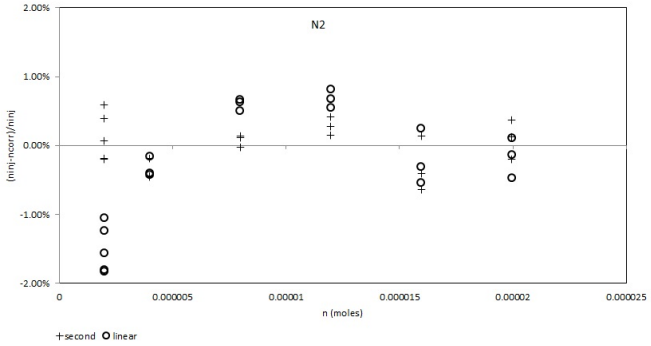

Figure B.4: Deviation between the number of moles injected in the GC and the number of moles obtained using a linear and a second order correlation for the Perichrom PR2100 GC TCD calibration for N_2.

Similarly, the number of moles of the second component j (CH_4 or N_2) has been obtained from the molar volume of the mixture (of composition $\mathbf{x}$):

$$n_j = \frac{V_{cell}}{v_j(T, p, \mathbf{x})} \tag{B.11}$$

The volume of the equilibrium cell (EC) has been accurately measured by injecting liquid methanol into the cell using a variable volume cell equipped with a Digital Display Displacement sensor (DDD). For measuring only the EC volume, valve V11 (see fig. 5.2) is closed. The measured volume (V_{cell}) is found to be 39.0824 cubic centimeters.

Once the volume of the EC has been measured,the mixture has been prepared by loading the CO_2 and the solvent (N_2 or CH_4) at atmospheric temperature. The pressure of loaded CO_2 has been measured by means of the 0.16 MPa pressure transducer. After that, valve V11 has been closed and the solvent loaded, using the 200 bar pressure transducer for measuring the pressure. The cell has been finally isolated by means of valve V1 and the stirrer turned on to ensure homogeneous mixing in the cell. A series of sampling then has been performed, and a new mixture loaded. The results of the calibration are shown in table B.4 and figures B.7 and B.8.

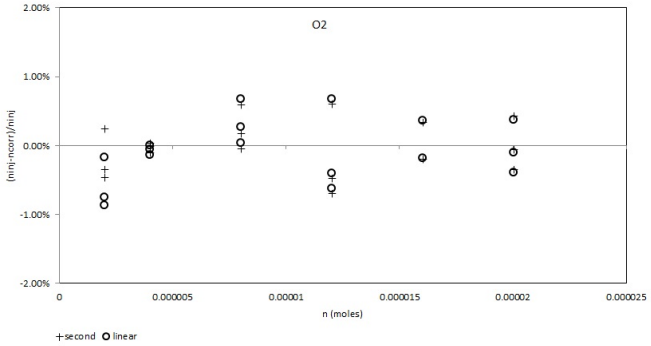

Figure B.5: Deviation between the number of moles injected in the GC and the number of moles obtained using a linear and a second order correlation for the Perichrom PR2100 GC TCD calibration for O_2.

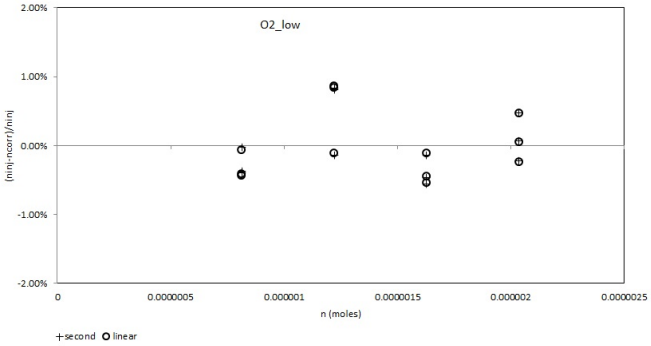

Figure B.6: Deviation between the number of moles injected in the GC and the number of moles obtained using a linear and a second order correlation for the Perichrom PR2100 GC TCD calibration for O_2 at lower injected volumes.

Table B.4: Results of GC calibration

Measurements	Component	F_{ij}	CO_2 range (ppm)	$max((n_i/n_j)_{calc} - (n_i/n_j)_{corr})$
Ternary SLVE	CO_2/CH_4	404.97	6 500 - 65	5.51E-05
Ternary SLVE	CO_2/N_2	310.93	5 600 - 18	1.33E-05
Quaternary SLVE	CO_2/CH_4	223.81	10 000 - 100	7.91E-05

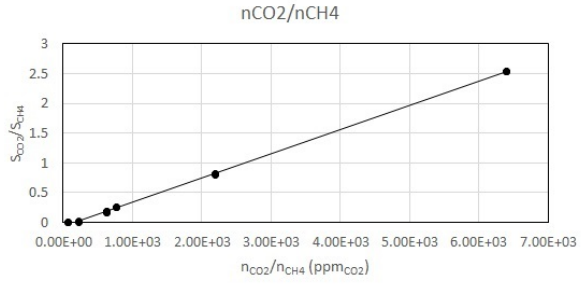

Figure B.7: Calibration of the TCD and FID with CH_4-CO_2 for the N_2-CH_4-CO_2 SLVE measurements.

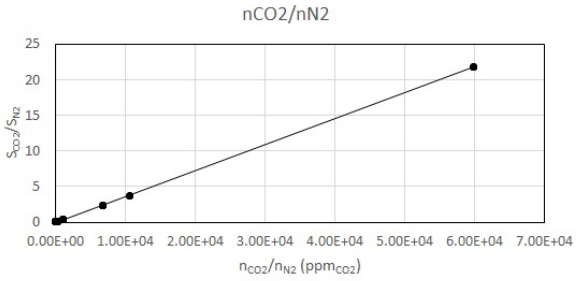

Figure B.8: Calibration of the TCD and FID with N_2-CO_2 for the N_2-CH_4-CO_2 SLVE measurements.

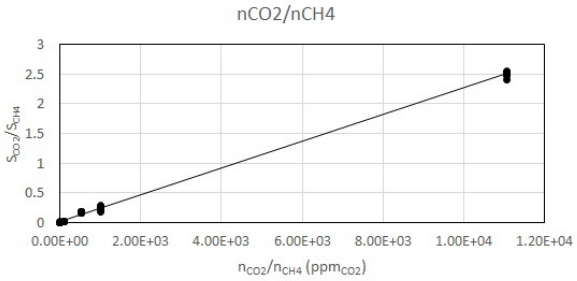

Figure B.9: Calibration of the TCD and FID with CH_4-CO_2 for the N_2–O_2-CH_4-CO_2 SLVE measurements.

Appendix C

Evaluating the uncertainties of experimental results

C.1 Uncertainties in temperature and pressure measurements

Uncertainty in temperature and pressure measurement are calculated as follows. The estimated value of pressure of temperature is expressed as

$$T = T_{exp} \pm U(T) \tag{C.1}$$

$$p = p_{exp} \pm U(p) \tag{C.2}$$

Where T_{exp} and p_{exp} are the values of temperature and pressure registered during the measurements and $U(T)$ and $U(p)$ the expanded uncertainty, obtained by multiplying the combined standard uncertainty $u_c(T)$ and $u_c(p)$ by a coverage factor k.

$$U(T) = k\ u_c(T) \tag{C.3}$$

$$U(p) = k\ u_c(p) \tag{C.4}$$

The coverage factor (k) defines the level of confidence to be associated to the interval defined by $U(T)$ and $U(p)$, and is taken equal to 2.

The combined standard uncertainty $u_c(T)$ and $u_c(p)$ is obtained by combining the uncertainty associated to the repeatability of the temperature and pressure measurement and the uncertainty associated to calibration of temperature and pressure sensors.

$$u_c(T) = \sqrt{u_{rep}(T)^2 + u_{calib}(T)^2} \tag{C.5}$$

$$u_c(p) = \sqrt{u_{rep}(p)^2 + u_{calib}(p)^2} \tag{C.6}$$

The repeatability of the measurement is the estimated standard deviation of the mean temperature and pressure at SLVE consitions, during the period at which the temperature was set constant and the pressures resulted stable. During this period, the composition analysis of vapor and liquid phases was performed.

$$u_{rep}(T) = \sqrt{\frac{1}{n(n-1)} \sum_{j=1}^{n} \left(T_j - \bar{T}\right)^2} \tag{C.7}$$

$$u_{rep}(p) = \sqrt{\frac{1}{n(n-1)} \sum_{j=1}^{n} (p_j - \bar{p})^2} \tag{C.8}$$

where n is the number of measurements taken, $\bar{T}$ and $\bar{p}$ are the average value of T and p over the n measurements.

The calibration uncertainty $u_{calib}(T)$ and $u_{calib}(p)$ is obtained considering the calibration correlation resulting from the temperature and pressure sensors calibration (see App. B). For the pressure calibration, the uncertainty considers also the uncertainty associated to the Druck PACE 5000 manometer used as a secondary measurement standard. The uncertainty on the secondary measurement standard is reported in the calibration certificates 25196 and 25197 (7 march 2016) provided by the Desgranges and Huot pressure calibration laboratory. For the temperature calibration, the uncertainty associated to the reference temperature (saturation temperature at measured pressure) used as secondary measurement standard is considered negligible compared to the uncertainty associated to the repetability.

$$u_{calib}(p) = \sqrt{u_{corr}(p)^2 + u_{stand}(p)^2} \tag{C.9}$$

where

$$u_{stand}(p) = 3.8\ 10^{-5} + 4\ 10^{-10} p\ (bar) \tag{C.10}$$

The correlation uncertainty u_{corr} has been calculated assuming that the values of T and p follows a rectangular probability distribution and thus

$$u_{corr}(p) = \frac{b_p}{\sqrt{3}} \tag{C.11}$$

$$u_{calib}(T) = \sqrt{u_{corr}(T)^2 + u_{sat}(T)^2} \tag{C.12}$$

$$u_{corr}(T) = \frac{b_T}{\sqrt{3}} \tag{C.13}$$

where b_p and b_T is the absolute value of the maximum deviation between the observed values and the values obtained by the polynomial expression outsourced from the calibration of the sensors (see Appendix B).

$u_{sat}(T)$ refers to the uncertainty on temperature due to the uncertainty on pressure measured for obtaining the saturated temperature (see App. B.2). It is computed as:

$$u_{sat}(T) = \frac{\partial T_{sat}}{\partial p} u(p) \tag{C.14}$$

where the derivative of the saturated temperature over pressure is obtained by numerical derivation of eq. (B.2) and $u(p)$ is the uncertainty on pressure, calculated as eq. (C.6).

C.2 Uncertainties in composition measurements

As described in Chap. 5, vapor and liquid composition are measured through Gas Chromatographic analysis. The composition x of each component i in mixture is expressed together with the estimation of the uncertainty, named expanded uncertainty $U(x_i)$

$$x_i = x_{exp,i} \pm U(x_i) \tag{C.15}$$

where $x_{exp,i}$ is the experimental value of x_i and $U(x_i)$ the expanded uncertainty, obtained by multiplying the combined standard uncertainty $u_c(x_i)$ by a coverage factor k.

$$U(x_i) = k\ u_c(x_i) \tag{C.16}$$

The coverage factor defines the level of confidence to be associated to the interval defined by $U(x_i)$, and is taken equal to 2.

The combined standard uncertainty $u_c(x_i)$ is obtained by combining the uncertainty associated to the repeatability of the composition measurement and the uncertainty associated to calibration of the GC device

$$u_c(x_i) = \sqrt{u_{rep}(x_i)^2 + u_{calib}(x_i)^2} \tag{C.17}$$

The measurement repeatability uncertainty associated with x_i is the estimated standard deviation of the mean, for each series of composition analysis at the same SLVE temperature and pressure, where n is the number of repeated measurements

$$u_{rep}(x_i) = \sqrt{\frac{1}{n(n-1)} \sum_{j=1}^{n} (x_{i,j} - \bar{x_i})^2} \tag{C.18}$$

where $\bar{x_i}$ is the average value of x_i over the n measurements.

The calibration uncertainty $u_{calib}(x_i)$ is calculated depending on the calibration method used for obtaining the calibration curve.

GC calibration by injecting a known volume

In case the calibration of the GC detector is performed by injection of known volumes of component i through a syringe, the calibration curve relates the number of moles n_i to the peaks surface measured by means of a TCD detector. The molar concentration of component i is obtained dividing the number of moles of component i (n_i) by the total amounts of moles ($n_{tot} = \sum_{j=1}^{nc} n_j$, where nc is the number of components)

$$x_i = \frac{n_i}{\sum_{j=1}^{nc} n_j} \tag{C.19}$$

The calibration uncertainty on x_i is thus

$$u_{calib}(x_i) = \sqrt{\sum_{j=1}^{n} \left[\frac{\partial x_i}{\partial n_j} u(n_j) \right]^2} \tag{C.20}$$

where, from eq. (C.19)

$$\frac{\partial x_i}{\partial n_j} = \begin{cases} -\frac{x_i}{n_{tot}} & \text{if } j \neq i \\ \frac{1-x_i}{n_{tot}} & \text{if } j = i \end{cases} \tag{C.21}$$

Uncertainty $u(n_j)$ is related to the polynomial correlation used for determining the number of moles n_j from the GC response ($u_{corr}(n_j)$). The correlation uncertainty has been calculated assuming that the values of n_j follows a rectangular probability distribution and thus

$$u(n_j) = u_{corr}(n_j) = \frac{b}{\sqrt{3}} \tag{C.22}$$

where b has been considered as the absolute value of the maximum deviation between the mole number calculated from the injected volume and the polynomial expression outsourced from the calibration of the TCD detector.

Calibration by sampling a synthetic mixture

In case of very low composition of one component (namely CO_2), injection into the GC line of the corresponding small volume by means of a syringe is not possible. The method used is thus by sampling a synthetic mixture of known composition prepared at this purpose. The procedure is explained in details in Chap. 5.

In this case the molar composition of generic component i is given by following equation:

$$x_i = \frac{1}{1 + \sum_{j=1}^{nc} \frac{S_i}{S_j} F_{ij}} \tag{C.23}$$

where S_i and S_j is the peak surface (integrated detector response measured by the GC) of component i and j respectively, F_{ij} is the relative response factor obtained by the calibration correlations and nc the number of components.

The uncertainty due to the calibration of the GC is thus

$$u_{calib}(x_i) = \sqrt{\sum_{j=1}^{nc} \left[\frac{\partial x_i}{\partial \frac{x_i}{x_j}} u\left(\frac{x_i}{x_j}\right) \right]^2} \tag{C.24}$$

Being

$$\frac{S_i}{S_j} F_{ij} = \frac{x_i}{x_j} \tag{C.25}$$

Uncertainty on $\frac{x_i}{x_j}$ is related to the linear correlation used for the calibration of the GC ($u_{corr}\left(\frac{x_i}{x_j}\right)$). The correlation uncertainty has been calculated assuming that the values of $\frac{x_i}{x_j}$ follows a rectangular probability distribution and thus

$$u\left(\frac{x_i}{x_j}\right) = u_{corr}\left(\frac{x_i}{x_j}\right) = \frac{b}{\sqrt{3}} \tag{C.26}$$

where b is the maximum deviation between the mole ration $\frac{x_i}{x_j}$ of the synthetic mixture and mole ratio calculated from the linear correlation obtained from the calibration of the GC.

Résumé

Le biométhane est en train de devenir un acteur majeur dans le contexte des biocarburants et dans le cadre des politiques de décarbonisation de l'énergie. Pour sa production, le biogaz brut obtenu á partir des déchets (agricoles ou de décharge), doit être traité pour éliminer le dioxyde de carbone et l'azote. Grâce á la demande croissante de biogaz liquéfié (LBG), les techniques de purification cryogéniques sont de plus en plus compétitives par rapport aux technologies classiques. L'optimisation énergétique et les défis techniques tels que la solidification du CO_2, exigent des modelés fiables pour la simulation du procédé. L'objectif de cette thè se est l'étude d'une technologie cryogénique appliquée à la purification et la liquéfaction du biogaz. La base de l'étude est la modélisation des diagrammes de phases du biométhane constitué de méthane, d'azote, de dioxyde de carbone et d'oxygène. La purification du biogaz est obtenue par solidification et séparation du CO_2, dans une plage de température de -160 à -90°C, à la pression de 1 à 30 bar. C'est pourquoi il est nécessaire d'étudier les équilibres de phases solide-fluide et de déterminer les conditions de formation de la phase solide. Afin de définir les diagrammes de phases comprenant une phase solide, ainsi que de tester et calibrer le modè le thermodynamique l'étude s'appuie sur des données expérimentales. Pour pouvoir étudier l'influence de l'azote et de l'oxygè ne, des mesures originales d'équilibre solide-liquide-vapeur sont produites. Les résultats obtenus sont enfin utilisés pour la compréhension et l'optimisation du procédé de purification et de liquéfaction.

Mots Clés

Purification du biogaz, Biomethane liquéfié, Modèle thermodynamique, Equilibre solide-liquide-vapeur, Mesures de solubilité, CO_2 solide

Abstract

Biomethane plays an important role in the context of bio-fuels consumption and energy decarbonisation policy. For its production, raw biogas obtained from agricultural or landfill wastes has to be upgraded by removing carbon dioxide and nitrogen. Thanks to the increasing demand of Liquefied BioGas (LBG), cryogenic upgrading techniques are becoming more competitive compared to classical upgrading technologies. Optimization of energy consumption and technical challenges such as CO_2 solidification, require reliable models for the simulation of the process. The objective of the thesis is the study of an optimized cryogenic technology applied to a biogas upgrading and liquefaction process. The base of the study is the thermodynamic modeling of the phase diagrams of biomethane mixture, constituted of methane as a major component and nitrogen, oxygen and carbon dioxide. The biogas upgrading is obtained through CO_2 solidification and separation in a range of temperature of -160 to -90°C at pressure from atmospheric to 30 bar. For this reason the study is focused on solid - fluid equilibria. In order to identify solid CO_2 conditions and define the phase diagrams the thermodynamic model is tested and calibrated on experimental data. In order to study the influence of nitrogen and oxygen, original solid-liquid-vapor equilibrium data are produced, providing the composition of the vapor and liquid phase. Results obtained from the model are used for understanding and optimizing the upgrading and liquefaction process.

Keywords

Biogas upgrading, Liquefied biomethane, Thermodynamic model, Solid-liquid-vapor equilibrium, Solubility measurements, Solid CO_2